# Developing 1,10-phenanthroline complexes towards their application as triplet sensitizers

**Niamh Mc Goldrick**

**A thesis submitted to the University of Dublin for the degree of**

**Doctor of Philosophy**

**School of Chemistry**

**Trinity College Dublin**

**February 2014**

## Declaration

This thesis has not been submitted as an exercise for a degree at this or any other university. Except where acknowledgement is given, all work is original and was carried out by the author alone. I agree that the library may lend or copy this thesis upon request.

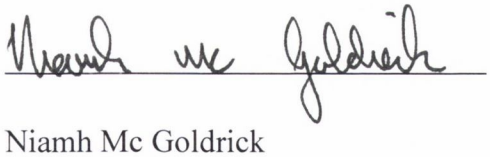

Niamh Mc Goldrick

## Summary

**Chapter 1:** This chapter begins with a general introduction to polycyclic aromatic hydrocarbons, followed by a focused review of recent 3,8-substituted 1,10-phenanthroline systems reported in the literature. The chapter also describes the synthesis a series of 3,8-aryl acetylene 1,10-phenanthroline ligands *via* a sequence of Sonogashira cross-coupling and Diels-Alder cycloaddition reactions, and the issues surrounding the use of copper catalysts in cross-coupling reactions with 1,10-phenanthrolines. The characterisation and spectroscopic properties of the ligands are discussed. In addition, brief computational investigations of both the neutral and protonated pyrene functionalised 1,0-phenanthroline ligand are also presented.

**Chapter 2:** This chapter contains a short literature review of the photophysical properties and selected applications of Ru(II) and Ir(III) 1,10-phenanthroline complexes. Also presented is the synthesis and characterisation of Ru(II) and Ir(III) complexes of the aryl acetylene 1,10-phenanthroline ligands described in Chapter 1.. The photophysical investigation has established the effect on the emission properties of both metal centres when the size of the appended aryl chromophore is increased.

**Chapter 3** contains a comprehensive literature review on the application of 1,10-phenanthroline complexes as triplet sensitizers for TTA based upconversion as well as illustrating the development of a new screening system for TTA triplet sensitizers using a typical fluorimeter setup. The Ru(II) and Ir(III) 1,10-phenanthroline complexes prepared in Chapter 2 are examined for their potential application in TTA as triplet sensitizers using DPA as an acceptor. The subsequent photophysical and computational investigation of two pyrene substituted 1,10-phenanthroline complexes is also presented.

**Chapter 4:** describes the synthesis and characterisation of a novel series of 3,8- aryl 1,10-phenanthroline ligands and two of their corresponding Ir(III) and Ru(II) complexes. These ligands have been designed with aim of investigating possible C-C bond formation to the 1,10-phenanthroline core through cyclodehydrogenation of polyphenylene based 1,10-phenanthrolines. The photophysical properties of the ligands and complexes are discussed, as well as screening of the complexes for TTA applications.

**Chapter 5:** provides a full account of the experimental work carried out in this research.

## Acknowledgements

I would like to sincerely thank my supervisor Prof. Sylvia Draper for her continuous support and encouragement over the course of my postgraduate study, particularly in the last twelve months. For both her guidance and suggestions, I am forever in her debt. I also wish to thank those in the School of Chemistry who allowed me the opportunity to continue my studies at postgraduate level.

I wish to acknowledge the experimental officers and technicians who have assisted me over the last five years. In particular, I would like to thank Dr John O'Brien for both his expertise and time. I also wish to extend my gratitude to Drs. Manuel Ruether, Martin Feeney and Gary Hessman, and Patsy Greene, each of whom have made valuable contributions to this work. I am grateful to Prof Jianzhang Zhao, and his postgraduate student Wanhua Wu for the collaborative work in this project and Dr Longsheng Wang for crystallographic support.

I would like to thank the past members of the Draper group especially Drs. Deanne Nolan, Frances Murphy and Belen Gil, for their advice and suggestions at the very beginning. To the current members; Lankani, thank you for being such a great listener, you are a real friend. Lu, Nitheen, Bryan and Rob, those little favours will forever be remembered. Special thanks to Colm, for your time and technical expertise, you are a star. Finally, this thesis would not have been completed without Gearóid. His endless patience and advice will never be forgotten.

To my parents, Kevin and Edel, and my sisters Treasa and Eadaoin; thank you for your love, understanding and unfailing support. To my extended family, especially Minnie and Annie, and my friends Munny, Niamh, Sarah and Róisin, thank you for your constant motivation and above all, for always being there. Finally, to my boyfriend Dean, thank you for your constant encouragement, belief and love. I could not have done this without you.

## Table of Contents

**Table of Figures**

**Table of Schemes**

# Abbreviations

| | |
|---|---|
| **1D** | one-dimensional |
| **2D** | two-dimensional |
| **A** | acceptor |
| **Å** | angstrom |
| **$Alq_3$** | tris(8-hydroxyquinolinato)aluminium |
| **Ar** | aryl |
| **a.u.** | arbitrary units |
| **bodipy** | iodophenyl boron-dipyrromethene |
| **BPEA** | bis(phenylethynl)anthracene |
| **BPEN** | 9,10-bis(phenylethynl)naphthacene |
| **bpy** | 2,2'-bipyridine |
| **Bu** | butyl |
| **C** | Celsius |
| **cm** | centimetre |
| **COSY** | correlation spectroscopy |
| **Cp** | cyclopentadiene |
| **D** | doublet |
| **dd** | doublet of doublets |
| **DDQ** | 2,3-dichloro-5,6-dicyano-1,4-benzoquinone |
| **DEPT** | distortionless enhancement by polarisation transfer |
| **DFT** | density functional theory |
| **dip** | 4,7-diphenyl-1,10-phenanthroline |
| **DMF** | dimethylformamide |
| **DMPD** | 1,4-dimethylpiperazine-2,3-dione |
| **DMSO** | dimethylsulfoxide |
| **DNA** | deoxyribonucleic acid |
| **DPA** | 9,10-diphenylanthracene |
| **DPBF** | 1,3-diphenylisobenzofuran |
| **dppz** | dipyrido[3,2-a:2′-3′-c]phenazine |
| **$e^-$** | electron |
| **EI-MS** | electron impact mass spectrometry |
| **em** | emission |
| **EPR** | electron paramagnetic resonance |
| **ESI-MS** | electrospray mass spectrometry |
| **EDTA** | ethylenediaminetetraacetic acid |
| **exc** | excitation |
| **ES** | excited state |
| **EXSY** | EXchange SpectroscopY |
| **FRET** | Forster Resonance Energy Transfer |
| **FTIR** | Fourier transform infrared spectroscopy |
| **G** | gram |
| **GS** | ground state |

| | |
|---|---|
| **HETCOR** | HETeronuclear CORrelation spectroscopy |
| **HBC** | hexa-peri-hexabenzocoronene |
| **HMBC** | Heteronuclear Multiple-Bond Correlation |
| **HMQC** | Heteronuclear Multiple-Quantum Correlation |
| **HOMO** | highest occupied molecular orbital |
| **HPLC** | high-performance liquid chromatography |
| **Hr** | hour |
| **Hz** | Hertz |
| ***I*** | iso |
| **IR** | infrared |
| ***J*** | coupling constant |
| **K** | Kelvin |
| **kJ** | kilojoule |
| **L** | ligand |
| **LD-TOF** | Laser desorption –time-of-flight mass spectrometry |
| **LMCT** | ligand-to-metal-charge transfer |
| **LUMO** | lowest unoccupied molecular orbital |
| **m** | multiplet |
| **M** | metal |
| **M** | Molarity |
| **Min** | minute |
| **Mol** | mole |
| **m.p.** | melting point |
| **m.u.** | mass units |
| ***m/z*** | mass to charge ratio |
| **MALDI-TOF MS** | matrix-assisted laser desorption/ionisation – time of flight mass spectrometry |
| **max** | maximum |
| **Me** | Methyl |
| **mg** | milligram |
| **MHz** | Megahertz |
| **mL** | millilitre |
| **MLCT** | metal to ligand charge transfer |
| **mmol** | millimole |
| **mol** | mole |
| **MS** | mass spectrometry |
| **mV** | millivolt |
| **N-½HSB** | half-cyclised nitrogen-heterosuperbenzene |
| **N-HSB** | nitrogen-heterosuperbenzene |
| **nm** | nanometer |
| **NMR** | nuclear magnetic resonance |
| **nOe** | nuclear Overhauser effect |
| **ns** | nanoseconds |
| **OLED** | organic light emitting diode |
| **ox.** | Oxidation |

| | |
|---|---|
| **PAH** | Polycyclic aromatic hydrocarbon |
| **PBS** | Phosphate buffered saline |
| **PDOEP** | Octaethylporphyrin palladium |
| **PDT** | Photodynamic Therapy |
| **ph** | phenyl |
| **phen** | 1,10-phenanthroline |
| **PIFA** | (bis(trifluoroacetoxy)iodo)benzene |
| **ppm** | part per million |
| **ppy** | 2-phenylpyridine |
| **RT** | room temperature |
| **S** | singlet |
| **sec** | second |
| ***sh*** | shoulder |
| **solv.** | solvent |
| **SOMO** | singly occupied molecular orbital |
| **T** | triplet |
| ***t* or *tert*** | tertio |
| **TD DFT** | Time dependent density functional theory |
| **th** | thiophene |
| **THF** | tetrahydrofuran |
| **TLC** | thin layer chromatography |
| **TMS** | tetramethylsilane |
| **TOCSY** | total correlation spectroscopy |
| **TPA** | two-photon absorption dyes |
| **tpphz** | tetrapyridophenazine |
| **tpy** | terpyridine |
| **TPP** | tetraphenylporphyrin |
| **TTA** | Triplet-Triplet Annihilation |
| **TTET** | Triplet-Triplet Energy Transfer |
| **UV/Vis** | ultraviolet-visible |
| ***vs.*** | versus |
| ° | degrees |
| **Δ** | chemical shift |
| **Δ** | heat |
| **ε** | molar absorption coefficient |
| **λ** | wavelength |
| μs | microsecond |
| **τ** | lifetime |
| **%** | percentage |

# 1 The synthesis, characterisation and photophysical study of 3,8-aryl acetylene 1,10-phenanthrolines

## 1.1 Polycyclic Aromatic Hydrocarbons

Polycyclic aromatic hydrocarbons (PAHs) are a class of compounds with an architecture of two dimensional graphitic segments of $sp^2$-hybridised carbons. High chemical and thermal stability, and an extensive π-electron delocalised carbon atom network makes them favourable candidates for many optoelectronic applications. Benzenoid PAHs can be further classified as; (a) polyacenes, (b) helicenes and (c) circulenes (Figure 1.1). Polyacenes consist of a series of linearly fused rings, such as naphthalene and tetracene, with their larger members forming valuable building blocks for graphene sheets and carbon nanotubes. Helicenes differ from polyacenes in their non-linear arrangement and are *ortho-* condensed in their structure e.g. phenanthrene and triphenylene. Meisenheimer first successfully isolated a member of the family by reduction of 2-nitronaphthalene in 1903,[1] though today a variety of synthetic pathways have since been a reported.[2] Circulenes are series of closed helicenes whose members form the basis of fullerene structures e.g. [5]circulene (corannulene) or [6]circulene (coronene) (Figure 1.1). Increasing the platform size of all of the benzenoid subclasses results in a corresponding decrease in the solubility, thus limiting their potential use in device application. Further synthetic modification is required to make these viable candidates for commercial use.

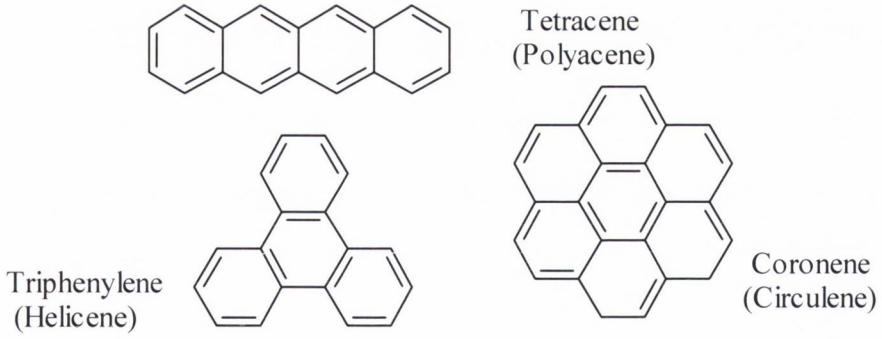


*Figure 1.1: Three members of the benzenoid family.*

### 1.1.1 Hexa-peri-hexabenzocoronene

Hexa-peri-hexabenzocoronene (HBC), commonly known as "superbenzene" is a 13 fused benzene ring structure with $D_{6h}$-symmetry. HBC is an extended coronene disc containing six additional benzene rings, with each peripheral benzene correlated to one $sp^2$ carbon of benzene. The addition of alkyl chains prevents aggregation of the discs, overcomes poor solubility and consequently enables the formation of columnar stacks with discotic liquid crystalline behaviour. These columns display directional charge transport and have been successfully developed for a variety of applications such a photovoltaics[3] and bio-imaging.[4]

### 1.1.1.1 Synthesis of Hexa-peri-hexabenzocoronene: cyclodehydrogenation

The oxidative cyclodehydrogenation of oligophenylenes is the principal step in the formation of HBC-type compounds. There are two key synthetic routes in the synthesis of the polyphenylenes HBC precursors. Cyclotrimerisation of diarylacetylenes is a one-step route to generate homo-substituted acetylene precursors [Scheme 1.1, (i)]. Route (ii) is based on a Diels-Alder [4+2] cycloaddition, in which the appropriate tetraarylcyclopentadienone (generated from a two-fold Knoevenagel condensation between a symmetrical diketone and prop-2-one), reacts with a suitable acetylene. This method allows for the incorporation of homo or hetero aryl groups into the periphery of the HBC framework, providing scope for the design of numerous derivatives, which would be synthetically unattainable using route (i).

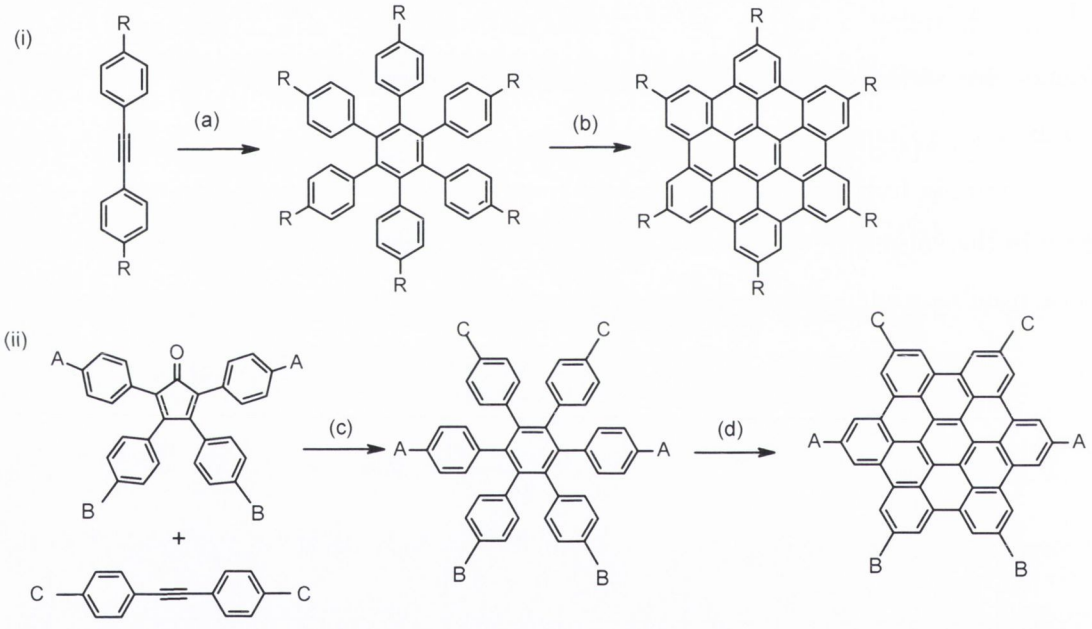


*Scheme 1.1: Synthesis of hexaphenylbenzene derivatives (i) $Co_2(CO)_8$, dioxane, reflux. (ii)$CuCl_2/AlCl_3$ or $Cu(OTf)_2/AlCl_3$ or $FeCl_3/CH_3NO_2$, (iii) benzophenone, 300 °C, (iv) $FeCl_3/CH_3NO_2$.A, B, C and R refer to alkyl groups.*

Intramolecular oxidative cyclodehydrogenation of hexaphenylbenzene, known as the Scholl reaction, generates the corresponding planarised polycyclic structure. The elimination of two aryl-bound hydrogen atoms initiates the formation of an aryl-aryl C-C bond between each adjacent phenyl ring pair. The C-C bonds are formed in a stepwise manner, with the formation of the first being the slowest. This is known as the "slippery slope" effect (Scheme 1.2).[5] The reaction becomes increasingly exergonic as each successive bond is formed. Many apposite oxidant conditions have been reported,

including $CuCl_2/AlCl_3$, and $Cu(OTf)_2/AlCl_3$ or $FeCl_3$ are suitable reagents for alkyl substituted HBC platforms. Wong *et al.* have recently reported the successful cyclodehydrogenation of electron-poor arenes containing bromine, fluorine and $CF_3$ substituents, using $DDQ/CF_3SO_3H$. Traditionally, the synthesis of these materials has been arduous, but this report should enhance their potential in electron transport applications.[6]

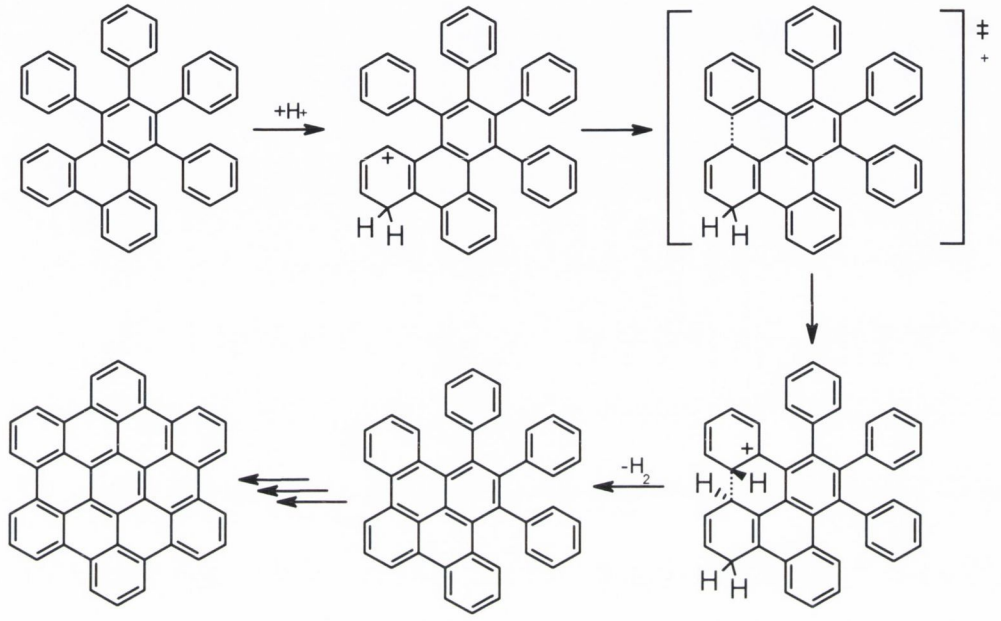


*Scheme 1.2: Hexaphenylbenzene condensation through the acid-catalysed Scholl reaction.*

### 1.1.2 Nitrogen Hetero-Superbenzene (N-HSB)

In 2002, Draper *et al.* reported the development of a new family of ligands. The nitrogen hetero-superbenzenes (N-HSB) are graphitic nanostructures containing electroactive imines on the periphery. The inclusion of the electronegative nitrogen atoms confers electron-accepting ability on the ligand, and allows for increased electron carrier transport, making the family suitable for optoelectronic applications such as LED based devices. These molecules also have the added advantage of increased solubility over their all carbon analogues, and are designed to accommodate bidentate coordination to a range of transition metals such as osmium and ruthenium. The group have reported the fully cyclised N-HSB, as well as the daughter compounds in the series N-½HSB , N-⅔HSB and N-5/6HSB. Draper et *al.* have also demonstrated that the remarkably low-lying $\pi^*$ orbital of the parent compound N-HSB has the ability to impart the highly desirable properties of a black MLCT absorber and a near IR emitter on the Ru(II) complex.

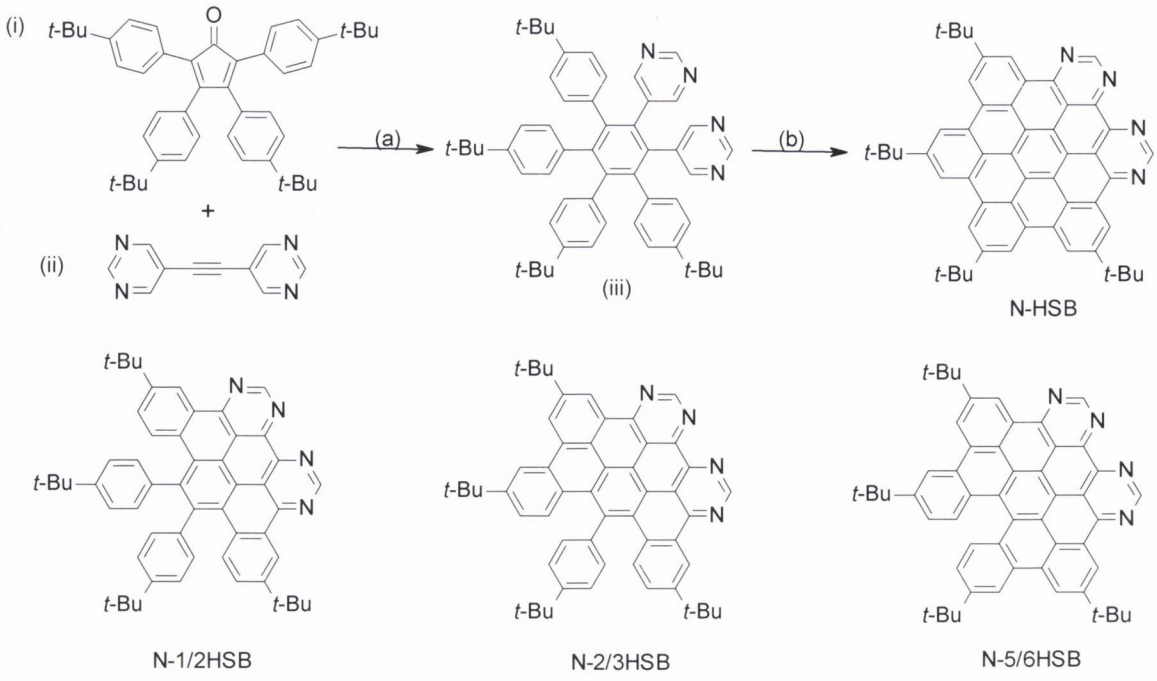


*Scheme 1.3: Synthetic route to N-HSB; (i) Cyclopentadienone (prepared by a double Knoevenagel condensation from the relevant diketone and monoketone) and (ii) diimine acetylene (a) benzophenone melt, 1 h, 81%; (b) $AlCl_3$, $CuCl_2$, $CS_2$, 72 hr, R.T., 49%.*

Incorporation of pyridyl nitrogens into polyphenylenes leads to significant disruption of the oxidative cyclodehydrogenation. The Draper group have previously demonstrated this effect in terpyridyl moiety containing polyphenylene molecule, where only *tert*-butyl group bearing phenyl rings undergo ring closure. Given that the initial protonation step should occur at the pyridyl ring, it is believed that the protonated pyridine ring may be inadequately electrophilic for the attack at the neighbouring phenyl ring. The inclusion of (*o,p*) directing methoxy substituents into the periphery of the structure has been shown to encourage bond formation at the para position.[7] The Draper group have successfully utilised this approach to extend the N-HSB family as well as pyridazine based ligands.[8 9]

### 1.1.3 The influence of an acetylene linker on the HBC chromophore

The incorporation of acetylene linkers into graphene-like systems has led to the development of their use in the building of carbon-rich scaffolds, nanoelectronic architectures, liquid crystalline materials and supramolecular systems.[10, 11] In order to understand and control the physical factors influencing these molecules, we need to

establish how best to interlock the components into ordered systems. Combining acetylene linkers with nitrogen containing moieties such as terpyridine and bipyridine units incorporates an additional degree of directionality, whilst conferring ligand functionality on these systems. The distance between the chromophoric centers can be controlled by the presence of additional acetylenic tethers, and the rigidity of the backbone can be improved with the addition of aryl moieties. Stroh *et al.* implemented these strategies in the design of segmented multitopic ligands which can be incorporated into larger arrays through selective cross-coupling reactions, and complexed to transition metals e.g. ruthenium(II) salts.[12, 13] The position of the acetylene is hypothesised to enable "shuttling" of the electrons between the metal centres.

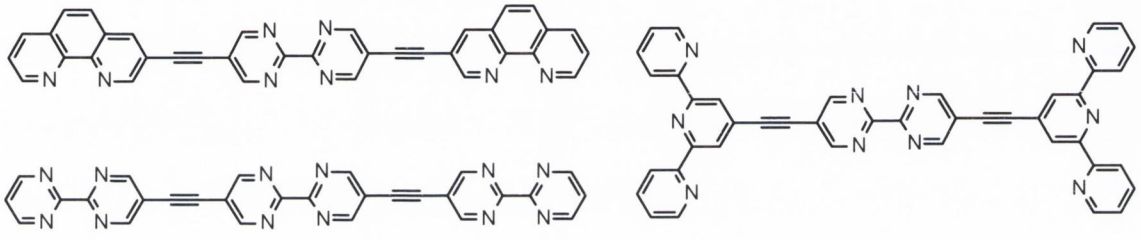

*Figure 1.2: Examples of Stroh's segmented multitopic ligands incorporating bipyrimidine, 1,10 phenanthroline and terpyridine units prepared by Sonogashira cross-coupling reactions.*[12]

As part of the Draper group's research into fused nitrogen systems, Dr Frances Murphy reported a study on the comparison of electronic communication between the HBC and the tridentate terpyridine unit (Figure 1.3). **HBC 1** differs from **HBC 2** by the inclusion of the acetylene linker which facilitates the enhancement of the lifetimes of the corresponding Ru(II) terpyridine complexes. For both **HBC 1** and **HBC 2**, the UV-Vis absorption spectra display characteristic HBC features, including a structured band centred at $\lambda$ = 360 nm. Both $\pi$-$\pi^*$ and n-$\pi^*$ terpyridine based transitions are also visible at $\lambda$ = 240-228 nm. Luminescence spectra for both compounds display a complex vibronic structure, which was also observed for the iodo and TMS protected HBC precursors (THF, 1 x$10^{-5}$M). The shape and position of the emission bands is independent of excitation wavelength, but the intensity is strongest when the excitation wavelength coincides with the maximum HBC absorption ($\lambda_{max\ abs}$= ~365 nm). When the excitation wavelength coincides with the high energy terpy absorption ($\lambda_{abs}$ = 243 nm and 228 nm), a lower intensity HBC based emission is observed for both **HBC 1** and **HBC 2**. The inclusion of the acetylene linker in **HBC 2** extends the emission tail to

lower energy wavelengths, and leads to increased vibronic structure of the emission bands. This suggests that better communication is achieved between the terpyridine and the HBC chromophore when an acetylene is incorporated into the framework of the ligand.

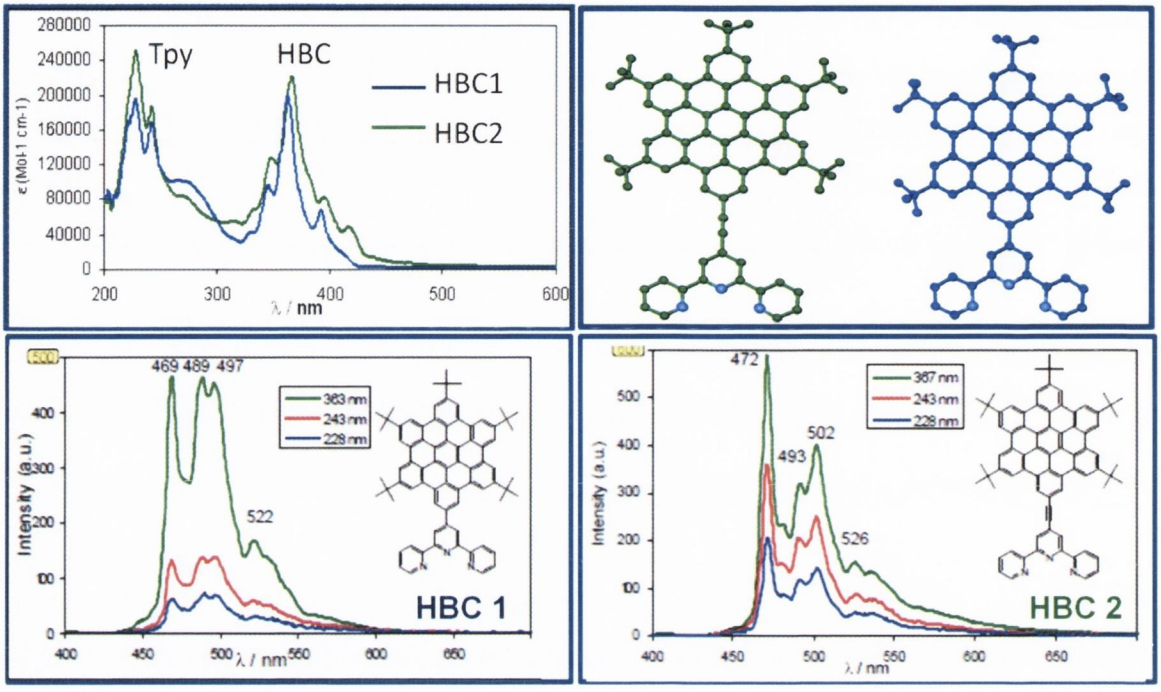


*Figure 1.3:(a) The UV-Vis absorption spectra of* ***HBC 1*** *and* ***HBC 2****, (b) crystal structures of the terpy ligands; (c) and (d) the corresponding emission spectra obtained by Murphy et al. for* ***HBC 1*** *and* ***HBC 2****.*

A similar study was carried out by Schanze *et al.* on *trans*-platinum(II) acetylides with long chain HBC functionality. The Pt(II) acetylide unit provides strong spin-orbit coupling into the HBC chromophore, which thereby enables moderate phosphorescence and extended triplet lifetimes.[14] To further build on the work on HBC platinum(II) acetylides,[15] Dr Deanne Nolan has investigated the geometrical effect of both HBC and its corresponding uncyclised polyphenylene derivative on *cis* and *trans* configurated platinum acetylides complexes (Figure 1.4).[15] The UV-Vis absorption spectra of **Ac-PP** is broad and featureless, and is typical of polyphenylene-type ligands [Figure 1.4 (a)].[16] Conversely, **Ac-HBC** displays structured, well resolved bands which is typical of other HBC ligands. **Pt-csPP** and **Pt-trPP** show both intense high energy bands, which are assigned as ligand based absorption bands, and the expected MLCT bands. **Pt-trPP** displays lower energy MLCT bands than **Pt-csPP**, due to more efficient communication through the platinum centre. The same trend is evident in the cyclised complexes,

however since the Pt-acetylide group breaks the symmetry of the HBC, an additional band was also reported at $\lambda \sim 415$ nm. This is assigned as having both intraligand and MLCT character, which has been previously reported for similar terpyridine derivatives.[17]

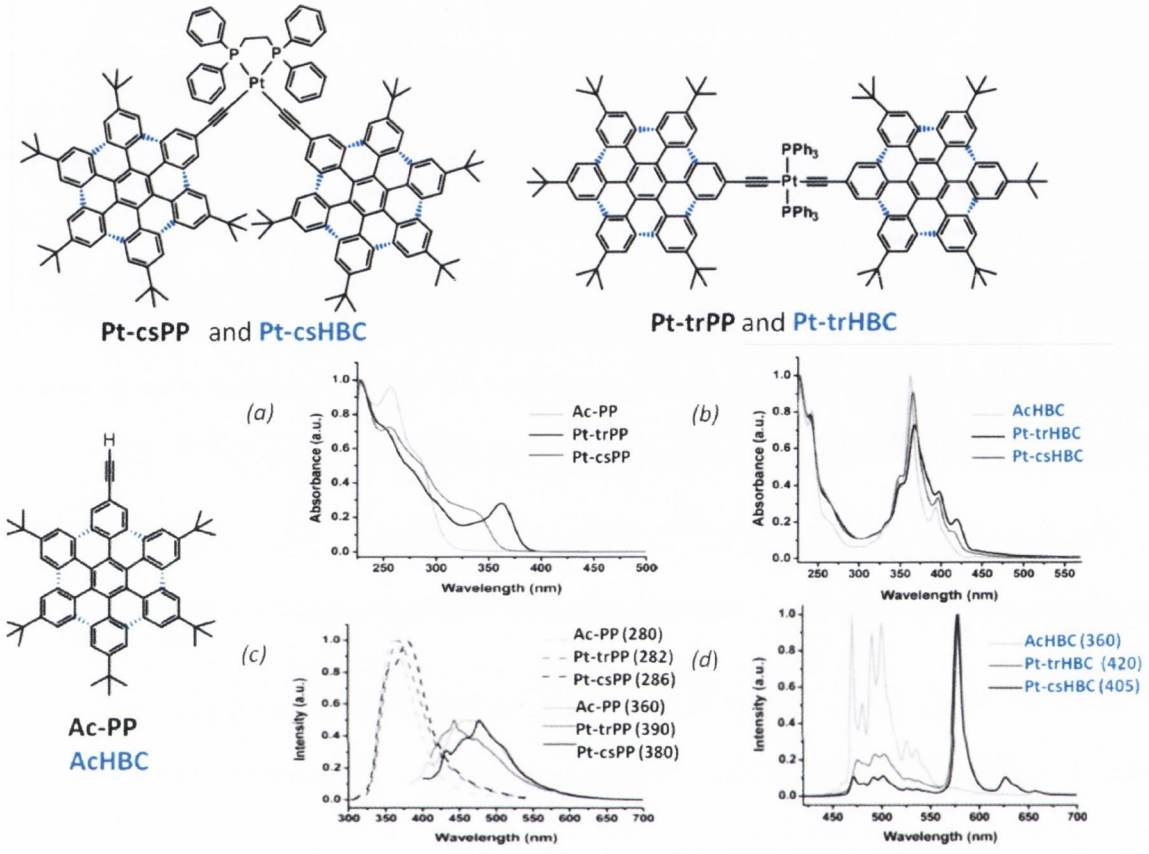


*Figure 1.4: cis and trans Pt(II) acetylide complexes synthesised by Nolan et al. with UV-Vis absorption spectra of (a) uncyclised compounds **Pt-trPP**, **Pt-csPP** and **Ac-PP**; and (b) cyclised compounds **Pt-csHBC**, **Pt-trHBC** and **AcHBC**. The normalised emission spectra for both sets of complexes and ligands are also shown in (c)and (d) at selected $\lambda_{exc}$ (298 K).*[18]

Figure 1.4(c) shows the emission spectra of **Ac-PP** and the polyphenylene complexes **Pt-csPP** and **Pt-trPP**. The emission produced by both complexes was found to be strongly dependent on excitation wavelength, and displayed structured low-energy emission. Figure 1.4(d) shows the corresponding emission profiles for the cyclised derivatives, **Pt-trHBC** and **Pt-csHBC**, with phosphorescence typical of HBC chromophores appearing at $\lambda$ = 577 nm. The geometrical significance of **Pt-trHBC** is evident, with a phosphorescence/HBC fluorescence ratio approximately four times that of **Pt-csHBC**. This effect is also reflected in the extended triplet lifetime observed for **Pt-trHBC** *vs.* **Pt-csHBC** (**Pt-trHBC** = 30.9 μs and **Pt-csHBC** =18.3 μs), which indicates that *trans* co-

ordinated π- conjugation is more effective at facilitating communication in the acetylide ligands.

## 1.2 1,10-Phenanthrolines

1,10-Phenanthrolines are a class of bidentate heterocyclic organic compounds with co-ordination chemistry similar to that of 2,2'-bipyridines. The synthesis requires two successive Skraup reactions[19] between glycerol and *o*-phenylenediamine using sulphuric acid as a catalyst and nitrobenzene or aqueous arsenic acid as an oxidising agent. 1,10-Phenanthrolines have been attractive as a chemical building block in the design of new fluorophores for the past number of decades due to its rigidity, planarity and ability to co-ordinate to metal centres. The planar structure of the molecule enables groove binding and intercalation with DNA and RNA, and the rigidity of the backbone means that the inwardly pointing pair of nitrogens makes it more entropically favourable for binding to metals than the bipyridine or terpyridine unit. Similar to bipyridine units, 1,10-phenanthrolines are also π-electron deficient, which confers excellent electron accepting properties onto the ligands. Arising from this, these diimines are capable of stabilising metal ions in their lower oxidation states. These properties have enabled this class to be extensively utilised for molecular recognition and sensing applications, and as building blocks for photo-switchable molecular devices.[20] On a supramolecular level, Sauvage *et al.* have successfully incorporated 1,10-phenanthroline into the structure of larger systems such as rotaxanes and catenanes using the template effect.[21] Compounds such as bathocuproine (2,9-dimethyl-4,7-diphenyl-l,10-phenanthroline, (see Scheme 1.4(b)) have already found application in optoelectronic devices as hole blocking materials, and can optimize the transport of electric charge.[20]

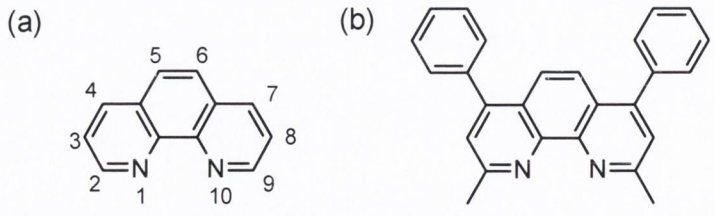


*Scheme 1.4: The numbering system adopted for 1,10-phenanthroline and (b) bathocuproine.*

1,10 Phenanthrolines display close π-π* and n-π* singlet excited states, with emission predominantly originating from the π-π* states. The parent compound, 1,10-

phenanthroline, possesses a low quantum yield of $\Phi_f \leq 0.01$, has a short singlet lifetime ($\tau < 1$ ns, $CH_2Cl_2$) and emits outside of the visible region ($\lambda_{em}$= 360 nm). Investigations to improve the emission efficiency have found that significant substitution to 1,10 phenanthroline produces an increased energy gap between the $\pi$-$\pi^*$ and n-$\pi^*$ levels, and leads to enhanced lifetimes.[22, 23] Symmetrical substitution in the 4,7- or 2,9- position has proven to be most popular, with the primary synthetic strategies aiming to extend the $\pi$-conjugation or incorporate electron donating/withdrawing groups to inject/withdraw electrons.[24]

### 1.2.1 1,10- Phenanthrolines: substitution in the 3,8- position

Investigations by Bosnich into the nature of $\pi$-$\pi^*$ transition dipole in bipyridyl and 1,10-phenanthroline ligands were found to be directed along either the short axis *(z)* or the long axis *(x)* (Figure 1.5), and appeared to be relatively unaffected by complexation.[25] Conjugation along the short axis results in weak changes to the circular dichroism of the ligand, but the corresponding transitions on the long axis results in strong electrostatic coupling of the electronic transition dipole. By increasing the conjugation through either the 2,7-position of bipyridyl ligands or the 3,8- position of 1,10-phenanthroline ligands, there is a stabilization of the charge-separated excited states. This enables access to the most intense electronic transitions and shifts the emission of the fluorophore into the visible region of the spectra. This suggests that modification of the 3,8- position of 1,10-phenanthroline is more favourable to the 4,7- or the 2,9- position.

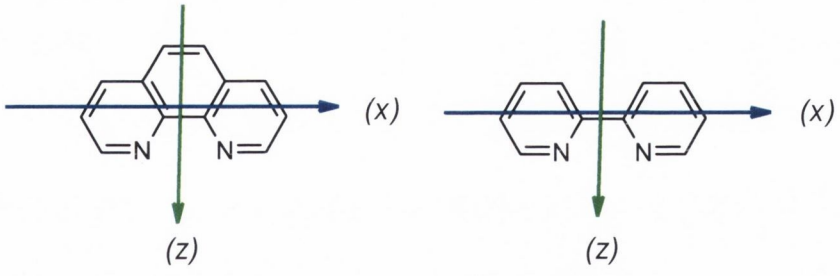


*Figure 1.5: Representation of the transitions in polypyridyl ligands; short axis (z) and long axis (x).*

The original synthesis of 3,8 substituted 1,10-phenanthrolines was reported by Case was both challenging and low yielding. Multi-step Skraup reactions produced carcinogens and other toxic arsenic-containing side products.[26] In 1995, Tor and Siegel developed a method to brominate 1,10-phenanthroline based on Kress' synthetic procedure for

bromination of quinoline salts.[27 28] This method provided the 3- and the 3,8-substituted starting materials, both of which are valuable and versatile synthetic building blocks.

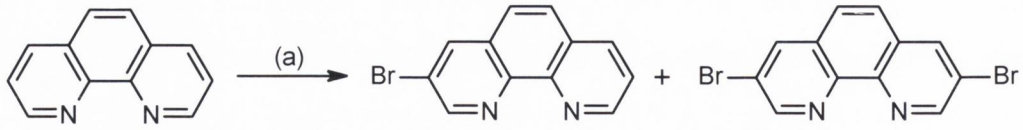


*Scheme 1.5: Bromination of 1,10-phenanthroline yielding the 3- and 3,8-substituted product; (a) $Br_2$, $PhNO_2$, heat.*

Unsymmetrical 1,10-phenanthrolines can also be prepared from a modified Friedländer condensation reaction between an *o*-aminoaldehyde and an enolizable ketone, with the loss of a molecule of water (Scheme 1.6).[29] This reaction has also been successfully reported by Thummel *et al.*, for the synthesis of phenanthroline based unsymmetrical terdentate ligands.[30]

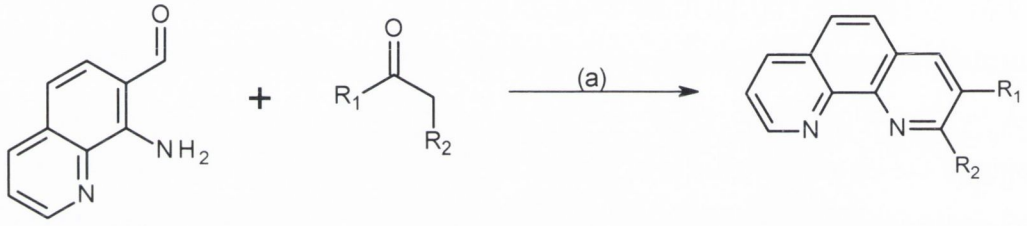


*Scheme 1.6: Modified Friedländer condensation between 8-amino-7-quinolinecarbaldehyde and an unsymmetrical ketone to produce the corresponding 1,10-phenanthroline (a) KOH, EtOH, heat.*[29]

### 1.2.2 Enhancing the photophysical properties of 1,10-phenanthrolines

Substitution in the 3,8-position with acetylenic linkers facilitates communication between the 1,10-phenanthroline core and appended moieties, by anchoring and controlling the spatial separation of the chromophores. Functionalised acetylenes can have a marked influence on the electron delocalization in the excited states of the chromophores, thereby inducing a substantial red shift in the emission wavelength and can increase the intensity of this emission.[31] Tor *et al.* have previously examined the variation in emission properties of phenanthroline cores substituted in various positions with acetylene linkers and have reported dual emission in Ru(II) complexes substituted in the 4-position of the phenanthroline.[31] This is as a result of spatially separated excited states, one of which appears on the phenanthroline moiety and produces a lower energy emission, the other on the bipyridine ligands attached to the Ru(II) metal which appears as a higher energy band. This enhanced electron delocalisation is thought to produce

larger σ donation to the metal centre, which is reflected by a more pronounced downfield shift being observed in the $^{13}C$ NMR spectrum i.e. the acetylene carbon appears at δ = 103.56 ppm *versus* δ = 96.14 and 98.19 ppm for the 3- or 5 -1,10-phenanthroline derivatives. This effect does not extend to the other carbons in the ring, which suggests that in the ground state, electron delocalisation is confined to the acetylene and appended chromophore.

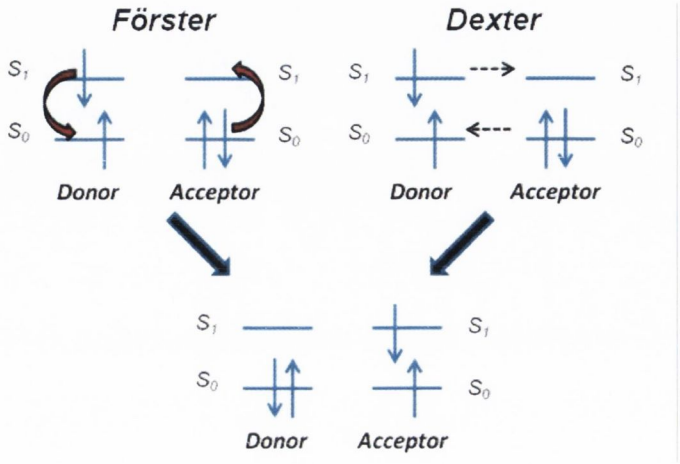


*Figure 1.6: Schematic depiction of Förster and Dexter energy transfers mechanisms.*

It is well understood that acetylene linkers act as "molecular wires" for electron transfer to metal centres. There are two possible methods of energy transfer; (i) through space dipole-dipole interactions (Förster mechanism, long range, non-radiative) or (ii) by a double exchange electron arbitrated by the bridge (Dexter mechanism, short range, requires contact between the orbitals of the donor and the acceptor) (Figure 1.6). The Förster energy transfer occurs through a dipole-dipole interaction between the electronic excited states of the donor and the acceptor, and does not result in the emission and re-absorption of light.[32] The Dexter mechanism involves the concurrent transfer of an electron through the bridging lowest unoccupied molecular orbitals (LUMO) and a positive hole *via* the bridging highest occupied molecular orbital (HOMO) from donor to the acceptor. It is a double electron exchange involving the transfer of one electron from the semi occupied LUMO of the excited donor to the empty LUMO of the acceptor. This occurs with a simultaneous transfer of an electron from the HOMO of the acceptor to the semi- occupied HOMO of the donor.[33]

### 1.2.3 Studying the effect of electron-donating substituents on 1,10-phenanthroline ligands

Tor and Jishi completed a systematic study of 3,8- substituted 1,10-phenanthrolines with phenylethynyl substituents of increasing electron donating abilities.[34] In all cases, there was a significant red-shifted in comparision with the parent compound ($\lambda_{em}$ =360 nm) and showed a gradual shift in accordance with their electronic donating abilities. High fluorescence quantum yields were reported, with the methyl derivative reaching unity (Figure 1.7). Both the methoxy and the -$N(CH_3)_2$ derivatives display a red shift in emission with increasing solvent polarity, unlike the parent compound which undergoes a hypsochromic shift. The -$N(CH_3)_2$ derivative exhibits a more prominent shift which can be attributed to stronger donating ability. Overall, solvent polarity was found to have a much more significant effect on the emission behaviour of the series than on the absorption behaviour. This is in line with a greater stabilisation of the excited state, and is commonly observed in polar molecules containing charge transfer behaviour in their excited states, as well as larger dipoles.[35]

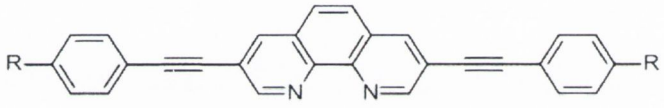


**a: R = H; $\Phi_fl$ = 0.41**
**b: R = $CH_3$; $\Phi_fl$ =1.0**
**c: R = $OCH_3$; $\Phi_fl$ = 0.64**
**d: R = $N(CH_3)_2$; $\Phi_fl$ n.a.**

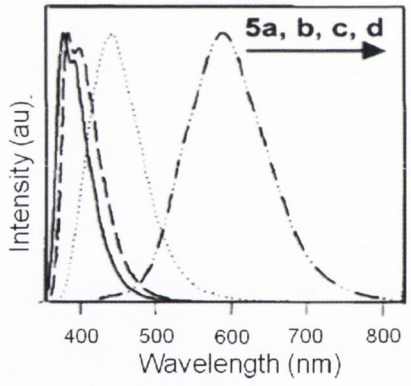


*Figure 1.7: Tor's normalised emission spectra showing an increasing bathochromic shift with corresponding increase in substituent (R) electron donating ability.*[20, 34]

### 1.2.4 Other applications for 1,10-phenanthroline systems

Chemical sensors that show a measurable response upon scavenging of heavy metals are in high demand for applications in environmental and biomedical fields. Designing an optical sensor that can be tuned to accommodate a variety of metal ions that can be rapidly measured upon exposure to the analyte is particularly attractive. Supramolecular metal-organic assemblies that can be synthesised *via* click chemistry have become increasingly popular, as they combine the properties of both organic and inorganic materials.[36] Stang and co-workers have successfully integrated the 1,10-phenanthroline core into a symmetrical rectangular clip (Figure 1.8).[37, 38] Titration of the sensor with a

variety of metal ions ($Ni^{3+}$,$Cd^{2+}$ and $Cr^{3+}$) produces a clean isosbestic point at 300 nm which indicates the successful binding of the cation without disturbing the geometry of the ligand. The rigid rectangular geometry of the clip offers the advantage of a preorganised architecture which is designed for metal uptake, unlike free 1,10-phenanthroline.

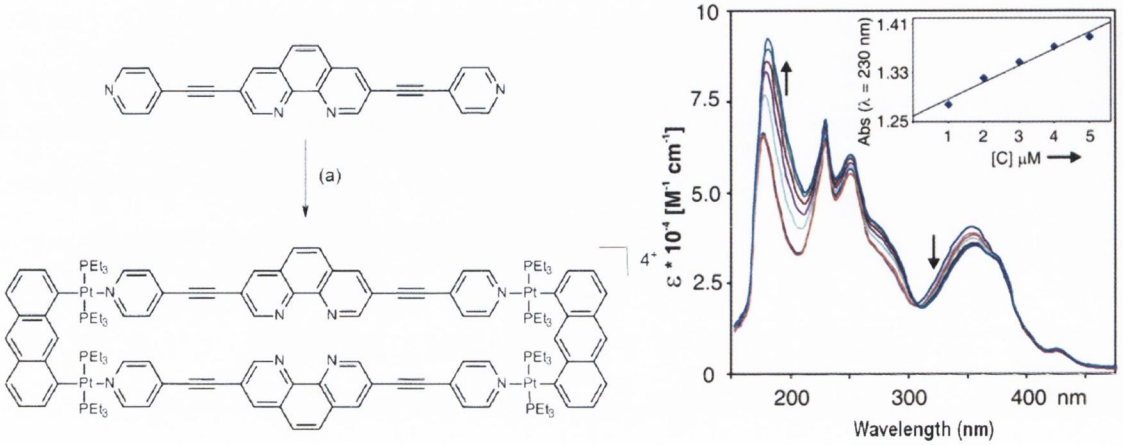


*Figure 1.8: The chromogenic 1,10-phenanthroline sensor formed via cross-coupling with an organometallic "clip" (a) 1,8-bis(trans-Pt($PEt_3$) anthracene)$_2$($NO_3$)), acetone/$H_2O$, 65°C, 2 hours; and the UV-Vis absorption titration of the sensor with $Ni(NO_3)_2.H_2O$ in MeOH.*

The use of pyridyl and bipyridyl moieties in the synthesis of mesogenic frameworks for liquid crystalline applications is a relatively well-developed field.[39, 40] The mesogenic nature of the crystal can be easily lost on complexation to transition metals, because of the introduction of charges, further dipoles, bulkiness of the metal centre etc., as well as the possibility of microsegregation (the non-uniform distribution of grain, crystal or microscopic particles resulting in localised concentrations) during the heating cycles.[41]

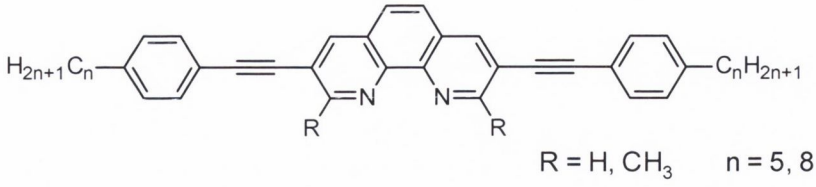


*Figure 1.9: Liquid crystal 1,10-phenanthrolines synthesised by Bruce and co-workers to investigate the effect of methyl substitution in the 2,9- position on structural anisotropy and clearing point temperature Tc.*[42]

Bruce *et al.* developed a series of uncomplexed 3,8-mesomorphic 1,10-phenanthrolines related to Ziessel's mesomorphic 3, 8-substituted copper 1,10-phenanthroline complexes generated from a non-mesomorphic 1,10 phenanthroline core.[40, 43, 44] Inclusion of a rigid

core such as 1,10-phenanthroline, enables the crystals to maintain intermolecular bonds as ligands. There is a switch to intramolecular bond formation when a metal centre is introduced, which stabilises the newly generated interlocked molecular structures. Bruce's design intended to demonstrate that clearing point temperatures $T_c$ (the temperature at which a liquid crystal transforms into an isotropic crystal, i.e. one that has uniform properties in all directions) could be reduced through the introduction of methyl groups in the 2,9 positions. This would reduce both the structural anisotropy into the molecule and the symmetry, thus reducing the risk of degradation on heating. This was found to be unsuccessful. The unsymmetrical ligands were non-mesogenic (i.e. displayed poor rigidity) in nature. Therefore, symmetrical 1,10-phenanthrolines, with unsubstituted 2,9- positions were found to be more promising for the development of these materials for liquid crystalline applications. This knowledge, combined with the overall simplicity and versatility of the design of the systems, makes this family of ligands attractive candidates for further optoelectronic application development.

## 1.3 Project Goals: Ligand Design

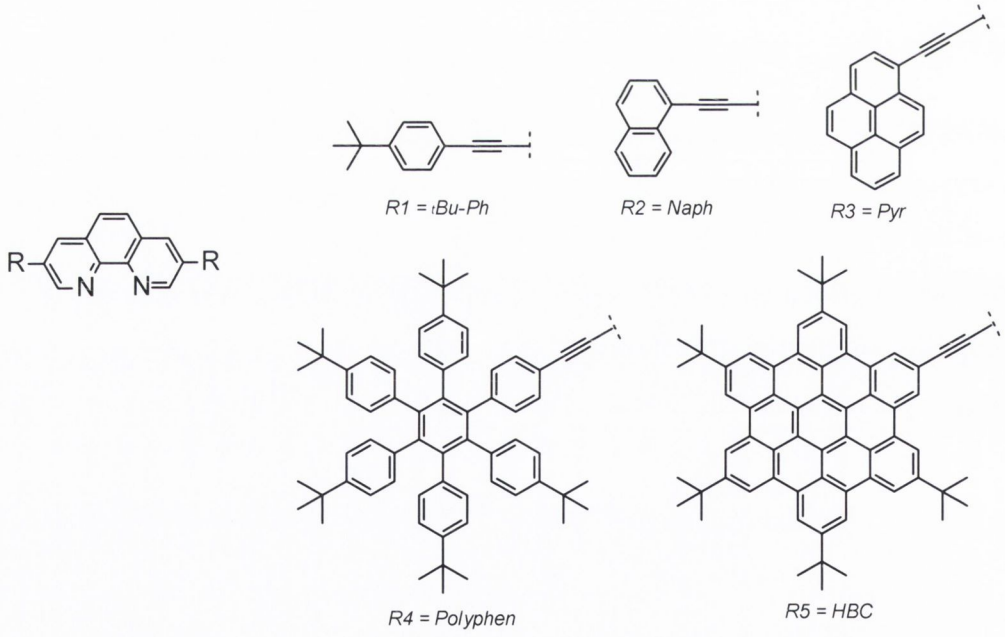


*Figure 1.10: The target 3,8-diaryl acetylene based 1,10-phenanthrolines.*

Series 1 of 1,10-phenanthroline ligands is designed in order of increasing aromaticity. (Figure 1.10). As discussed, substitution in the 3,8-position is carried out specifically to allow for stabilisation of the excited states and the incorporation of the acetylene linker is to facilitate communication from the 1,10-phenanthroline core. Tor *et al.* refer to the *t*-

butyl phenyl derivative in the supplementary information of previous work, but did not discuss the synthetic procedure, or photophysical data on the ligand or any corresponding complexes in the publication.[45] It has been included in our series, as the ligand also acts as a precursor to the larger supergraphene-like ligands, which will be discussed in Chapter 4. The synthesis of the pyrene ligand was previously reported by Ziessel *et al.*, [12] but to our knowledge, no photophysical study on the ligand, or its corresponding complexes has been carried out. The pyrene unit provided us with a chromophore that is intermediate in platform size to the smaller units and the HBC derivatives in the series. The inclusion of the uncyclised polyphenylene unit, and the fully cyclised HBC unit allows for additional comparison between this study and work previously carried out within the Draper group by Dr. Frances Murphy on HBC-terpyridine derivatives, and Dr. Deanne Nolan on HBC-platinum acetylides. To aid solubility, the *tert*-butyl HBC derivative was chosen, and the inclusion of a flexible linker should allow the HBC unit to twist with respect to the 1,10-phenanthroline core, and prevent aggregation. Chapter 2 outlines the synthesis, characterisation, electrochemical and photophysical studies of the corresponding ruthenium(II) bipyridyl, and iridium(III) 2-phenylpyridine complexes.

### 1.3.1 Synthesis of 3,8 substituted 1,10-phenanthroline aryl-acetylenes.

This section details the synthesis and characterisation of the 3,8-aryl 1,10-phenanthroline ligands using amodified Sonogashira cross-coupling reactions, and the use of microwave synthesis towards a more efficient generation of acetylene precursors.

#### 1.3.1.1 Synthesis of 3,8-dibromo-1,10-phenanthroline

Bromination of 1,10-phenanthroline was achieved by a modified version of Siegel's synthetic procedure, first developed by Yamamoto *et al.*[46] This method offers improved yields to the nitrobenzene-based synthesis (discussed previously, Scheme 1.5). The addition of pyridine was found to further improve yields, and enabled the 3,8-brominated derivatives isolation by recrystallization. Siegel's original method produces a high yield of the mono substituted product, which has to be separated by silica column chromatography.[27] After multiple attempts at optimisation of the reaction, it was found that the product could be successfully isolated without purification on silica column chromatography, but by precipitation with diethyl ether. The white solid was filtered, to give the pure product in a yield of 52%.

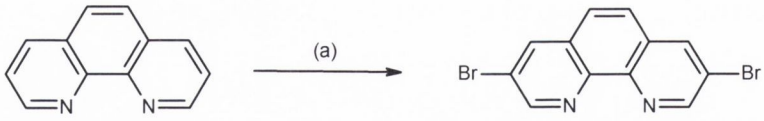


**(sm1)**

*Scheme 1.7: Yamamoto's synthesis of 3,8-dibromo-1,10-phenanthroline (**sm1**) using a modified version of Siegel's procedure.(a) $Br_2$, $S_2Cl_2$, pyridine, 85 °C, 12 hr.*[27, 46]

### 1.3.1.2 Synthesis of aryl acetylenes

*tert*-Butyl phenyl acetylene and 1-ethynyl pyrene are commercially available starting materials. 1-Ethynyl pyrene was subjected to additional purification by silica column chromatography before Sonogashira coupling to the 3,8-1,10-phenanthroline core was attempted. Although the preparation of 1-ethynyl naphthalene *via* a traditional Sonogashira coupling has previously been reported,[47] the target compound was successfully synthesised *via* a modified version of Gourdon's microwave assisted Sonogashira coupling, which was recently established by Dr Gearóid Ó'Máille in the Draper group.[48 49]

Microwave heating is a recent development in the synthetic field. It offers many advantages over traditional experimental methods, including reduced preparation time of reagents, and faster reaction times, and has rapidly developed the area of cross-coupling reactions. Reactions such as Stille[50], Heck[51], Suzuki [52] and Negishi [53] type cross-coupling reactions have been reported. Reactions can be carried out in modified domestic microwaves, but variable power levels are produced when the magnetron is switched on/off, making it difficult to keep the reaction parameters constant. Another disadvantage of irradiating with a domestic microwave is that the heating pattern is inconsistent. "Hot and cold spots" are generated as the microwaves bounce off the walls in the cavity, which can result in overheating within the vessel. In a commercial system, although considerably more expensive, the internal temperature and the pressure can be easily modified, and the source of the microwave irradiation can be accurately controlled and kept continuous.

One of the most important considerations in all microwave reactions is the choice of solvent. The boiling point is not the main consideration, but the dielectric constant. The heating mechanism is not through traditional conductive-convective heat transfer, which begins at the boundaries and reaches the interior of the vessel, but instead originates in

the interior and works its way to the boundary.[54] Dipoles have the ability to orientate themselves in the direction of the electric field, and any change that occurs in the direction of the electric field causes a corresponding change in the orientation of the dipoles. This mechanism is known as dielectric heating. If the molecules have a high dielectric constant, they have a greater ability to align themselves with the direction of the field applied. If the molecule is in a liquid or gaseous state, the field frequency of the molecule can be $10^6$ Hz or greater. The choice of solvent also affects the choice of reaction vessel. If an open-vessel system is required, both the flammability of the solvent and the volatility need to be considered. Solvents such as DMF, $CH_2Cl_2$ and MeCN have been successfully used, all of which can be heated above their boiling points using microwave irradiation. This is known as "superheating", and has been shown to enhance the rate of the reaction. [55]

Irradiation of 1-bromonaphthalene and trimethylsilylacetylene (TMSA) in a solution of $NHEt_2$:DMF (5:2) for 20 minutes produced the desired protected product (Scheme 1.8). The yellow oil was purified by silica column chromatography eluting with hexane, and deprotected overnight using KF. Following work-up, the product (**1**) was obtained as a pale yellow oil in a higher yield (64 %) than literature reports using traditional methods (50 %). [47]

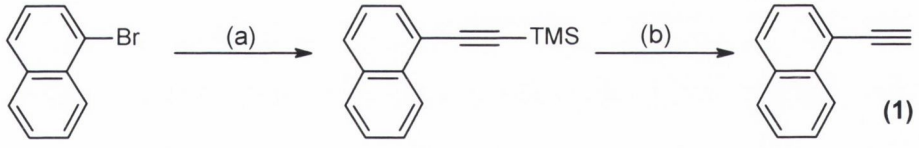


*Scheme 1.8: Sonogashira cross-coupling of 1-bromonapthalene to give 1-ethynylnaphthalene (1) (a) TMSA (1.05 eq.), $Pd(PPh_3)_4$ (10 mol%), DMF: $NHEt_2$ (2:5, v/v), μλ, 125 °C, 20 mins; (b) KF (110 eq.), THF: MeOH (1:1, v/v), 18 hrs, under Ar.*

Coupling of the aryl acetylenes to 3,8-dibromo-1,10-phenanthroline was attempted by traditional room temperature Sonogashira cross-coupling methods previously reported by Tor[34] and Ziessel,[12] using $PdCl_2(PPh_3)_2$ and CuI as catalysts. As two cross-coupling reactions are required to generate the desired 3,8-substiuted 1,10-phenanthroline ligands, more than twice the equivalents of catalysts are required to avoid the formation of multiple products. This proved to have significant consequences in this study. In the case of the *tert*-butylphenyl acetylene (**2**) and 2-ethynyl naphthalene derivatives (**3**), the products were successfully isolated, but mass spectrometry analysis showed one

additional product for both reactions [i.e. at m/z = 1051.4749 for (**2**) and m/z/ = 1027. 2864 for (**3**)]. These correspond to copper coordination to both products, and the formation of the corresponding tetrahedral copper (I) complex such as (4) as shown in Scheme 1.9 ($[C_{72}H_{68}CuN_4]^+$ calculated m/z = 1051.4750 and ($[C_{72}H_{44}CuN_4]^+$, calculated *m/z* = 1027.2862). Despite several attempts to remove the coordinated metal using a potassium cyanide wash, this proved to be unsuccessful.[56] Although only trace amounts of the Cu(I) complexes were present, the photophysical study of the ligands persistently showed the presence of a $^1$MLCT band at ~ $\lambda_{abs}$ = 400 nm.

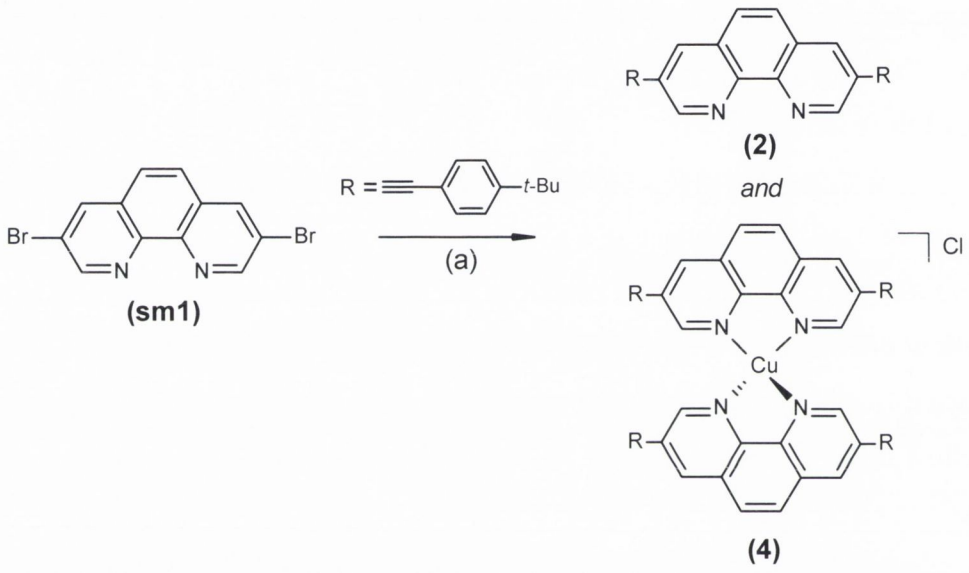


*Scheme 1.9: Sonogashira cross-coupling reaction of tert-butyl phenylacetylene and 3,8-dibromophenanthroline(**2**) which generated trace amounts of the corresponding copper species shown (i) $PdCl_2(PPh_3)_2$ (10 mol %) and CuI (12 mol %), THF: $^iPrNH_2$ (3:1; v/v), R.T., Ar, overnight.*[34]

To verify the formation of the tetrahedral copper complex, 3,8-di-bromo-1,10-phenanthroline was reacted directly with a copper salt $[Cu(MeCN)_4]PF_6$ in $CH_2Cl_2$. The complex was precipitated from hexane, washed with diethyl ether and dried. The Sonogashira cross-coupling between *tert*-butylphenyl acetylene and the isolated copper complex was carried out using the conditions described in Scheme 1.9. The crude mixture was purified using silica column chromatography, eluting with $CH_2Cl_2$. The product (**4**) was isolated by precipitation with diethyl ether as a yellow/orange solid (82%). This was verified by mass spectrometry, which, as before displayed a peak at *m/z* = 1051.4734 which corresponds to the $[M\text{-}PF_6]^+$ ion ($[C_{72}H_{68}CuN_4]^+$, calculated *m.z.* = 1051.4740) Further analysis by UV-Vis absorption spectroscopy displays the same

$^1$MLCT band at $\lambda_{abs}$= 405 nm (Figure 1.11). Similar copper(I)-1,10-phenanthrolines have previously been reported and exhibit comparable absorption profiles.[56, 57]

The persistent formation of Cu(I) complexes required an alternative strategy to be adopted. As the incorporation of potassium cyanide into the experimental work-up proved to be both undesirable and unsuccessful, therefore it was decided to reattempt the cross-coupling reactions using an alternative catalyst i.e. $Pd(PPh_3)_4$. The reactions were heated to 70 °C and refluxed for 2 days. The crude mixtures were isolated after extraction into diethyl ether, washing with water and drying with $MgSO_4$. Both **2** and **3** were further purified by silica column chromatography eluting with either diethyl ether or $CH_2Cl_2$/hexane (1:1, v/v). **2** was isolated as a pale yellow solid in a yield of 56% and **3** as a pale orange yellow solid in a yield of 48%. The electrospray mass of **2** displays a peak centred at *m/z* = 493.2653 for $[M+H]^+$, which agrees with the calculated value of 493.2644 for $[C_{36}H_{33}N_2]^+$. No evidence of copper coordination was found by mass spectrometry analysis. Similarly, the electrospray mass of **3** displays a peak centred at *m/z* = 482.1687 for $[M+H]^+$, which agrees with the calculated value of *m/z* = 482.1699 for $[C_{36}H_{22}N_2]^+$.

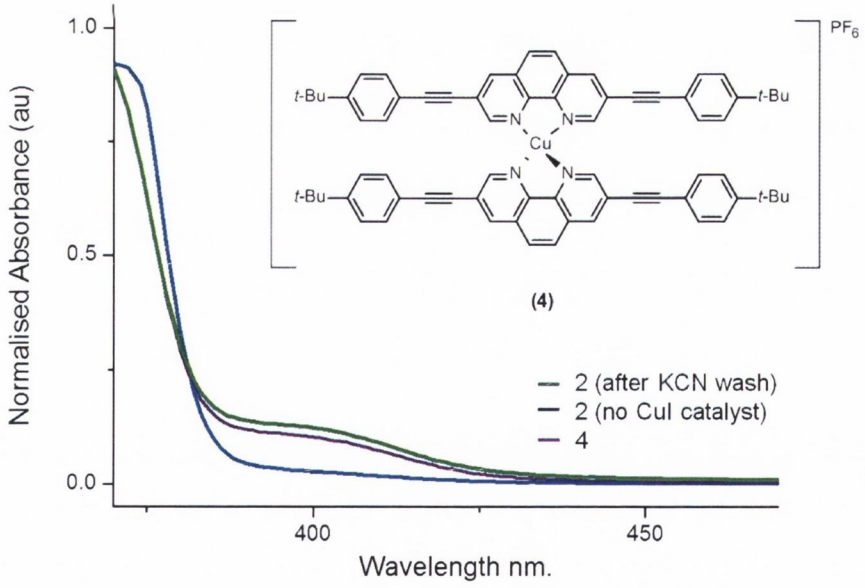


*Figure 1.11: The lower energy absorption bands of* ***2*** *after KCN wash,* ***2*** *prepared without the copper catalyst and reference copper tetrahedral complex (****4****) showing additional $^1$MLCT absorption band at $\lambda_{abs}$ = 405 nm ($CH_2Cl_2$, 1 x $10^{-5}$M).*

Figure 1.12 shows the $^1$H NMR spectra obtained for compound **2**. Five distinct peaks are observed in the aromatic region. The ligand is symmetrical, which further simplifies the spectrum. Two doublets appear at δ = 7.45 and 7.6 ppm, both with larger $^3J$ coupling

constants of 8.36 Hz, and integrate for 4 H. The proton adjacent to the acetylene moiety is slightly more deshielded than its neighbouring proton, and therefore is assigned as the doublet appearing at 7.65 ppm (●). The remaining three signals appear as singlets, but are more accurately assigned as doublets. Their proximity to the electronegative nitrogen atom on the ring causes broadening of their signals which is reflected in their smaller coupling constants of 1-2 Hz. The aliphatic region of the spectra displays one signal at 1.35 ppm, which integrates for 18 H and is therefore assigned as the protons on the *tert*-butyl functional group.

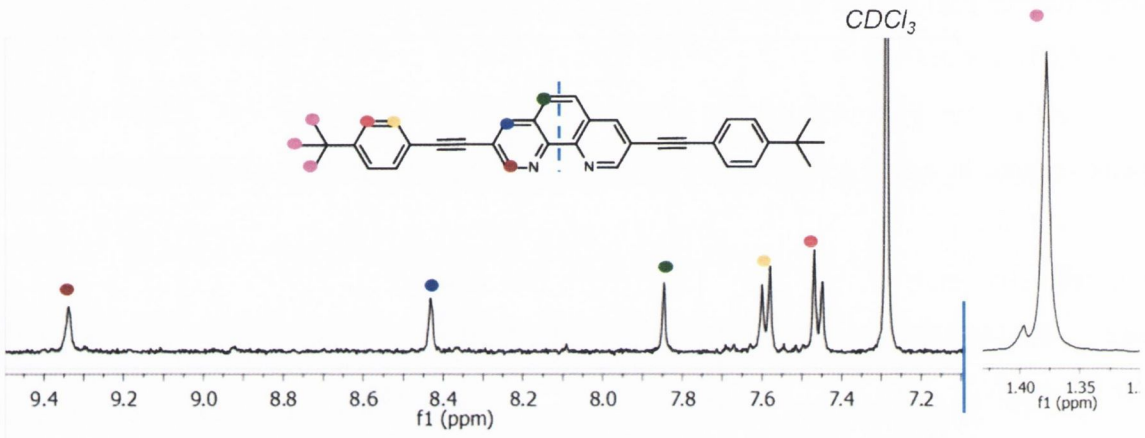


*Figure 1.12: $^{1}H$ NMR spectra of **2** in $CDCl_3$ (400.1 MHz, R.T.)*

The $^{1}H$ NMR spectrum of **3** is presented in Figure 1.13, and is compromised of three protons on the 1,10-phenanthroline moiety, with an additional 3 doublets and four triplets allocated to the naphthyl group. A $^{1}H$-$^{1}H$ COSY experiment for **3** successfully identified one three spin system, and one four spin system as expected. The sole triplet of the three spin system is easily distinguished at δ 7.55 ppm (●). It couples to two of the four doublets at δ = 8.0 ppm and 7.88 ppm. As before, the doublet adjacent to the acetylene appears slightly more upfield, and is therefore assigned as the doublet at δ = 7.88 ppm (●).The proton residing next to the acetylene is the more deshielded of the remaining two doublets, and has been labelled accordingly at δ = 8.2 ppm (●). The two triplets situated on the four spin system appear at δ = 7.67 ppm and δ = 7.65 ppm. They were distinguished using a 1D selective ROESY experiment which identified the doublet at δ = 7.67 ppm as the proton adjacent to the doublet at δ = 8.2 ppm (●).The three proton signals of the 1,10-phenanthroline assigned in the same manner as in the $^{1}H$ NMR spectrum of **2** and appear only marginally shielded with respect to their corresponding signals in Figure 1.12.

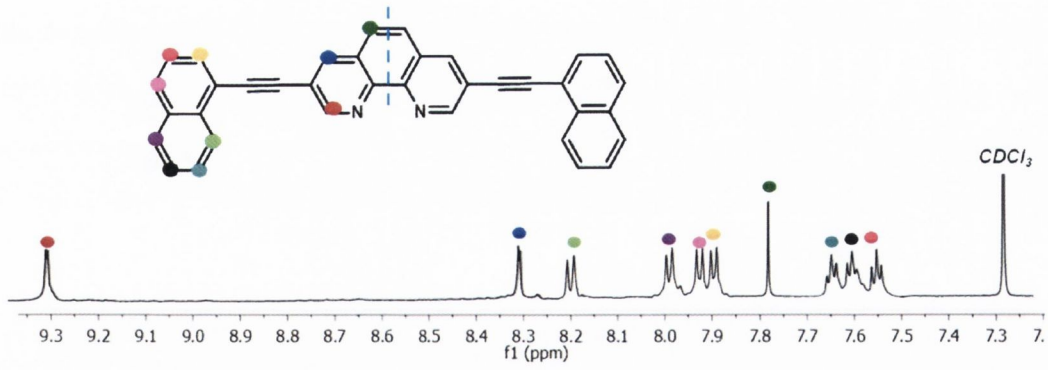


*Figure 1.13: The $^{1}H$ NMR spectrum of **3** ($CDCl_3$, 400 MHz, R.T.)*

### 1.3.1.3 Synthesis of 3,8-bis(2-(1-pyrenyl) ethynyl)-1,10-phenanthroline (5)

Cross-coupling of 1-ethynyl pyrene to 3,8-dibromo-1,10-phenanthroline was attempted using $Pd(PPh_3)_4$ as catalyst. The reaction was carried out in excess solvent (THF: $^{i}PrNH_2$, 3:1, v/v) as the poor solubility of 3,8-dibromo-1,10-phenanthroline had led to reduced yields and unreacted starting materials in previous reactions. A highly blue-fluorescent product which was poorly soluble in all chlorinated solvents was isolated. The electrospray mass of the sample revealed a peak centred at m/z = 451.1490 which corresponds to the homo-coupled pyrenyl product (calculated m/z = 451.1481, $[C_{36}H_{18}+H]^{+}$). This was further confirmed by $^{1}H$ NMR analysis which did not contain any of the three downfield aromatic singlets previously assigned to the 1,10-phenanthroline unit in **2** and **3**. This compound has previously been synthesised by Rostron and co-workers using Glaser coupling. [58] The reaction was repeated using the procedure reported by Ziessel *et al.*, [12] however this also produced in the homo-coupled product with no evidence of the formation of the target ligand.

Based on the previous success of Sonogashira cross-coupling with microwave irradiation, the synthesis of **5** was reattempted using similar conditions. 3,8-dibromo-1,10-phenanthroline was added to the microwave vessel with the catalyst, $Pd(PPh_3)_4$, and pre-dried solvents ($NHEt_2$:DMF, 5:2 v/v). Despite sonication and stirring, the starting material did not fully dissolve. To circumvent the formation of homo-coupled ethynyl-pyrene, the synthetic procedure was modified. The reaction vessel was sealed, and irradiated for 5 minutes at 85 °C, and automatically cooled to 60 °C. 1-Ethynyl pyrene was quickly added, the vessel resealed and the mixture irradiated for an additional 20 minutes at 125 °C. The reaction mixture was purified as before, and precipitated from $CH_2Cl_2$/MeOH to give an orange/yellow powder in a poor yield of 32 %. Although further attempts to scale-up the reaction were attempted, the size of the microwave vessel

restricted the volume of solvent, thus preventing greater amounts of the poorily soluble 3,8-dibromo-1,10-phenanthroline from being reacted. **5** was fully characterised using NMR spectroscopy. The electrospray mass spectrum of **5** displays a peak centred at *m/z* = 629.2015 corresponding to $[M+H]^+$, which agrees with the calculated value for $[C_{48}H_{24}N_2+H]^+$ (*m/z* = 629.2012.).

Figure 1.14 presents the $^1H$ NMR spectrum obtained for **5**. The large overlapping multiplet between δ = 8.3 and 8.05 ppm contains the majority of the signals attributed to the pyrene system. Examination of the $^1H$-$^1H$ COSY experiment proved to be futile in the assignment of many of the spin systems, therefore alternative ID experiments were employed.

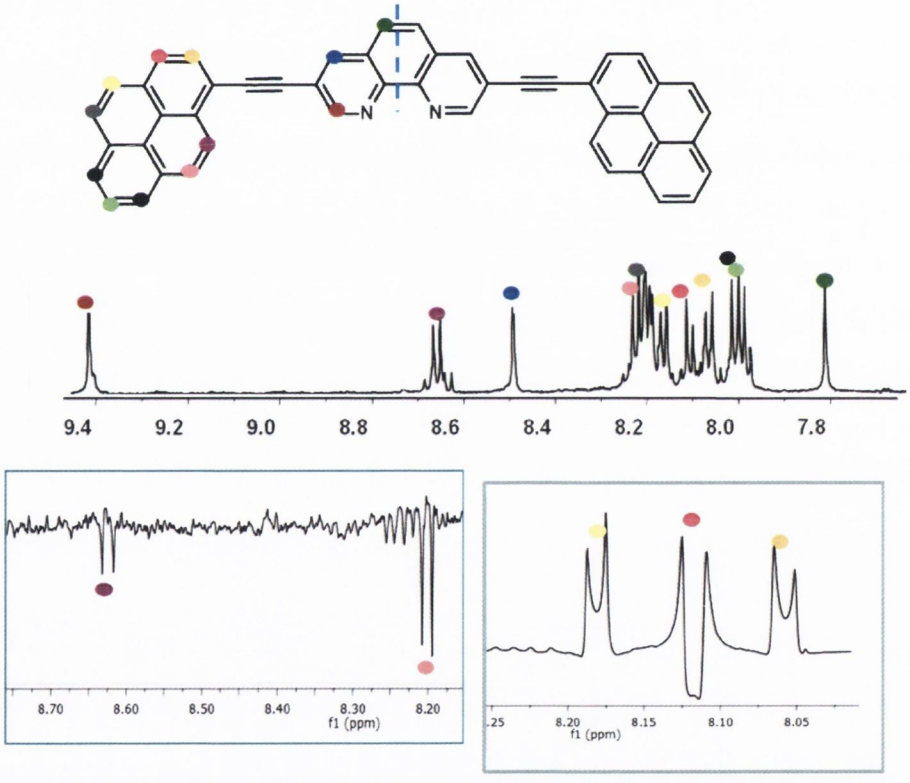


*Figure 1.14: Above the $^1H$ NMR spectra of **5** and below; a portion of the selective ROESY experiment and an example of the selective TOCSY experiment used to establish the various spin systems in the aryl moiety ($CDCl_3$, 600 MHz, R.T.).*

Selective ROESY experiments through irradation at various resonances enabled the assignment of neighbouring spins, such as the one below the acetylene linker (●●). Selective TOCSY experiments also proved to be very fruitful in identifying the remainder of the signals on the chromophore. The TOCSY mixing sequence causes the magnetism to spread to its nearest neighbours over various periods of time. Shorter

experiments establish connectivity between a proton and its adjacent protons. Longer periods of time can be employed to verify long range connectivity. A selective TOCSY experiment was used in the analysis of **5** to establish the relative order of the three doublets between δ = 8.15 and 8.05 ppm, each of which integrate for 1H (Figure 1.14). Irradiation of the central doublet reveals connectivity to the other two. This experiment was repeated by irradiating for a short period at δ = 8.05 ppm (●), which revealed a correlation to the doublet at δ = 8.10 ppm (●) only, thus verifying the order in which the doublets have been assigned. As in ligands **2** and **3**, three signals are easily identified as those on the 1,10-phenanthroline ring, and have been assigned as shown. They appear relatively unaffected by the presence of the larger chromophore

### 1.3.1.4 Synthesis of 3,8-bis[2-[4-[2,3,4,5,6-pentakis(4-tert-butylpheynl) phenyl] phenyl]ethynyl]-1,10-phenanthroline (6)

The synthesis of the polyphenylene ligand **6** was achieved using synthetic precursors previously prepared within the Draper group toward the synthesis of N-HSB.[59] 1,3-bis-*tert*-butylphenyl-propan-2-one (**sm2**) was synthesised from the commercially available 4-*tert*-butylbenzyl bromide by a phase-transfer carbonylation reaction with $^{t}Bu_4N^{+}(HSO_4)^{-}$ (phase transfer catalyst) and $Fe(CO)_5$.[60]

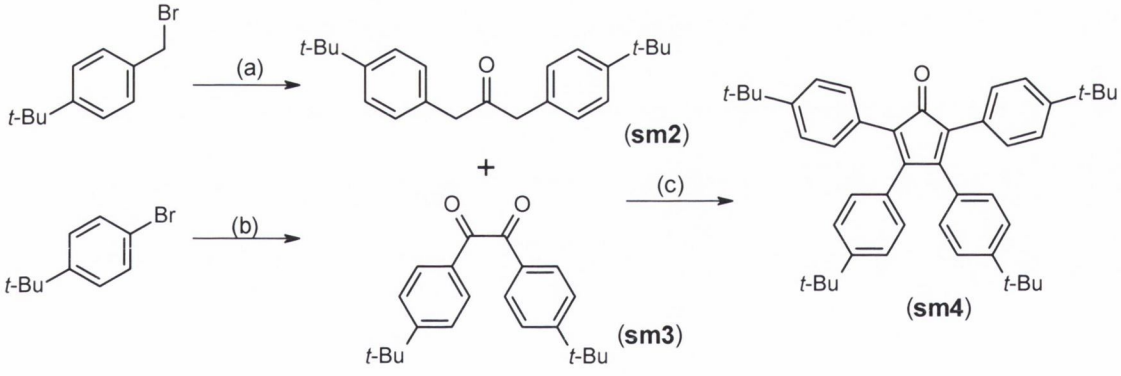


*Scheme 1.10: The synthetic procedure adopted for the precursors to the t-butyl derivative of cyclopentadienone (6). (a) $Ca(OH)_2$, $^{t}Bu_4N^{+}(HSO_4)^{-}$, $Fe(CO)_5$, $CH_2Cl_3$:$H_2O$ (1:1) v/v), R.T. (Yield 63 %) (b) $^{n}$BuLi, -78 °C, THF; DMPD; HCl soln. (10%) (Yield 81 %). (c) KOH, EtOH, 75 °C (Yield 59 %)*

Lithiation of 4-*tert*-butylbromobenzene with $^{n}$Bu-Li in THF at -78 °C, proceeded by reaction with a solution of 1,4-dimethylpiperazine-2,3-dione (DMPD) in THF at -78 °C, and acidifying with aq. HCl (10 %), yielded 2,5-bis-(4-*tert*-butylpheyl)ethane-1,2-dione (**sm3**). [61] 2,3,4,5-tetra-(4-*tert*-butylphenyl)cyclopenta-2,4-dienone (**sm4**) was prepared

by a two-fold Knoevenagel condensation reaction with KOH between the two precursors in ethanol to yield the purple solid in a comparative yield (59%). [59]

4-iodo-4`-*tert*-butylphenylacetylene (**sm5**) and iodo-hexaphenylbenzene (**sm6**) have previously been reported by the Draper group in the synthesis of the terpyridine substituted HBC derivatives (Scheme 11).[17] 4-iodo-4`-*tert*-butylphenylacetylene (**sm5**) was synthesised *via* a Sonogashira palladium catalysed cross-coupling reaction between two commercially available synthons, 1,4-diiodobenzene and 4-*tert*-butylphenyl acetylene. In the interest of time efficiency, the reaction was initially attempted using the microwave procedure described for the synthesis of (**2**), although this produced the two-fold coupled product, rather than the target compound. The reaction was then attempted *via* the traditional procedure and gave the product as a white solid in good yield (69 %).[18] Iodo-hexaphenylbenzene (**sm6**) was prepared *via* a [2+2] Diels Alder cycloaddition reaction between the iodo-acetylene (**sm5**) and the previously prepared cyclopentadienone (**sm6**). This reaction was carried out in a high temperature benzophenone melt. Precipitation from cold methanol produced the product as a cream powder in 77 % yield

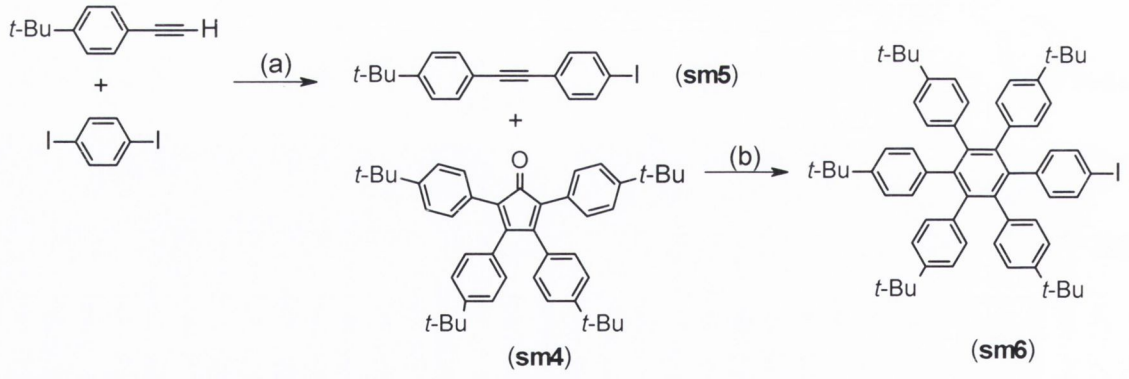


*Scheme 1.11: Synthesis of iodo-hexaphenylbenzene (a) cis-$PdCl_2(PPh_3)_2$ (6 mol %), CuI (6 mol %), THF, $^iPr_2NH$ (3:1 v/v) , R.T. (b) Benzophenone, 200 °C, 1.5 hrs, 320 °C, 18 hours, under Ar.*

Iodo-hexaphenylbenzene was cross-coupled to TMSA and then deprotected to form ethynyl-hexaphenylbenzene (**sm8**), which had been previously reported by Drs. Fran Murphy and Deanne Nolan within the Draper group in the synthesis of extended aromatic terpyridines and Pt(II) acetylides.[17, 18] The white powder was isolated following precipitation with cold MeOH to afford the product (**sm8**) in 81% yield.

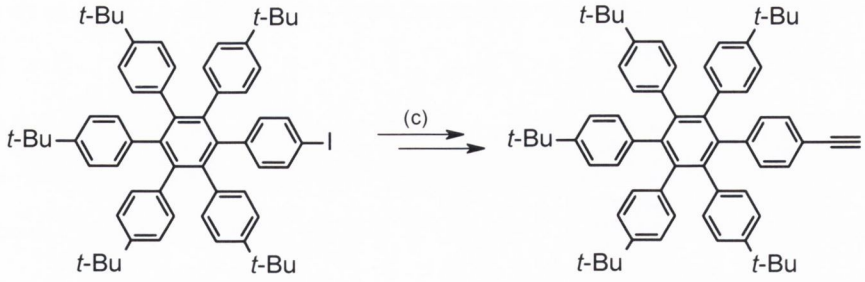


(sm6) (sm8)

*Scheme 1.12: Synthesis of ethynyl-hexaphenylbenzene (**sm8**); TMSA (1.05 eq) cis-$PdCl_2(PPh_3)_2$ (6 mol %), THF:$^iPr_2NH$ (3:1; v/v), R.T. ; KF (10 eq), MeOH: THF (1:1 v/v), R.T.*

The synthesis of the target ligand was carried out by a Sonogashira cross-coupling of ethynyl-hexaphenylbenzene (**sm8**) with 3,8-di-bromo-1,10-phenanthroline (**sm1**). Higher temperatures were required to ensure that (**sm1**) had fully dissolved before a solution of the acetylene in DMF was transferred *via* cannula. The reaction was continuously monitored, and a new product was finally detected after three days. Purification by silica column chromatography produced a pale brown solid in a moderate yield (46 %) which was confirmed by MALDI-TOF analysis as the desired product **6** (Scheme 1.13) ($[C_{140}H_{145}N_2]^+$: calculated *m/z* = 1854.1402, found 1854.1396). Although the cross-coupling was repeated using elevated temperatures and longer reaction periods, this yield was not optimised any further. Small amounts of unreacted starting material (**sm8**) were recovered after all attempts.

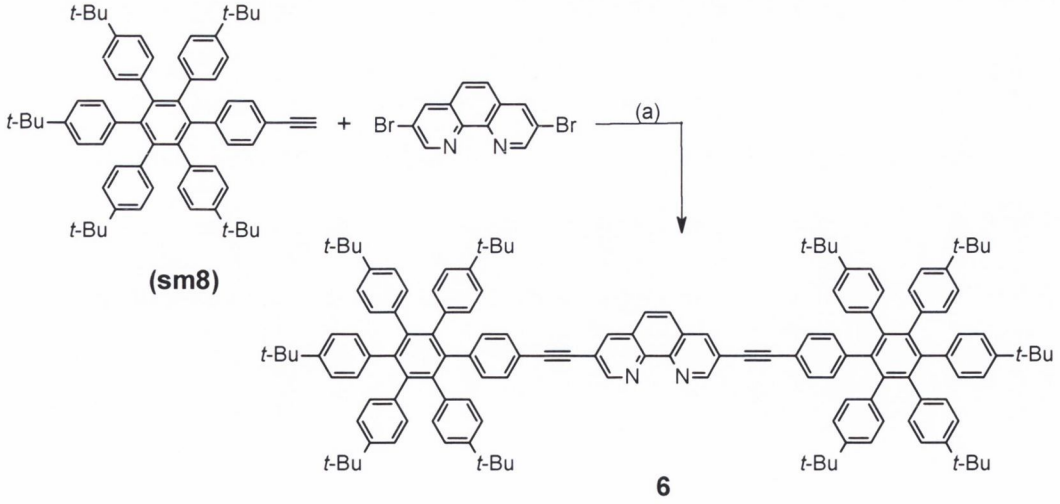


(sm8) 6

*Scheme 1.13: Sonogashira coupling of 3,8-dibromo-1,10-phenanthroline to ethynyl-hexaphenylbenzene (a) $Pd(PPh_3)_4$ (12 mol %), DMF:$NHEt_2$ (3:1; v/v) 90 $^oC$, R.T., 3 days, Ar.*

The $^{1}$H NMR spectrum of **6** is presented in Figure 1.15. The three protons residing on the 1,10-phenanthroline moiety appear as three distinct singlets as shown. The majority of the polyphenylenes protons appear as 2 multiplets at δ = 6.7 ppm and 6.9 ppm, each of which integrate for 20 H. Two additional doublets are visible on either side of the shielded multiplet at δ = 6.7 ppm. A selective TOCSY experiment irradiation at δ = 6.6 ppm (see inset, Figure 1.15) showed no correlation to the *tert*-butyl groups appearing in the aliphatic region, thereby confirming the identity of the doublets as those situated on the phenyl ring attached to the acetylene.

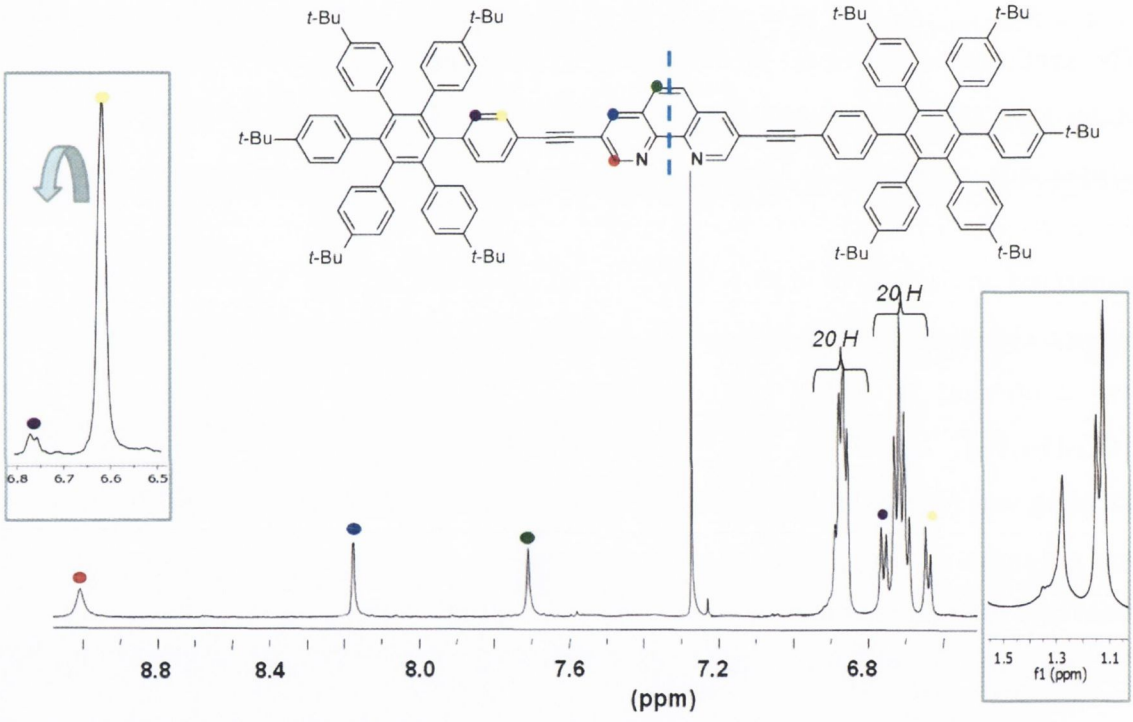


*Figure 1.15: The $^{1}$H NMR spectrum of **6** with inset showing selective TOCSY experiment used to identify the neighbouring protons on the phenyl ring attached to the acetylene ($CDCl_3$, 400 MHz, R.T.)*

The $^{13}$C NMR spectrum for **6** is shown in Figure 1.16, and is dominated by the presence of the carbon signals on the polyphenylenes moiety which appear at δ = 131 and 123 ppm. Three carbons at δ =148 ppm (●), δ =137 ppm (●) and δ =130 ppm (●) were assigned using a HSQC experiment, and are located on the 1,10-phenanthroline ligand centre. Also visible are two C-H carbons assigned to the phenyl carbon attached to the acetylene ring. The two acetylene carbons are shielded with respect to the other carbon signals and appear at δ = 85.7 ppm and 77.2 ppm. The unassigned signals are attributed to the 15 quaternary carbons of **6**.

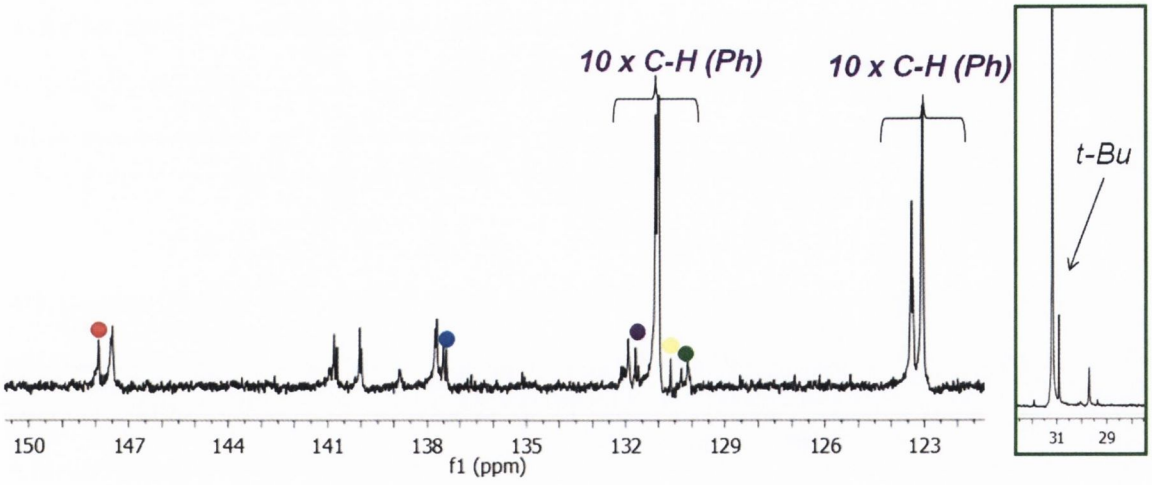


*Figure 1.16: The $^{13}C$ NMR spectrum of **6** with inset showing $CH_3$ carbon signals. ($CDCl_3$, 600 MHz, R.T.)*

### 1.3.1.5 Sonogashira cross-coupling reactions with 2-ethynyl-5, 8, 11, 14, 17-penta-tert-butylhexa-peri-hexabenzocoronene (ethynyl-HBC).

Oxidative cyclodehydrogenation of 6 could potentially generate the fully fused ligand 3,8-bis[2—ethynyl-5,8,11,14,17-penta-tert-butylhexa-peri-hexabenzocoronene]-1,10-phenanthroline, however the scale of the reaction would be restricted by the poor yielding cross-coupling reaction between ethynyl-polyphenylene (**sm8**) and 3,8-dibromo-1,10-phenanthroline (**sm1**) (Scheme 1.13). A more viable option is direct cross-coupling of the prefused ethynyl-HBC (**sm9**) to 3,8-dibromo-1,10-phenanthroline (**sm1**). This synthetic route also minimises the number of cross-coupling reactions with **sm1**, thereby reducing the possibility of copper coordination to the ligand centre.

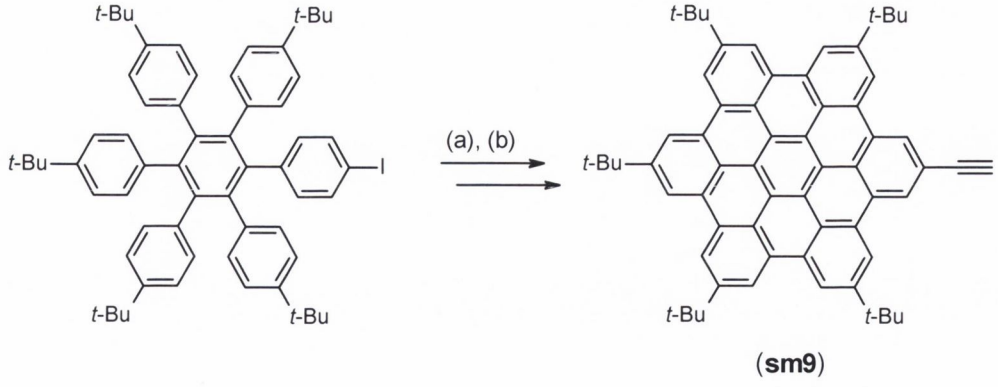


(**sm9**)

*Scheme 1.14: The synthetic route towards ethynyl-HBC (**sm9**) (a) $FeCl_3/CH_3NO_2$, $CH_2Cl_2$, R.T., overnight, Ar (b) TMSA (1.05 eq), $Pd(PPh_3)_2Cl_2$ (6 mol%), CuI (6 mol%) THF:$^{i}PrNH_2$ (3:1; v/v,), overnight, Ar; KF, THF: MeOH (1:1; v/v), overnight, R.T., Ar.* [18]

The oxidative cyclodehydrogenation of the iodo-polyphenylene (**sm8**) to give ethynyl-HBC (**sm9**) was carried out in using the oxidant conditions $FeCl_3/CH_3NO_2$, according to the procedure adopted within the Draper group (Scheme 1.14). The yellow/orange solid was isolated in a comparative yield of 57 %.[18]

The cross-coupling reaction between ethynyl-HBC (**sm9**) and 3,8-dibromo-1,10-phenanthroline (**sm1**) was initially attempted using the same conditions used for the cross-coupling of the polyphenylenes precursor (**sm8**), in THF and $^{i}PrNH_2$. Despite augmented heating to aid the solubility of both starting materials, and increased volumes of the solvents, no new product was detected. Other solvent systems were employed in additional attempts. These included THF/MeOH/$^{i}PrNH_2$ (2:1:1, v/v), and THF:$CH_2Cl_2$ (2:1:1, v/v). Ziessel *et al.* have previously reported the successful Sonogashira cross-coupling of bipyrimidine-based platforms and ethynyl functionalised terpyridines using a heated mixture of benzene and $^{i}PrNH_2$.[12] Based on this knowledge, the reaction was reattempted in a mixture of toluene and $^{i}PrNH_2$.

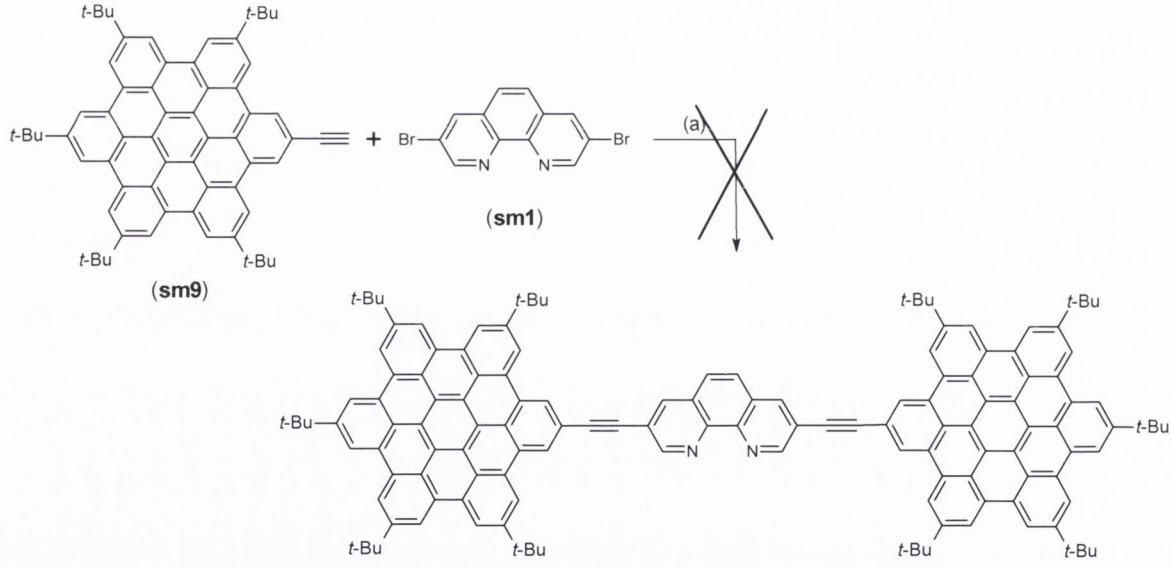


*Scheme 1.15: The attempted cross-coupling reaction between ethynyl-HBC and 3,8-dibromo-1,10-phenanthroline to produce 7; (a) $Pd(PPh_3)_4$, THF: Toluene: MeOH $^{i}PrNH_2$ (3:1, v/v), 90 °C, 3 days, Ar.*

**Sm1** and the Pd catalyst were dissolved in still-dried toluene and $^{i}PrNH_2$, sonicated for several minutes, and heated to 90 °C. The ethynyl-HBC was dissolved in excess toluene, and added dropwise. The reaction was left refluxing at 80 °C under argon for three days. A strongly fluorescent product was isolated from the crude mixture by silica column

chromatography in $CH_2Cl_2$ and precipitation from cold methanol (42 %). However, the poor solubility of the compound, in combination with the omission of 3 signals from the 1,10-phenanthroline core in the $^1H$ NMR spectrum (Figure 1.17) suggested that it was not the target product but homo-coupled ethynyl-HBC (**7**). This was confirmed by MALDI-TOF analysis, which displayed a peak at m/z 1651.8999 ($[C_{130}H_{122}+H]^+$: calculated m/z = 1651.8993. This product (**7**) has not been previously reported. The molecule shows a two-fold degree of symmetry, as shown, which greatly simplifies the aromatic region of the $^1H$ NMR spectrum.

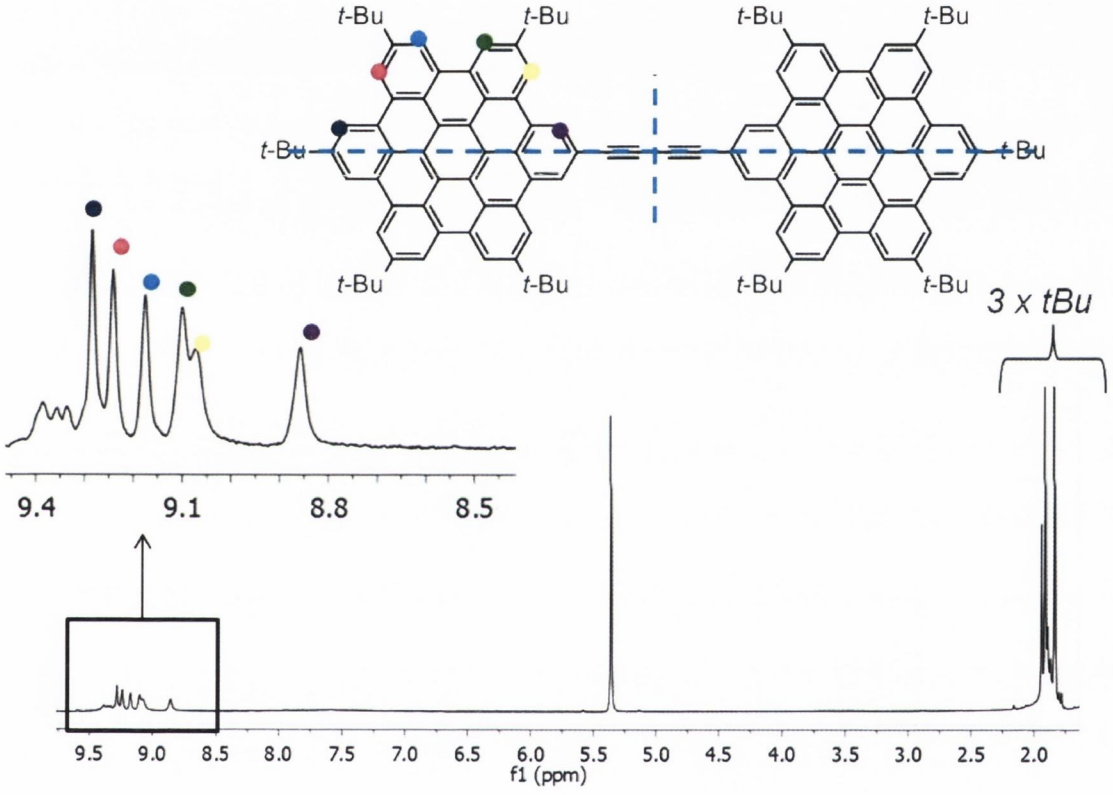


*Figure 1.17: The aromatic region of the $^1H$ NMR spectrum recorded for 7 ($CD_2Cl_2$, 600 MHz, R.T).*

Each of the signals are broadened with respect to the corresponding spectrum for the starting material 1-ethynyl HBC (**sm9**) (previously reported by Dr Deanne Nolan), however, the assignment of the signals remains the same. The presence of the homo-coupled product is further verified by the absence of a C≡CH signal in the aliphatic region, which previously appeared at δ = 3.52 ppm. Analysis of the IR spectrum of **7** revealed the absence of the C≡C*H* band at 3289 $cm^{-1}$, which had been reported for 1-ethynyl-HBC. An additional multiplet is also present at δ = 9.4 ppm but cannot be attributed to any specific proton on the molecule. It is believed that this is a feature

resulting from aggregation of the molecule in solution. The $^{13}C$ NMR spectrum for the molecule mirrors that obtained for the starting material (see experimental section).

To date, the cross-coupling of ethynyl-HBC to 3,8-dibromo-1,10-phenanthroline has not been successful despite several modifications to the reaction conditions employed in the synthesis of the other ligands. An additional route, the cross-coupling of the iodo-HBC precursor to 3,8-diethynyl-1,10-phenanthroline has also proved to be unsuccessful. This synthetic design required two sequential Sonogashira cross-coupling reactions on the 1,10-phenanthroline moiety with the $Pd(PPh_3)_4$ catalyst, which as previously discussed, results in compromised reaction scales and reduced yields. Alternative cross-coupling reactions have also been explored using the conditions reported by Gau and co-workers. Gau successfully developed cross-coupling conditions for a range of terminal alkynes and benzyl bromides, using $NiCl_2(PPh_3)_2$ and aluminium acetylide as reagents in up to 99 % yields. [62] Unfortunately, this study was restricted to smaller benzyl systems, and could not be modified to accommodate larger aryl units such as the pyrene and HBC acetylenes in this work. The current focus of the project is to examine the feasibility of refluxing solvents with higher boiling points, such as xylene, in sealed pressure tube reactions.

### 1.3.2 Photophysical study of aryl-acetylene substituted 1,10-phenanthroline ligands (2, 3, 5, 6) and 7.

The UV-Vis absorption spectra of the 3,8-bis-(aryl)1,10-phenanthroline ligands (**2**), (**3**), (**5**), (**6**) as well as the homo-coupled ethynyl-HBC compound (**7**) are presented in Figure 1.18. The UV-Vis spectra were recorded in $CH_2Cl_2$ at ~1 x $10^{-5}$ M. The absorption spectra of the five compounds feature strong broad absorption bands indicating rotation in the compounds, and is frequently seen for acetylene-containing systems. Ligand centred $\pi$-$\pi^*$ transitions at $\lambda$ = 286 nm are apparent for the four ligands and are due to the 1,10-phenanthroline moiety.[31] **2** exhibits similar absorption band structure to that reported for 3,8-diethynyl-1,10-phenanthroline and comparable derivatives.[34] The lowest energy absorption ($\lambda_{max}$ = 348 nm) is red shifted with respect to the parent 1,10-phenanthroline, and can be assigned as $\pi$-$\pi^*$ transitions on the extended phenanthroline moiety.

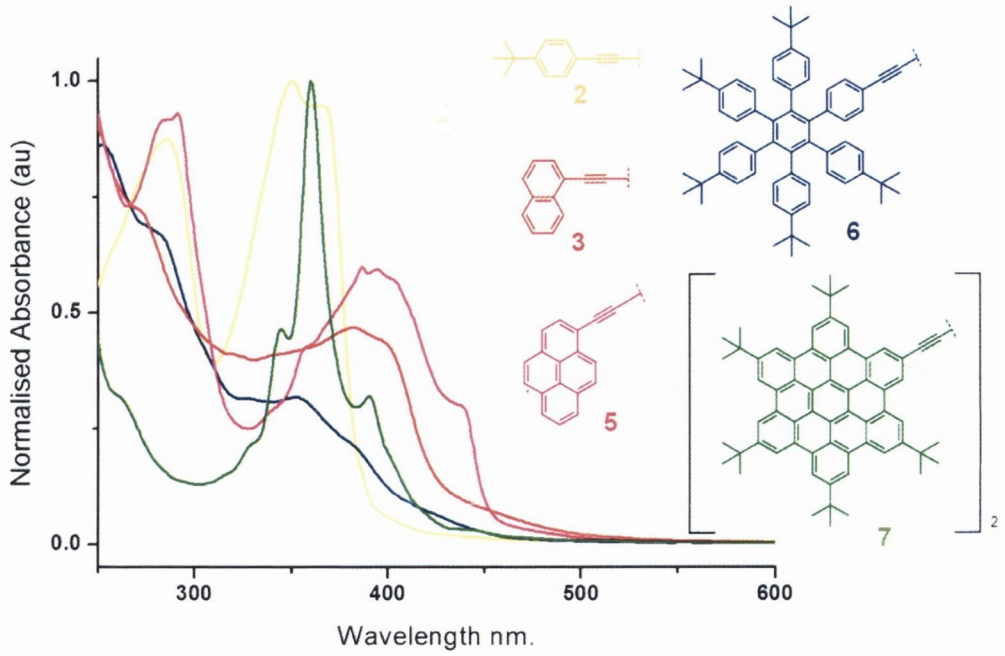


*Figure 1.18: Normalised UV-Visible absorption spectra of* ***2****,* ***3****,* ***5****,* ***6*** *and* ***7*** *in* $CH_2Cl_2$ *(~*$10^{-5}$ *M).*

Both ligands **3** and **5** shows intense absorption bands appearing at $\lambda$ = 350 nm to 400 nm which have been assigned as absorption bands characteristic of 1,10-phenanthroline ligands with larger $\pi$-conjugation in their framework.[63] The increase in degree of conjugation on going from naphthyl to pyrenyl chromophores leads to a bathochromic shift, and results in a more intense lower energy n-$\pi^*$ transition. The polyphenylene ligand **6** shows typical broad and featureless absorption profiles which have been previously observed within the Draper group for other nitrogen doped polyphenylenes, and is due to the non-planar conformation of the attached chromophores.[8, 64] The absorption bands of **6** are chiefly comprised of high energy ligand centred $\pi$-$\pi^*$ and n-$\pi^*$ transitions ($\lambda$ = 200-320 nm). Overall, the addition of aryl ethynyl groups to the 1,10-phenanthroline causes a red shift in absorption with increasing conjugation and electron delocalisation. The UV-Vis absorption spectrum of the homo-coupled ethynyl-HBC compound (**7**) is well-resolved and displays significant fine structure which is characteristic of hexa-*peri*-hexabenzocoronenes. Clar has previously attributed $\lambda_{max}$ = 365 nm to the ß-band, which corresponds to the electronic interaction between benzenoid rings, and the weaker transition at $\lambda_{abs}$ = 393 nm as the p-band, which involves the localisation of electrons in their excited state. [65] In general, the absorption maxima appear at the same wavelengths as the monomer, ethynyl-HBC, but the fine structure of the transitions are slightly broadened.[18] The lowest energy absorption bands do not

undergo a bathochromic shift in the UV-Vis absorption spectrum of the dimer (**7**) with respect to those reported for ethynyl-HBC. This is unusual, and is normally observed in systems with extended π-conjugation. Table 1.1 contains a summary of the UV-Visible spectral data for the four 1,10-phenanthrolines and the dimer **7**.

*Table 1.1: The UV-Vis absorption maxima observed for compounds in $CH_2Cl_2$ (~$10^{-5}$ M).*

| Compound | $\lambda_{max}$[nm]($\varepsilon$ x $10^4$ [$M^{-1}$ $cm^{-1}$]) |
|---|---|
| **2** ($^t$Bu) | 232 (4.05), 254 *sh* (5.35), 285 (8.1), 344 (9.85), 362 (8.48) |
| **4** (Naph) | 235 (5.3), 334 (4.02), 360 (4.14), 395 (0.5) |
| **5** (Pyr) | 246 (9.92), 282 (8.47), 292 (8.87), 340 (2.88), 360 (4.22), 387 (5.83), 395 (5.7), 405 *sh*, 439 (2.85) |
| **6** (Polyphen) | 232 *sh* (4.4), 256 (6.72) , 280 (6.94), 327 (1.05) |
| **7** (HBC) | 230 (19.2), 243 (18.5), 260 *sh* (4.9), 327 ( 8.1), 345 (19.1), $365_{max}$ (29.6), 389 *sh* (11.2), 410 (5.8), 443 (0.5), 459 (0.1). |

### 1.3.2.1 The solvent dependency of 1,10-phenanthroline derivatives UV-Vis absorption

The parent compound, 1,10-phenanthroline is blue shifted in solvents of increasing polarity, [Figure 1.19 (a)] which can be justified in terms of the relative energies of the singlet excited states. [66] In polar solvents, such as water, the $^1$n-π$^*$ and $^1$π-π$^*$ singlet excited states lie very close together [Figure 1.19(c)]. The first excited state is the $^1$π-π$^*$ state, which results in the fluorescence emission spectrum of 1,10-phenanthroline closely resembling phenanthrene, its parent hydrocarbon [Figure 1.19(b)]. Because the $^3$(n-π$^*$) state is situated between the $^1$(π-π$^*$) and $^3$(π-π$^*$) states, intersystem crossing is symmetry allowed, and occurs very quickly. The fluorescence singlet state lifetime and quantum yield are therefore notably less than phenanthrene where intersystem crossing is not observed. Changing the solvent to cyclohexane consequently reverses the $^1$(n-π$^*$) and $^1$(π-π$^*$) states. The $^1$(n-π$^*$) is now the highly populate state, and the fluorescence maximum moves to lower energy. Intersystem crossing is no longer symmetry allowed, but the non-radiative processes occur much quicker than in polar solvents. This reasoning explains the low quantum yields observed for 1,10-phenanthroline in non-polar solvents.

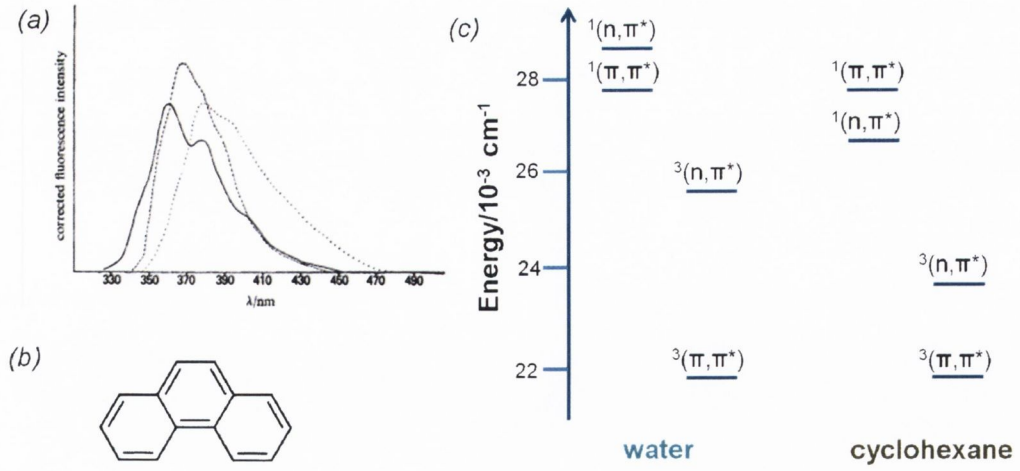


*Figure 1.19: (a) Fluorescence spectra of 1,10-phenanthroline in water(—), ethanol (--) and cyclohexane (···) (b) phenanthrene and (b)energy level diagram for the excited states of 1,10-phenanthroline which behaves similarly to (b) in polar solvents such as water.*

Compounds with lone pairs, which happen to have lower n-π* states, are stabilized in non-polar solvents. Similar to the parent compound 1,10-phenanthroline, 3,8- substituted derivatives of 1,10-phenanthroline with strongly electron-donating substituents exhibit considerable charge transfer character in their excited states. This has been observed for the methoxy and dimethylamino derivatives of **2** reported by Joshi *et al.* which results in both the absorption and emission maxima of the spectra being red shifted.[34]

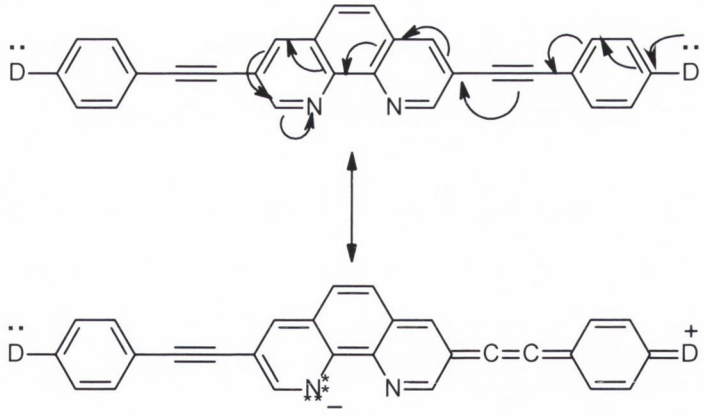


*Figure 1.20 : Promotion of charge-transfer of a conjugated 1,10-phenanthroline in the excited state by the electron-donating groups.*[34]

Table 1.2 contains the absorption maxima of the lowest energy band for each of the ligands, which exhibit marginal dependence on solvent polarity. This suggests that the stabilization effect reported by Joshi and co-workers does not extend to aryl groups with extended electron delocalisation such as the naphthyl (**4**) and pyrenyl (**5**) chromophores. Ligand **2** and **6** contain weakly electron-donating substituents which do not enable a

sufficient amount of charge transfer to the 1,10-phenanthroline core. Marginal shifts in absorption wavelength with a change in solvent polarity are typical of $\pi$-$\pi^*$ electronic transitions, which does not require a significant change in the dipole moment. This mirrors the behaviour of the methyl derivative reported by Joshi in his study.

*Table 1.2: UV-Visible absorption maxima ($\lambda$, nm) of the lowest energy absorption band for the ligand series in various solvents (~$10^{-5}$ M ) * Indictates sample was insoluble in ($^{i}Pr)_2O$ and measurement was carried out in toluene.*

| | **THF** | **$CH_2Cl_2$** | **$(^{i}Pr)_2O$** |
|---|---|---|---|
| **2** ($^{t}$Bu) | 362 | 363 | 365 |
| **4** (Naph) | 394 | 395 | 395 |
| **5** (Pyr) | 410 | 405 | 403* |
| **6** (Polyphen) | 324 | 327 | 327 |

### 1.3.2.2 Photophysical properties of ligands at room temperature ($CH_2Cl_2$ solution) and at 77 K in frozen butyronitrile glass ($10^{-5}$ M)

The emission spectra for compounds **2**, **4**, **5**, **6** and **7** were recorded in $CH_2Cl_2$ (1 x$10^{-5}$M) at 298 K and are presented in Figure 1.21. As anticipated, there is a significant red shift in all emission maxima with respect to the parent compound ($\lambda_{em}$= 360 nm). The ligands show a marginal dependence on excitation wavelength which verifies the poor electron donating ability of the series. The emission profile of **2** illustrates that the incorporation of the aryl ethynyl linker into the dimine structure results in a red-shift into the visible region ($\lambda_{em}$ = 385 nm) when compared with the parent compound ($\lambda_{em}$ = 360 nm). This is attributed to the presence of the electron-donating group, and mirrors the observations reported by Joshi and Tor for the methyl derivative of **2**. The fluorescence lifetime of **2** at room temperature also compares favourably with other 3,8-phenyl acetylene 1,10-phenanthrolines ligands, although a bi-exponential fit was observed for the ligand. [$\tau$ = 1.7 ns (89 %), 2.1 ns (11%)]. [29]

The emission profiles of the naphthyl and pyrenyl derivatives **3** and **5** are broad and featureless at room temperature [$\lambda_{em}$ = 445 nm (**3**) and $\lambda$ = 470 nm (**5**)] however the size of the appended chromophore causes a substantial bathochromic shift in emission maxima when compared with **2**. Both free naphthalene and free pyrene display structured

higher energy emission bands at room temperature, however Constable *et al.* have reported a similar broad emission profile for a dipyrene substituted bipyridine ligand, and attributes this behaviour to the emission arising from the diimine moiety rather than the pyrene chromophore. [67, 68]

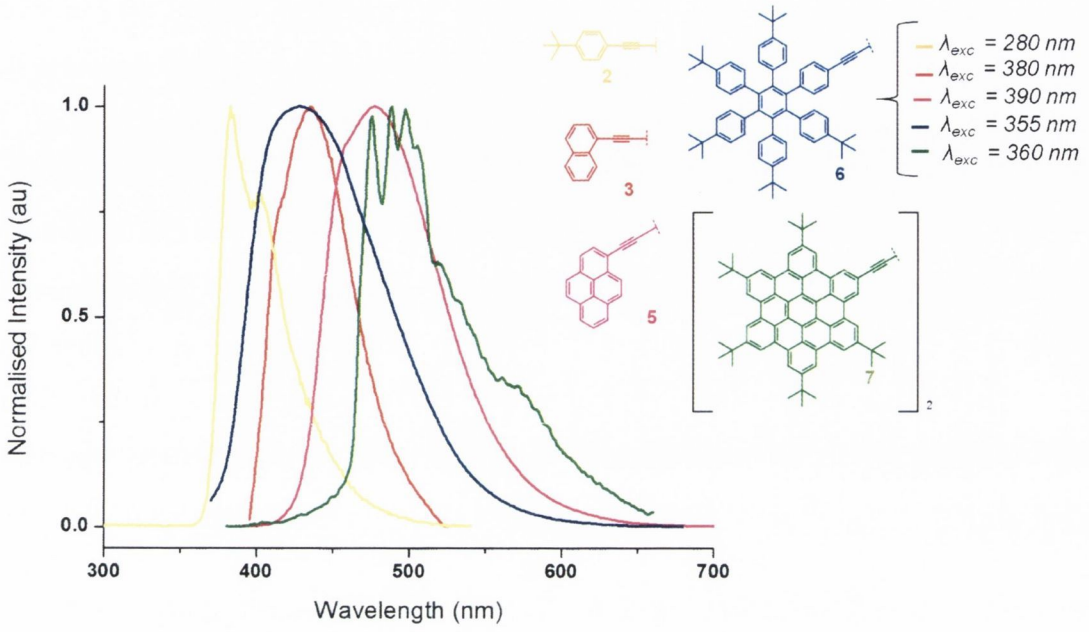


*Figure 1.21: Normalised emission spectra for compounds **2,3,5,6** and **7** in $CH_2Cl_2$ (1 x $10^{-5}$M) at 298 K with excitation wavelengths shown.*

The singlet state lifetimes of the two ligands are marginally longer than the *tert*-butyl derivative (**2**), with ligand **3** also displaying a biexponential fit [$\tau$ = 2.2 ns (73%) 2.9 ns (27%) (**3**) and $\tau$ = 2.4 ns (**5**)], but considerably shorter than their free aryl chromophores. The polyphenylenes derivative (**6**) exhibits a broad emission band ($\lambda_{em}$= 365 nm), which overlays the emission profiles of the smaller aryl ligands. This emission is dominated by $^1(\pi\text{-}\pi^*)$ fluorescence from the polyphenylene chromophore, which is reflected in the short singlet lifetime measured for the ligand ($\tau$ =2.7 ns). This is typical behaviour for polyphenylene based emission, and will be discussed in further detail in Chapter 4.

The emission spectra of **7** is comparable to ethynyl-HBC, and is composed of an extended band with a degree of vibronic structure between $\lambda$ = 450-590 nm at room temperature. The emission profile is slightly broader to that reported by Dr Deanne Nolan for the monomer, but is also invariant to solvent polarity.[18] The emission of **7** is assigned as singlet emission $^1(\pi\text{-}\pi^*)$ arising from the HBC chromophore.

The overlaid normalised UV-Vis absorption, excitation and emission spectra are presented for **2** and **7** in Figure 1.22(a) and (b) illustrate the difference in the photophysical behaviour of the 1,10-phenanthroline ligands and the dimer. The similarity in the overlaid absorption and excitation spectra for **2** [Figure 1.22(a)] is indicative of a single emitting species at room temperature. There is a marginal Stokes shift ($\Delta E$ =1069 $cm^{-1}$), which suggests very little conformational change occurs between the ground state ($S_0$) and the excited state ($S_1$). The magnitude of the Stokes shift is larger for the 1,10-phenanthroline ligands with larger aryl chromophores (e.g. **5** $\Delta E$ = 3786 $cm^{-1}$ and **6** $\Delta E$ = 3663 $cm^{-1}$), which indicates a more significant change in the conformation is occurring. Figure 1.22 (b) illustrates the significant Stokes shift observed between the excitation and emission spectra of the HBC-dimer **7**. There is also an additional low energy band visible at $\lambda$ = 467 $cm^{-1}$ that is detected in the absorption spectra for the compound (see inset). This is assigned as the forbidden 0→0 transition, and is not present in the other 1,10-phenanthroline ligands. Both of these observations have been previously reported by Schanze and co-workers in their photophysical study of HBC platinum(I) acetylide derivatives, and by Dr Deanne Nolan for ethynyl-HBC. [14, 18]

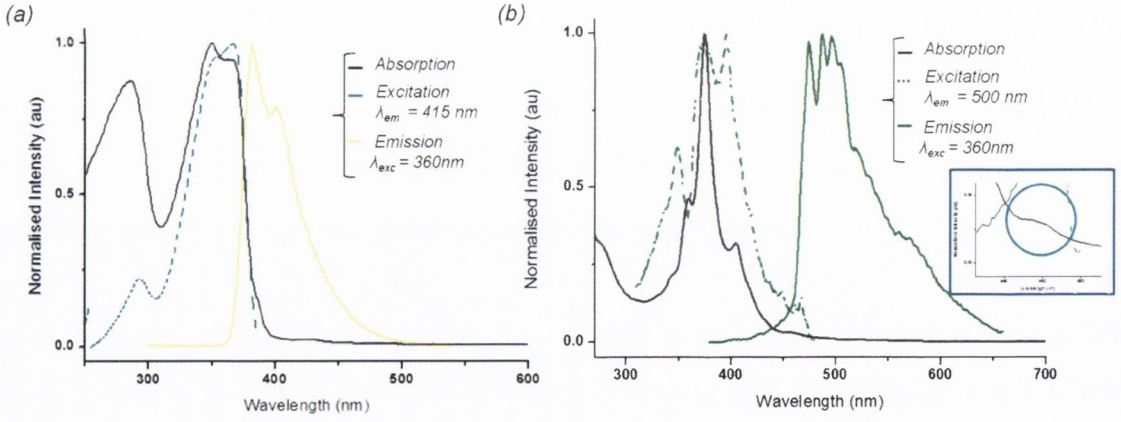


*Figure 1.22: The overlaid absorption, excitation and emission spectra for (a) tert-butyl derivative **2** and (b) the ethynyl-HBC dimer (**7**) in $CH_2Cl_2$ at room temperature. Inset magnified region of the absorption spectrum showing 0→0 transition in **7**.*

The corresponding emission spectra for the five compounds were recorded in butyronitrile at 77 K and are presented in Figure 1.23. There is a distinct increase in the vibronic structure in all five emission spectra and several vibronic progressions are particularly apparent in the emission spectra of **3**, **5** and **7**. The smaller vibronic progression detectable in the naphthyl ligand **3** is attributed to the naphthyl C-H wagging vibration (809 $cm^{-1}$). Three vibronic progressions in the emission spectrum of **5** are

assigned as (i) C≡C stretching (2383 $cm^{-1}$) (ii) C=C stretching (1346 $cm^{-1}$) and (iii) pyrene C-H wagging (730 $cm^{-1}$). The C=C stretching mode is also detectable in the emission spectra of **7** (1427 $cm^{-1}$).

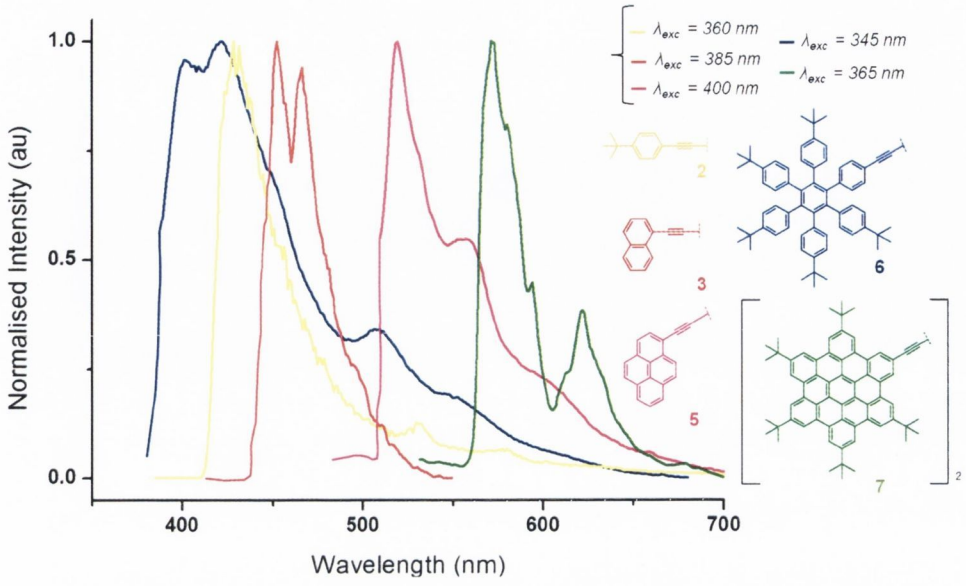


*Figure 1.23: Normalised emission spectra for compounds **2**, **3**, **5**, **6** and **7** in butyronitrile at 77 K (1 x $10^{-5}$M) with excitation wavelengths shown..*

The emission spectra at 77 K of all five compounds are red-shifted with respect to their emission maxima at room temperature. The values for the triplet lifetimes of the compounds could not be determined using the experimental set-up available at the time of measurement, but values reported for comparable diimine ligands range from microseconds to seconds.[24, 68, 69] The phosphorescence lifetime of free pyrene is reported to be 0.5 s at $\lambda_{exc}$ = 590 nm. This observation, in combination with the extended lifetimes of the emissive state at low temperature suggest that the emission is now derived from the $^3(\pi\text{-}\pi^*)$ state. An alternative assignment is proposed for the emissive state of **6**. The broad emission band observed for the polyphenylene ligand (**6**) at room temperature is replaced by an emission band with two components. The higher energy band at λ = 405-450 nm is characteristic of singlet derived emission $^1(\pi\text{-}\pi^*)$, and has a longer singlet lifetime than that measured at 298 K, i.e. τ = 13 ns. The weaker emission band centred at ~ λ = 510 nm is derived from the $^3(\pi\pi^*)$ emissive state, whose triplet lifetime also lies outside the range of the instrumentation set-up. This observation agrees with the emissive behaviour of other polyphenylene functionalised 1,10-phenanthroline ligands which will be discussed in Chapter 4.

Finally, the emission spectrum of **7** at 77 K deviates from that reported by Dr. Deanne Nolan for ethynyl-HBC. The monomer displayed higher energy emission ($\lambda$ = 475 nm, frozen $CH_2Cl_2$) and was assigned as singlet emission ($^1\pi\pi^*$) derived from the HBC chromophore. The emission maxima of the dimer compound **7** appears at $\lambda$ = 573 nm, with no trace of residual fluorescence observed despite excitation at various wavelengths. This is consistent with emission now derived solely from the triplet state $3(\pi\pi^*)$, and mirrors the behaviour of HBC metal complexes, despite the fact that there is no coordination site available in the dimer. Similar observations have been reported by Rostron *et al.* for the homo-coupled pyrenyl dimer.[58] The presence of the rigid linker between the two chromophores is believed to prevent the formation of intramolecular excimer which is reported for dipyrene molecules with saturated bridges. Based on the extensive vibronic structure and the large bathochromic shift observed at 77 K, this has been tentatively assigned as a $S_1 \rightarrow T_1$ transition, which must now lie closer in energy. Further investigations are on-going to see if similar behaviour is observed for other homo-coupled fused aryl chromophores. Table 1.3 summarises the photoluminescence data for the ligands in argon degassed $CH_2Cl_2$ and at 77 K.

*Table 1.3: Summary of emission data for **2**, **4**, **5**, **6**, **7** in solution at 298 K and 77 K.*

| | **Medium (T[K])** | **$\lambda_{em}$[nm]( $\lambda_{exc}$[nm])** | **$\tau$[ns] ]( $\lambda_{exc}$[nm])[b]** |
|---|---|---|---|
| **2** ($^t$Bu) | $CH_2Cl_2$ (298)[a] | $385_{max}$, 398 (350) | 1.7 (89 %) 2.1 (11%) (294/470) |
| | Butyronitrile (77) | $429_{max}$, 588 (360) | * |
| **3** (Naphth) | $CH_2Cl_2$ (298)[a] | $445_{max}$ (380) | 2.2 (73 %), 2.9 (27%) (294/ 445) |
| | Butyronitrile (77) | $452_{max}$, 466 (385) | * |
| **5** (Pyr) | $CH_2Cl_2$ (298)[a] | $470_{max}$, 525 *sh* (370) | 2.4 (100%) (340/470) |
| | Butyronitrile (77) | $519_{max}$, 558, 602 *sh* (400) | * |
| **6** (Polyphen) | $CH_2Cl_2$ (298)[a] | $365_{max}$, 378 (325) | 3.7 (72 %), 8.6 (28%) |
| | Butyronitrile (77) | 383, 423, $451_{max}$, 481, 531, 573 (300) | 13 ns[#*] |
| **7** (HBC) | $CH_2Cl_2$ (298)[a] | 488, $496_{max}$, 522 *sh*, 564 | 26 (100%) (370/488) |
| | Butyronitrile (77) | 571, 580 *sh*, 594, 622 (365) | * |

Solutions ~ $10^{-5}$ M [b] Estimated uncertainty on $\tau \pm 10$ %; [c] Measurement refers to fluorescent component of the emission band only[#] Lifetime measurement could not obtained using instrumentation set-up available.[*]

### 1.3.3 Protonation of 1,10-phenanthrolines

The facile ability of the nitrogen atoms of 1,10-phenanthrolines to undergo protonation in the presence of acid has led to comprehensive studies of this family of ligands.[20, 70] Symmetrical 1,10-phenanthrolines undergo strict mono-protonation upon addition of dilute acid, with $^1$H NMR studies confirming that a rapid shuttling of the proton occurs between the two nitrogen. This has been confirmed by the formation of isobestic and isoemissive points in the UV-Vis absorption and emission spectra, and is reversible upon addition of base.[69] The newly formed bands are red-shifted, and emission now arises predominately from $\pi$-$\pi^*$ transitions. Unsymmetrical 1,10-phenanthrolines behave differently, the proton can been situated on either of the nitrogens, depending on the nature and position of the appended substituents.[69] Protonation of 1,10-phenanthrolines has become a valuable tool for tuning the luminescence of larger chromophores, especially in terms of the self-assembly of supramolecular structures.[71] It can also be utilised to tune the direction of photo-induced energy transfer (Figure 1.24). Armaroli *et al.* have shown that if spectral overlap occurs between the absorption and emission of two units such as oligophenylenevinylene (OPV) and a phenanthroline proton acceptor, the requirements for FRET are fulfilled.[72] This process enables the on-off switching of luminescence from the OPV unit, and could be further exploited in sensor based applications.

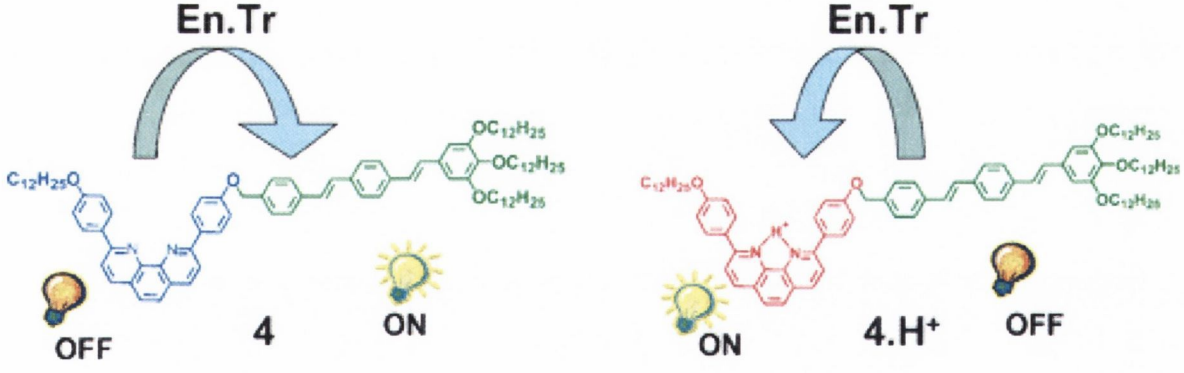


*Figure 1.24: Armaroli's on/off luminescence switching through protonation of 1,10-phenanthrolines.*[20]

The unusual behaviour of 1,10-phenanthrolines upon protonation is also observed for other diimine ligands, as reported by Constable *et al.*[68] Similar photophysical investigations of the bipyridyl derivative of **5** which contains no acetylene linker, shows the double protonation of the diimine moiety can occur to form $[(pyr_2bpy)H_2]^{2+}$ upon

addition of TFA. This species then undergoes strict dissociation back the mono-protonated dimine ($[(pyr_2(bpy)\text{-}H]^+ + H^+$) due to the acid strength of the 2,2'-bipyridyl dication.[73] Three isosbestic points were observed, ($\lambda$ = 306, 340 and 394 nm), and a broad shoulder of weaker intensity is formed ($\lambda$= 440 nm, which is consistent with the formation of a charge transfer state. Constable *et al.* believe that this charge transfer state indicates that a change in the ligand conformation occurs upon protonation of the diimine centre as shown in Figure 1.25. This has been verified computationally where the most stable neutral structure of the ligand was calculated to by the *trans* conformer, however the *cis* conformer is predicted to be the most stable conformer of the protonated species (5.2 kcal /mol lower in energy). Analysis of the crystal structure of the unprotonated "*trans*" ligand shows that the pyrene moiety is twisted out of the plane by 45.8° with respect to the bipyridyl centre.

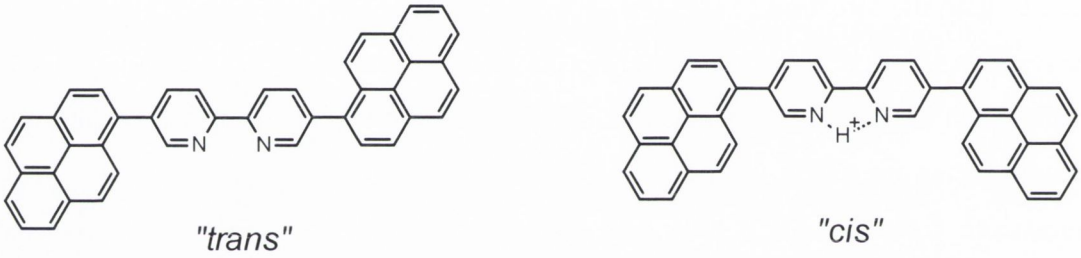


*Figure 1.25: The cis and trans conformation adopted by Constable's pyrene substituted ligand.*

Figure 1.26 shows the acid titration of **5** (1 x$10^{-6}$ M) with increasing 10 µl alliquots of trifluoroacetic acid (1 x $10^{-7}$ M). The strong fluorescence band at 410 nm is promptly quenched upon addition of the acid, with a new band of lower energy forming at $\lambda$ = 470 nm. The new emissive state is ICT in nature and assigned as (pyr → $phenH^+$).[20, 68] This charge transfer is more likely to occur in the protonated acceptor, and has been verified by computational studies which will be discussed in the next section. Three isosbestic points are observed at $\lambda$ = 325 nm, 370 nm and 440 nm, indicating an equilibrium between the neutral and newly formed protonated species. Increasing additons of acid causes these isobestic points to be perturbed, which is attributed to solvent affects caused by a change in the solvent polarity on acid addition.

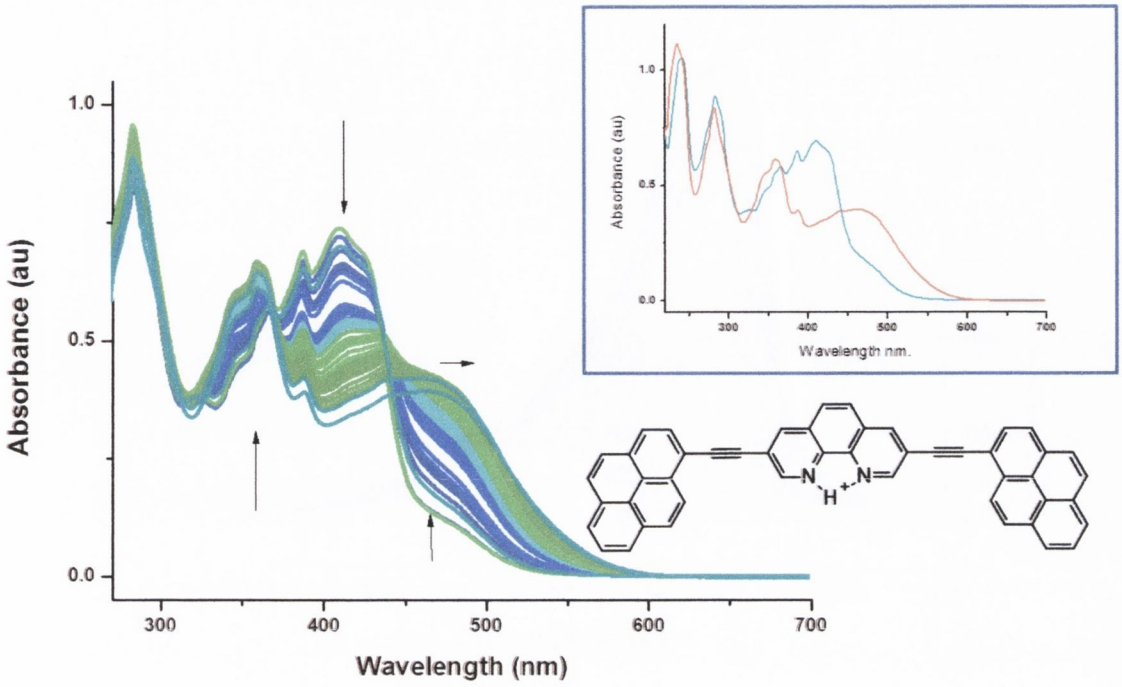


*Figure 1.26: The absorption spectra of* ***5*** *upon addition of increasing amounts of trifluoroacetic acid in $CH_2Cl_2$, showing three isosbestic points at (λ= 325, 370, 440 nm), and the shift of the CT band to lower energy. Inset also shows overall change between neutral (blue) and protonated species (red) after 1000 equivalents of acid.*

The corresponding emission acid titration of **5** shows that quenching of the emission maxima at λ = 475 nm is observed upon addition of 10 μL alloquots of TFA (1 x $10^{-7}$ M), and a new weaker low energy band is formed (λ = 575 nm). The newly formed band is dramatically red shifted with respect to the emission maxima of the neutrals species i.e. 3661 $cm^{-1}$. This band displays intramolecular charge transfer (ICT) character, and becomes more pronounced on successive additions of TFA. The fluorescence at λ = 475 nm is almost completely quenched after 300 equivalents of acid. This observation is consistent with Constables observations for the bipy pyrene derivative (Figure 1.25) and suggests the formation of *cis* conformer of the ligand, which is stabilised by the N-$H^+$ bond. In contrast, the unprotonated form of the ligand preferentially forms the *trans*-conformer of the ligand. This has been verified computationally for similar diimine systems. [68]

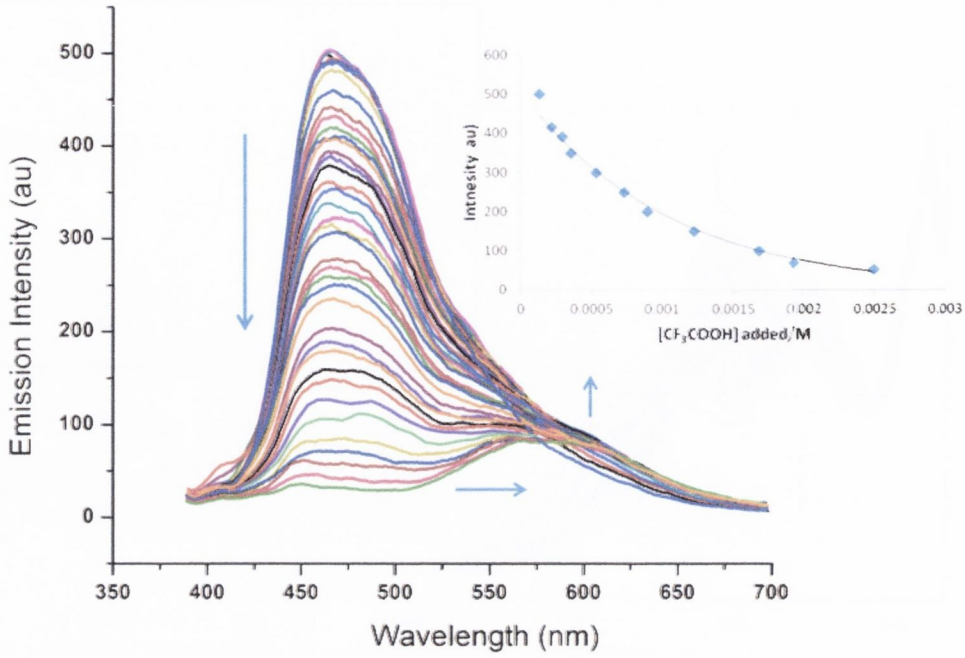


*Figure 1.27: Emission spectral changes of 5 (1 x $10^{-6}$ M) on addition of increasing amounts of trifluoroacetic acid (10 μL aliquots, 1 x $10^{-7}$ M) in $CH_2Cl_2$ at room temperature ( $\lambda_{exc}$ = 340 nm), which corresponds to the isosbestic point shown in Figure 1.26). Inset shows the change in intensity observed at $\lambda_{max}$ =475 nm with increasing concentration of acid in the cuvette.*

### 1.3.3.1 Computational investigation of 5 and $[5+H]^+$

To investigate the lowest lying triplet states of the ligand **5** and the protonated ligand $[\mathbf{5}+H]^+$, the spin density of the surface of both molecules was calculated by DFT calculations in collaboration with Prof. Jianzhang Zhao in the University of Dalian. Figure 1.28(a) illustrates that the spin density is distributed over the entire ligand **5**, which is agreement for the results previously reported by Prof Zhao and co-workers for the corresponding 3-substituted pyrenyl 1,10-phenanthroline ligand. Protonation of the ligand results in a localisation of electron density of the HOMO and LUMO on the pyrene and 1,10-phenanthroline moiety respectively. Figure 1.28 (c) and (d) show the calculated frontier molecular orbitals for both species, which shows the topology of the HOMO→LUMO calculations performed. The high oscillator strengths (f) for both transitions mirrors the strong absorptions observed for the lowest energy bands in the neutral and protonated species. Upon protonation of the ligand, a reduction in the HOMO-LUMO gap is observed which causes a stabilization of the molecular orbitals. This is reflected in a corresponding red shift in the lowest energy absorption band upon

protonation, for which the calculated value of $\lambda$ = 452 nm (2.74 eV) agrees closely to the experimental value obtained earlier ($\lambda$ = 470 nm, 2.63 eV).

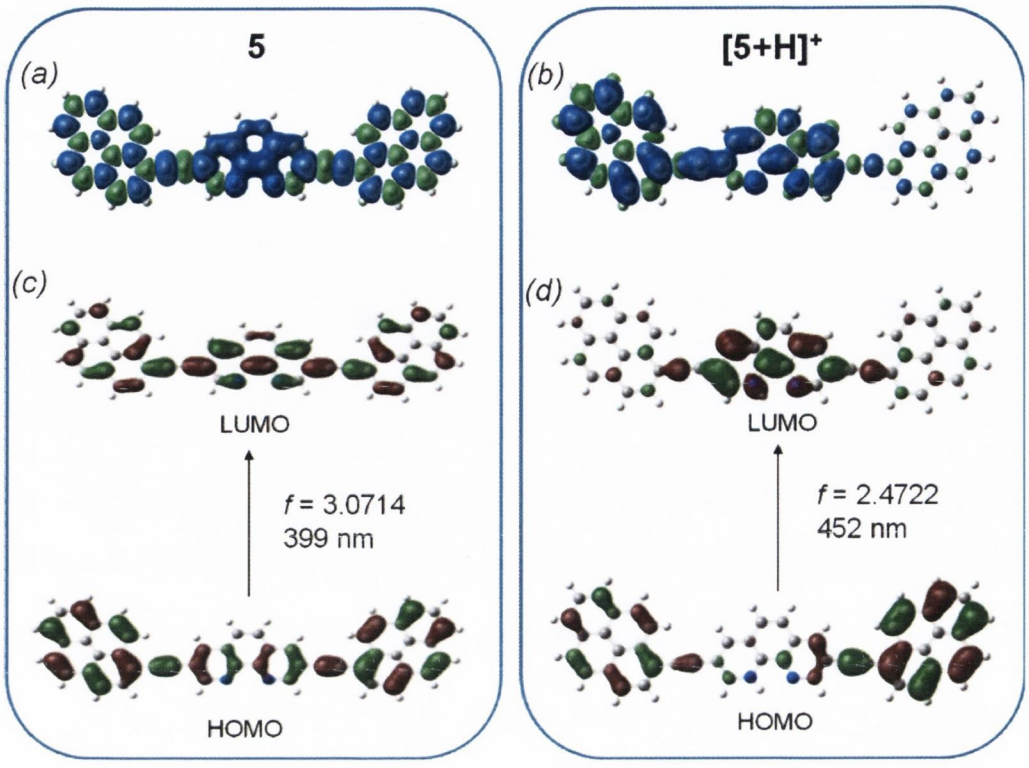


*Figure 1.28: (a) and (b) Isosurfaces of spin density of* ***5*** *and [****5****+H]$^+$ respectively at the optimized triplet state geometries, (c) and (d) the corresponding frontier molecular orbitals depicting the HOMO-LUMO gaps for* ***5*** *and [****5****+H]$^+$. Calculations are at the B3LYP/6-31G(d) / LanL2DZ level using Gaussian 09W and toluene as solvent.*

Figure 1.29 shows the selected frontier orbtials for the neutral and protonated ligand **5** both of which are presented in the *cis*-conformation. Figure 1.29 confirms that the lowest lying singlet excited states for the neutral species is distributed across the entire ligand. The DFT calculations verify that the lower energy transitions in the unprotonated ligand arise mainly from the electronic transitions $S_1$ and $S_2$ excited singlet states. These have been assigned as HOMO-1→ LUMO+1, HOMO→LUMO ($S_0 \rightarrow S_1$), and the less intense HOMO-1→LUMO and HOMO→LUMO+1 ($S_1 \rightarrow S_2$) excitations respectively. This is concurrent with an electronic density charge transfer from the tangential pyrene moieties to the inner phenanthroline core. Unlike the 5,5′-bis(pyren-1-yl)-2,2′-bipyridine ligand reported by Constable *et al*, **5** shows an extended lower energy absorption band with a higher extinction coefficient. This is attributed to the presence of the acetylene linker

between the 1,10-phenanthroline core and the pyrene chromophore. This concurs with the enhanced oscillator strengths calculated for the transition (f = 3.0714 vs. 1.21) and is assigned as intramolecular pyr→ phen charge transfer transition. The slight solvent dependency exhibited by the lowest energy band in the experimental measurements (toluene = 403 nm, THF = 410 nm) further supports the ICT assignment of the band. The calculated higher energy transitions (λ = 271 nm and 263 nm) are in good agreement with the experimental values of λ = 246 nm, and 282 nm. The weaker oscillator strengths (f = 0.4325 and 0.9615) indicate pyr→pyr and phen→phen excitations.

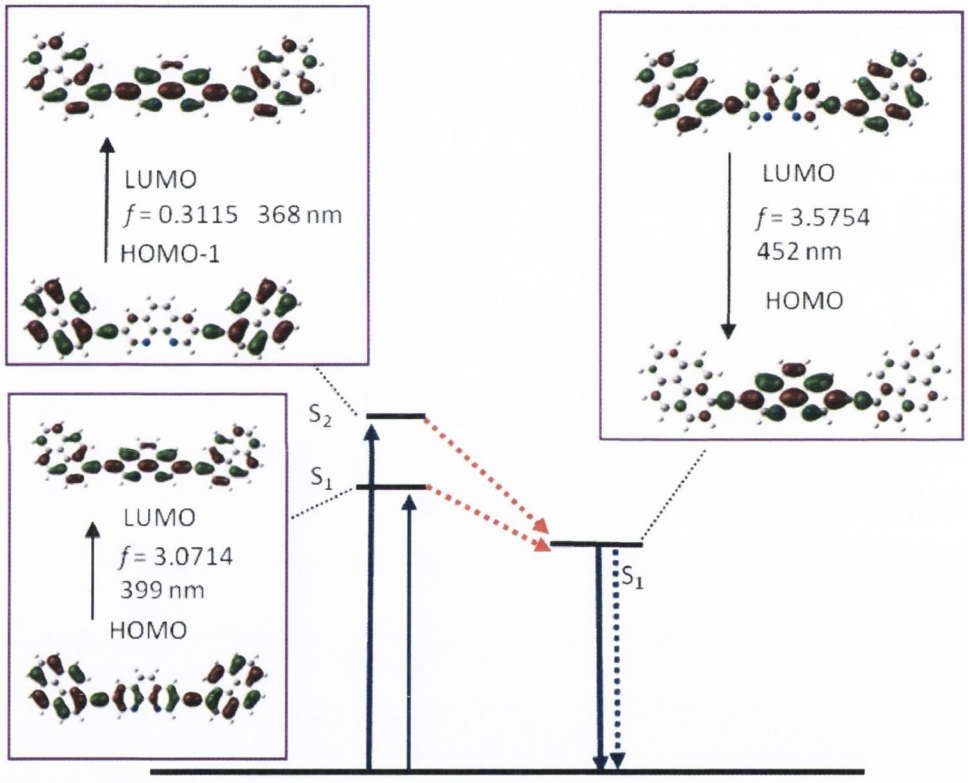


*Figure 1.29: Selected frontier molecular orbitals involved in the excitation and emission of 5. The calculations are at the B3LYP/6-31G(d)/ level using Gaussian 09W.*

Table 1.4 shows a summary of the selected electronic transitions (absorption and emission) calculated for the neutral ligand showing corresponding electronic excitation energies (eV), oscillator strengths (f) and configurations of the low-lying excited state.

*Table 1.4: Selected parameters for the vertical excitation (UV-Vis absorption and fluorescence emission) of the neutral ligand* ***5****.*

| | *Electronic transition* [a] | *TDDFT/B3LYP/6-31G(d)* | | | |
|---|---|---|---|---|---|
| | | *Excitation energy* | *f* [b] | *Composition* [c] | *CI* [d] |
| *Absorption* ***(5)*** | $S_0 \rightarrow S_1$ | 3.11 eV (399 nm) | 3.0714 | H–1→ L+1<br>H → L | 0.3202<br>0.5929 |
| | $S_0 \rightarrow S_2$ | 3.37 eV (368 nm) | 0.3115 | H–1 →L<br>H → L+1 | 0.5123<br>0.4413 |
| | $S_0 \rightarrow S_9$ | 4.57 eV (271 nm) | 0.4325 | H–2 → L+1 | 0.3139 |
| | $S_0 \rightarrow S_{13}$ | 4.71 eV (263 nm) | 0.9615 | H–4 → L+2 | 0.4122 |
| *Emission* ***(5)*** | $S_1 \rightarrow S_0$ | 2.74 eV (452 nm) | 3.5754 | H–1 → L+1<br>H → L | 0.2878<br>0.6151 |
| | $S_9 \rightarrow S_0$ | 4.34 eV (286 nm) | 0.8308 | H–6 → L<br>H–3 → L<br>H–2 → L+1<br>H–1 → L+2<br>H → L+4 | 0.2532<br>0.2149<br>0.3269<br>0.2122<br>0.2548 |

*Calculated by TDDFT/CAM-B3LYP/6-31G(d), based on the optimized ground state geometries ($CH_2Cl_2$ was employed as solvent in all the calculation) a Only selected excited states were considered. The numbers in parentheses are the excitation energy in wavelength. b Oscillator strength. c H stands for HOMO and L stands for LUMO. Only the main configurations are presented. d Coefficient of the wavefunction for each excitations. The CI coefficients are in absolute values.*

DFT calculations were also performed for the protonated species, $[5+H]^+$ a summary of which is presented in Figure 1.30 and Table 1.5. The newly formed red-shifted band at $\lambda$ = 475 nm was previously assigned as an ICT pyr→ $phenH^+$ transition in the experimental study presented in Figure 1.26. DFT calculations confirm this assignment and predict a new excited state at $\lambda$ = 452 nm, which has been attributed to a HOMO→ LUMO excitation. This new state is now assigned as $S_0 \rightarrow S_1$ excited singlet state. The calculations further predict additional new excited states at $\lambda$ = 359 nm and 300 nm respectively. These have been assigned as $S_0 \rightarrow S_3$ and $S_0 \rightarrow S_9$ excited singlet states, and are contained within the experimentally observed absorption bands at $\lambda$ = 283 nm and 360 nm. As previously assigned in the neutral species, the weaker values determined for their respective oscillator strengths ($f$ =0.427 and 0.327) suggest pyr→pyr and phen→phen transitions.

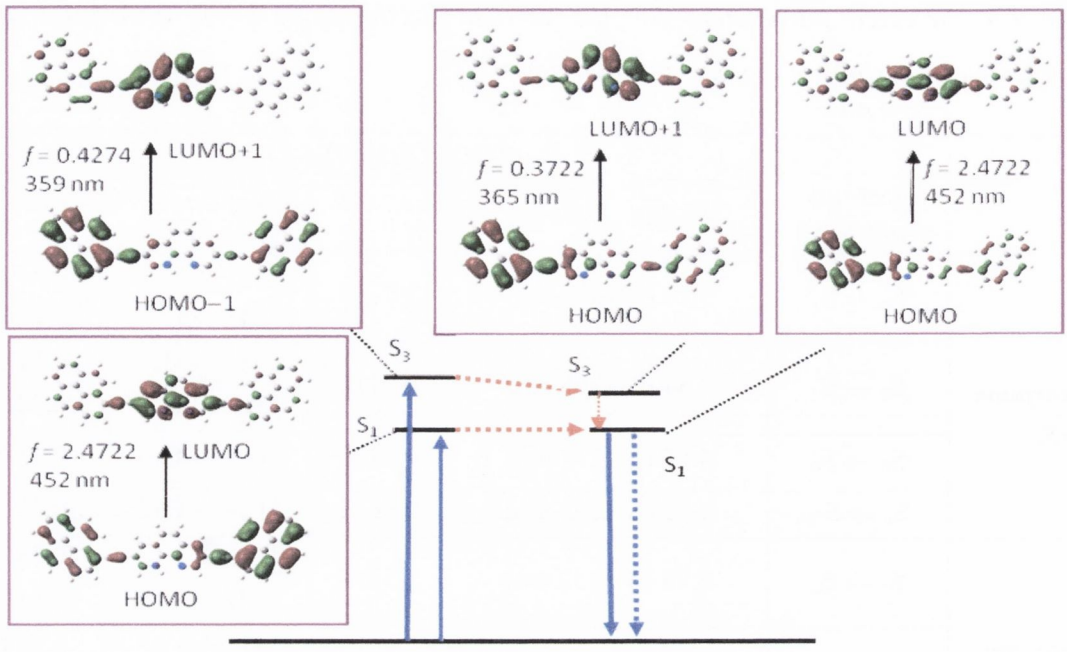


*Figure 1.30: Selected frontier molecular orbitals involved in the excitation and emission of [**5**+H]$^+$. The calculations are at the B3LYP/6-31G(d)/ level using Gaussian 09W.*

*Table 1.5: Selected parameters for the vertical excitation (UV-Vis absorption and fluorescence emission) for [**5**+H$^+$]. including electronic excitation energies (eV), oscillator strengths (f), configurations of the low-lying excited states of **5**.*

| | *Electronic transition* [a] | *TDDFT/B3LYP/6-31G(d)* | | | |
|---|---|---|---|---|---|
| | | *Excitation energy* | *f* [b] | *Composition* [c] | *CI* [d] |
| *Absorption (**5**+H$^+$)* | $S_0 \rightarrow S_1$ | 2.75 eV (452 nm) | 2.4722 | H → L | 0.5887 |
| | $S_0 \rightarrow S_3$ | 3 45 eV (359 nm) | 0.4274 | H–1 →L+1<br>H → L+1 | 0.4201<br>0.4091 |
| | $S_0 \rightarrow S_9$ | 4.13 eV (300 nm) | 0.3273 | H–4 → L<br>H–2→L<br>H → L | 0.4066<br>0.2783<br>0.2330 |
| *Emission (**5**+H$^+$)* | $S_1 \rightarrow S_0$ | 2.32 eV (535 nm) | 2.7422 | H →L | 0.6354 |
| | $S_3 \rightarrow S_0$ | 3.40 eV (365 nm) | 0.3722 | H–1 → L+1<br>H–1 → L+2<br>H → L+1 | 0.2943<br>0.2892<br>0.4414 |
| | $S_4 \rightarrow S_0$ | 3.51 eV (353 nm) | 0.3823 | H–1 → L<br>H–1 → L+1<br>H → L+2 | 0.2507<br>0.3088<br>0.4704 |

[a] *Calculated by TDDFT/CAM-B3LYP/6-31G(d), based on optimized ground state geometries ($CH_2Cl_2$). Only selected excited states were considered. The numbers in parentheses are the excitation energy in wavelength.* [b] *Oscillator strength.* [c] *H = HOMO and L = LUMO.* [d] *Coefficient of the wavefunction for each excitations. The CI coefficients are in absolute values.*

## 1.4 Conclusions and Future Work

In this chapter, a family of 3,8-substituted 1,10-phenanthroline ligands were prepared through Sonogashira cross-coupling reactions in order to study the affect of increased electron delocalisation on the photophysical properties of the diimine moiety. The tradition synthetic approaches have been adapted where possible to enable the use of microwave synthesis in Sonogashira cross-coupling reactions. This process not only led to optimised yields over traditional routes reported in the literature, but also increased the time efficiency of the reactions. The study has also led to the development of alternative copper-free Sonogashira cross-coupling conditions in the preparation of larger 1,10-phenanthroline systems, using $Pd(PPh_3)_4$ as catalyst. Optimisation of these conditions are currently underway in an attempt to synthesise the final member of the 3,8-aryl 1,10-phenanthroline family, the HBC derivative. The synthesis and characterisation of a homocoupled HBC acetylene has also been discussed, which to our knowledge, has not been previously reported.

The photophysical study of the compounds has revealed that in general, an increase in aryl platform size, [i.e. *tert*-butyl phenyl (2) → pyrene (5)] leads to a bathochromic shift in emission maxima, both at room and low temperature. The fluorescence lifetimes of compounds **2**, **3**, **5** and **6** are comparable to those reported for other 3,8-substituted 1,10-phenanthroline systems, and are not significantly affected by the presence of larger chromophores. The emissive behaviour of homo-coupled ethynyl-HBC (**7**) at low temperature is under further investigation. The strong phosphorescence observed at 77 K, combined with the absence of residual fluorescence has been tentatively attributed to an $S_0 \rightarrow T_1$ transition. Studies of other homo-coupled aryl acetylenes are underway to establish alternative possible explanations for this emissive behaviour in the absence of metal centres. Quantum yield measurements of the ligands are also currently underway, and attempts are being made to perform low temperature lifetime measurements on all of the compounds through collaborative work.

An extensive photophysical and computational study of the pyrene ligand (**5**) and the corresponding protonated species has also been completed. This approach has enabled the conclusive assignment of the lowest energy absorption band of **5** ($\lambda$ = 450-500 nm) as an intramolecular charge transfer singlet state, arising from electronic density charge transfer from the pyrene chromophore to the diimine centre. DFT calculations on the

protonated species concur with the observation of a new excited state at $\lambda$ = 475 nm, which has now been assigned as a $S_0 \rightarrow S_1$ excited state. Additional higher energy excited states have also been assigned as pyr→pyr and phen→phen transitions.

## 2 Comparing the photophysical properties of Ru(II) and Ir(III) complexes of 3,8- aryl acetylene 1,10-phenanthrolines.

## 2.1 Metal Diimine Acetylenes and Their Role in Information Transfer

This chapter focuses on the synthesis, photophysical and electrochemical study of the effect of increased chromophore size on 3,8 substituted Ru(II) bipyridyl and Ir(III) 2-phenylpyridyl 1,10 phenanthroline acetylene complexes. A short literature review will be presented which describes various recent examples of ruthenium(II) and iridium(III) 1,10-phenathroline complexes and their applications to date. This chapter also includes relevant studies on the effect of increased conjugation on other dimine ligands,

### 2.1.1 Ruthenium(II) polypyridine complexes

Ruthenium(II) diimine complexes are one of the most extensively studied classes of luminescent compounds, with well established synthetic, photophysical and electrochemical behaviour. Development of these materials has led to successful applications in photocatalysis, luminescent probes for biological systems and energy conversion.[74-76] The properties of Ru(II) polypyridyl complexes that make them suitable for these applications include high thermal and electrochemical stability, as well as ground state and excited state stability, and strong absorption throughout the visible region of the spectra (λ 380-750 nm), which can be further extended to include the near-infrared (> λ 750 nm) with careful ligand modification.[77] This enables maximum absorption of sunlight photons, making the complexes appropriate for light-harvesting in solar cells.

#### 2.1.1.1 Luminescence in ruthenium(II) polypyridyl complexes and other metal systems

Coordination complexes are typically classified by their electronic structure which is governed by the interaction of the transition metal and the surrounding ligands. Ruthenium(II) polypyridyl complexes with octahedral symmetry, and have the formula ($ML_6$), where L refers to a ligand. The five degenerate *d*-orbitals are split into two doubly degenerate orbitals ("$e_g$") and three lower lying triply degenerate orbitals ("$t_{2g}$"). The main electronic transitions for an octahedral metal comples are also depicted in Figure 2.1. (**1**) A ligand centred (LC) transition which occurs between molecular orbitals on the same ligand [$\pi_L \rightarrow \pi_L^*$]; (**2**) A metal-to-ligand charge transfer (MLCT) transition which arises from an electron being promoted to a $\pi^*_L$ acceptor orbital from a metal-centred ($\pi_c$) orbital [$\pi_M \rightarrow \pi^*_L$]. These transitions frequently take place when the metal present is in a low oxidation state, and if one of the coordinated ligands is readily

reducible; (3) A ligand-to-metal charge transfer transition [$\pi_L \rightarrow \sigma^*_M$], which occurs when the ligand is readily oxidised, and the metal centre is present in a higher oxidation state; (4) Metal centred (MC) transitions occur when an electron is promoted from a $\pi_M$ to a $\sigma^*_M$ orbital. MC transitions are spin forbidden. [$\pi_M \rightarrow \sigma^*_M$ ].[74, 78] Heteroleptic $[Ru(bpy)_2(L)]^+$ complexes distinctively exhibit two absorption bands in their UV-Vis absorption spectrum which have been attributed to charge transfer transitions from the bipyridyl and "L" ligands.

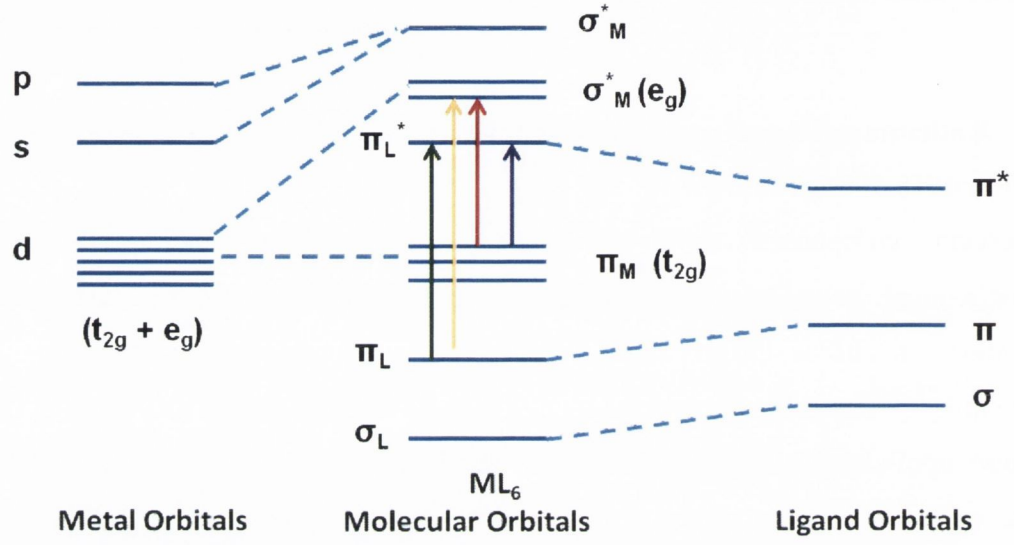


*Figure 2.1: Simplified molecular orbital diagram for an octahedral $ML_6$ complex such as Ru(II) polypyridyl complexes:(1) $\pi_L \rightarrow \pi_L^*$ (LC), (2) $\pi_M \rightarrow \pi^*_L$ * (MLCT), (3) $\pi_L \rightarrow \sigma^*_M$, (LMCT), (4) $\pi_M \rightarrow \sigma^*_M$ (MC).*

Further analysis of these transitions comes from the Jablonski diagram (Figure 2.2), where an excited state transition is classified as being either radiative (e.g. fluorescence) or non radiative (e.g. quenching). When a molecule in its ground state absorbs a photon of light of a suitable wavelength, it is promoted to populate an excited state. According to Kasha's rule, this excited state will promptly undergo internal conversion (IC) to an excited state which is lower in energy. The molecule can release the absorbed energy in the form of fluorescence, or by intersystem crossing (ISC) to a parallel spin triplet excited state where it can produce phosphorescence as it returns to the ground state. Single low energy emissive triplet MLCT excited states are as a result of non-radiative decay pathways *via* intersystem crossing (ISC). ISC from the $^1$MLCT state to the $^3$MLCT state is enhanced by the presence of the heavy metal centre. High spin-orbit coupling enables spin-forbidden mixing of the singlet and triplet molecular orbitals. The spin selection rule deems this process as forbidden ($\Delta S = 0$). Spin-allowed transitions must

involve the promotion of an electron, and this must occur without a change in spin. The remaining energy of the molecule can be dissipated through non-radiative processes such as bimolecular quenching.

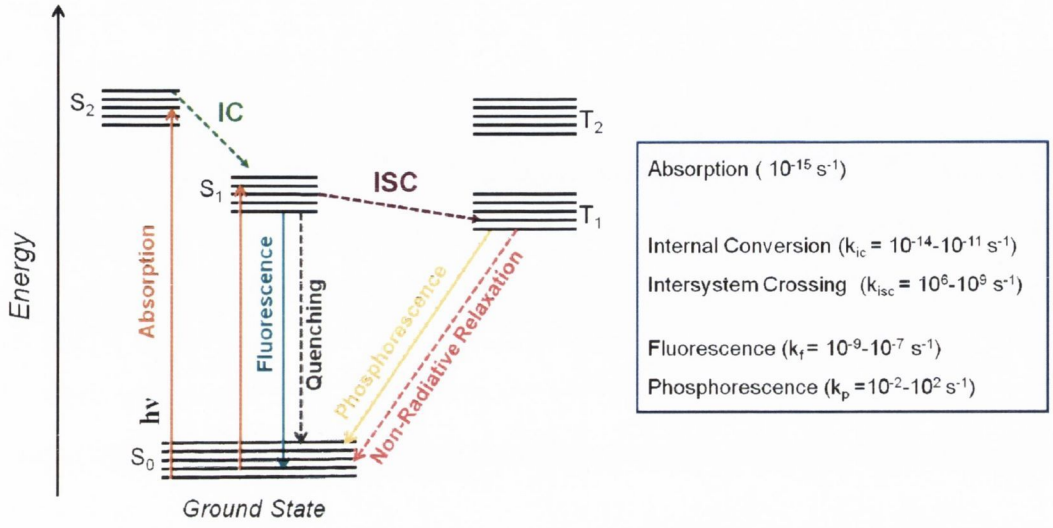


*Figure 2.2: Simplified Jablonski diagram indicating the various excited state decay pathways. (—) denotes radiative and (---) denotes non-radiative processes. Inset gives approximate values for the rate constants (k) of each pathway.*

The rate constant of fluorescence ($k_r$) can be approximated by summing the individual rates of the non-radiative processes ($k_{nr}$). The same approach cannot be used for the approximation of the radiative processes, as phosphorescence is intersystem crossing to the ground state, and is affected by quenching. The magnitude of the rate of the radiative processes is directly proportional to the square of the transition dipole moment (TM).

$$TM = \int X_i \cdot X_f dQ \cdot \int S_i \cdot S_f d\tau_e \cdot \int \Phi_i \cdot \mu \cdot \Phi_f d\tau_e$$

The first term refers to the Frank-Condon factor [the overlap of the nuclear configuration of initial and final states ($\chi$)]. The second term refers to the electron spin component which is governed by the spin selection rule. The spin overlap integral is zero if there is a change in multiplicity between the initial and final spin states (S). This rule can be relaxed by spin orbit coupling which mixes the $M_S$=0 constituent of the singlet and triplet states, and can be further maximised through the incorporation of metals with larger spin-orbit coupling constants. The last term in the equation refers to the symmetry of the states of the vector $\mu$, and is referred to as the electronic transition moment.

### 2.1.1.2 Luminescent ruthenium(II) polypyridine complexes and their selected applications.

Michael Grätzel first reported the use of a Ru(II) polypyridine redox-active dye in a dye sensitized solar cell in the early 1990's.[79] The dye was covalently linked to a semiconductor surface with a redox mediator situated in the electrolyte. Once the dye has been excited with visible light, the complex is promoted to the excited state, with the electrons passing into the conduction band of the $TiO_2$ layer. These electrons pass through an external circuit, and gather at a counter electrode. The Ru(II) state is regenerated through reduction back to the ground state by the redox mediator, and the result is conversion of sunlight to electricity. One of the most successful dyes to be reported is the $[Ru(dcbpy)_2(NCS)_2]$ (dcbpy = 4,4'-dicarboxyl-bipyridine) which has an incident photon-to-current conversion efficiency of 90%, with the thin layer photoelectrochemical device producing an overall solar-electric conversion efficiency of 10%.[80] The potential of Ru(II) polypyridyl complexes for solar-based applications has resulted in a surge of photophysical research in the past 25 years, of which the highlights relevant to this work will now be discussed.

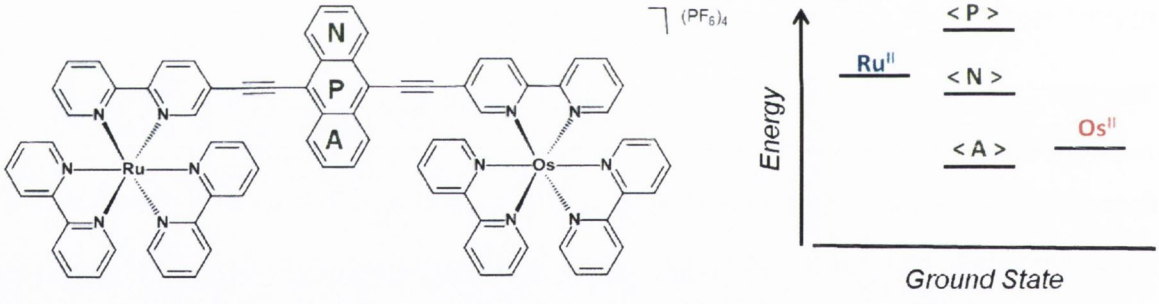


*Figure 2.3: The Ru(II) and Os(II) molecular dyad design reported by Harriman and co-workers and the energy level diagram showing the relative triplet states of the molecular dyads with respect to the aromatic bridging units. Naming scheme refers to substitution with ; P =1,4 phenylene, N= 1,4 naphthalene and A= 9,10-anthracene.*[81]

To establish the significance of long range vs. stepwise triplet energy transfer, Harriman *et al.* designed a series of molecular triads with increasingly aromatic diethynylated bridges (Figure 2.3).[81] The molecular triads incorporate two ethynyl connectors which ensure the molecule remains geometrically constrained. The connectors simultaneously ensure that the lowest-energy triplet state of each of the terminal metal fragments participates in charge injection to the ligand. [33, 82] The phenylene spacer acts as a mediator in the super energy exchange process, and a systematic lowering of the triplet state with respect to the Ru(II) state is observed with increasing aromaticity of the spacer

to naphthyl and anthracene derivatives. As the triplet energy of the phenylene spacer lies above the Ru(II) donor, it cannot participate in the overall energy transfer process to the same extent as the naphthalene and anthracene derivatives. Long-range energy transfer takes places between the two metal centres and is assisted by the phenylene moiety. The naphthalene intermediate lies lower than the Ru(II) state, and the energy transfer process occurs in a two step process. The naphthalene based triplet intermediate is produced, with a small degree of reverse energy transfer, followed by energy transfer from the bridge to the Os(II) bipy fragment. Both steps occur rapidly, and the overall energy transfer is quantitative. Replacing the naphthalene unit with the anthracene derivative lowers the triplet state of the bridge to the extent that it now results in a "bottle-neck" situation, and the transfer mechanism is restricted. Energy transfer takes place from both metal terminals to the bridge, with reverse transfer occurring from the bridge to the Os(II) terminal. This prolongs the length of the triplet lifetime of the Os(II) terminal.

The corresponding 2,2': 6',2''- terpyridine derivatives have also been investigated as well as the dinuclear Ru(II) terpyridine derivatives[83] with similar trends reported as the aromaticity of the bridge increases.[84] The dinuclear phenylene and naphthalene Ru(II) triad showed an increase in conjugation leads to a corresponding increase in triplet lifetime and quantum yield. ($\tau$ = 110 ns and $\Phi$ = 0.6% for the 1,4- phenylene and $\tau$ = 415 ns and $\Phi$ = 0.8% for the 1,4-naphthalene derivative). This trend did not extend to the anthracene bridged system, ($\tau$ = 0.09 ns and $\Phi$ = 0.2%) because of irreversible triplet energy transfer from the Ru(II) terminals to the bridge, which can again be quantified by the relative positions of the anthracene to metal triplet energy levels.

To investigate the effect of larger conjugated systems, the pyrenyl Ru(II) complexes and their corresponding Os(II) complexes were synthesised (Figure 2.4). [85] The pyrene subunit has the ability to display excimer/monomer emission and notably long fluorescence lifetimes ($\tau$ = approx 400 ns in deaerated solution, with $\tau$ < 10 ns for most other organic fluorophores). Reversible energy transfer was observed for **Ru-Bpy-P** which is justified by the pyrene triplet state being situated just below the triplet state of the metal. However, in the case of **Ru-Tpy-P** the triplet energy levels are reversed, and the pyrene triplet state now sits above the metal triplet state. The presence of the ethylene group provides an increased stabilisation factor ($S=k_R\tau_T$) for **Ru-Bpy-P** that is 35 times greater than in the case of **Ru-Tpy-P**. The stabilisation factor has a similar effect to

solvatochromic changes on a complex, and can further stabilize or destabilize the triplet/singlet states.[86] These values are significant in terms of applications in analytical or electro-chemiluminescence devices. The effect of the ethynyl bridge is also reflected in the triplet lifetimes of the complexes with complex (b) exhibiting a lifetime of $\tau$ = 40 μs, and $\Phi$ = 2.6% for the MLCT triplet state, whilst $\tau$ = 580 ns and $\Phi$ = 0.5% for **Ru-Tpy-P**. Shorter triplet lifetimes were observed for both corresponding Os(II) derivatives (e.g. $\tau$ = 12 ns), which can be justified by the fact that the Os triplet energy level is situated below the pyrene triplet, and the pyrene triplet must therefore remain unpopulated.

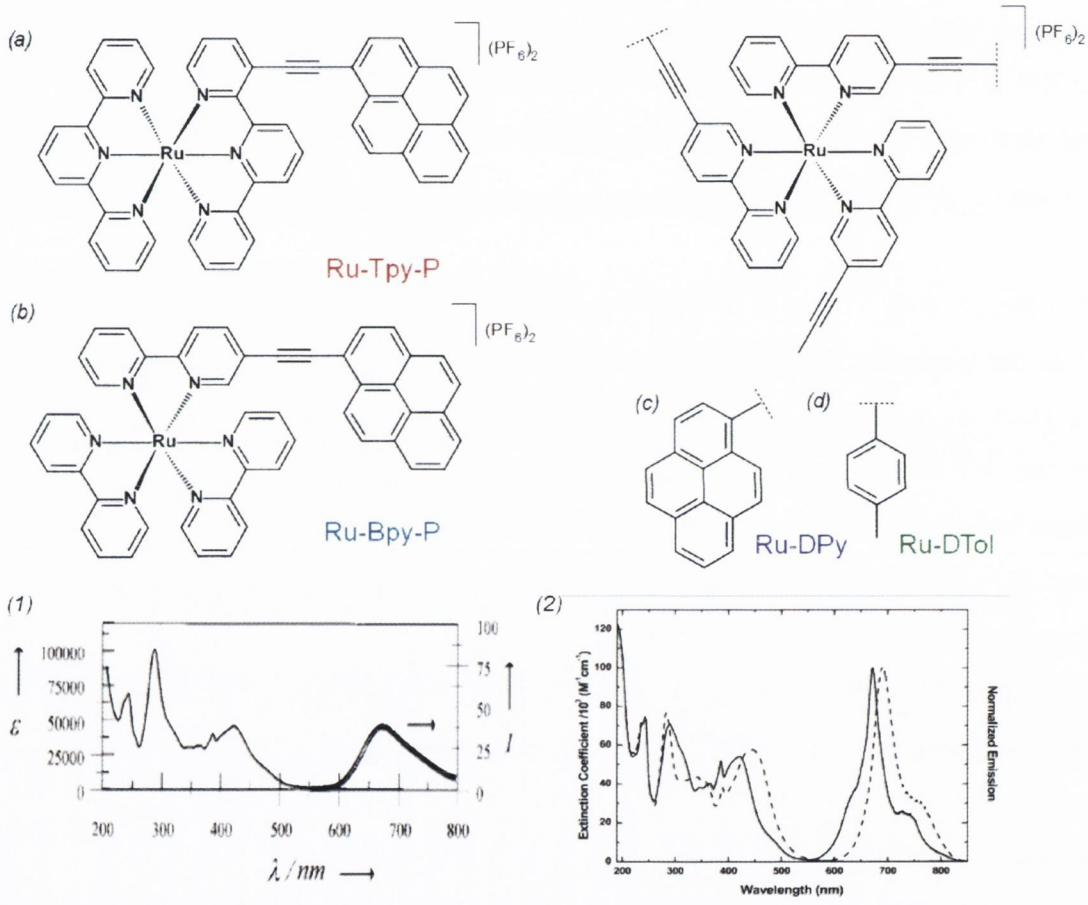


*Figure 2.4: Photoactive Ru(II) complexes (a) and (b) bearing ethynyl pyrene terminal unit*[85] *and Castellano's study of multiple pyrenyl (c) and ethynyltolyl (d) chromophores.*[87] *Included is the absorption and emission data for the Ru(II) bipy derivatives (a) spectrum 1 and (c) spectrum ($CH_3CN$, R.T. ).*

Castellano *et al.* prepared a series of Ru(II) dimine chromophores possessing increasing numbers of ethynylpyrene and ethynyl toluene substituents [**Ru-DPy** and **Ru-DTol**, Figure 2.4]. While the incorporation of ethynyl toluene subunits results in the characteristic $d\pi(Ru) \rightarrow \pi^*(L)$ MLCT excited states, pyrenyl substitution results in $^3$IL

excited states producing room temperature phosphorescence (Figure 2.4, spectrum 2). The increase in conjugation renders the $^3$IL states, relative to the MLCT states, so low in energy that no significant electronic interactions were detected.[88] The photophysical data also displayed no appreciable dependence on the number of appended pyrenyl units, with the only noteworthy influence of the chromophore occuring on the RT emission lifetime measurement, where a ten-fold increase was observed on-going from mono to dipyrenyl substituted bipy. The close proximity of the $^3$MLCT and the $^3$IL states encourages an interaction between the two states making it difficult to assign the photophysics as either pure $^3$MLCT or $^3$IL, an observation that has been previously reported.[89-91] **Ru-DTol** shows a greater dependence with increased substitution, leading to a corresponding hypsochromic shift in absorption wavelength i.e. ($\lambda_{abs}^{max}$ 440 nm → 460 nm → 468 nm, room temperature), and a corresponding red shift in emission wavelength ($\lambda_{em}^{max}$ 675 nm →640 nm →634 nm, room temperature).

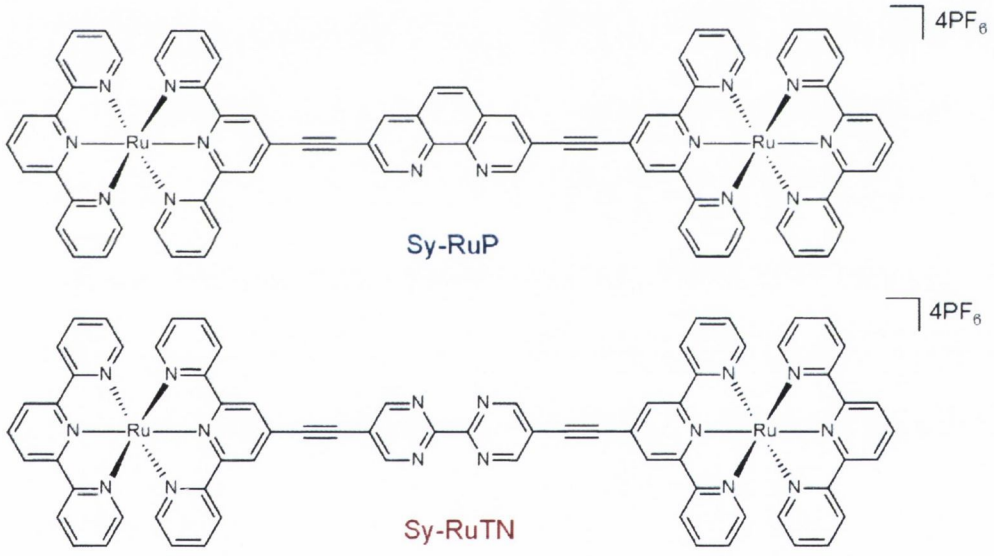


*Figure 2.5: Binuclear Ru(II) polypyridyl complexes featuring central diimine units.*[83, 92, 93]

Designing molecular triads with incorporated diimine bridges confers ligand capability on the central unit (Figure 2.5). This enables fine tuning of the triplet lifetime through complexation. The coordination of various cations to the bridge can lead to increased electron delocalisation at the triplet level. Enhanced energy transfer can take place, as the bridge energy has been lowered below that of the Ru(II) triplet state. Incorporating a rigid spacer such as 1,10-phenanthroline or 2,2'-bipyrimidine also has the ability to lock the geometry of the bridge, which has been proven to further enhance the energy of the triplet lifetime.[92, 93]

The application of luminescent transition metal polypyridyl complexes as molecular probes in bioanalytical tools offers multiple advantages over corresponding organic systems. These include photostability, chemical inertness and photophysical insensitivity to environmental change (e.g. ionic strength, pH). Long-lived excited states facilitate their incorporation into polarization assays, with their large molecular weight inhibiting rotation when excited. The resulting emitted light is therefore more highly polarised then typical organic compounds.

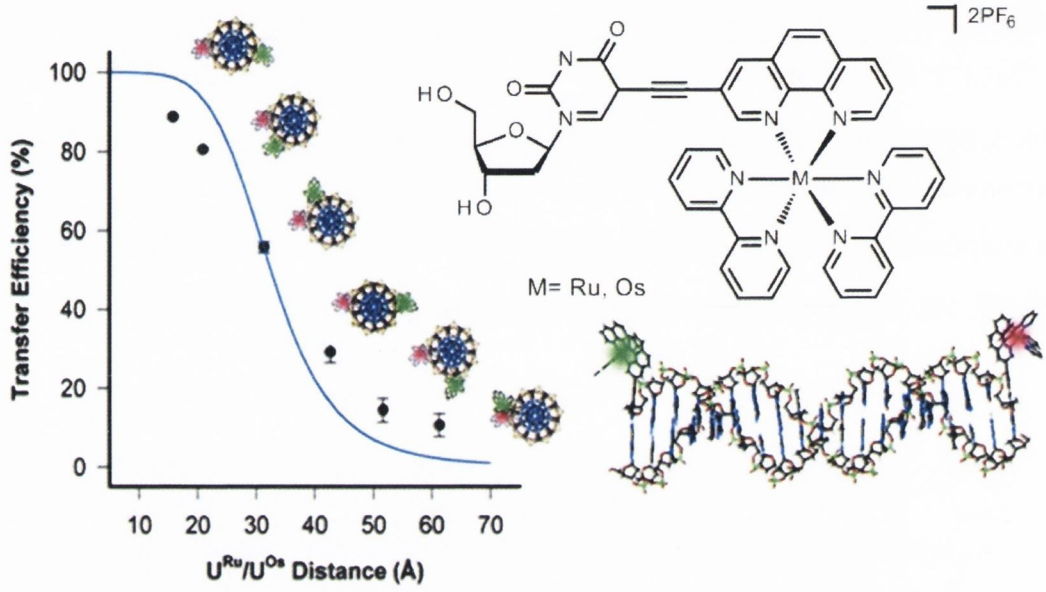


*Figure 2.6: The structure of Tor's 1,10-phenanthroline molecular beacon complexes [Ru(II) and Os(II)]. Luminescence quenching of the Ru(II) complex was observed with increasing distance between the two metal complexes. Figure adapted from reference.*[94]

Tor *et al.* have designed 3-substituted 1,10-phenanthroline complexes which includes an acetylene bridged oligonucleotide (Figure 2.6). This linker allows for communication between the metal centres, increases electronic delocalization due to its positioning along the 3 position of the 1,10-phenanthroline, and prevents back-intercalation into the DNA duplex.[95] [94]Attaching the oligonucleotide in the 5 position allows for projection into the major groove of the DNA double helix structure which minimises distortion and reduces the impact of the complex on the stability of the sequence. Both complexes display solvatochromic behaviour, with a hypsochromic shift observed in their UV-Vis absorption and a bathochromic shift observed in their corresponding emission spectra. This suggests a destabilization of the ground state, and a stabilization of the emissive states, and implies that the emissive charge separated MLCT excited state is located on the substituted 1,10-phenanthroline ligand, and not delocalised on the bipyridyl ligands. Tor and co-workers examined the relationship between luminescence and increased

distance between the two metal centres. The Ru(II) complex was placed on the 5' terminus of a modified DNA duplex. The Os(II) complex was placed on the complimentary DNA strand, and subsequently moved away from the Ru(II) metal complex in three base pair increments. Figure 2.6 shows the correlation between transfer efficiency and the distance between the metal centres. While Förster dipole-dipole energy transfer is considered to be the primary mechanism of interaction between the donor and acceptor, Dexter triplet energy transfer is expected to participate at shorter distances. This unusual behaviour has not been reported for similar systems.[96]

### 2.1.2 Cyclometalated Polypyridyl Ir(III) complexes

#### 2.1.2.1 The synthetic development of iridium(III) cyclometalated complexes.

Although, *cis*-$[Ir(phen)_2Cl_2]Cl$ was first successfully prepared by Chiswell *et al.*[97] Brewer adapted the method in the early 1990's to a synthesis requiring lower temperatures in a $EtOH/H_2O$ reflux. This produced many more diimine derivatives, all of which were isolated in higher yields (up to 70%).[98] The most popular synthesis was reported by Watt's *et al.*[99] Refluxing iridium trichloride hydrate with the required ligand in 2-ethoxyethanol and water for one day gave the dichloro-bridged iridium dimer [Figure 2.7(a)], which can be further reacted with a second ligand in a $CH_2Cl_2$ reflux, and precipitated with an appropriate hexafluorophosphate salt to give the desired $[Ir(N^C)_2(N^N)]^+$ or $[Ir(N^C)_2(N^C)]$ complex. This procedure was later adapted to produce iridium dimers where each iridium centre is surrounded by one N^C and one N^N ligand [Figure 2.7(b)].

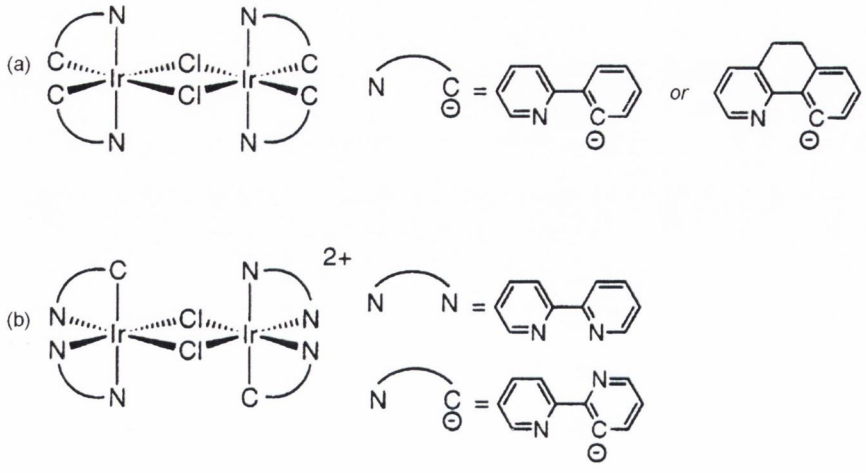


*Figure 2.7: Schematic representation of the dichloro-bridged iridium dimers reported by Watts et al.*[99, 100]

Although the synthesis of cyclometalated iridium(III) complexes was well established in the 1970's, the geometry of these complexes was unknown until crystallographic data on $[Ir(bpy)_2(bpy\text{-}C,N)]^{3+}$ from Wickramasinghe and Serpone was produced.[101] This work revealed that orthometalated carbon atoms remain *cis* to each other, and in an overall *trans* geometry with respect to the N^N ligand. The explanation proposed by Watts from his study of the formation of *fac*-tris $Ir(ppy)_3$ by the displacement of $acac^-$ ligands from $[Ir(acac)_3]$ is now widely accepted. As each successive ppy ligand is added, it is subjected to the *trans* effect from the previously formed Ir-C bond.

### 2.1.2.2 The photophysical properties of Ir(III) cyclometalated complexes

The photophysical and electrochemical properties of iridium(III) complexes can be tuned through careful modification of the cyclometalating and ancillary ligands. Iridium (III) complexes have an added advantage over their corresponding Ru(II) diimine derivatives as they possess increased ligand–field stabilization energy (LFSE), making thermal population of their non-emissive metal-centred states ($^3$MC) more challenging, and producing a reduced value for $k_{nr}$, the magnitude of the non-radiative processes. Cyclometalated iridium(III) complexes are more attractive than their corresponding tris-diimine derivatives due to the enhanced ability of the C^N ligand to back bond to the metal, producing higher energy MC states than diimine derivatives. Although Ir(III) is considered to be isoelectronic with Ru(II), iridium complexes have higher spin-orbit coupling constants which produces an elevated $k_r$ , the rate constant of the radiative processes. These factors enable colour tunability and enhanced splitting of their *d*-orbitals, making them potential candidates for optoelectronic devices. Figure 2.8 (a) illustrates the electronic transitions available for a $d^6$ metal centre containing 2-phenylpyridine type ligands. For Ir(III) complexes, the ligand field splitting is larger than that observed for Ru(II) complexes, which makes the MC levels non-thermally accessible and subsequently non-emissive [Figure 2.8(b)]. The observed MLCT emission for Ir(III) complexes is typically greater than that observed for Ru(II) complexes (2.1 - 3.0 eV *vs* ~2.1 eV). This means that Ir(III) complexes are not affected by the contribution from the MC levels towards the radiationless deactivation of the MLCT emission level that is commonly observed in Ru(II) complexes.

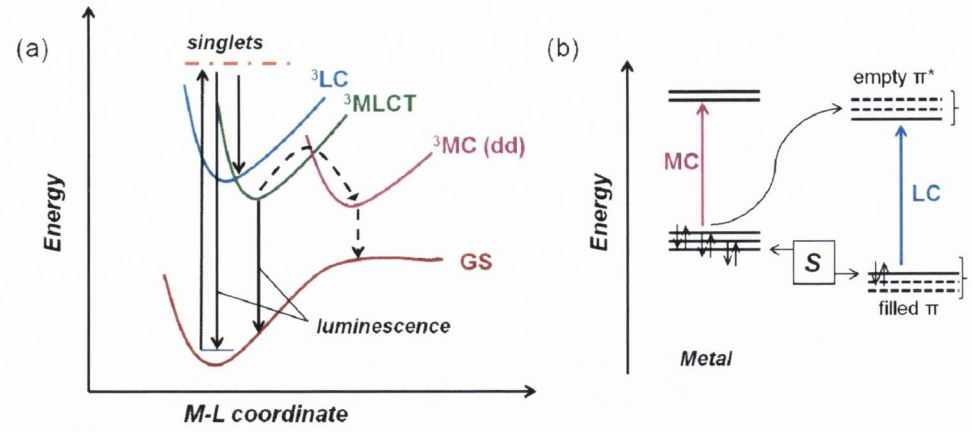


*Figure 2.8: (a) Schematic molecular orbital diagram showing various transitions available for octahedral complex with ppy type ligands. (b) S is a substituent group with the ability to stabilize or destabilise the energy level of the filled d and π orbitals.*

The emissive state of iridium(III) cyclometalated complexes are usually assigned as (i) $^3$MLCT (ii) $^3$LC or (iii) $^3$MLCT/$^3$LC mixed. Analogous to (iii), if a complex displays irreversible oxidation, the emissive state can also be denoted as a sigma bond to ligand charge transfer (SBLCT) state. The MO diagram in Figure 2.9 illustrates the difference between the MLCT and SBLCT state.[102] Unlike the MLCT state, the SBLCT state does not result in oxidation of the metal centre to $Ir^{4+}$. An electron is promoted from the Ir-C bond, which causes the interaction between the metal and the ortho-metalated carbon (highlighted in Figure 2.9) to be weakened. This causes an overall distortion to the geometry of the complex. However, the concept of the "SBLCT" term is not fully endorsed, as the theory does not consider the contribution to the HOMO made by the remainder of the ppy ligand. Therefore, many prefer the overall assignment of this state as the mixed '$^3$MLCT/$^3$LC' state.[103]

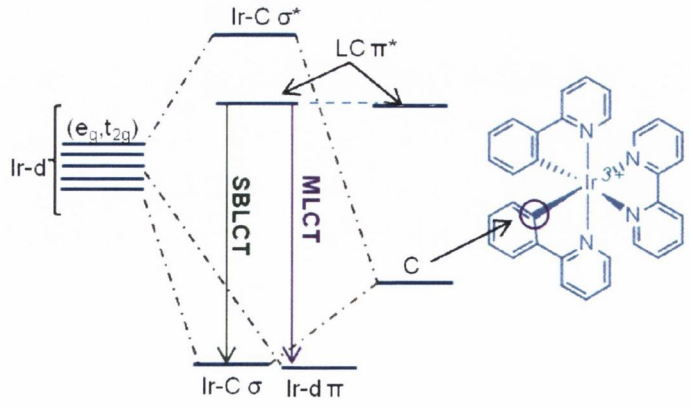


*Figure 2.9: Qualitative MO diagram illustrating SBLCT and MLCT in iridium(III) cyclometalated complex. C refers to the ortho-metalated carbon on the ppy ligand as shown. Adapted from Kirsch-de Mesmaeker and Watts.[102]*

The design of iridium(III) 1,10 phenanthroline derivatives is a relatively under-developed area of research, with literature reports mainly focusing on the 2,7 substituted 1,10-phenanthroline complexes rather than the 3,8 substituted complexes that this research centres on. Functionalisation with azo-crown ethers has lead to applications in metal cation sensing,[104] but iridium(III) 4,7 substituted phenanthroline complexes have also potential use in non linear optics[105] and catalysts for hydrogen transfer.[106] The incorporation of the N^N ligand into cyclometalated iridium complexes is known to improve complex stability over their corresponding *tris*-cyclometalated complexes. The mobility of the counter-ions under an applied bias results in the accretion of the negative charge at one electrode and the diminution of charge at the other. This generates high electric fields around the electrodes causing a corresponding increase in the total electric charge injection into the metal complex, meaning that a lower operating voltage is required, and offers the benefit of necessitating the presence of air stable complexes.[107] These complexes can feature as emitting guests in electrophosphorescent organic/polymer light emitting devices (O/PLEDS), where spin orbit coupling enables the mixing of the singlet and triplet excited states. Light emission is therefore based on contributions from both the singlet and triplet states, making the devices overall more efficient. Incorporating 1,10 phenanthroline units over other diimine derivatives infers additional stability on the complexes. Extending the π-conjugation of the appending units should reduce the non–radiative intermolecular charge recombination, which has been reported by Bolink for similar 4,7-diphenyl 1,10-phenanthroline complexes. [108]

$Eu(tta)_3$-phen is one of the most efficient rare earth molecular phosphors[109], and it and similar systems have found applications in liquid crystals,[110] polymer matrices [111] and sol-gel glasses. [112] Rare earth diketonates are known for their poor photochemical stability and suffer from photodecomposition under standard ultra-violet light. To combat this problem, Nockemann *et al.* have incorporated an ethynyl ferrocene moiety into the backbone of the ligand. This expands the π-system of the ring (*via* the ethynyl bridge) and ferrocene functionalisation improves solubility in organic solvents while shifting the excitation wavelength into the visible region.[113] Schmittel *et al.* have successfully synthesised the corresponding iridium *bis*(2-phenyl-quinoline-$C^2$-$N^1$) complex of the ligand and utilised it as a cyanide and fluoride probe (Figure 2.10).[114] The iridium centre displaces the 1,10-phenanthroline ligand through a classic ligand displacement mechanism and successfully binds the cyanide ions directly to the iridium

centre. **Ir-CN** was synthesised as a control compound. The ECL spectra of **Ir-phFc** and the emission spectra of **Ir-CN** are overlaid in Figure 2.11(a). The complex also displayed selectivity towards fluoride ions. Figure 2.11 (b) shows the ECL emission spectra of 1 (10 μM), after addition of 200 equivalents of a range of anions such as $Cl^-$, $HSO_4^-$ and $AcO^-$. The emission enhancement observed is 60-fold upon addition of the fluoride ions. The detection method for the fluoride ion must be different to the cyanide ion as it has been shown that the complex does not interact with the fluoride ion in its ground state and therefore the ligand displacement mechanism cannot occur.

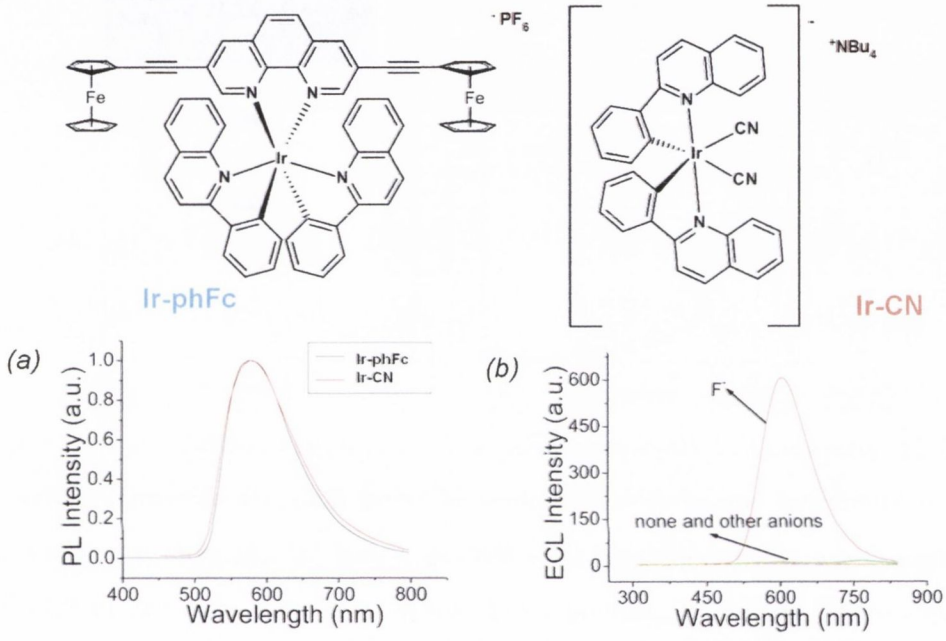


*Figure 2.10: (a) Normalised PL response ($\lambda_{exc}$ 330 nm) of* ***Ir-phFc*** *and control* ***Ir-CN*** *after 180 ±1 min of reaction in 0.1 M Tris $ClO_4$/MeCN (10/90, v/v, pH 7.24), and (b) the selective ECL response of* ***Ir-phFc*** *to fluoride ions vs other anions.* [115]

The development of iridium(III) 1,10-phenanthroline complexes as luminescent sensors has led to their application as labelling reagents for biological substrates and as phosphorescent dyes for living-cell imaging. Improved water-solubility through incorporation of biocompatible non-immunogenic polymers such as poly(ethylene) glycol (PEG), in combination with the iridium centre acting as a luminescent probe, affords a synthetically accessible probe with low toxicity. Yang *et al* successfully developed a water soluble iridium complex of this design, prepared *via* click chemistry (Figure 2.11). The unsymmetrical design allows for further ligand functionality, which enables tuning of the photophysical properties of the complex. The combination of low energy MLCT absorption [Figure 2.11(b) (λ = 450-500 nm)] and intense emission in the visible region [Figure 2.11(c)] in various solvents makes this system suitable for bio-

imaging applications. The complex displays low cytotoxicity, good membrane permeability and showed elective staining when introduced into the cytoplasm of cells [incubation with 0.1mM in phosphate buffered saline (PBS) for 10 mins at 37 °C ($\lambda_{ex}$=488 nm), Figure 2.11 (a)]. [116]

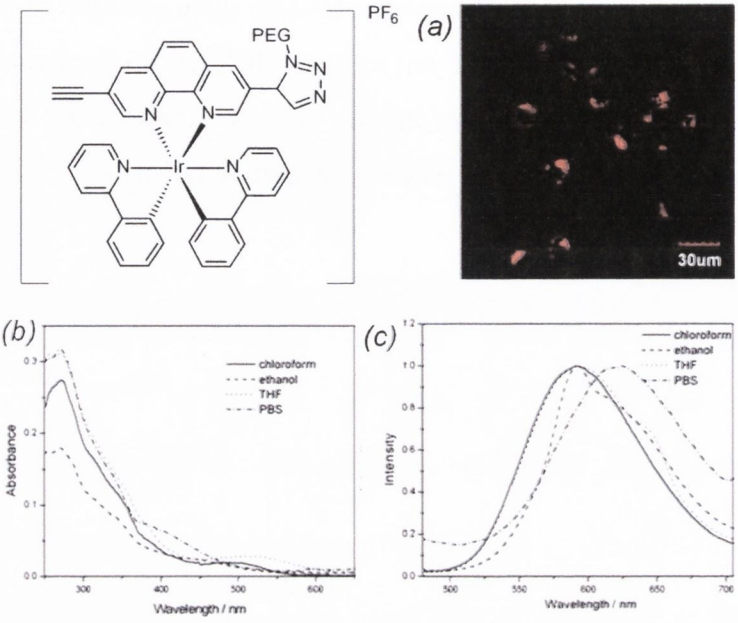


*Figure 2.11: Iridium(III)1,10-phenanthroline PEG complex synthesised by Yang and co-workers (a) confocal luminescence imaging of living KB cells showing elective staining after incubation with the complex ($\lambda_{ex}$=488 nm ) and (b) absorption and (c) emission spectra in various solvents displaying a red shift ($\lambda$ =592 nm →625 nm) in PBS buffer.*[116]

## 2.2 Project Goals: Heteroleptic Ru(II) polypyridyl complexes and cyclometalated Ir(III) complexes of symmetrical 3,8-substituted 1,10-phenanthrolines.

This chapter describes the synthesis and characterisation of a series of Ru(II) and Ir(III) complexes incorporating the symmetric 1,10-phenanthroline series described in Chapter 1, and the photophysical comparison of the communication pathways between the aromatic chromophores and two different metal centres. Although there are many accounts of 1,10-phenanthroline complexes in the literature, no investigation to date has examined the effect of different metal centres on the charge separated excited states created through aryl acetylene substitution in the 3,8 position. To our knowledge, no comparison has been made between two alternative metal centres coordinated to the same 1,10-phenanthroline substituted ligand. This work is designed to build on the investigations of both ruthenium(II) polypyridyl and cyclometalated iridium(III) complexes previously synthesised and studied within the Draper group, as well as initiate further exploration into 1,10-phenanthroline complexes for potential optoelectronic

applications. The synthesis and photophysical properties of [iridium(III)(ppy)$_2$(3,8-dibromo-1,10-phenanthroline)](PF$_6$) has not been previously reported, and has therefore been included in the study. The synthesis of [ruthenium(II)(bpy)$_2$(3,8-dibromo-1,10-phenanthroline)](PF$_6$)$_2$ has already been reported by Tor *et al.* along with a photophysical investigation of the complex. [117]

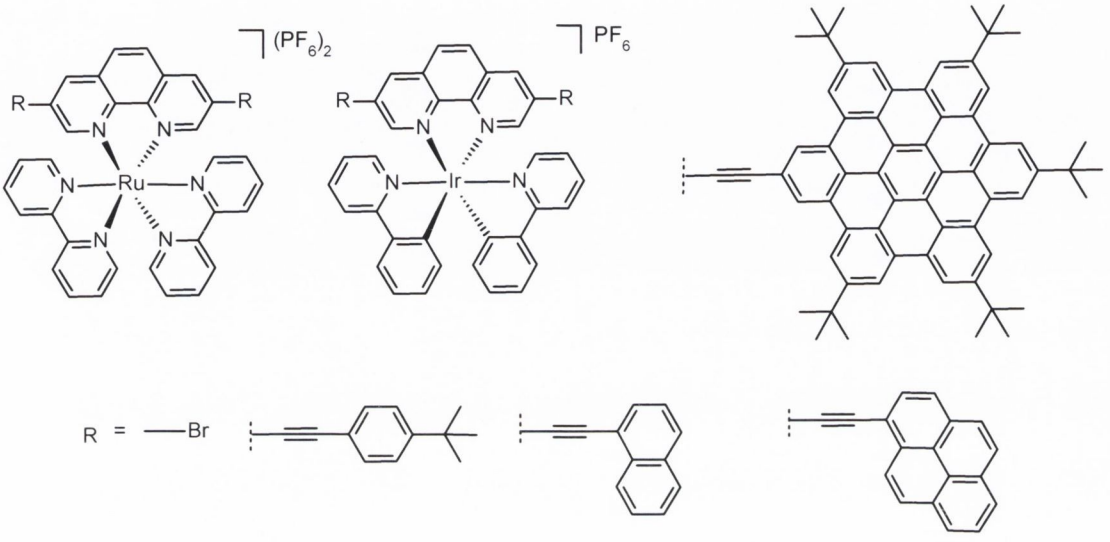


*Figure 2.12: The structure of the symmetrical ruthenium(II) and iridium(III) 1,10-phenanthroline substituted aryl acetylenes to be synthesised and investigated in this study.*

### 2.2.1 Synthesis of [Ru(II)(bipy)$_2$(1,10-phenanthroline)](PF$_6$) complexes

Ruthenium polypyridyl complexes are typically prepared from salts such as [Ru(bpy)$_2$Cl$_2$].H$_2$O or [Ru(dmso)$_4$Cl$_2$]. The size of the ligand field stabilisation energy for second row transition metals dictates higher boiling point solvents are required for the ligand exchange reaction to be successful e.g. ethylene glycol or diethylene glycol monoethyl ether. The complexes are prepared *via* high temperature reflux with the chosen ligand under inert conditions, and can be isolated in the form of the hexafluorophosphate salt. Careful consideration of the metal precursors enables selective exchange of the ligands, whilst maintaining the stereochemistry of the overall complex. The thermal stability of Ru(II) polypyridyl complexes is extremely high, and the synthetic behaviour of the coordinated ligand is analogous to the uncoordinated ligand. These properties make Ru(II) polypyridyl complexes favourable for a wide range of commercial applications such as molecular electronics and biosensors.

### 2.2.1.1 Synthetic route A: Synthesis of Ru(II) 1,10-phenanthroline complexes from *cis*-Ru(II)(bpy)$_2$Cl$_2$

The initial attempts to synthesise the ruthenium(II) bipyridyl complexes **8**, **9**, **10**, and **11** were based on previously reported methods, using ethylene glycol as solvent.[118, 119] Many of the aryl acetylenes were poorly soluble, despite heating the reaction mixture to ~ 60 °C before addition of the *cis*-Ru(bpy)$_2$Cl$_2$ salt. This was circumvented by the addition of either acetone or ethanol (~3 mL) to the ethylene glycol. All complexes were obtained in yields above 70 %, however, as previously discussed in Chapter 1, copper coordination to the 1,10-phenanthroline centre resulted in compromised overall yields for the ligands, thereby reducing the scale of the reaction for all complexes.

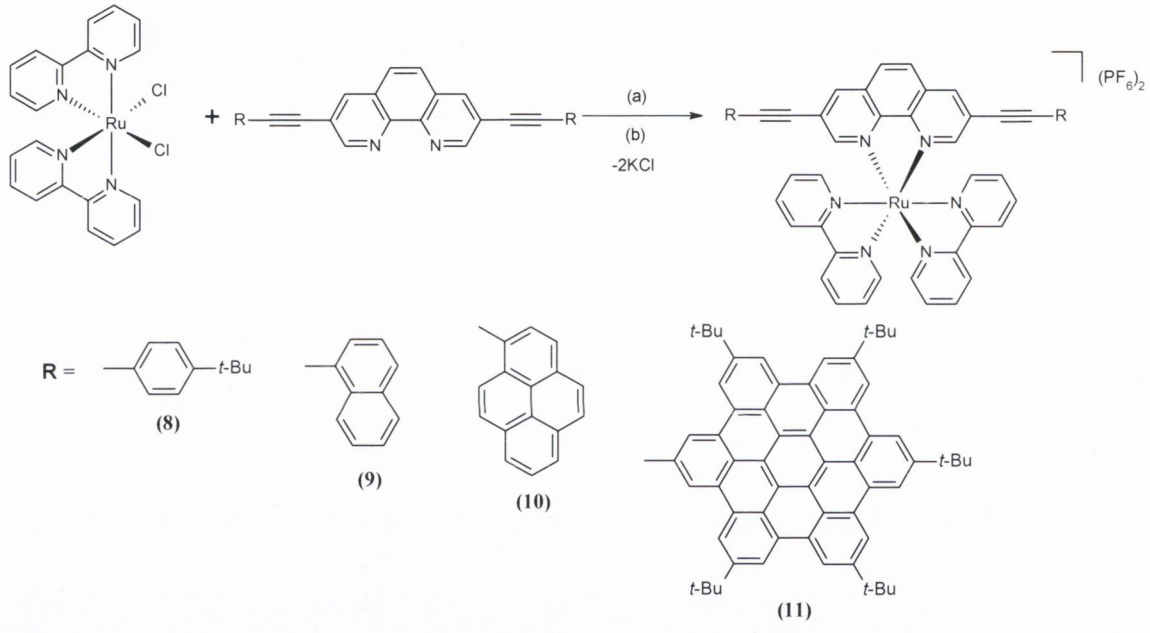


*Scheme 2.1: Synthetic route **A** to Ru(II) heteroleptic complexes (a) ethylene glycol, 150 °C, argon, 16 hours. (b) Sat. aqueous $KPF_6$*

### 2.2.1.2 Synthetic route B: Direct Sonogashira coupling of aryl acetylenes to [Ru(II)(bpy)$_2$(3,8-dibromo-1,10-phenanthroline)] ($PF_6$)

The synthesis of [(Ru(bpy)$_2$(3,8-dibromo-1,10-phenanthroline)]($PF_6$)$_2$ has been previously reported, and the direct coupling to Ru(II) complexes has be successfully utilised for bipyridyl and 1,10-phenanthroline ligands. [31, 87, 88] In order to optimise the final yield of all of the complexes, a second synthetic route was proposed. 3,8-dibromo-1,10-phenanthroline was reacted with Ru(bpy)$_2$Cl$_2$.H$_2$O, and six coordinate species was isolated. To aid the solubility of 3,8-dibromo-1,10-phenanthroline, diethylene glycol monoethyl ether and acetone (4:1, v/v) were chosen as solvents for the reaction.The desired ruthenium(II) complex was isolated by direct precipitation with saturated

aqueous $KPF_6$ from the crude reaction mixture in a yield of 79%. The Sonogashira cross coupling of each of the substituted aryl acetylenes to [Ru(bpy)$_2$(3,8-dibromo-1,10-phenanthroline)] $(PF_6)_2$ was first attempted using the microwave synthesis described in Chapter 1 to prepare the ligands. Despite multiple attempts, the starting materials were recovered each time, however this method has been successfully adapted for the coupling of 1-ethynylsilane to the [Ru(bpy)$_2$(3,8-dibromo-1,10-phenanthroline)] $(PF_6)_2$. Traditional methods were then employed and optimised yields were finally achieved using still-dried, degassed DMF: $iPr_2NH$ (2:1, v/v) as solvents. The complexes were purified by silica column chromatography using acetonitrile: $KNO_3$: $H_2O$ as eluent, with the exception of the HBC acetylene complex (**11**). The poor solubility of the complex was deemed to be unsuitable for any chromatographic purification methods, and it was therefore isolated by repeated precipitations from ethylene glycol, and washing with diethyl ether. All of the complexes were obtained in yields above 65%, as either dark orange or brick-red crystalline powders.

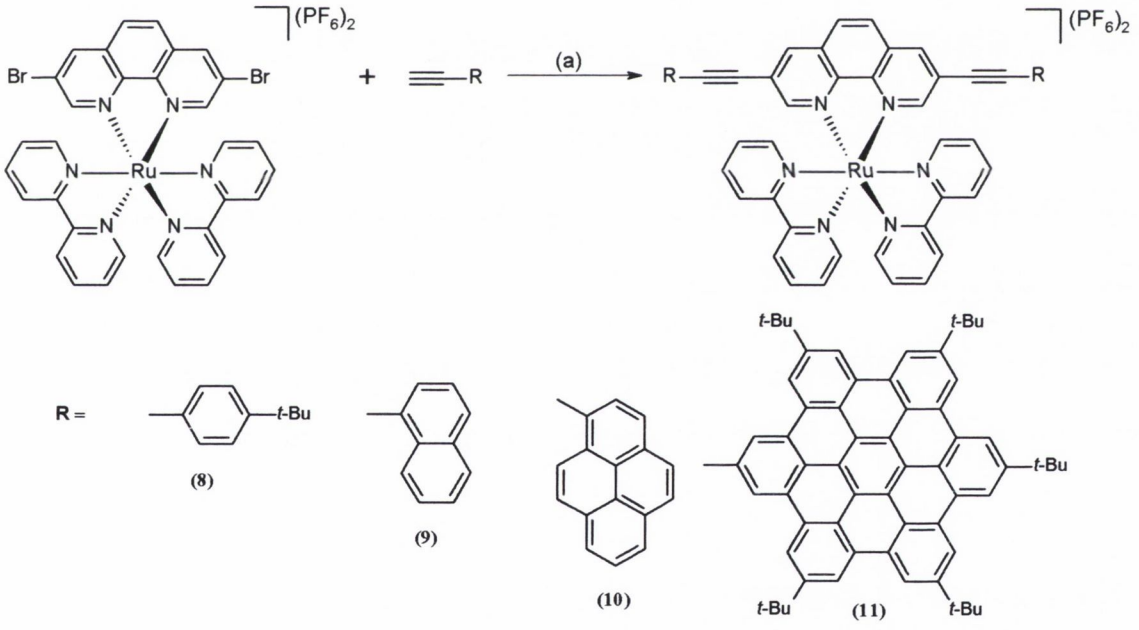


*Scheme 2.2: Synthetic route B adopted in the synthesis of the Ru(II) complexes* ***8, 9, 10, 11*** *through Sonogashira cross-coupling, (a) $Pd(PPh_3)_2Cl_2$ (12 mol%), CuI (12 mol%), DMF: $^iPr_2NH$ (2:1, v/v).*

MALDI-TOF mass spectral data for all of the complexes in either $CH_3CN$ or $CH_2Cl_2$ revealed a major peak which correlates to the $[M-(2PF_6)]^{2+}$ cation. This indicates the displacement of two $PF_6^-$ counterions from the cationic species. The mass spectral data displays ½ m.u. intervals which is consistent with a molecular ion with a $2^+$ charge. The

characteristic Ru(II) isotopic distribution pattern was observed for all complexes in the series. A second peak was also observed for all complexes and identified as the $[M-(PF_6)]^+$ ion.

*Table 2.1: Mass spectrometry analysis for each of the four Ru(II) polypyridyl complexes*

| | Molecular Ion | Formula | Found *m/z* (%) | Calculated *m/z* |
|---|---|---|---|---|
| **8** | $[M-2(PF_6)]^{2+}$ | $[C_{56}H_{48}N_6Ru]^{2+}$ | 908.2979 | 908.2984 |
| | $[M-(PF_6)]^+$ | $[C_{56}H_{48}F_6N_6PRu]^+$ | 1051.2623 | 1051.2626 |
| **9** | $[M-2(PF_6)]^{2+}$ | $[C_{56}H_{36}N_6Ru]^{2+}$ | 894.2026 | 894.2045 |
| | $[M-(PF_6)]^+$ | $[C_{56}H_{36}F_6N_6PRu]^+$ | 1039.1493 | 1039.1512 |
| **10** | $[M-2(PF_6)]^{2+}$ | $[C_{71}H_{52}N_6Ru]^{2+}$ | 1045.2590 | 1045.2593 |
| | $[M-(PF_6)]^+$ | $[C_{71}H_{52}F_6N_6PRu]^+$ | 1190.1436 | 1190.1434 |
| **11** | $[M-2(PF_6)]^{2+}$ | $[C_{160}H_{136}N_6Ru]^{2+}$ | 2242.9812 | 2242.9870 |
| | $[M-(PF_6)]^+$ | $[C_{160}H_{136}F_6N_6PRu]^{2+}$ | 2387.3112 | 2387.3127 |

**2.2.1.3 IR spectroscopic data for ruthenium(II) complexes 8-11**

To further verify the presence of the aryl-ethynyl bond, each of the four Ru (II) complexes were measured by IR spectroscopy. The ν(C≡C) stretching frequency was observed in all four complexes in the region of 2200 $cm^{-1}$ (Table 2.2). As expected, the reported C-Br stretching frequency for [Ru(II) 3,8-dibromo-1,10-phenanthroline] $(PF_6)_2$ at 664 $cm^{-1}$ is no longer evident in any of the four spectra, further indicating successful cross-coupling to the starting material. Finally, multiple weak bands appear in the region of 1400-1600 $cm^{-1}$. These are assigned as aromatic C=C stretching frequencies from both the 1,10-phenanthroline moiety and the aryl chromophores, thus further supporting the presence of the target complexes.

*Table 2.2: IR spectroscopic data for ruthenium(II) complexes **8-12***

| | IR [ν (C≡C), $cm^{-1}$] |
|---|---|
| **8** | 2210 |
| **9** | 2202 |
| **10** | 2199 |
| **11** | 2195 |

### 2.2.1.4 NMR spectroscopic characterisation of 8, 9, 10, and 11

The spectroscopic characterisation of $[(Ru(bpy_2)(L)](PF_6)_2$ complexes **8**, **9**, **10**, and **11** was achieved through a series of multiple NMR 1D and 2D experiments. The symmetrical nature of the complexes aided the characterisation of the aryl acetylene 1,10-phenanthroline and each of the four pyridyl rings ligands. For the sake of brevity, only some of the 2D experiments used to assign the complexes have been included in the figures provided. The complexes will be discussed individually at first, and an overall discussion on the trends observed within the characterisation e.g. the acetylenic carbons signals, and the effect of larger chromophores on the 1,10-phenanthroline signals will be included at the end of this section.

### 2.2.1.5 The $^{1}H$ and $^{13}C$ NMR spectra of 8, 9 10 and 11

Figure 2.13 shows the fully assigned $^{1}H$ NMR spectra of the symmetrical ruthenium bipyridyl complex **8**. The three signals at 8.73 ppm, 8.28 ppm and 8.19 ppm correspond to the proton signals on the 1,10-phenanthroline ring. Each of the signals appear as broad doublets, due to their proximity to the nitrogen on the ring ($^{3}J$ = 1.2 Hz).

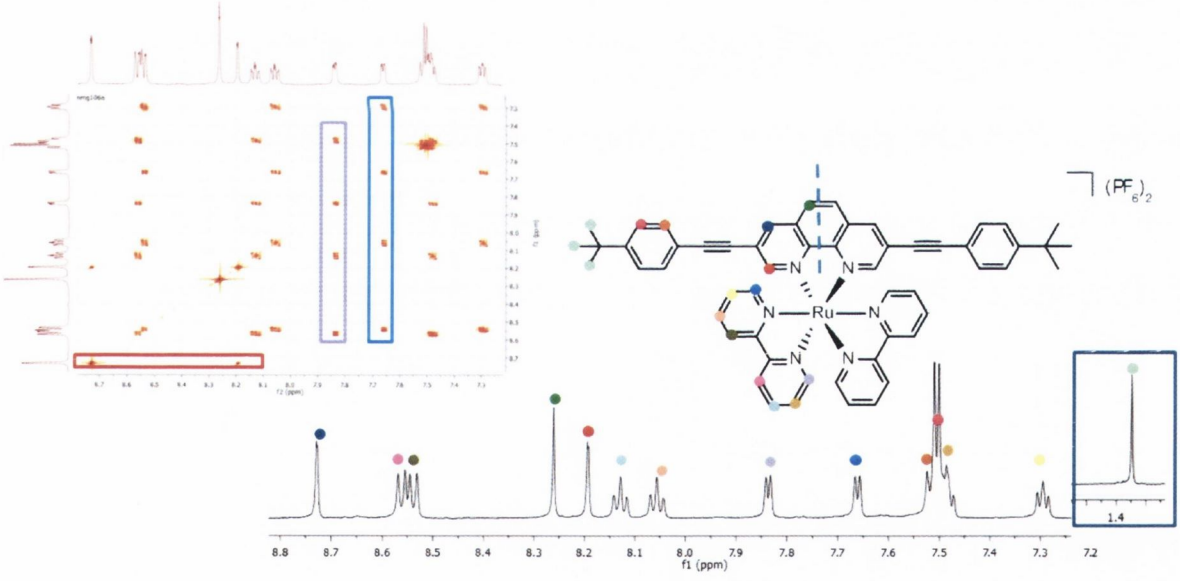


*Figure 2.13: $^{1}H$ NMR spectrum of **8** in $CD_3CN$, with inset showing aliphatic region with one tert-butyl environment. Inset $^{1}H$-$^{1}H$ COSY experiment used to identify the bipy spin systems (labelling refers to the colour of the proton adjacent to the N ring for each respective ring) (600 MHz, $CD_3CN$, R.T.)*

Examination of the $^{13}C$-$^{1}H$ COSY 2D experiment reveals that the proton alpha to the nitrogen is no longer the most deshielded proton i.e. the carbon signal located at δ = 153 ppm couples to the proton appearing at 8.19 ppm and is therefore assigned as (●). The

doublet at δ = 8.73 ppm (●) can be assigned based on its correlation to a more deshielded $^{13}C$ signal (δ = 138 ppm) than the doublet at 8.28 ppm (●). This is due to its proximity to the acetylene linker in the ligand framework. The doublets appearing at δ = 7.85 ppm ($^3J_{HH}$ = 6 Hz) and 7.65 ppm ($^3J_{HH}$ = 6 Hz) are assigned as the protons next to the nitrogens on the pyridyl rings, and have also been distinguished based on their carbon signals at δ = 152 ppm (● and ●, Figure 2.14). Two overlapping doublets appear at δ = 8.55 ppm must be attributed to the protons at the back of the bipy ligand, with one correlating to each bipyridyl spin system in the $^1H$-$^1H$ COSY experiment (Figure 2.13).[120,121] Selective TOCSY analysis was used to confirm the identity of the remaining four triplets. The previously assigned resonances at δ = 7.85 ppm and 7.65 ppm were irradiated and showed an intense correlation with the two triplets at δ = 7.45 ppm (●) and 7.45 ppm (●), which confirms the pair as " nearest neighbours". Weaker intensity signals were observed at δ = 8.15 and 8.05 ppm, indicating that the two triplets are situated further away on the phenyl rings. The protons on the *tert*-butyl phenyl ring (● and ●) have shifted slightly upfield upon complexation and now appear as a multiplet at δ =7.5 ppm. There is one *tert*-butyl signal at δ =1.38 ppm, integrating for 18 H as expected, which further confirms the symmetrical nature of the complex (inset, Figure 2.13 ●).

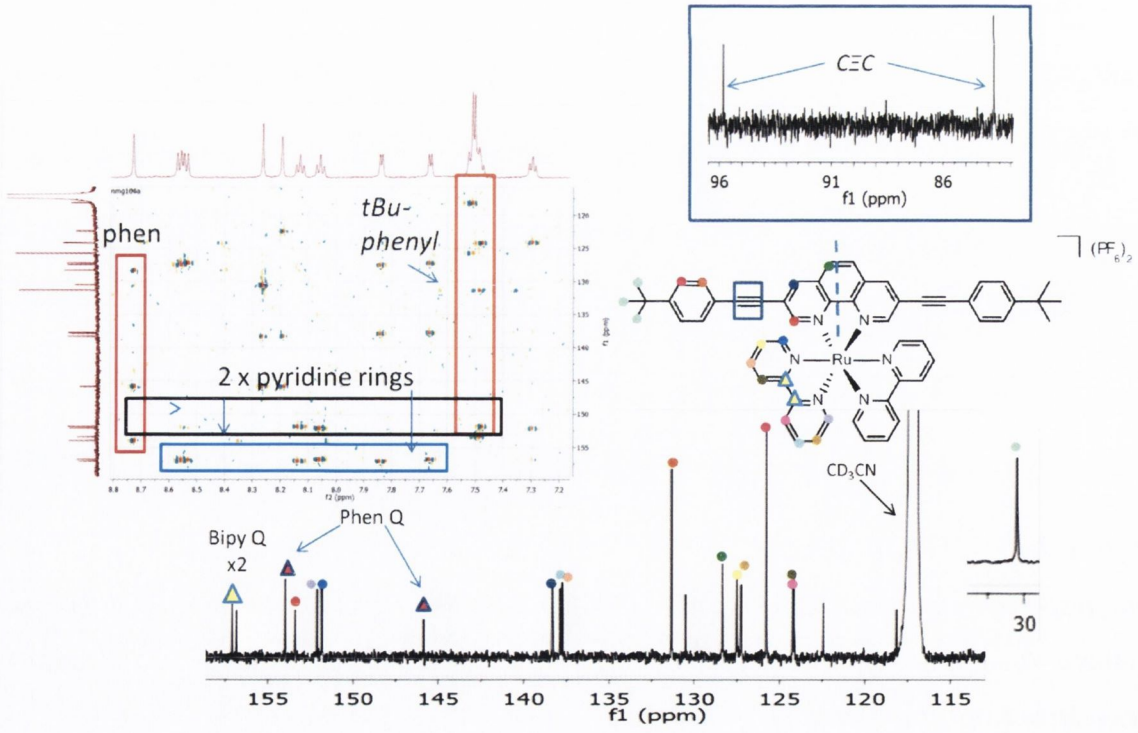


*Figure 2.14: The fully assigned $^{13}C$ spectrum of **8** with inset showing HMBC experiment to allocate the remaining quaternary carbon signals on the individual rings (151 MHz, $CD_3CN$, R.T.).*

The assignment of the $^{13}$ C spectrum of **8** was achieved through a series of DEPT and HMBC (Heteronuclear Multiple Bond Connectivity) experiments. HMBC is a highly sensitive 2D experiment which incorporates a long range pulse delay into the HSQC pulse to enable the identification of one bond correlations, which can extend to neighbouring quaternary carbon signals. In this study, it enabled not only the identification of two quaternary carbons on the 1,10-phenanthroline core at $\delta$ = 146 ppm and 153 ppm but also the two quaternary carbons on the bipyridyl rings (Figure 2.14). The two acetylenic carbon signals appear at $\delta$ = 95.85ppm and 83.93 ppm and are shown in the inset.

The $^{1}$H NMR of the naphthyl derivative **9** is presented in Figure 2.15 and consists of eighteen well defined signals, each integrating for 2H. The bipyridyl spin systems were identified in a method analogous to **8**. The three doublets corresponding to the 1,10-phenanthroline ring are slightly deshielded with respect their corresponding signals in **8** and now appear at 8.93 ppm (●), 8.45 ppm (●) and 8.30 ppm (●). The $^{3}J$ coupling constants for all three doublets is unaffected by the presence of a more conjugated aryl ring, and remains at 1.2 Hz for each doublet.

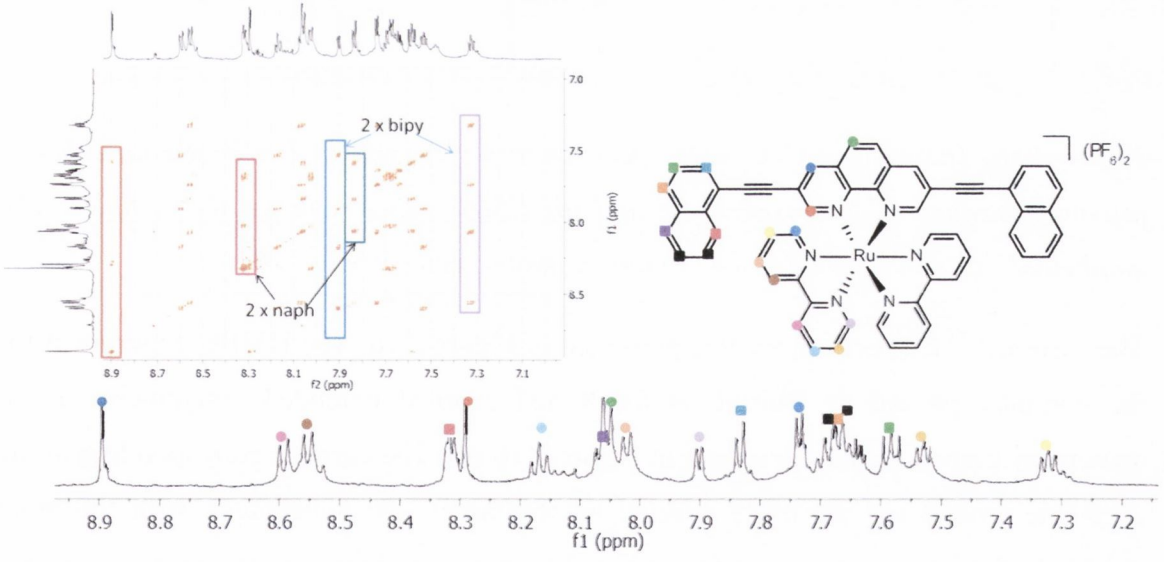


*Figure 2.15: Aromatic region of the $^{1}$H NMR spectrum of* ***9****. Also shown is the $^{1}$H-$^{1}$H COSY experiment of* ***9*** *showing the identification of the various spin systems (600 MHz, $CD_3CN$, R.T.).*

The seven protons on the naphthyl ring appear as two spin systems as expected, however the two triplets on the four spin system appear as a multiplet at $\delta$ = 7.65 ppm. The proton adjacent to the acetylene in the four spin system has been identified as the most

deshielded doublet, appearing at δ = 8.25 ppm (■).The $^{1}$H-$^{1}$H COSY experiment indicates that the remaining doublet on this spin system is buried within the multiplet at δ = 8.05 ppm.

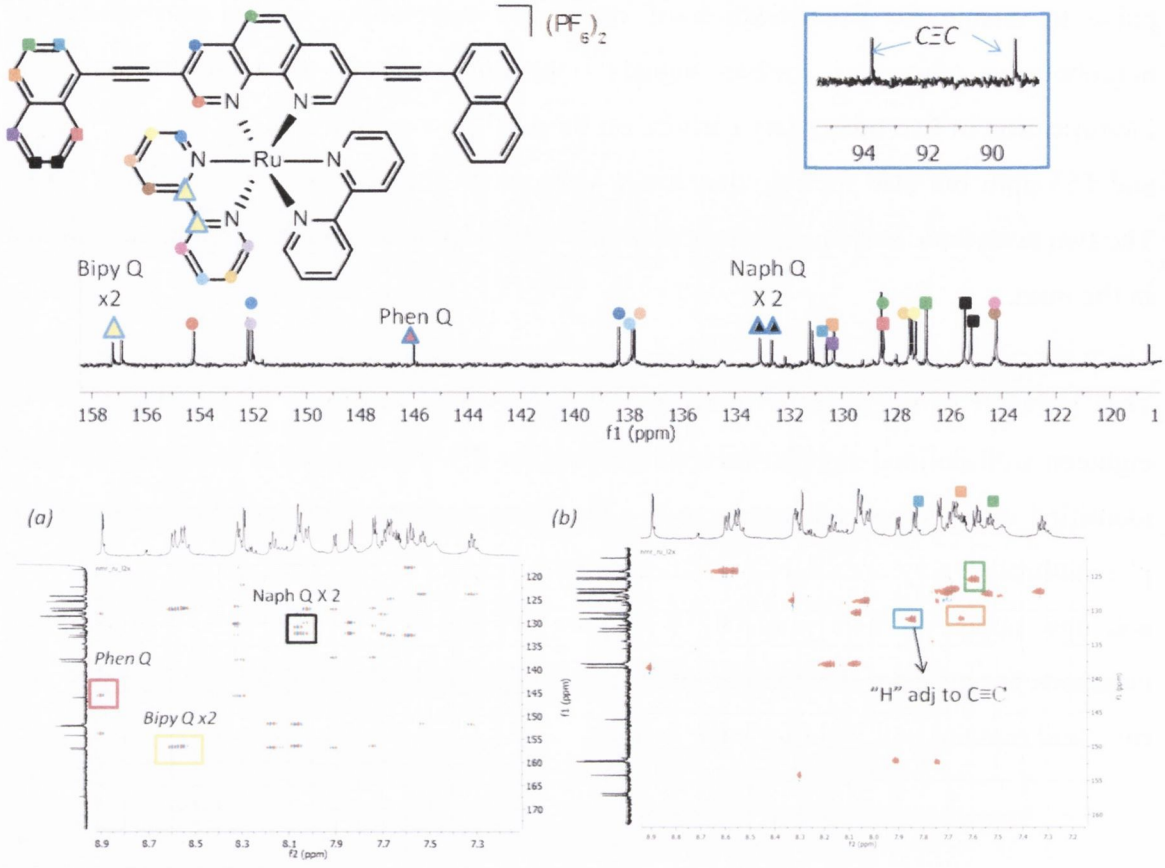


*Figure 2.16: The assigned $^{13}$C NMR spectrum of* ***9*** *(151 MHz, $CD_3CN$, R.T.).and below (a)complimentary HMBC experiment and (b) HSQC experiment for the complex. The unlabelled $^{13}$C signals refer to the remaining quaternary carbons in* ***9****.*

The assigned $^{13}$C spectrum for **9** is presented in Figure 2.16. The HMBC experiment for the complex proved as fruitful as for **8** and enabled extended assignment of the quaternary carbon signals as shown in Figure 2.16 (a). The carbons corresponding to the acetylene moiety are the most affected by the larger aryl substituent, with the more shielded of the two now appearing at δ = 89.2 ppm, as shown in the inset, *versus* δ = 83.93 ppm. This is due to the omission of the electron-donating *tert*-butyl substituent from the aryl moiety which causes the acetylene carbon to become more deshielded with respect to its corresponding signal in **8**. Although selective TOCSY experiments on the naphthyl moiety were attempted, no affirmative data was obtained from the analysis. For example, irradiation of the resonance at δ =7.9 ppm generated multiple overlapping signals of various intensities between δ = 7.7 ppm and 7.5 ppm. However, investigation of the HSQC experiment presented in Figure 2.16 (b) revealed that the doublet at δ =

7.85 ppm correlated to a $^{13}C$ resonance which is marginally more deshielded than the doublet residing in the multiplet at $\delta$ = 7.7 – 7.5 ppm. It is therefore more likely that this is the proton adjacent to the acetylene linker, and on this basis has been assigned as (■).

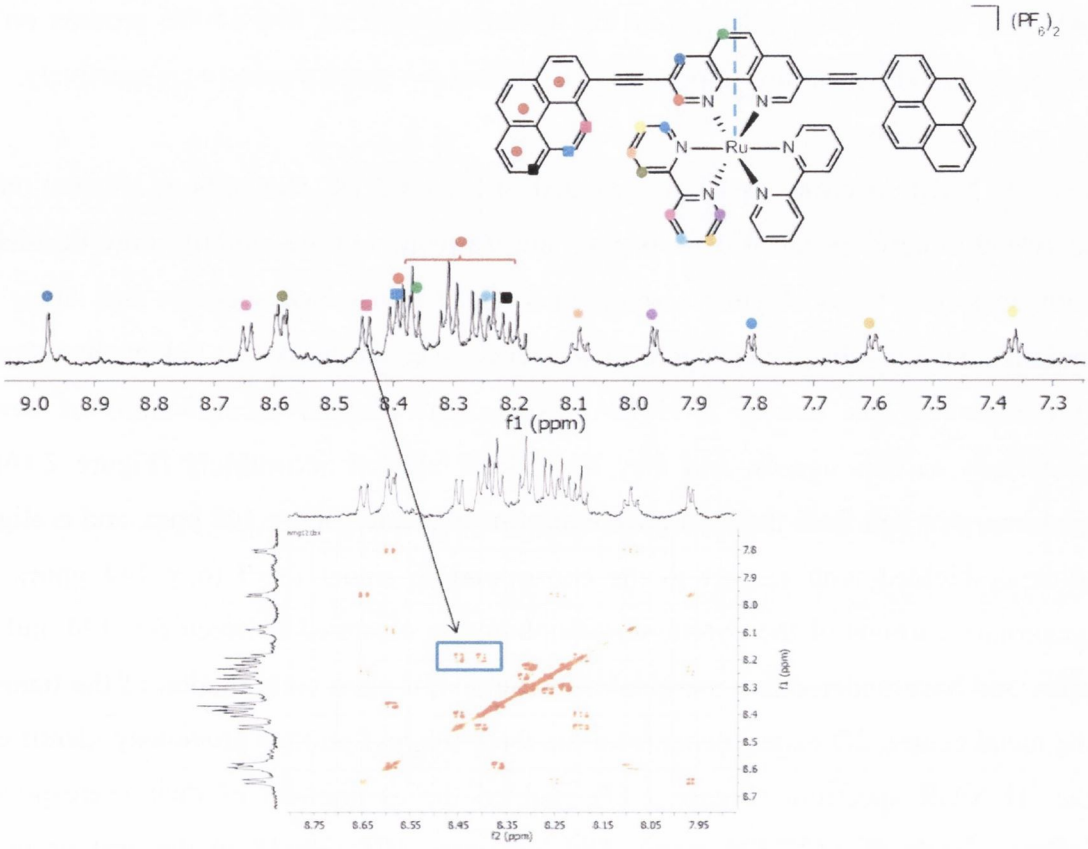


*Figure 2.17: Aromatic region of the $^{1}H$ NMR spectrum of **10** with inset $^{1}H$-$^{1}H$ COSY showing the only identifiable spin system on the pyrene unit (600 MHz, $CD_3CN$, R.T.).*

The ruthenium(II) complex **10** is only moderately soluble in deuterated solvents such as $CD_3CN$. At higher concentrations, the complex exhibits a high degree of aggregation. The $^{1}H$ NMR presented in Figure 2.17 was obtained after continuous sonication and heating. The doublets and triplets of the pyrenyl moiety appear as an undefined multiplet between $\delta$ = 8.45 ppm and 8.2 ppm, and superimpose two of the three 1,10-phenanthroline signals. This prevented the full assignment of the pyrene pendant, however, one spin system has been identified as indicated by the highlighted region of the $^{1}H$-$^{1}H$ COSY presented in Figure 2.17. As observed in the $^{1}H$ NMR of **9**, this corresponds to the protons in the two spin system adjacent to the acetylene [$\delta$ = 8.45 ppm (■) and $\delta$ = 8.4 ppm (■)]. This is verified by a similar assignment made by Zhao *et al.* for the 3-pyrenyl-1,10-phenanthroline derivative of the complex. [122] Full assignment of the pyrenyl chromophore is typically not achieved, with many similar systems in the literature reporting a general assignment of the unit as a whole.[123, 124] The proton signals

attributed to the bipyridyl moieties were assigned in the same manner as complexes **8** and **9**. The influence of the more conjugated aryl group emerges with the proton adjacent to the acetylene more deshielded than the equivalent proton in **8** and **9** i.e. δ = 8.95 ppm (●). The trend is also reflected in the downfield shift of two of the protons on the auxiliary ligand which now appear at δ =8.65 ppm (●) and 8.6 ppm (●) respectively.

The $^{13}C$ NMR spectrum of **10** is presented in Figure 2.18. The carbons situated on the acetylene moiety appear at δ = 96 ppm and 91 ppm, and are slightly more deshielded with respect to the analogous carbons in **8** and **9**. This trend suggests that larger aryl moieties have a substantial degree of influence over the acetylene linker, than smaller chromophores. As before, a HMBC experiment enabled identification of several quaternary carbon signals, and they have been labelled accordingly (Figure 2.16). A quaternary carbon from the 1,10-phenanthroline is located at δ = 147 ppm, and is slightly more deshielded with respect to the corresponding signal for **9** (δ = 144 ppm). The quaternary carbons of the pyrene chromophore are clustered between δ = 134 and 131 ppm, and have undergone a marginal downfield shift upon coordination of the ligand to the metal centre. 2D experiments from the three pyrenyl protons previously identified in the $^{1}H$ NMR spectrum (Figure 2.17) enabled the assignment of their corresponding carbon signals (δ =127-126 ppm). The remaining CH signals on the aryl group are centred at δ =128 ppm (●).

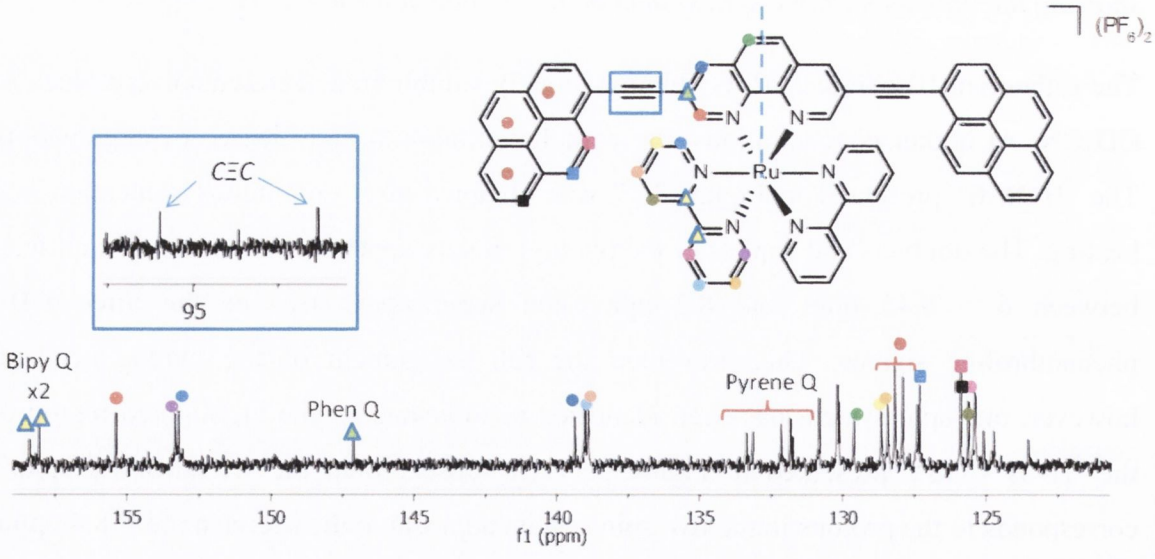


*Figure 2.18: The assigned $^{13}C$ NMR spectrum of **10** with inset verifying the presence of two acetylenic carbons (151 MHz, $CD_3CN$, R.T.).*

Table 2.3 contains the chemical shifts of each of the protons residing on the 1,0-phenanthroline moiety for the complexes **8-10** in $CD_3CN$. Each of the C-H signals become marginally more deshielded as the size of the attached aryl pendent increases. The effect is more significant on-going from **8** to **9**, than **9** to **10**. The $^{13}C$ signals for the quaternary carbons on the acetylene moiety are also presented in Table 2.3. In general, the position of the more deshielded carbon resides between $\delta$ = 96-94 ppm. More variation is evident for the second quaternary signal, which appears to be significantly influenced by the appending aryl moiety. This is attributed to a combination of increasing aryl size which causes the signal to become more deshielded e.g (**9** vs **10**) and the contrasting shielding affect of the electron-donating *tert*-butyl group on the phenyl ring in **8**.[45]

*Table 2.3: The relative $^{1}H$ positions of the three protons on the 1,10-phenanthroline moiety ($CD_3CN$, 600MHz, R.T.) and the $^{13}C$ signals for the two acetylenic carbons for each complex ($CD_3CN$, 151 MHz, R.T.)*

| | ● $\delta$ $^{1}H$ and $^{13}C$ (ppm) | ● $\delta$ $^{1}H$ and $^{13}C$ (ppm) | ● $\delta$ $^{1}H$ and $^{13}C$ (ppm) | $C\equiv C$ $\delta$ $^{13}C$ (ppm) |
|---|---|---|---|---|
| **8** | 8.19, 154.5 | 8.73, 138.6 | 8.28, 128.5 | 95.9, 83.9 |
| **9** | 8.38, 154.3 | 8.98, 138.7 | 8.30, 129.8 | 93.7, 89.2 |
| **10** | 8.39, 155.2 | 8.98, 139.4 | 8.36, 129.7 | 96.1, 91.3 |

The HBC functionalised derivative **11** undergoes considerable stacking in solution and is poorily soluble in all available deuterated solvents. Despite continuous sonication, and heating, the $^{1}H$ NMR spectrum obtained for the complex showed a broad downfield signal centred at $\delta$ = 9.25 ppm, which overlays the majority of the downfield aromatic region (Figure 2.19). Three poorily visible signals, which have been attributed to the bipyridyl moiety are also detectable at $\delta$ = 7.25 ppm, as well as three *tert*-butyl signals in the aliphatic region of the spectrum. The T.L.C for the complex confirms the presence of one product, however the integration values for the *tert*-butyl region do not correlate with the integration of the broad band in the aromatic region. This is attributed a significant amounts of aggregation. The poor solubility of **11** also prevented the $^{13}C$ NMR spectrum for the complex from being obtained.

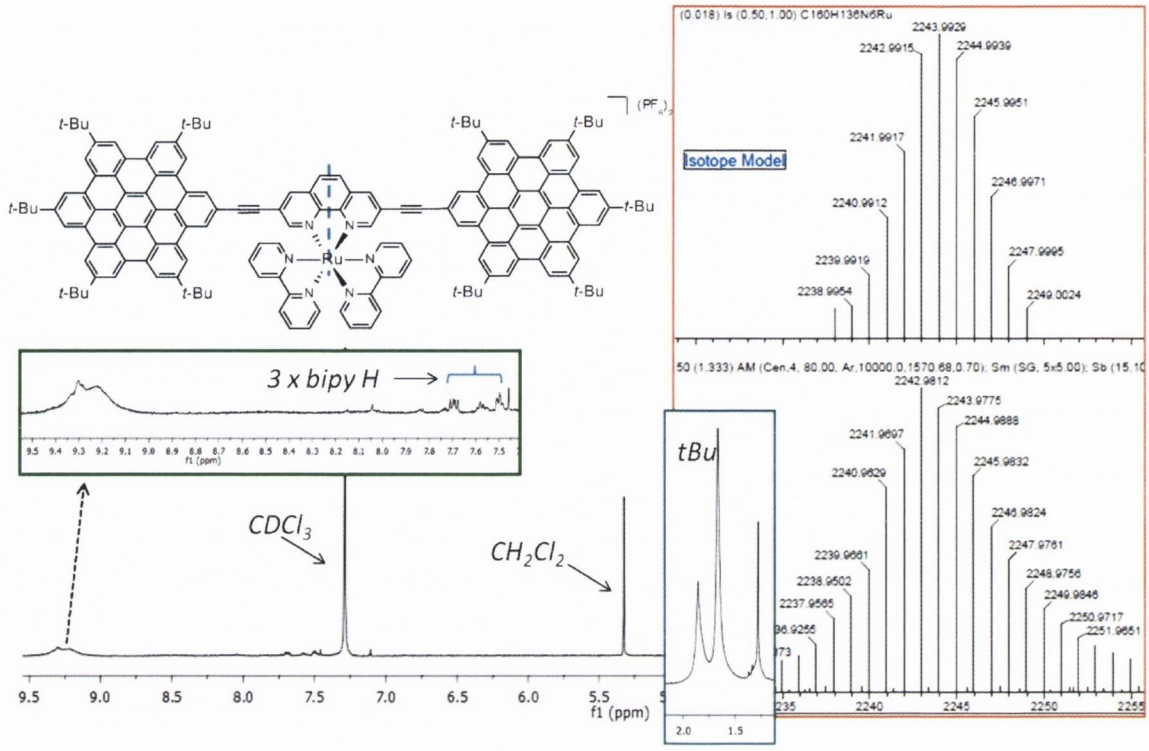


*Figure 2.19: The $^{1}H$ NMR spectrum (600 MHz, $CDCl_3$, R.T. ), along with the isotopic model and magnified MALDI-TOF analysis for complex **11** confirming the presence of the desired product.*

MALDI-TOF analysis was also obtained for the product and is presented in Figure 2.19 along with the isotope model calculated for the complex ($[C_{160}H_{136}N_6Ru]^{2+}$found *m/z* = 2242.9812 calculated *m/z* = 2242.9870). No evidence of the monosubstituted product was observed, or any residual traces of ethynyl-HBC. This further supports the observation that the inconsistency in integration values in the $^{1}H$ NMR spectrum is due to aggregation of the complex.

### 2.2.2 UV-Visible Absorption Spectra of Ru(II)(3, 8-aryl acetylene-1,10-phenanthroline) complexes.

The overlaid UV-Vis absorption spectra of Ru(II) polypyridyl complexes **8-11** are presented in Figure 2.20. This is followed by a summary of their absorption maxima, and corresponding extinction coefficients in Table 2.4. The absorption profiles of the four complexes contain high energy transitions ($\lambda$ = 250 - 300 nm) which can be assigned as imine and acetylene based IL transitions and are evident for all four of the complexes. Ru(II) bipyridyl complexes typically display two intense bands in the visible region of their absorption profiles between (i) $\lambda$ = 420-425 nm and (ii) ) $\lambda$ = 445- 455 nm. These bands are also observed in the UV-Vis absorption spectrum of $Ru(bipy)^{2+}$, and are

assigned as spin-allowed MLCT transitions [d(Ru)→π*(N^N)] with extinction coefficients (ε) ~1 x$10^4$ $M^{-1}cm^{-1}$.[74]

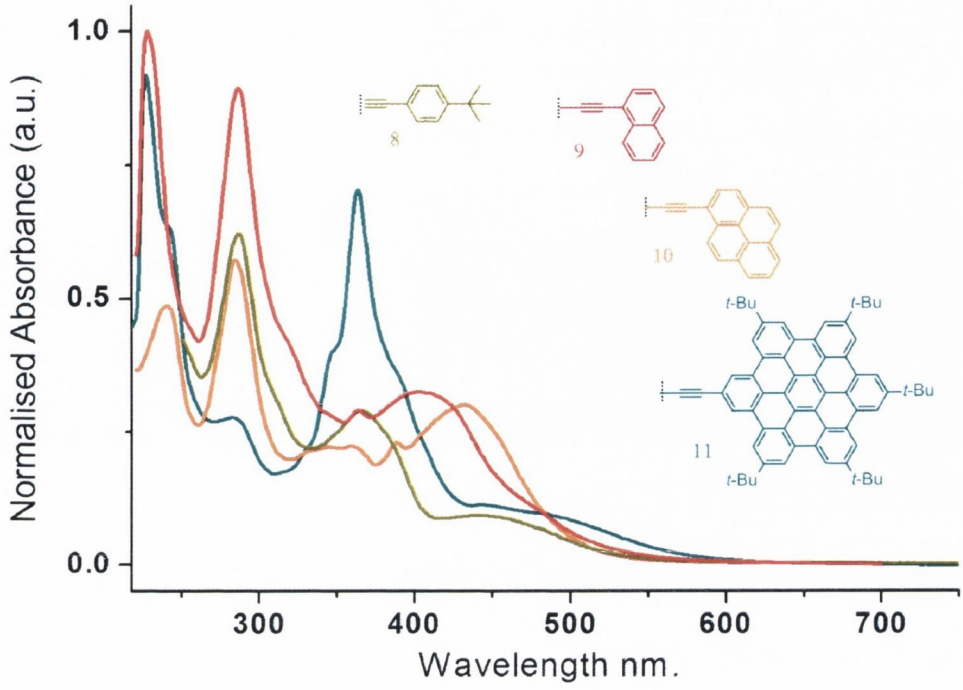


*Figure 2.20: The UV-Vis absorption spectra of Ru(II) aryl acetylenes* ***8- 11*** *in* $CH_2Cl_2$ *(1 x$10^{-5}$M).*

The absorption profile of Ru(II) diimine complexes also typically contain weak metal centred d-d transitions between λ = 310-340 nm, however they cannot be identified in absorption profiles of the complexes in Figure 2.20. Absorption bands between λ = 360-445 nm are indicative of an absorption band commonly seen in 1,10 phenanthroline ligands with heavily conjugated substituents, and are visible for all four complexes. The new lower energy bands which are not reported for the parent compound $[Ru(bipy)_2(phen)]^{2+}$ suggests a strong electronic coupling between the aryl pendants and the 1,10-phenanthroline. [125]

Both the naphthyl and pyrenyl complexes **9** and **10** display strong broad low energy absorption bands between 400-500 nm, which is again indicative of $S_0 \rightarrow {}^1IL$ (chromophore-localised) and the $S_0 \rightarrow {}^1MLCT$ transition. [126, 127] Zhao *et al.* have previously reported an absorption band due to the pyrenyl chromophore at λ = 385 nm, however, this band is not apparent in the absorption profile of **10**.[128, 129] The hexabenzocoronene acetylene **11** possesses well-defined, highly structured low energy absorption bands, particularly between λ = 350-400 nm, which are characteristic of π-π* transitions on the appended chromophore.[17] The most interesting feature however, is that

MLCT band of the *tert*-butyl phenyl derivative **8** is more red-shifted than the MLCT band of the naphthyl derivative **9**. This disrupts the overall trend of the UV-Vis absorption profile of the complexes, i.e. an increase in aryl acetylene conjugation does not result in lower energy absorption bands. This suggests that the lowest energy band of the complexes maybe also be comprised of some IL or LLCT character.

*Table 2.4: Room temperature UV-Visible spectral data for Ru(II) complexes* ***8-11***

| Complex | $\lambda_{max}$ [nm] ($\varepsilon$ x $10^4$ [$M^{-1}$ $cm^{-1}$]) |
|---|---|
| (**8**) (*tert*-butyl) | 288 (6.16), 366 (2.87), 386 *sh* (2.33), 446 (0.9), 487 *sh* (0.6) |
| (**9**) (naphthyl) | 285 (8.59), 318 (4.42), 363 *sh* (2.69), 407 (3.27), 480 *sh* (1.26) |
| (**10**) (pyrenyl) | 284 (8.48), 348 (3.74), 366 (3.77), 389 (2.79), 438 *sh* (3.77),490 *sh* (0.8) |
| (**11**) HBC | 243 (6.3), 277 (9.1), 285 (2.69), 345 (3.89), 364 (6.9), 390 *sh* (3.6), 446 (0.93) |

To establish the solvatochromic behaviour of the four Ru(II) complexes, their absorption spectra were recorded in three solvents of decreasing polarity i.e. $CH_3CN$, $CH_2Cl_2$ and toluene. The maxima of the lowest energy bands are presented in Table 2.5 below. In general, the high energy transitions of the complexes show a small or negligible dependence with increasing solvent polarity ($\Delta E$ ~5 nm), which is indicative of $\pi$-$\pi^*$ transitions and was observed in the solvent polarity study of the free ligands. The parent complex $Ru(bipy)_2$ (phen) displays a bathochromic shift with increasing solvent polarity i.e. $\lambda$ = 433 nm to $\lambda$ = 450 nm to $\lambda$ = 482 nm. However the lower energy absorptions derived in the naphthyl, pyrenyl and HBC complex display no obvious trend, which indicates mixed identity i.e. MLCT and $^3$IL/LLCT in nature.

*Table 2.5: UV-Visible Absorption maxima ($\lambda$, nm) of the lowest energy absorption bands for complexes* ***8-11*** *in various solvents. (~$10^{-5}$M).*

| | *$CH_3CN$* | *$CH_2Cl_2$* | *Toluene* |
|---|---|---|---|
| (**8**) (*tert*-butyl) | 286, 347, 448 | 286, 347,448 | 286, 347,448 |
| (**9**) (naphthyl) | 297, 317, 386 | 318, 363, 407 | 290, 317, 395 |
| (**10**) (pyrenyl) | 345, 364, 391, 432 | 336, 362, 388, 439 | 345, 362, 438, 444 |
| (**11**) HBC | 345, 364, 390, 472 | 338, 358, 397,480 | 345, 363, 394, 473 |

### 2.2.3 Photoluminescence properties

The photoluminescence spectra of all of the complexes were recorded in optically dilute argon-degassed $CH_2Cl_2$ solutions at 5 x $10^{-6}$ M concentration. Figure 2.21 shows the room temperature excitation and emission spectra obtained for each of the four ruthenium(II) diimine complexes **8**, **9**, **10** and **11**.

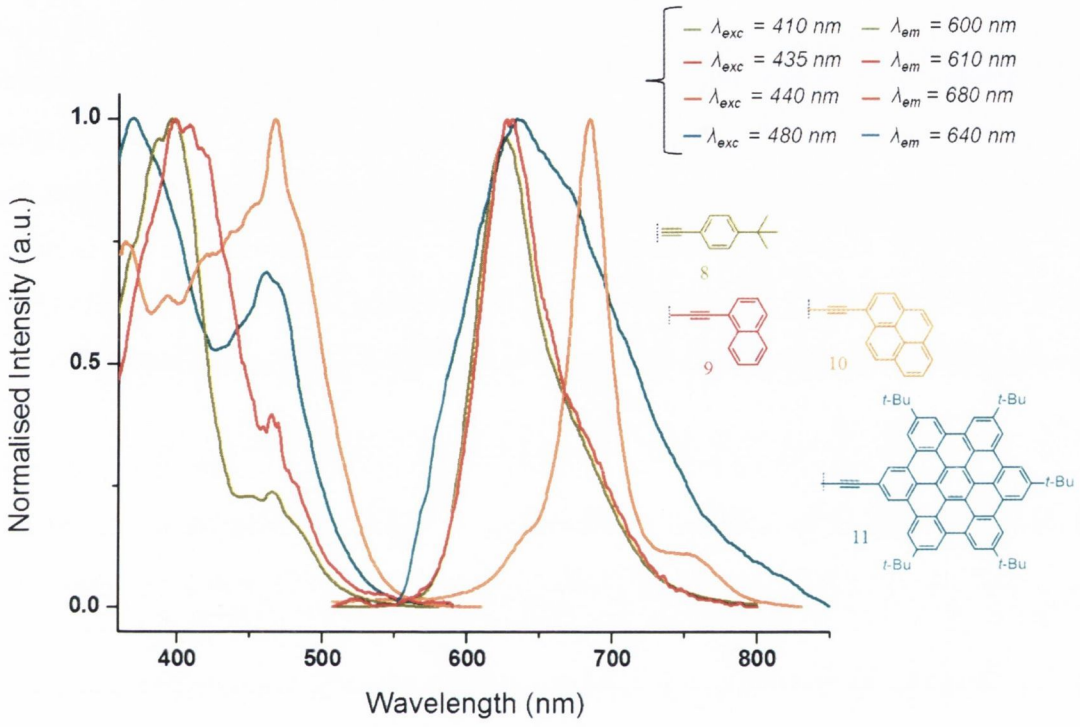


*Figure 2.21: Luminescence emission (—) and excitation (---) data for* ***8*** *,* ***9****,* ***10*** *and* ***11*** *in $CH_2Cl_2$ (5 x $10^{-6}$ M) at 298 K. Colour labelling for individual excitation and emission wavelengths as shown.*

The excitation spectra recorded for the complexes are superimposable with the UV-Vis absorption spectra recorded previously. This confirms that emitting compound is the expected one. Both the emission spectra of complexes **8** and **9** appear as a single structureless broad band centred at λ= 600 nm, with the *tert*-butyl derivative **8** slightly red-shifted with respect to the naphthyl derivative. This reflects the pattern observed in the excitation spectra, and is likely to be due to the presence of the electron donating group. Both have been assigned as $^3$MLCT emission, and are typical of other Ru(II) aryl 1,10-phenanthrolines substituted with smaller chromophores previously reported in the literature.[63] The recorded room temperature emission lifetimes for the phosphorescent bands are (**8**) 3.7 μs ($\lambda_{em}$ = 645 nm) and (**9**) 1 μs ( $\lambda_{em}$ = 620 nm) both within the expected range for Ru(II) polyimine complexes displaying $^3$MLCT emission.

The emission spectra of **10** shows more vibronic structure than the other complexes, with features at $\lambda$= 630 nm, 677 nm and 745 nm. The energy difference of 2098 $cm^{-1}$ is assigned as the C≡C triple bond stretching vibration. The energy difference between 630 nm and 677 nm is 1102 $cm^{-1}$, and is assigned as the pyrene C-H wagging vibration. Finally, the calculated vibration progression of 997 $cm^{-1}$ which is the energy difference between $\lambda$ = 677 nm and 726 nm is due to the phenanthroline C-H rocking vibration.[125] The near-IR luminescence spectra for the complex is red-shifted with respect to the three other complexes to an extent that suggests a different emissive state e.g. $^3$IL in nature. This is supported by the extended triplet lifetime measurement of 56.9 μs. Despite numerous attempts to perform this measurement within the group, it was found that the triplet lifetime of **10** lay outside the range of the on-site spectrofluorometer. The lifetime of the complex was therefore measured by Prof Jianzhang Zhao at the University of Dalian in China by nanosecond transient decay methods (see discussion, Chapter 3).

Finally, the emission profile of **11** is centred at $\lambda$ = 640 nm, but overlays the spectra of all the other complexes with broad, structureless emission stretching from $\lambda$= 550 nm into the near IR. Although complexes with $^3$IL emissive states typically display some vibronic structure at room temperature (such as that observed in the emission spectrum of **10**), based on the $^1$H NMR data obtained for the complex, it is likely that **11** undergoes considerable stacking in solution. As a result, it is possible that the structureless emission observed is not indicative of $^3$MLCT emission but a degree of aggregation in solution. The lifetime of the complex at 298 K extends beyond the scope of the available experimental set-up. This further supports phosphorescence from the HBC chromophore i.e a $^3$IL emissive state. It is hoped that a value will be ascertained for the triplet state lifetime through on-going collaborative efforts in the near future.

The corresponding emission spectra for all the complexes were recorded at 77K in butyronitrile glass, and are shown in Figure 2.22. The broad emission profiles recorded at room temperature for **8**, **9** and **11** have been replaced by narrower structured bands with enhanced vibronic progression. Rigidochromic blue shifts are observed for three of the complexes, however there is no overall correlation between the size of the appended chromophore and the extent of the shift observed (Table 2.6). The emission lifetimes of complexes **8** and **9** are extended, although only marginally in the case of **8** [~ 4 μs

(100%)]. This confirms the previous assignment of the $^3$MLCT emissive state of both complexes.

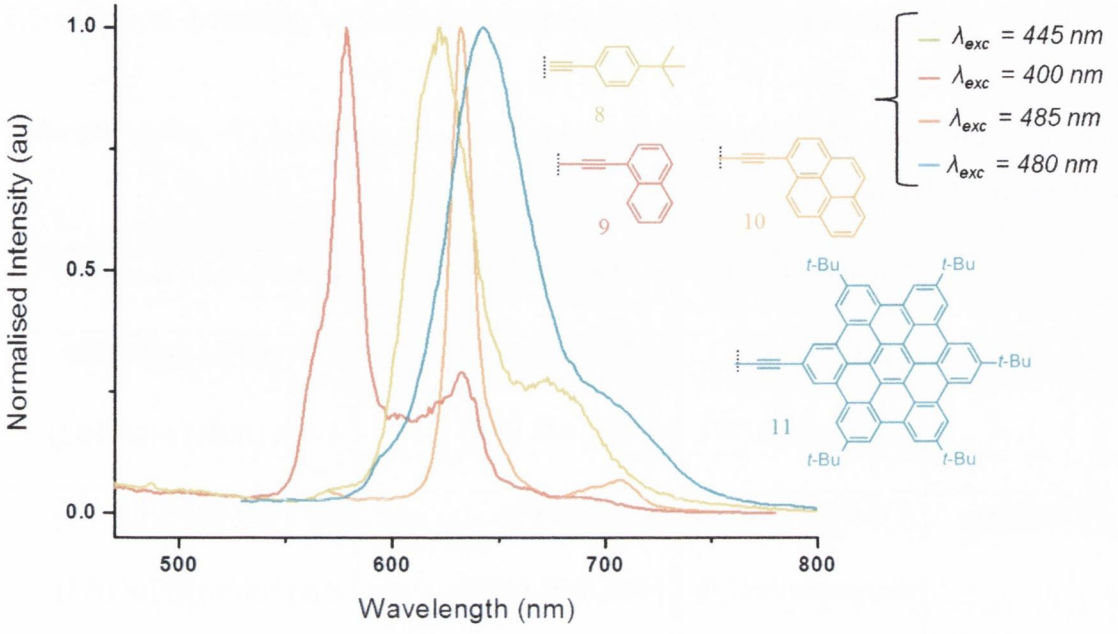


*Figure 2.22: Luminescence emission and excitation data for* ***8*** *,* ***9****,* ***10*** *and* ***11*** *in $CH_2Cl_2$ (5 x $10^{-6}$ M) at 77 K.*

Examination of the emission profile of the HBC complex **11** shows a marginal red shift of the emission band of the complex at 77 K which suggests an alternative emissive state for the complex to **8** and **9**, which again supports the assignment of the $^3$IL emissive state.

*Table 2.6: The calculated rigidochromic shift for the four ruthenium(II) complexes ($\Delta E_{rt\text{-}77K}/cm^{-1}$).*

| Complex | $\Delta E_{rt\text{-}77k}/cm^{-1}$ |
|---|---|
| **8** (t-Bu) | 206 |
| **9** (Naph) | 745 |
| **10** (Pyr) | 1178 |
| **11** (HBC) | -98 |

Complex **10** displays a thermally induced Stokes shift of 1178 $cm^{-1}$, which is in agreement with the value reported by Castellano *et al.* for Ru(II) complexes bearing multiple pyrenyl subunits. [130] The low temperature triplet state lifetime for the complex is predicted to be greater than 100 μs, and therefore well beyond the range of the experimental setup currently available within the group. However, based on the room

temperature and low temperature data presented, it is highly likely that the emissive state of the complex is $^3$IL as expected, and is in agreement with the observations reported by Zhao and Castellano for the similar complexes. An overall summary of the photophysical luminescent properties for the Ru(II) bipyridyl complexes is presented in Table 2.7 below.

*Table 2.7: Emission data and lifetimes for the ruthenium(II)1,10- phenanthroline complexes at 298 K and 77 K.*

| | Medium (T[K]) | $\lambda_{em}$[nm] ($\lambda_{exc}$[nm]) | $\tau$ [us] ( $\lambda_{exc}$ / $\lambda_{em}$ nm) |
|---|---|---|---|
| **8** (t-Bu) | $CH_2Cl_2$ (298) | $623_{max}$, 680 (445) | 3.7 (100%) (460/620) |
| | Butyronitrile (77) | $620_{max}$, 682 (490) | 4.41 (100%) (460/682) |
| **9** (Naph) | $CH_2Cl_2$ (298) | $600_{max}$ (400) | 3.9 (100%) (430/630) |
| | Butyronitrile (77) | $580_{max}$,635 (400) | 8.6 (100%) (370/ 635) |
| **10** (Pyr) | $CH_2Cl_2$ (298) | 640, $685_{max}$, 755 (485) | 56.6 μs * |
| | Butyronitrile (77) | 640, $675_{max}$, 745 (485) | # |
| **11** (HBC) | $CH_2Cl_2$ (298) | $541_{sh}$, 644, 681 (480) | # |
| | Butyronitrile (77) | $660_{max}$ 707 (480) | # |

* Measured by Prof Jianzhang Zhao and co-workers. # Could not be determined using the instrumentation set-up available.

### 2.2.4 Synthesis of Ir(III)($ppy_2$)(3,8-dibromo-1,10-phenanthroline) $PF_6$ (12)

To alleviate the competing formation of the copper complexes in the ligand synthesis, the decision was also taken to perform direct Sonogashira coupling to isolate the iridium(III) 1,10-phenanthroline aryl acetylene complexes. The iridium dichlorobridged dimer, $[Ir(ppy)_2Cl]_2$ was synthesised in a 2-ethoxyethanol reflux, according to literature procedure,[131] and isolated to give the yellow/green powder in comparative yields. The 3,8-dibromo-1,10-phenanthroline derivative was synthesised according to the procedure for the synthesis of other diimine ligands reported by Sprouse *et al.* [131] The product was isolated as a pale orange solid in a yield of 73%, with NMR and mass spectrometry confirming the product **12**.

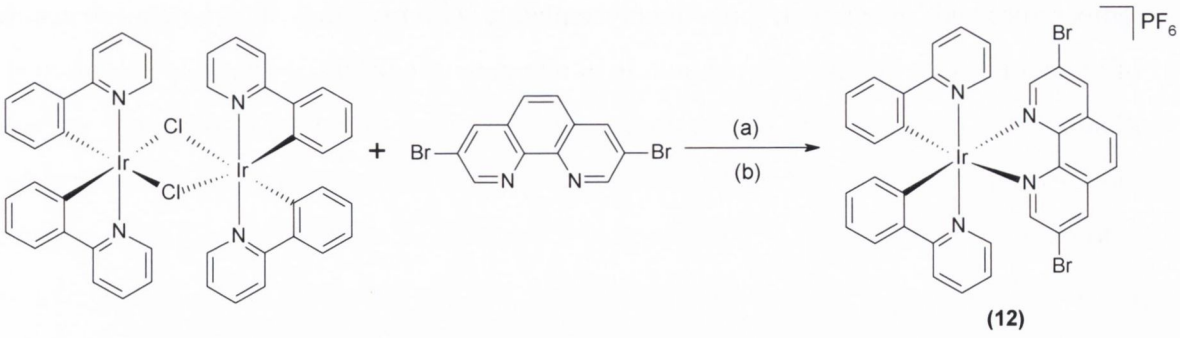


*Scheme 2.3: Synthesis of [Ir(ppy)$_2$ (3,8-dibromo-1,10-phenanthroline)](PF$_6$) (**12**) from [Ir(ppy)$_2$(μ-Cl)]$_2$ (a) $CH_2Cl_2$, reflux, 2 hours, (b) [$NH_4$][$PF_6$] in MeOH.*

The $^1$H NMR spectra for **12** is presented in Figure 2.23. The three proton signals on the 1,10-phenanthroline moiety are more deshielded than the equivalent protons on the ruthenium(II) bipyridyl derivative ( i.e. δ = δ = 8.85 ppm (●), 8.23 ppm (●) and 8.1 ppm (●), the assignment of which was carried out using the same method described for the Ru(II) complexes. As expected, the auxiliary 2-phenylpyridine ligand appears as two spin systems. The shielded doublet at δ = 6.4 ppm is assigned as the proton adjacent to the carbon *trans* to the metal centre. The remaining triplets and doublets for the two spin systems are assigned as shown, using a comparative method to that used for the bipyridyl ligands in **8-10**. Also shown in Figure 2.23 is the DEPT 90° experiment carried out for **12** which displays eleven C-H signals, confirming the presence of the product (see experimental for quaternary carbons).

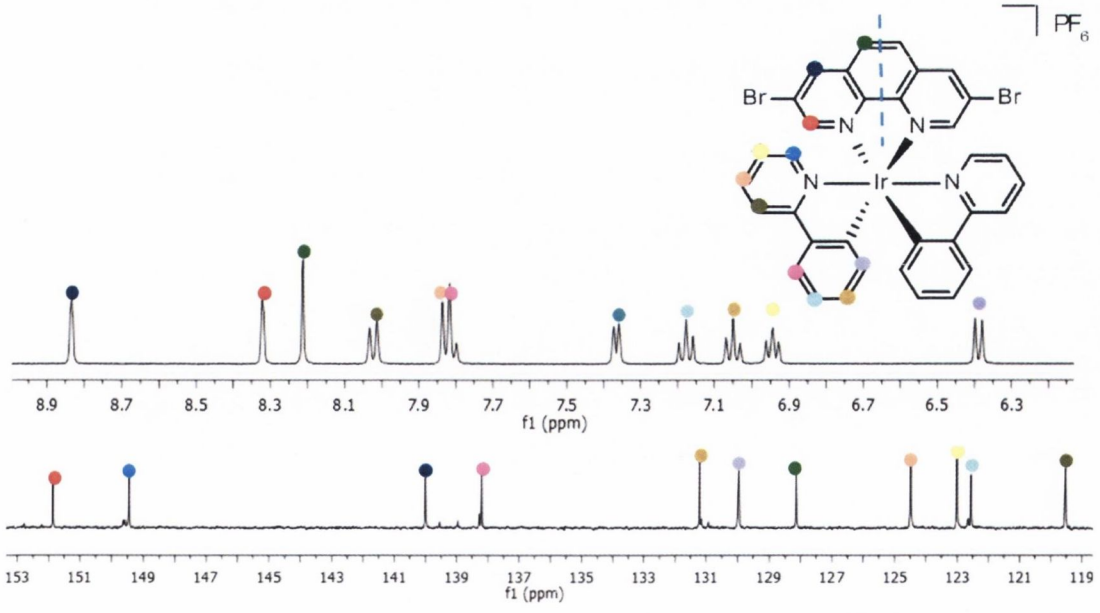


*Figure 2.23: $^1$H NMR spectrum ($CD_2Cl_2$, 600 MHz, R.T.) and DEPT 90° experiment for **12**. ($CD_2Cl_2$, 151 MHz, R.T.).*

### 2.2.4.1 General procedure for direct Sonogashira coupling of aryl acetylenes to Ir(III)(ppy)$_2$(3,8-dibromo-1,10-phenanthroline) $PF_6$

Coupling of the aryl acetylenes was attempted using a variety of conditions, but was finally optimised using the reaction conditions described in section 2.2.1.2 using either DMF or THF as solvent. The organic layers were concentrated, and purified on silica column chromatography elueting with either a mixture of MeCN: sat. $KNO_3$: $H_2O$ (10: 0.5: 1.5), or $CH_2Cl_2$/MeOH as solvent. The complexes were dissolved and precipitated by addition of a concentrated solution (~1 mL) of ammonium hexafluorophosphate in MeOH, and filtered to give orange/ red solids in yields of 53- 67 %. The HBC derivative **16** could not be purified by silica column chromatography, therefore repeated precipitation from $CH_2Cl_2$/hexane and washing with cold diethyl ether gave a dark red/black crystalline solid (yield = 55 %).

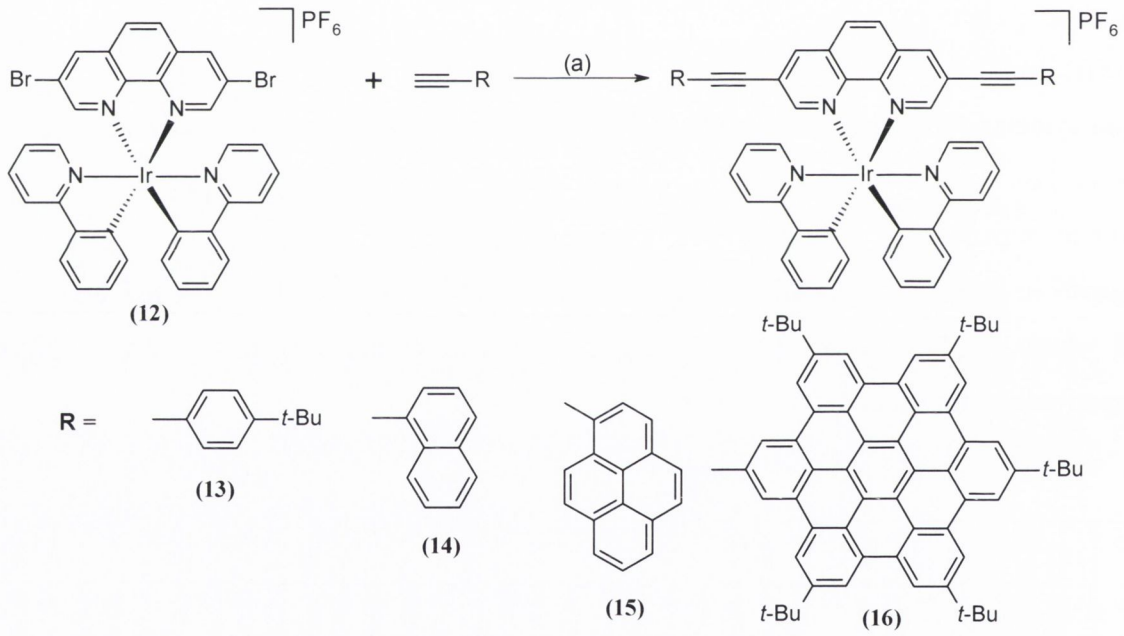


*Scheme 2.4: Synthetic route to aryl acetylene functionalised Ir(III) complexes from [(Ir(ppy)$_2$(3,8-dibromo-1,10-phenanthroline)](PF$_6$) (**12**).*

Table 2.8 shows the MALDI-TOF mass spectral data for all of the complexes in either $CH_3CN$ or $CH_2Cl_2$ and revealed a major peak which correlates to the $[M-(PF_6)]^+$ cation. This indicates the displacement of one $PF_6^-$ counterion from the cationic species.

*Table 2.8: The MALDI-TOF data obtained for each of the five Ir(III) cyclometalated complexes.*

| | Molecular Ion | Formula | Found *m/z* (%) | Calculated *m/z* (%) |
|---|---|---|---|---|
| **12** | $[M-(PF_6)]^+$ | $[C_{34}H_{22}Br_2IrN_4]^+$ | 836.9845 | 836.9841 |
| **13** | $[M-(PF_6)]^+$ | $[C_{58}H_{48}IrN_4]^+$ | 993.3540 | 993.3508 |
| **14** | $[M-(PF_6)]^+$ | $[C_{58}H_{36}IrN_4]^+$ | 981.2568 | 981.2574 |
| **15** | $[M-(PF_6)]^+$ | $[C_{70}H_{48}IrN_4]^+$ | 1133.3187 | 1133.3195 |
| **16** | $[M-(PF_6)]^+$ | $[C_{162}H_{136}IrN_4]^+$ | 2331.0532 | 2331.0439 |

Table 2.9 presents the corresponding IR spectroscopy data observed for the iridium(III) (1,10-phenanthroline) complexes. The ν(C≡C) stretching frequency was observed for four of the complexes (**13-16**) in the region of 2200 $cm^{-1}$ (Table 2.9). The C-Br stretching frequency for [Ir(III) 3,8-dibromo-1,10-phenanthroline] $(PF_6)_2$ at 669 $cm^{-1}$ is no longer evident in any of the four spectrum. As discussed for the Ru(II) complexes, the addition of multiple weak bands between 1400-1600 $cm^{-1}$ in the IR spectrum of **13-16** are attributed to aromatic C=C stretching, and is evidence for the formation of the target compounds.

*Table 2.9: The IR spectroscopic data for iridium(III)cyclometalated complexes **12-16**.*

| | IR [ν (C≡C), $cm^{-1}$] |
|---|---|
| **12** (Br) | 669* |
| **13** (t-Bu) | 2207 |
| **14** (Naphth) | 2202 |
| **15** (Pyr) | 2200 |
| **16** (HBC) | 2197 |

### 2.2.4.2 The $^1H$ and $^{13}C$ NMR characterisation of 13, 14, 15, and 16

The $^1$H NMR for the *tert*-butyl complex **13** is presented in Figure 2.24, and shows a broad multiplet which integrates for 10 H (δ = 7.65-7.5 ppm). The $^1H$-$^1H$ COSY experiment confirms the assignment of the proton adjacent to the nitrogen on the pyridine ring within the multiplet (2H, δ = 7.6 ppm, •). The remaining 8 H are attributed to the protons on the aryl acetylene ring (••). By comparing the spectrum with the

corresponding $^{1}$H NMR spectrum of **12**, it is clear that the three deshielded doublets of the 1,10-phenanthroline are only marginally affected by the introduction of the aryl acetylene functionality.

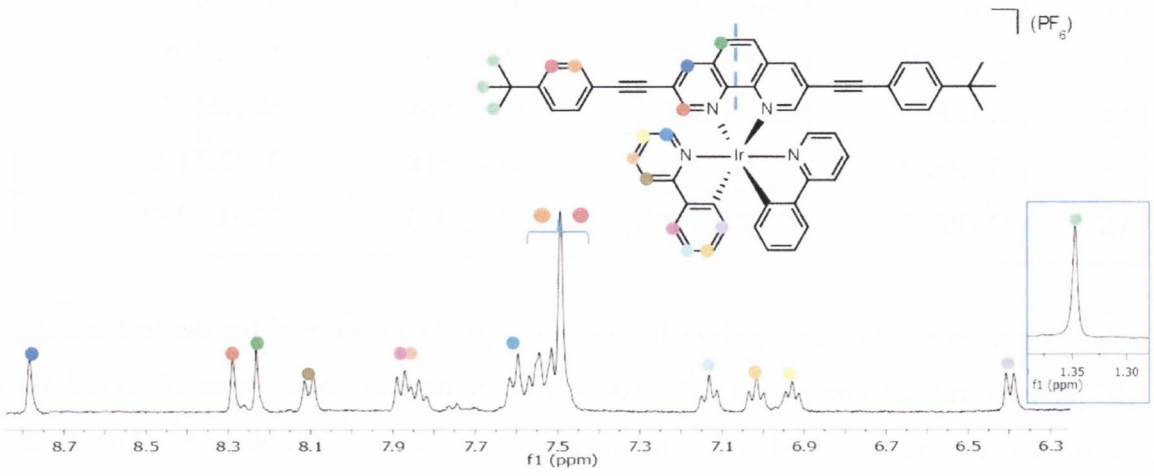


*Figure 2.24: The aromatic region of the $^{1}$H NMR of **13** with inset showing one $(CH_3)_3$ signal in the aliphatic region ($CD_2Cl_2$, 400 MHz, R.T.)*

Unlike the ruthenium(II) derivative **9**, the protons residing on the naphthyl and phenylpyridyl spin systems appear as a series of well defined doublets and triplets. The $^{1}$H- $^{1}$HCOSY experiment verifies the presence of four of the aryl spin systems and is shown in Figure 2.25. The sole three spin system was selected as the phenyl ring attached to the acetylene linker. It comprises of a well defined triplet appearing at δ = 7.55 ppm (■), and two deshielded doublets at δ = 8.05 and 7.6ppm. Analysis of the HMBC experiment revealed that the doublet at δ = 7.36 ppm correlates to a considerably more deshielded $^{13}$C signal at δ = 131.5 ppm. This is due to the close proximity of the carbon to the quaternary carbon on the acetylene linker, and is therefore assigned as (■). The signal appearing at δ = 8.25 ppm ($^{3}J$=12 Hz) was identified as the proton below the acetylene linker on the naphthyl moiety. A DEPT 90 experiment was used to identify the C-H signals in the $^{13}$C NMR spectrum of the complex. The assignment of the eighteen signals, is also shown in Figure 2.25. This assignment was conclusively achieved a 2D HSQC experiment through long range interactions between the individual protons and carbons. The two acetylenic carbons appear further upfield in the spectrum, at δ = 96 and 91 ppm respectively.

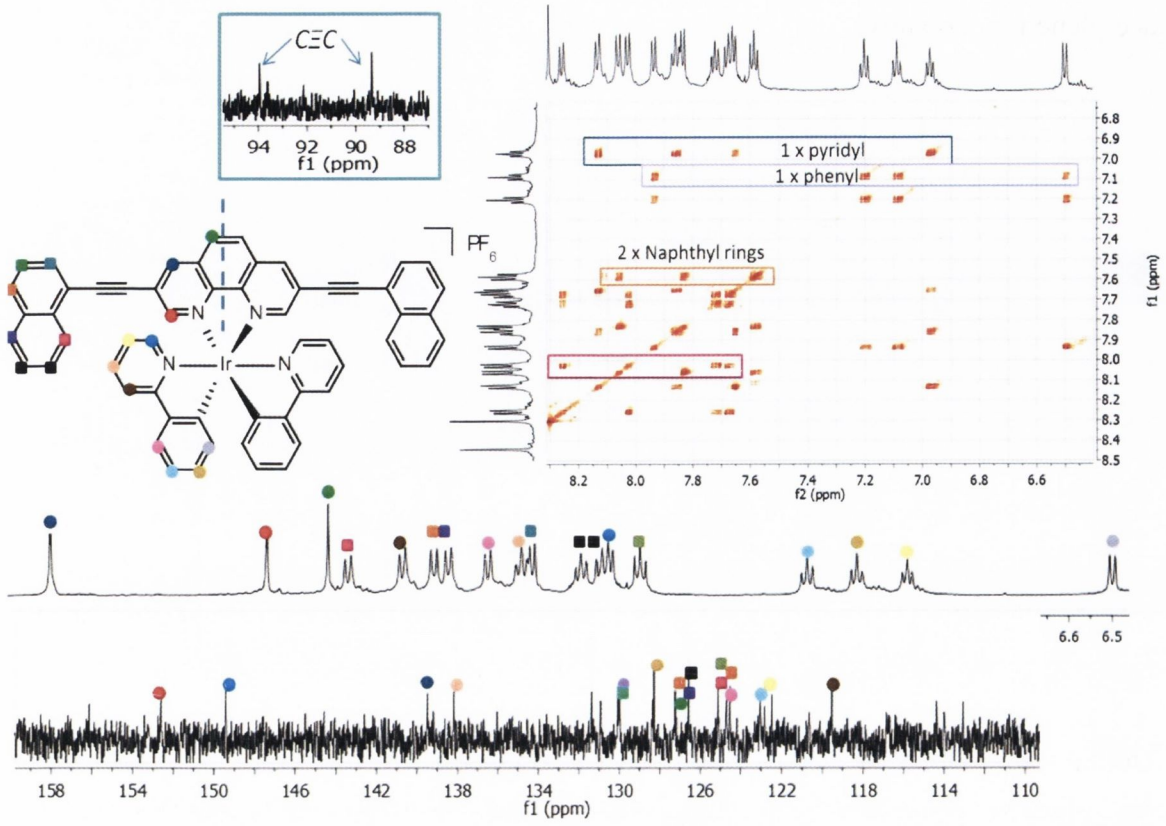


*Figure 2.25: The $^{1}H$ NMR spectrum ($CD_2Cl_2$, 600 MHz, R.T.) and DEPT 90 experiment for the naphthyl complex **14**. Inset; four spin systems were identified as shown using the $^{1}H$-$^{1}H$ COSY experiment.*

The majority of the pyrenyl protons appear as a series of overlapping multiplets between δ = 8.4 ppm and 8.0 ppm, however, two doublets residing on the same spin system have been identified at δ = 8.7 ppm and 8.5 ppm (▮ and ▮) using the $^{1}H$-$^{1}H$ COSY experiment shown in the inset of Figure 2.26. Both signals weakly correlate to the multiplet centred at δ = 8.25 ppm, which is tentatively assigned as the proton on the adjacent phenyl ring. This could not be conclusively confirmed with selective TOCSY experiments, as irradiation of both resonances resulted in a variety of "nearest neighbour" interactions across the entire multiplet. No improvement was observed by attempting to vary the mixing-time of the TOCSY experiment

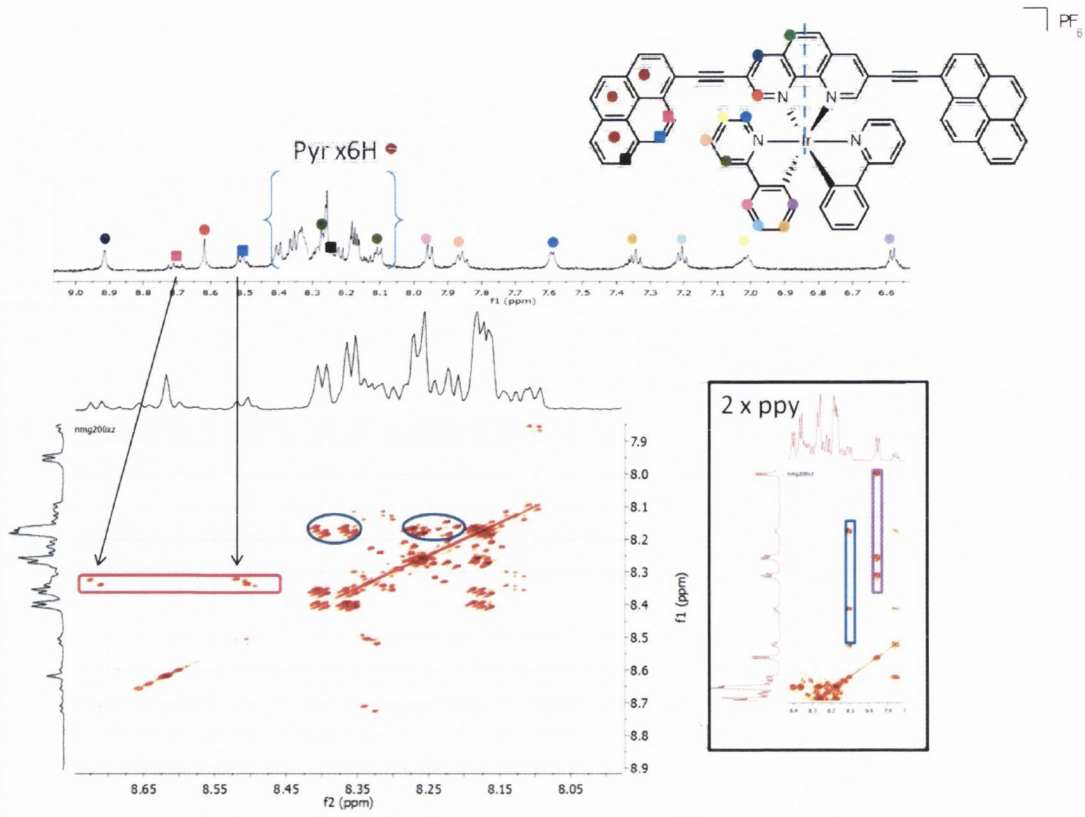


*Figure 2.26: Above, the aromatic region of the $^{1}H$ NMR of **15** and below, two sections of the $^{1}H$-$^{1}H$ COSY experiment used to locate two adjacent pyrene signals, and the phenylpyridine spin systems ( $CD_2Cl_2$, 600 MHz, R.T.).*

Figure 2.27 shows the assigned $^{13}C$ NMR spectrum for **15** in $CD_3CN$. The separate phenyl and pyridyl systems, previously linked in the 2D COSY experiment in Figure 2.25 were further studied using their connectivity in a long rang HMBC experiment. All four protons residing on the pyridyl ring of the auxiliary ppy ligand correlate to a quaternary carbon signal at δ = 167.5 ppm [Figure 2.27 (a)]. This has been highlighted in the $^{13}C$ NMR spectrum. The quaternary carbon located on the phenyl component of the ligand is buried within the overlapping signals at δ =132-130 ppm. In addition, one quaternary carbon from the 1,10-phenanthroline system was identified. The $^{13}C$ signal at δ = 144 ppm correlates to the protons residing on either side of the acetylene, but shows no long range connectivity to the proton at the back of the aryl moiety (●). On this basis, the quaternary carbon is assigned to the carbon directly attached to the acetylene. One shielded quaternary carbon was identified at δ = 111 ppm and correlated to the overlapping protons in the multiplet at δ = 8.3 ppm. On this basis, it has been allocated to one of the quaternary carbons on the pyrene pendant. The remaining quaternary carbons, as well as the C-H carbons attributed to the pyrene chromophore appear between δ =130

ppm and 125 ppm as indicated by the portion of the HSQC experiment presented in Figure 2.27(b).

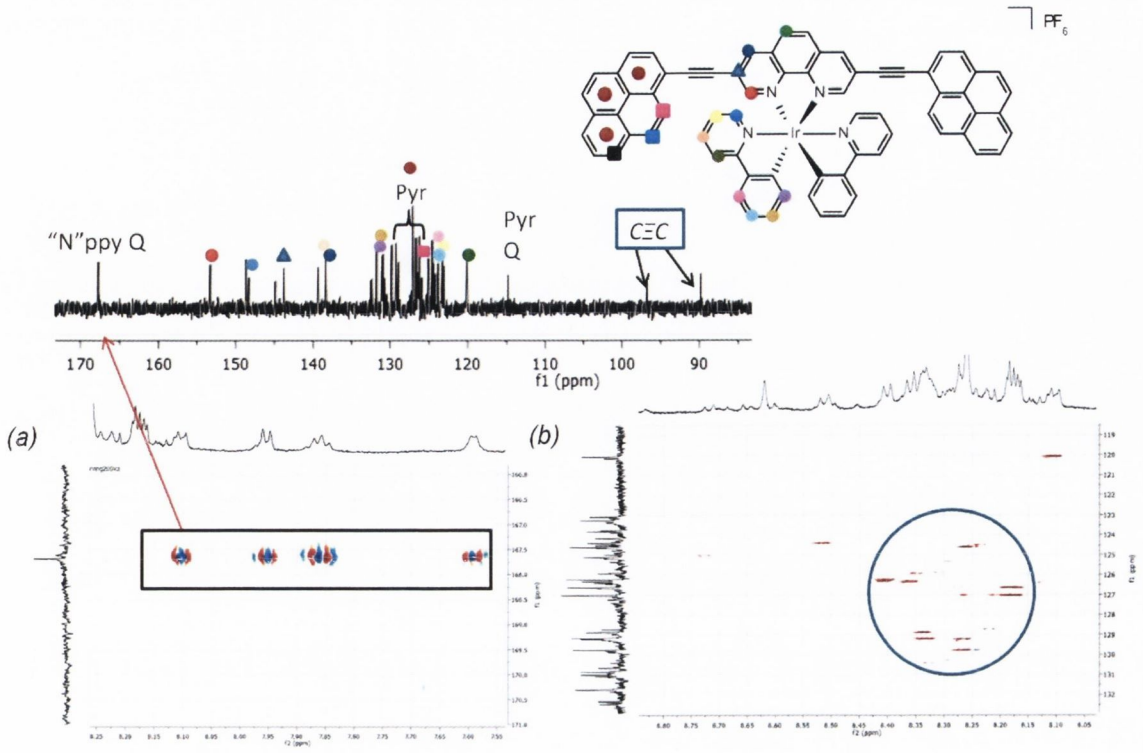


*Figure 2.27 Above: the assigned $^{13}C$ NMR spectrum for **15** and below; (i) HMBC experiment used to identify the quaternary carbon on the "ppy" pyridine ring and (ii) the HSQC experiment highlighting the overlapping C-H interactions for the pyrene moiety.*

Finally, the $^{1}H$ NMR spectrum of the iridium(III) HBC complex **16** in deuterated $CH_2Cl_2$ is presented in Figure 2.28. The solubility of the complex in deuterated solvents with higher boiling points (such as $CD_3CN$ and deuterated DMSO) prevented variable temperature $^{1}H$ NMR analysis from being attempted. Unlike the corresponding $^{1}H$ NMR spectrum for the Ru(II) analogue, nine signals are detectable in the aromatic region, eight of which are attributed to the auxiliary 2-phenylpyrdine ring. The most upfield of these signals is a doublet, which integrates for 2H, and appears at $\delta$ = 6.7 ppm. As previously seen in the other iridium(III) complexes, this is assigned as the proton closest to the metal centre (●). Selective TOCSY experiments carried out at each of the individual resonances of the ppy ring were unsuccessful in enabling a more definitive assignment of the individual spin systems, so the remaining ppy signals have been arbitrarily assigned. An additional downfield signal at $\delta$ = 8.6 ppm, is attributed to the 1,10-phenanthroline centre, however, the remaining two signals are expected to lie within the broad large multiplet appearing between $\delta$ = 9.4 and 9.0 ppm. The aliphatic region of the spectra shows two broad *t*-butyl peaks, which integrate in the ratio of 4:1. The integration values

of both the *tert*-butyl peaks (105 H), and the broad aromatic multiplet (32 H) are higher than expected (90 H and 28H). This discrepancy is believed to be a result of considerable aggregation occurring in solution. This would also account for the broad baseline present beneath the ppy protons.

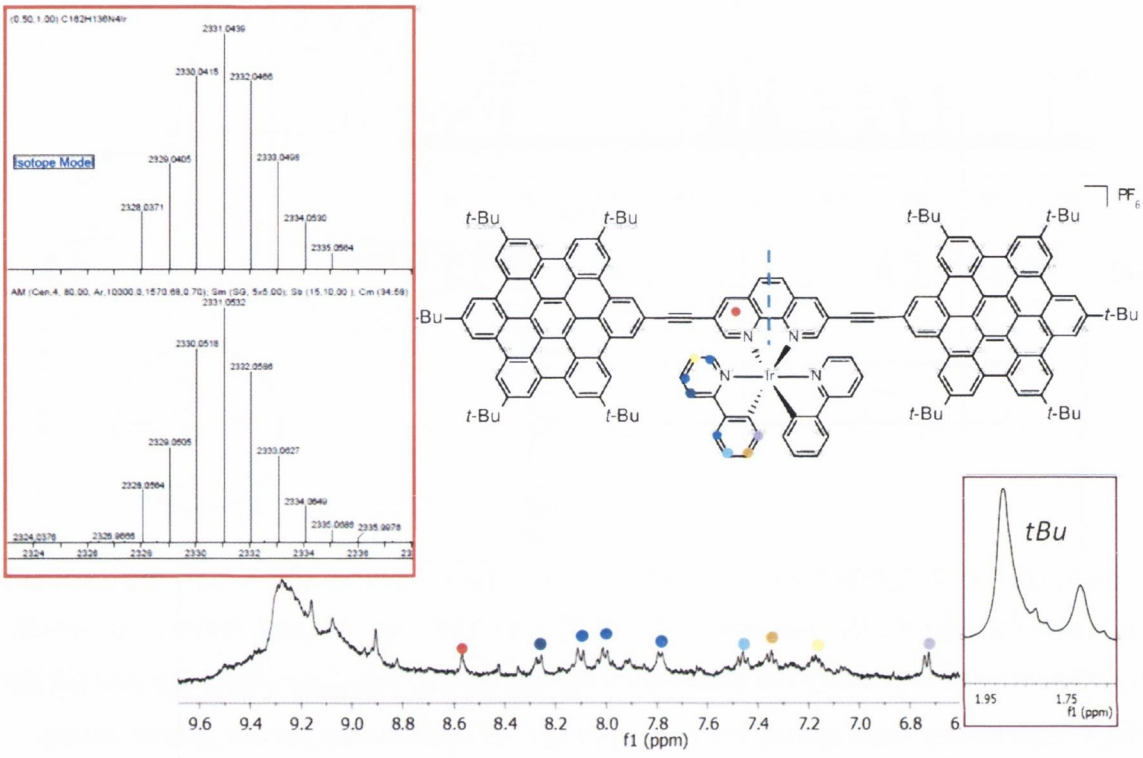


*Figure 2.28: Above; the model and MALDI-TOF isotopic distribution pattern obtained for* ***16****, below; the aromatic region of the* $^1H$ *NMR spectrum and inset showing the aliphatic region with two broad tert-butyl signals (*$CD_2Cl_2$*, 600 MHz, R.T.).*

Also shown in Figure 2.28 is the MALDI-TOF model and isotopic distribution pattern obtained for the complex in $CH_2Cl_2$. The main peak at *m/z* = 2331.0532 corresponds to the $[C_{162}H_{136}N_4Ir]^+$ ion (calculated m/z = 2331.0439). The MALDI-TOF analysis confirmed that only the symmetrical 3,8-disubstituted complex had been formed.

Table 2.10 shows the corresponding chemical shifts observed for the three doublets on the 1,10-phenanthroline moiety for Ir(III) complexes **12-15** in $CD_2Cl_2$. As observed for the Ru(II) derivatives, the proton adjacent to the nitrogen (●) become marginally more deshielded when larger aryl groups are cross-coupled to the diimine ligand. This is the only tangible trend observed; the remaining protons remain unaffected by the change in aryl chromophore.

*Table 2.10: Comparison of the relative chemical shifts of the three protons on the 1,10-phenanthroline moiety the two acetylene carbons for each of the iridium(III) complexes.*

| | ● δ $^{1}$H and $^{13}$C (ppm) | ● δ $^{1}$H and $^{13}$C (ppm) | ● δ $^{1}$H and $^{13}$C (ppm) | $C\equiv C$ δ $^{13}$C (ppm) |
|---|---|---|---|---|
| **12** | 8.20, 151.5 | 8.81, 140.3 | 8.19, 128.1 | ------- |
| **13** | 8.29, 152.1 | 8.83, 140.1 | 8.30, 128.3 | 95.9, 84.2 |
| **14** | 8.42, 155.7 | 8.92, 139.9 | 8.29, 128.5 | 95.9, 89.3 |
| **15** | 8.62, 154.5 | 8.91, 139.1 | 8.31, 129.6 | 96.4 89.8 |

### 2.2.4.3 UV-Visible Absorption Spectra of Ir(III)(3, 8-aryl acetylene-1,10-phenanthroline) complexes

The UV-Vis absorption profiles of the iridium(III) aryl acetylene complexes **12-16** are presented in Figure 2.29. As previously discussed, the 3,8-dibromo 1,10-phenanthroline complex (**12**) has not been reported, therefore a full photophysical investigation of the complex will also been included.

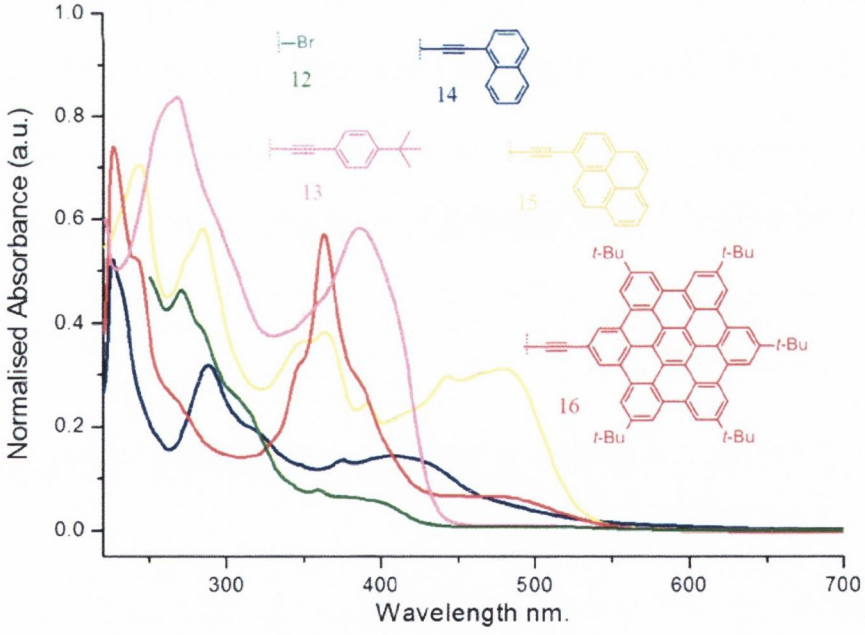


*Figure 2.29: The UV-Vis absorption spectra of Ir(III) aryl acetylenes **12-16** in $CH_2Cl_2$ (1 x$10^{-5}$M ) with inset showing the lower energy absorption in the extended tail of **16**.*

Cyclometallated iridium(III)diimine complexes display intense absorptions below 320 nm which are assigned as spin allowed π→π* ligand centred transitions that commonly

occur in cyclometallated 1,10-phenanthroline based and phenyl pyridine based ligands.[115] More specifically these absorption bands can be assigned as ppy centred ($\lambda$ < 270 nm) and diimine centred ($\lambda$ < 270-300 nm range) transitions. Spin allowed CT transitions to a phen-ligand based $\pi^*$ orbital result in weaker absorption bands at slightly lower energies ($\lambda$ = 320-440 nm). These can be of either MLCT [$d\pi(Ir) \rightarrow \pi^*(phen)$] or ligand-to-ligand LLCT [$\pi(ppy) \rightarrow \pi^*(phen)$] character. The nature of these CT transitions is dependent on the character of the HOMO and the degree of delocalisation over the phenylpyridine ligand and the iridium(III) metal centre.

Previous studies by Monkman *et al.* on iridium(III) 1,10-phenanthrolines functionalised with carbazole ligands showed a direct correlation between increased conjugation and higher extinction coefficients of the lower energy bands.[103] This trend does not hold for this study. The extinction coefficients of the naphthyl derivative (**14**) are lower than the tert-butyl phenyl derivative (**13**) (see Table 2.11). This is also the case for the pyrenyl complex (**15**) when its absorption spectrum is compared to that of the HBC functionalised complex (**16**). Unlike the trend observed in the ruthenium(II) analogues however, the larger the appending chromophore, the larger the red-shift observed in the lower energy absorption band [see inset, Figure 2.29 showing the extended tail observed for the lowest energy band of (**16**)].

*Table 2.11: UV-Visible Absorption maxima ($\lambda$ nm) of the lowest energy absorption bands observed for complexes* ***12-16*** *($CH_2Cl_2$, ~$10^{-5}$ M)*

| Complex | $\lambda_{max}$ [nm] ($\varepsilon$ x $10^4$ [$M^{-1}$ $cm^{-1}$]) |
|---|---|
| (**12**) Br | 270 (4.70), 308 *sh* (2.43), 360 (0.76), 400 (0.63) |
| (**13**) (*tert*-butyl) | 265 (8.2), 292 *sh* (6.08), 384 (5.86) |
| (**14**) (naphthyl) | 226, (5.1), 288 (3.2), 324 *sh* (1.94), 373 (1.49), 417 (1.36), 435 *sh* ( 1.28) |
| (**15**) (pyrenyl) | 240 (7.2), 282 (5.75), 347 (3.73), 391 (2.47), 439 (2.87), 481 (3.2) |
| (**16**) (HBC) | 269, 342 (3.0) , 363 (5.6), 390 (2.7) *sh*, 475 (0.71) |

To establish the solvatochromic behaviour of the complexes, their absorption spectra were recorded in three solvents of decreasing polarity i.e. $CH_3CN$, $CH_2Cl_2$ and toluene. The maxima of the obtained spectra are presented in Table 2.12. The poor solubility of

**12** percluded the measurement of the complex in toluene, therefore the UV-Vis absorption spectra was carried out in THF. The lower energy bands of the complexes display a small hypsochromic shift with increasing solvent polarity ($CH_3CN \rightarrow$toluene), which confirms assignment of partial MLCT nature of the transition.

*Table 2.12: UV-Visible Absorption maxima (λ, nm) of the lowest energy absorption bands for complexes* ***12-16*** *in various solvents. (~$10^{-5}$M). *THF*

| Complex | $CH_3CN$ | $CH_2Cl_2$ | Toluene |
|---|---|---|---|
| (**12**) Br | 358, 383, 409 | 358, 383, 409 | 358, 383, 409* |
| (**13**) (*tert*-butyl) | 386 | 385 | 387 |
| (**14**) (naphthyl) | 412 | 417 | 416 |
| (**15**) (pyrenyl) | 387, 435, 460 | 389, 442, 485 | 381, 441, 471 |
| (**16**) (HBC) | 390, 355, 396, 490 | 346, 363, 383, 486 | 343, 360, 390,471 |

**2.2.4.4 Photophysical study of iridium(III) cyclometalated complexes 12-16**

As previously discussed, emission from iridium(III) cyclometalated complexes is derived from either (i) a predominately $^3$MLCT emissive state (ii) a predominately $^3$IL state or (iii) a mixed $^3$IL/$^3$MLCT state. Emission displaying vibronic character is suggestive of emission derived from an excited state possessing some $^3$IL character. [132] Although it would be expected that increasing the conjugation of the N^N ligand would cause a significant shift in emission maxima, this is not always the case. The series of four iridium(III) 1,10-phenanthroline complexes reported by Monkman *et al.* with carbazole functionality displayed marginal variability in emission maxima at room temperature (i.e. ~5 nm). Each of the four complexes in the series displayed a broad structureless emission band centred at λ = 595 nm. This result is not an isolated case, with similar observations reported by the group on dimeric iridium(III) [9,9-dihexyl-2-(pyridin-2-yl)fluorene] complexes.[133] Guerchais *et al.* have also described a study of phenylated bipyridine iridium(III) complexes where she reported no significant bathochromic shift throughout the series.[134]

The normalised room temperature excitation and emission data for the iridium(III) complexes is presented in Figure 2.30. The excitation profiles of all five complexes correlate well with the UV-Vis absorption spectra presented in Figure 2.29. All five

complexes display intense emission profiles, which are independent of excitation wavelength.

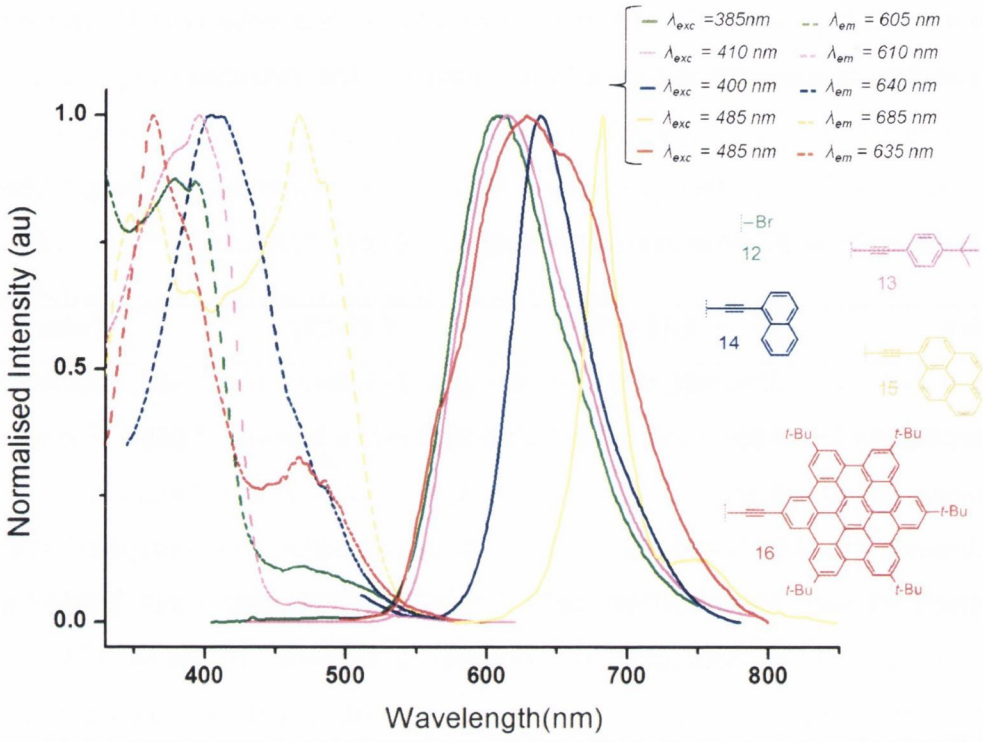


*Figure 2.30: Normalised excitation (---) and emission spectra (—) for iridium(III) cyclometalated complexes* ***12-16*** *($CH_2Cl_2$, 1 x$10^{-5}$M, 298 K). Emission and excitation wavelengths as shown.*

The variation between the emission maxima of **12** and **15** is small but considerably greater than that reported by Monkman and Guerchais i.e. ~80 nm. **12** undergoes a considerable red-shift with respect to the emission maxima reported by Wilson *et al.* for the parent complex in the same solvent [$\lambda_{em}$ = 584 nm $[Ir(phen)(ppy)_2]^{3+}$ *vs* $\lambda_{em}$ = 606 nm (**12**)]. This is due to a decrease in the energy gap between the metal $t_{2g}$ and the ligand $\pi^*$ orbitals.[135] The broad and featureless appearance of the emission spectra **12**, as well as that observed for **13** and **14**, suggest the assignment of their emissive state as CT in nature. Conversely, the vibronic structure present in **15** is more indicative of $^3$IL character. Similar to the ruthenium analog **10**, the energy differences between the band maxima of **15** were calculated and correlate well with those obtained for **10** i.e. 2190 $cm^{-1}$ (the C≡C triple bond stretching vibration), 1233 $cm^{-1}$ (pyrene C-H wagging vibration) and 957 $cm^{-1}$ (phenanthroline C-H rocking vibration).[125] The near-IR luminescence spectra for the complex is red-shifted with respect to the three other complexes to an extent that suggests, like **10**, a different emissive state e.g. principally $^3$IL in nature. There is no direct correlation across the series between the size of the appended

chromophore and the wavelength of the emission maxima, as the emission profile of **16** spans the width of the emission bands of the other complexes, which again is most likely attributed to aggregation in solution. However, **12** is marginally more blue shifted than the *tert*-Bu derivative **13**, and the emission tails of complexes with larger chromophores (**15** and **16**) extend further into the near-IR.

The lifetimes of the triplet state of each of the iridium(III) complexes are presented in Table 2.14. The emission of each complex decayed as a single exponential lifetime in degassed solutions of $CH_2Cl_2$. The duration of the triplet lifetimes of **12**, **13** and **14** are comparative i.e. 0-5 μs. The complexes are assigned as mixed $^3$MLCT character, and agree with similar systems in the literature.[133] As discussed for the Ru(II) complex **10**, the triplet lifetime of **15** was also found to be outside the range of our experimental set-up. The measurement was therefore performed by Prof Jianzhang Zhao's research group in Dalian university, and ascertained to be $\tau$ = 34.6 μs. The lifetime is considerably longer than any of the other iridium(III) complexes in the study. This concurs with the provisional assignment of the $^3$IL emissive state, and indicates that the emissive state of both the ruthenium(III) complex **10** and **15** are dominated by the organic chromophore, rather than the metal centre. The lifetime of **15** is also considerably longer than Constable's disubstituted pyrene bipyridyl iridium(III) complex, despite comparative emissive properties ($\lambda_{em}$ = 667 nm, $\tau \sim 1$ μs). The design of both **15** and Constable's complex have incorporated the pyrene moiety along the x-axis of the diimine core (see Chapter one), and should therefore enable access to the most intense electronic transitions in both complexes. The difference in the two triplet lifetimes must then be accounted for by the incorporation of the acetylene linker in the framework of **15** that is not present in Constable's ligand.[25]

The HBC functionalised complex displays emissive behaviour similar to that observed for the ruthenium(II) analogue **11**, i.e. broad, unstructured and overlaying the emission of the other complexes. This is also attributed to the complex undergoing stacking in solution, and therefore cannot be used as an indication of its emissive nature. Based on the extended emission tail into the near-IR, and the triplet lifetime also lying outside the range of the experimental set-up, it is more likely that the complex displays a $^3$IL emissive state.

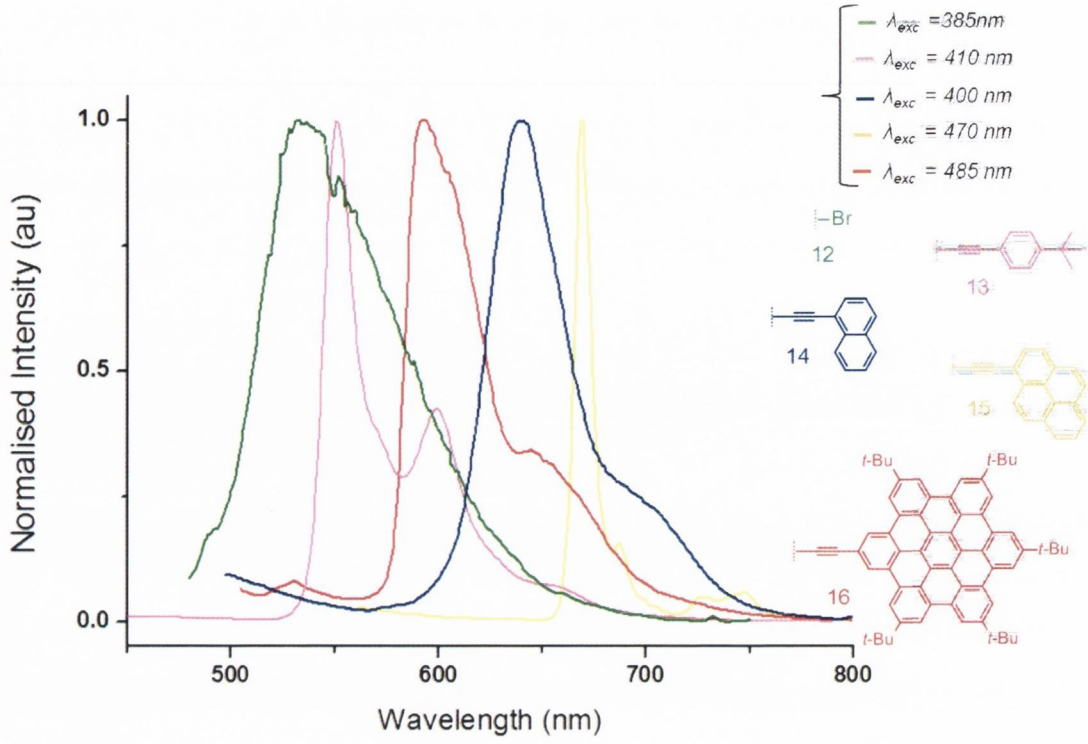


*Figure 2.31: Normalised emission spectra for iridium(III) cyclometalated complexes* ***12-16*** *(butyronitrile, 1 x10$^{-5}$M, 77 K). Emission wavelengths as shown.*

The emission spectra for each complex was also recorded at 77 K in butyronitrile, and is presented in Figure 2.31. Three of the complexes (**12-14**) display rigidochromic shifts which are overall considerably larger than the comparative values calculated for the Ru(II) complexes (Table 2.13). Although the rigidochromic shift displayed by **14** is considerably smaller than that typically reported for iridium(III) MLCT emitters (~2000 cm$^{-1}$),[136] the triplet lifetime values at room and low temperature are within the range expected for $^3$MLCT emissive states ($\tau$ = 0-5 μs).[115] The smaller $\Delta E_{rt\text{-}77\ K}$ values for the pyrenyl and HBC derivatives **15** and **16** are consistent with those reported by Constable *et al.* for the pyrene substituted bipyridyl derivative of **15** i.e. 112 cm$^{-1}$.[68] Similar to the ruthenium(II) analogues **10** and **11**, a value for the lifetime of the triplet state of **15** and **16** could not be determined at 77 K using the experimental set-up available. However, based on the extended room temperature lifetime of the triplet state for **15** ($\tau$ = 34.6 μs), as well as the vibronic character displayed by both at room temperature the emissive state of **15** has also been assigned as being predominately $^3$IL in character.The most apparent observation is that the magnitude of the shift is also proportional to the size of the appending chromophore. This trend was not previously observed for the Ru(II) analogues.

*Table 2.13: The rigidochromic shift calculated for the Ir(III) complexes ($\Delta E_{rt\text{-}77\ K}/cm^{-1}$).*

| Complex | $\Delta E_{rt\text{-}77k}/cm^{-1}$ |
|---|---|
| 12 (Br) | 2217 |
| 13 (t-Bu) | 1934 |
| 14 (Naph) | 1018 |
| 15 (Pyr) | 327 |
| 16 (HBC) | -24 |

A summary of the photophysical data obtained for the five complexes is presented in Table 2.14 below and suggests a correlation between the size of the appended aryl chromophore and the emissive properties of the complexes. Larger chromophores with enhanced electron delocalisation generate a $^3$IL emissive state (**15-16**), whilst smaller chromophores restrict the emission of the complex to the $^3$MLCT state. As this trend is also evident in the ruthenium(II) series, it is therefore evident that the choice of appending chromophore has substantially more influence on the photophysical properties of 3,8-1,10-phenanthrolines, than the choice of metal centre.

*Table 2.14: Emission data and lifetimes for Ir(III)complexes **12-16** at 298 K and 77 K.*

| | Medium (T[K]) | $\lambda_{em}$[nm] ($\lambda_{exc}$[nm]) | $\tau$ [μs] ( $\lambda_{exc}$ / $\lambda_{em}$ nm) |
|---|---|---|---|
| (**12**) Br | $CH_2Cl_2$ (298) | $610_{max}$ (385) | 0.63 (100%) (460/610) |
| | Butyronitrile (77) | $535_{max}$ (385) | 1.9 (100%) (460/535) |
| (**13**) *t*-Bu | $CH_2Cl_2$ (298) | $620_{max}$ (410) | 0.72 (100%) (370/620) |
| | Butyronitrile (77) | $550_{max}$, 600 (410) | |
| (**14**) Naph | $CH_2Cl_2$ (298) | $635_{max}$ (400) | 0.8 (100%) (460/650) |
| | Butyronitrile (77) | 640, 695 (490) | |
| (**15**) Pyr | $CH_2Cl_2$ (298) | $682_{max}$, 754 (485) | 34.6 * |
| | Butyronitrile (77) | $675_{max}$,692, 730, 745 (485) | # |
| (**16**) HBC | $CH_2Cl_2$ (298) | $475_{max}$, 505, $545_{sh}$, 660, (435) | # |
| | Butyronitrile (77) | $660_{max}$ , 707 (480) | # |

**Measured by Prof Jianzhang Zhao and co-workers. # Could not be determined using the instrumentation set-up available.*

## 2.3 Conclusions and Future Work

The aim of this chapter was to investigate the effect of varying an aryl acetylene chromophore on the 1,10-phenanthroline ligand whilst coordinated to two different metal centres. The synthesis of both the Ru(II) and Ir(III) complexes were optimised using Sonogashira cross-coupling reactions to the 3,8-dibromo-1,10-phenanthroline derivatives of both metal complexes. This method has not been previously reported for di-substituted 1,10-phenanthroline complexes, and is currently been explored for cross-coupling to other nitrogen doped systems. The Ru(II) and Ir(III) ethynyl-HBC complexes have been successfully isolated, although the solubility of both complexes may hinder their potential application as emissive materials.

The photophysical study of both sets of complexes has demonstrated that the emissive state at both room temperature and 77 K is dominated by the size of the aryl chromophore and not the choice of metal centre. Smaller aryl acetylenes such as *tert*-butyl phenyl or naphthyl groups, generate phosphorescence arising from the $^3$MLCT state. The incorporation of larger aryl groups, such as pyrene or HBC switches the emissive behaviour of the complexes so that it is predominately $^3$IL in origin. This is reflected in the extended triplet lifetimes measured for both pyrene complexes (**10** and **15**) at room temperature. Collaborative work is on-going to establish the corresponding values for the triplet lifetimes at low temperatures, as well as the triplet lifetimes for the ethynyl-HBC complexes **11** and **16**. Electrochemical studies of both the Ru(II) and Ir(III) complexes are in progress, however, the solubility of the pyrenyl and ethynyl HBC complexes at higher concentrations (~1 x $10^{-4}$ M) have so far prevented any conclusive electrochemical data from being obtained.

# 3 Developing Ru(II) and Ir(III) 1,10-phenanthroline complexes for application as triplet sensitizers.

## 3.1 Metal complexes as triplet sensitizers in upconversion

### 3.1.1 Upconversion

Upconversion was first reported by Parker and Hatchard after an observation of high energy fluorescence from a solution containing phenanthrene (as the donor) and naphthalene (as the acceptor).[137] The process required selective excitation of the phenanthrene chromophore which resulted in blue-shifted photoluminescence with respect to the excitation wavelength. The initial interpretation of the discovery invoked a two-quantum process involving the combination of two triplet excited states, producing an anti-Stokes delayed fluorescence derived from the singlet excited state of the acceptor. Research in the area mainly centred around investigations with polycyclic aromatic hydrocarbons,[138] as well as metal based systems such as delayed singlet excited state fluorescence in metalloporphyrins.[139] Further developments did not emerge until the 21$^{st}$ century upon the introduction of metal based triplet sensitizers,[140] which allowed access to the near IR region of the spectrum.

#### 3.1.1.1 Requirements for the sensitize and acceptor/annihilator

The upconversion process is now understood to be the energy transfer between a sensitizer molecule (donor) and an acceptor/annihilator. Sensitizers appropriate for upconversion must possess; (i) a relatively long triplet excited state lifetime to enable efficient diffusional based quenching, usually in the tens of microseconds range (ii) the ability to absorb light in the visible-to-near-IR region of the spectrum (iii) efficient intersystem crossing (ISC) (iv) the energy levels of the sensitizer must also match those of the acceptor in order for maximum triplet-triplet energy transfer [the energy transferred to the acceptor, (TTET)] to be achieved. This will give emission at higher energy level than the excitation. Based on these requirements, systems containing heavy metals are frequently chosen because of the enhanced spin-orbit coupling they provide. Porphyrins are often used, as they have the added advantage of containing π-conjugated systems which shift absorption and emission further into the red and near-IR spectral region. [141] [142] In addition, metal-based systems possessing MLCT excited states, which can exhibit relatively high extinction coefficients in the visible spectrum are also used. Although these criteria are widely recognised, designing potential triplet sensitizers has proven to be a considerable challenge as greater understanding of the relationship between ISC and molecular structure is needed. Acceptors with fluorescence quantum yields approaching unity are also beneficial to upconversion quantum yield

measurements. Organic molecules such as diphenylanthracene (DPA) and perylene are widely used as acceptors, and are commercially available. Research has shown that chemical modification of these popular acceptors does not necessarily generate more efficient acceptors. Cheprakov *et al.* have shown that derivatization of of chromophores, [such as 9,10-bis(phenylethynyl)anthracene (BPEA) and 9,10-bis(phenylethynyl)naphthacene (BPEN)] frequently causes the triplet excited state to shift above the singlet excited state, which can lead to a corresponding reduction in quantum yield. This can be seen when comparing DPA with its parent molecule anthracene as it has an ISC quantum yield which is fifteen times greater. Cheprakov has also shown using selectively modified porphyrin systems as triplet sensitizers with DPA acceptors can generate upconverted fluorescence that covers the visible UV-range [Figure 3.1, where PdOEP = 2,7,8,12,13,17,18-octaethylporphyrin palladium, $PdPh_4TBP$ = meso-tetraphenyl-tetrabenzoporphyrin palladium and $PdPh_4OMe_4TN$ = meso-tetraphenyl-octamethoxide-tetranaphtho[2,3] porphyrin palladium].

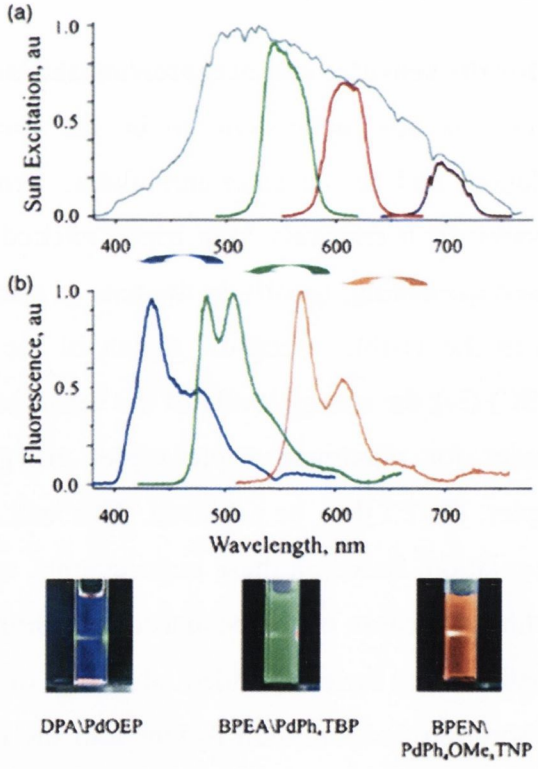


*Figure 3.1: Metal based triplet sensitizers generating "useable" light by Cheprakov et al. (a) The excitation spectra of the three sensitizers (coloured lines) with the solar spectrum overlaid (grey line) and (b) the upconverted fluorescence obtained after addition of the individual triplet acceptor to triplet sensitizers, excitation intensity 1 W $cm^{-1}$ Image reproduced from reference* [143]

### 3.1.1.2 Upconversion techniques and triplet-triplet annihilation

Studies into upconversion have invoked the development of a range of techniques which include upconversion with two photon absorption dyes (TPA), upconversion with rare earth materials,[144] and upconversion with inorganic crystals.[145] Triplet-Triplet Annihilation (TTA) is a type of upconversion that requires a low excitation power density, and is therefore achievable using solar light. TTA typically generates higher upconversion quantum yields than other upconversion techniques. It has stronger absorption in the visible range, making the overall upconversion capability of TTA materials higher ($\eta = \varepsilon \times \Phi_{uc}$, where $\eta$ is the upconversion capability, $\varepsilon$ is the extinction coefficient of the material at the excitation wavelength and $\Phi_{uc}$ is the upconversion quantum yield), and therefore more suitable for practical applications that require excitation with solar light.[146] Importantly, the excitation source for TTA does not need to be coherent. Both the excitation and the emission wavelength can be tuned easily by variation of the sensitizer and the acceptor, provided that the energy levels of both excited states have been matched. This flexibility makes TTA suitable for many applications, including photovoltaics,[147] solar fuel chemistry[148] and photocatalysis.[149]

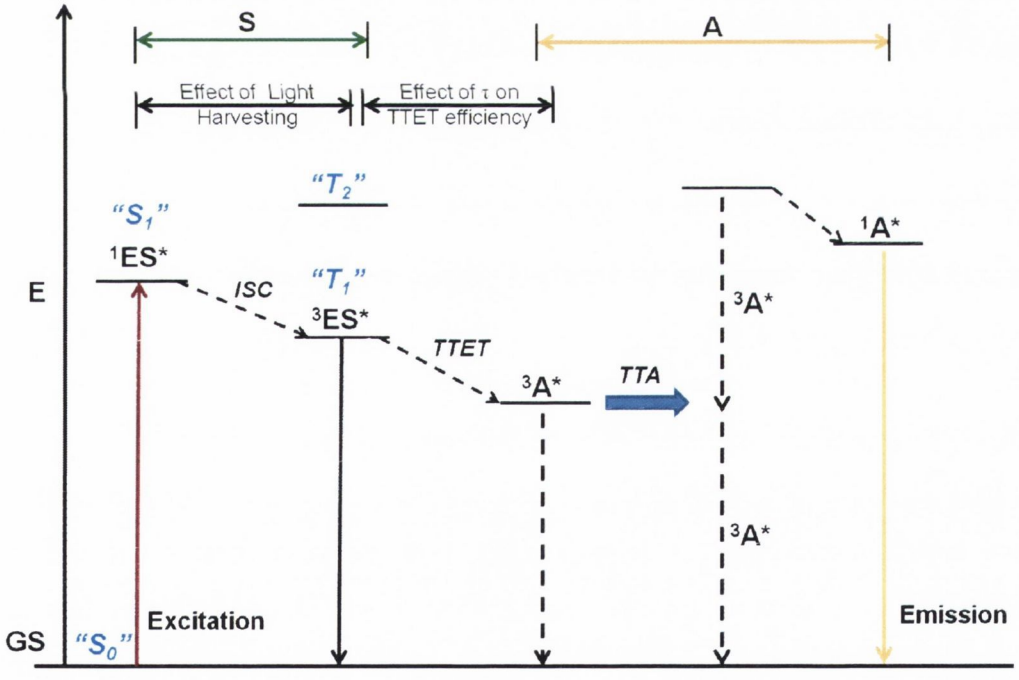


*Scheme 3.1: Generalised Jablonski diagram illustrating the upconversion process between the triplet sensitizer and acceptor resulting in singlet delayed fluorescence (GS is ground state, ES is excited state, S is sensitizer, A is acceptor, TTET is triplet-triplet energy transfer, ISC is intersystem crossing and TTA is triplet-triplet annihilation. "$S_0$", "$S_1$", "$T_1$" and "$T_2$" refer to the naming scheme adopted previously in the Jablonski diagram in Chapter 2).*

Scheme 3.1 illustrates the photophysics of the TTA upconversion process in a Jablonski diagram. Upon photo-irradiation, the sensitizer becomes excited ($^1$ES*), resulting in promotion to the singlet excited state ($S_o \rightarrow S_1$). Since the sensitizer cannot undergo direct excitation to the triplet state ($S_0 \rightarrow T_1$), ISC is required for population of the triplet excited state to occur ($^3$ES*) and is usually enhanced by the presence of a heavy metal. When the two components meet, Dexter energy transfer from the triplet sensitizer to the triplet acceptor occurs by the TTET process, and is facilitated by the extended lifetime of the triplet excited state.[150] The triplet acceptor molecules ($^3$A*) that are produced by this reaction can then combine to form the acceptor in its singlet excited state ($^1$A*) which is verified in the manifestation of upconverted fluorescence at a higher energy than the fluorescence previously observed from the triplet sensitizer.

### 3.1.1.3 Upconversion quantum yield ($\Phi_{uc}$)

The upconversion quantum yield of a process can be calculated using the following equation, where $\Phi_q$ is the energy transfer efficiency known as triplet-triplet energy transfer (TTET), $\Phi_{TTA}$ is the efficiency of the TTA process to produce a singlet excited state, and $\Phi_F$ is the fluorescence quantum yield of the acceptor.

$$\Phi_{UC} = \Phi_q \times \Phi_{TTA} \times \Phi_F$$

Several criteria must be met for successful TTA upconversion.[151]

(1) The triplet excited state lifetime of the sensitizer must be long so that there is an increased probability of an encounter between it and the acceptor, resulting in a more efficient TTET process and increase in the diffusion distance.

(2) The TTA process dictates that a high concentration of the sensitizers in the triplet excited state must be present. This enables a higher concentration of the acceptor molecules in the triplet excited state to be generated by TTET, which can then combine to produce the new singlet acceptor. By this reasoning, a better method of evaluating the upconversion capability ($\eta$) of the triplet sensitizer is therefore to use $\varepsilon$ x $\Phi_{UC}$ instead of $\Phi_{UC}$.

(3) The triplet excited state quantum yield of the sensitizer must be sufficiently high. This is because it is the triplet excited state that is produced after photoexcitation that is engaged in the TTET process, not the singlet excited state. Based on these criteria,

transition metal complexes are frequently selected as triplet sensitizers as they produce a high degree of ISC.

(4) To maximise the TTET efficiency, the relative energy levels of the triplet acceptor and triplet sensitizer must be matched.

(5) The fluorescence quantum yield of the acceptor must be high $\Phi_F$.

To assess the TTA upconversion of a system, two parameters need to be calculated, the TTET process efficiency and the upconversion quantum yield. The TTET process efficiency is calculated through quenching experiments, where the quenching result is fitted to the Stern-Volmer equation.

$$I_o / I = 1 + K_{sv}[Q], K_{sv} = k_q \times \tau_o$$

This provides a value for $K_{sv}$ and $k_q$, the bimolecular quenching constants. $\tau_0$ is the lifetime of the sensitizer of the triplet excited state in the absence of a quencher, and [Q] is the quencher's concentration. Time-resolved transient absorption spectroscopy can also be used to measure lifetime of the $T_1$ excited state of the sensitizer. This method is particularly useful when the triplet sensitizer is not phosphorescent. Finally, the upconversion quantum yield ($\Phi_{unk}$), can be calculated from the absorbance ($A_{unk}$), integrated photoluminescence intensity ($I_{unk}$) and the refractive index of a sample ($\eta_{unk}$). The corresponding "$_{std}$" terms are for the reference quantum counter. The incorporation of the multiplicative factor of two is to account for the fact that two photons must absorb for every one upconverted photon to be observed.

$$\Phi_{unk} = 2\Phi_{std}\left(\frac{A_{std}}{A_{unk}}\right)\left(\frac{I_{unk}}{I_{std}}\right)\left(\frac{\eta_{unk}}{\eta_{std}}\right)^2$$

### 3.1.1.4 The limits of the upconversion quantum yield; the spin statistical equation

As previously discussed, if a sensitizer absorbs low energy light, it is excited from the $S_0$ to the $S_1$ state, and can undergo rapid ISC to the $T_1$ state. This triplet energy is transferred to the acceptor species, and when two of these triplets collide in solution, they can form encounter species, which can be in one of three states. From the spin statistical equation below, we can deduce that nine spin states are produced, when two triplet states ($^3A_1$) collide. These spin states are five quintets ($^5A_2$), three triplets ($^3A_1$) and one singlet ($^1A_0$), each with equal probability of occurring. If this assumption is true, then since all triplet states react in the same way, than N/2 upconverted photons are created for every N number of photons absorbed. The spin-statistic equation below

dictates that the maximum quantum yield of the upconversion process is (2S+1)/9 or 11.1%, given that the quenching efficiency ($\Phi_q$) and the acceptors quantum yield of fluorescence are both 100%.

$$^3A_1^* + {}^3A_1^* \longleftrightarrow {}^5(AA)_2^* \longleftrightarrow {}^5A_2^* + {}^1A_0$$

$$^3A_1^* + {}^3A_1^* \longleftrightarrow {}^3(AA)_1^* \longleftrightarrow {}^3A_1^* + {}^1A_0$$

$$^3A_1^* + {}^3A_1^* \longleftrightarrow {}^1(AA)_0^* \longleftrightarrow {}^1A_0^* + {}^1A_0$$

*Scheme 3.2: The spin statistical equation showing five quintets, three triplets and one singlet spin states.*

Schmidt *et al.* recently investigated a $PQ_4Pd$ sensitizer and rubrene acceptor/annihilator system and reported an upconversion quantum yield of 16%.[152, 153] Castellano *et al.* have also reported a figure of 19.8%, which was obtained for a iodophenyl boron dipyrromethene (BODIPY) derivatives.[154] According to Schmidt, the predication of the 11.1 % limit is based on the quintet and triplet encounter complexes quenching directly to the singlet ground states. This has been refuted in a report by Saltiel and co-workers in 1981. They examined the mechanism for the TTA of anthracene, and proposed a mechanism to explain the dissociation of the anthracene triplet and quintet states (Scheme 3.3). It suggests, and has been experimentally verified by Schmidt *et al.*, that the quintet encounter complex is incapable of assuming a spin-allowed radiationless transition to a lower state, but instead undergoes dissociation back to two triplets, or alternatively, may dissociate into one singlet and one ground state molecule, with the energy of the stored photons being conserved in both cases.

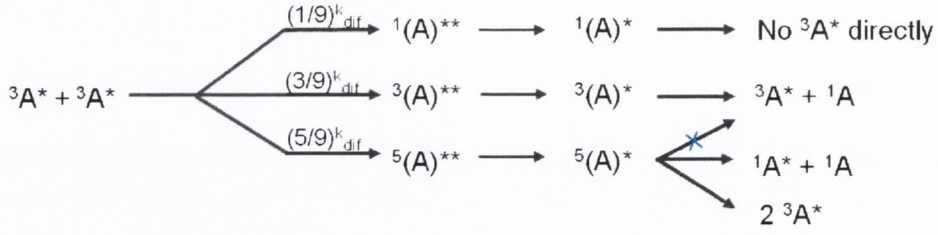


*Scheme 3.3: The proposed mechanism for anthracene TTA reported by Saltiel and co-workers adopted by Schmidt et al, showing the nine spin states produced by a TT encounter (**), and the lowest energy states produced by internal conversion (*).*[153, 155]

If this theory is correct, and assuming the TTA mechanism still holds, then the triplets ($^3A^*$) may interchange with a state of similar energy, which Schmidt assigns as a $T_2$ state, provided the energy of the $T_2$ state is less than twice the energy of the ($^3A^*$) state. This results in one of the triplets being quenched. If the quintets are ignored, five

emitters must be quenched for one photon to be upconverted. Schmidt further predicts that the maximum yield is substantially higher than previously estimated, (40%), and that this could be further improved. $T_2$ states can undergo reversible ISC crossing to $S_1$, which produces fluorescence.[156] Furthermore, if the $T_2$ energy exceeds the triplet energy by a factor many times greater than $k_BT$, it is possible that the three triplets may behave in the same manner as the quintets. This would raise the limit of upconversion quantum yield up to 100%. i.e. other excited states could generate singlet excited states, not just the triplet excited states as was previously believed.

### 3.1.2 Singlet oxygen quantum yields ($\Phi_\Delta$)

Singlet oxygen [$O_2(^1\Delta_g)$] plays a key role in many biological processes, such as the initial agent in photo dynamic therapy (PDT)[157] and the photooxidation of many organic compounds e.g. sulfides[158] and phenols.[159] The singlet oxygen quantum yield $\Phi_\Delta$ is defined as the number of molecules of $^1O_2$ generated for each photon absorbed by a photosensitizer. Excitation of the sensitizer results in a one photon transition between the ground state $S_0$ and a singlet excited state $S_n$. The lowest excited state $S_1$ is formed after relaxation of the $S_n$ state, which is followed by ISC to the $T_1$ of the sensitizer. As the lifetime of the $T_1$ state (~ μs) is considerably longer than that of $S_1$ (~ ns), $T_1$ can react *via* one of two mechanisms. Type A (indicated by △, Scheme 3.4) is a hydrogen-atom abstraction or electron transfer between the sensitizer in its excited state and the substrate, which generates free radicals. These radicals then react with oxygen to form the superoxide radical anion. Type B mechanism (indicated by ▮, Scheme 3.4), is the energy transfer between the colliding excited sensitizer and triplet oxygen to generate singlet oxygen. [160]

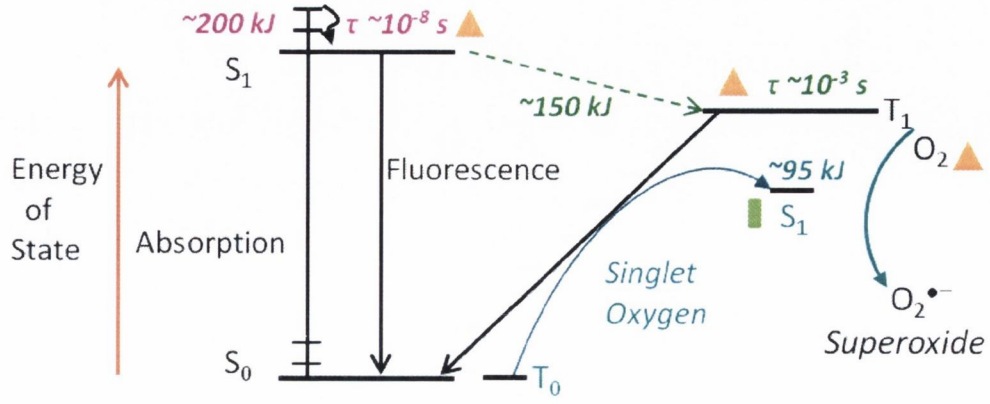


*Scheme 3.4: The generation of singlet oxygen via the excited states of the sensitizer.*

The generation of singlet oxygen is also only permitted if the energy difference between $T_1$ and $S_0$ of the sensitizer is greater than 0.98 eV (the energy gap between the triplet ground state of oxygen ($^3\Sigma_g^-$) and $O_2$ ($^1\Delta_g$)].[161] The majority of all of the reported measurements of $\Phi_\Delta$ are scaled to reference substances such as methylene blue (0.52), rose bengal (0.79) and $C_{60}$ (1.00).[160, 162] Examples quoted in the literature typically show considerable variation with solvent, measurement technique and reaction conditions.

The singlet oxygen quantum yield of ruthenium(II) polypyridyl complexes have been shown to be highly dependent on the choice of solvent but typically range from $\Phi_\Delta$ = 0.28 to unity.[163] Garcia and co-workers reported the singlet oxygen quantum yield of several ruthenium tris complexes including $[Ru(phen)_3]^{2+}$ and $[Ru(dip)_3]^{2+}$ (where phen = 1,10-phenanthroline and dip = 4,7diphenyl-1,10-phenanthroline). The values reported for $Ru(phen)_3^{2+}$ in deuterated methanol and water are $\Phi_\Delta$ = 0.52 and 0.54, however substitution to the 1,10-phenanthroline moiety in the 4,7-position enhances the efficiency of the photosensitizer substantially, with the comparative singlet oxygen quantum yield of $[Ru(dip)_3]^{2+}$ measured to be 0.87 and 0.95 respectively.[164] The inferior values for the tris-1,10-phenanthroline complex are most likely due to competing monomolecular processes (such as radiative and non-radiative deactivation), and bimolecular processes which Garcia suggests to be either physical deactivation of $^3[RuL_3]^*$ by $O_2$ (known as oxygen-enhanced intersystem crossing), and electron transfer to generate the superoxide anion and the oxidised form of the complex $[RuL_3]^+$. Singlet oxygen quantum yields for iridium(III) cyclometalated complexes typically range from 0.5 - 0.9. Iridium(III) complexes typically suffer from a combination of electron and energy transfer processes, therefore luminescence quenching may typically occur, which lowers the overall value of $\Phi_\Delta$. For iridium complexes with low emission energies, the physical deactivation of the ground state is also a competing process with energy transfer to the $O_2$ ground state.

### 3.1.2.1 Designing suitable materials for TTA upconversion

Organic triplet acceptors such as pyrene and anthracene derivatives have demonstrated their suitability for the TTA process. Others have the disadvantage of exhibiting photochemical instability e.g. rubrene photo-oxidises in solution to form rubrene endoperoxide.[165] Rubrene is only suitable if used in vacuum degassed solvents such as toluene, and is therefore unlikely to find real commercial value as a triplet acceptor.

Although the area of metal-organic upconverting composites is relatively under developed, zinc,[142] palladium[166] and platinum[167] porphyrins are amongst those which

have successfully been utilised as triplet sensitizers (Figure 3.2). Porphyrins contain anellated aromatic rings which extend the π-conjugation, red shifting both the absorption and the emission of the systems. The presence of a heavy metal in the ring system results in $\Phi_{isc}$ values near unity. This heavy atom effect induces large spin-orbit coupling, thereby enhancing ISC. It is a nuclear-charge effect, and scales with $Z^4$ ($Z$ is the nuclear charge).

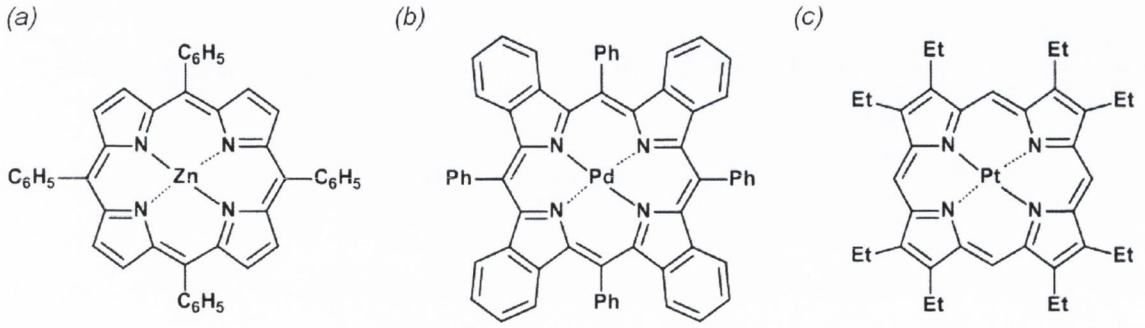


*Figure 3.2: Three examples of metalloporphyrin triplet sensitizers (a) ZNTPP[142] (b) $PdPh_4TBP$[166] and (c) PtOEP ($\Phi_{uc}$= 0.02).[167] Upconversion quantum yields were not reported for (a) and (b).*

Other methods used to enhance ISC in triplet sensitizers include utilizing chromophores with low-lying n-π* states.[151] For ISC to occur, the angular momentum energy must be strictly conserved, which necessitates that the energy difference between the two states in the transition must be close to the perturbation energy. For n-$\pi^*$ transitions, the energy gap between the $S_1/T_1$ states is small, which increases the chances of ISC occurring. However, the opposite is true for π-$\pi^*$ transitions, and this is reflected in the weak ISC observed for aromatic chromophores with larger π-conjugated networks, making them poor triplet sensitizers. Smaller molecules such as benzophenone are much more efficient.

### 3.1.2.2 Ruthenium(II) polyimine complexes and their potential applications in upconversion

Ruthenium(II) polyimine complexes are one of the most extensively studied classes of luminescent complexes, and have been successfully utilised in a wide range of applications which have previously been discussed in chapter two. These systems possess long-lived $T_1$ excited states, undergo highly efficient ISC and have the ability to populate the triplet excited states upon photoexcitation. These features make them ideal potential candidates for TTA applications. Despite this, they have not been sufficiently exploited in the development of TTA sensitizers. This may be as a result of the paucity

of reported Ru(II) complexes that display both UV-Vis absorption with high extinction coefficients and phosphorescence above $\lambda$= 500 nm. The number of literature citations for Ru(II) triplet sensitizers is currently fewer than twenty publications and these are limited to ruthenium(II) polyimine complexes such as $Ru(dmb)_3^{2+}$ and coumarin derivatives of 1,10-phenanthrolines.[140, 168] These reports have displayed TTA sensitizers with promising upconversion efficiencies of up to 10%, which compares favourably with similar reports for iridium(III) systems. These initial results warrant further photophysical investigation of Ru(II) polyimine complexes for this application.

Castellano and co-workers first reported a successful TTA upconversion with $[Ru(dmb)_3][PF_6]_2$ as a TTA sensitizer and using DPA as a triplet acceptor.[140] Upconverted fluorescence was observed at $\lambda$ = 430 nm, when the DPA and $[Ru(dmb)_3]^{+2}$ solution was excited with a green laser ($\lambda_{ex}$ = 514.5 nm, 24 mW). Although the quantum yield of upconversion and the efficiency of the TTET process were not reported, the work demonstrated that TTA upconversion is achievable with low-power density irradiation. Zhao *et al.* later reported a fluorescence quantum yield ($\Phi_f$) of 7.3 % for the complex and an upconversion quantum yield ($\Phi_{uc}$) of 1%.[125] The $T_1$ excited state lifetime of the sensitizer should ideally be long, on comparison of the N^N *vs* N^N^N geometry of the Ru(II) centre if was found that the $T_1$ lifetime is considerably higher for $[Ru(bpy)_2]^{2+}$ and $[Ru(dmb)_3]^{+2}$ than for the terpyridine derivative $[Ru(tpy)_2]^{2+}$ (1.0 µs and 0.84 µs, *vs* 0.25µs respectively).[169] The rapid deactivation of the lowest emissive state *via* thermal depopulation of the non emissive triplet states ($^3$MC) has been acknowledged as the reason for the shorter excited state lifetime of the Ru(II) tridentate complex. This suggests that extending the triplet lifetime of bidentate ligands is more promising for potential commercial application of the upconversion process.

### 3.1.2.3 Enhancing Ru(II) polyimine complex fluorescence lifetimes.

As previously discussed, sensitizers appropriate for TTA upconversion must possess a relatively long lived triplet state to enable efficient diffusional based quenching. Several strategies have been reported for the design of new sensitizers. These include (i) switching the emissive state of the complex to the intraligand excited state ($^3$IL) from the $^3$MLCT state e.g. by inclusion of an acetylenic linker, or (ii) generating an equilibrium between the $^3$MLCT and ($^3$IL) states e.g. by inclusion of C-C bond linker.[126, 170-172] Zhao *et al.* reported an investigation of these strategies through the design of the Ru(II) 1,10-

phenanthroline complexes in Figure 3.3.[63] This work was the first comparative report of upconversion with Ru(II) triplet sensitizers.

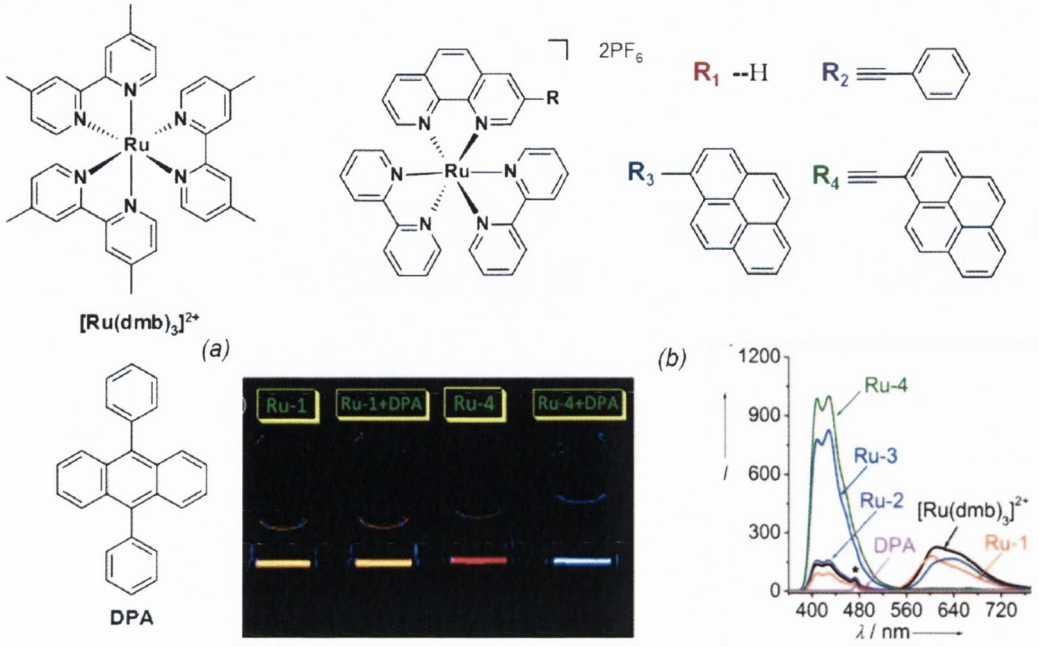


*Figure 3.3: Structure of the Ru(II) complexes studied by Zhao et al., the reference complex [Ru(dmb)3]$^{2+}$, and the structure of the acceptor DPA (a) Photograph of the upconversion of Ru-1 and Ru-4 upon addition of DPA (excited with a λ = 483 nm laser) (b) The upconverted DPA fluorescence and the residual phosphorescence of the mixture of DPA (4.3 x 10$^{-5}$ M) and the complexes*

As expected, the emission lifetimes of the four complexes in the series increases with extended π-conjugation (Ru-1 = 0.45 μs, Ru-2 = 2.44 μs, Ru-3 = 9.22 μs and Ru-4 = 108.0 μs). Inclusion of the acetylenic linker gives a ten-fold increase in the $T_1$ lifetime from Ru-3 to Ru-4, because the emission has been switched from the $^3$MLCT to the $^3$IL/$^3$LLCT state. The fluorescence generated by the two of the complexes when DPA is added is shown in Figure 3.3 (a). Ru-4 displays a pyrene centred phosphorescence band at $\lambda_{max}$ = 667 nm and has previously reported by the group to be a successful candidate for luminescent oxygen sensing, which involves a similar mechanism of triplet-triplet energy transfer to the TTA process.[125] This evidence suggested that it was the most suitable candidate for triplet sensitizing. DPA was chosen as the acceptor/annihilator because of its high fluorescence quantum yield ($\Phi_f$=0.95) and it's $T_1$ energy level (1.77 eV) matches well with the four complexes.[173, 174] Figure 3.3(b) shows the upconverted DPA fluorescence and the residual phosphorescence of the complexes after mixing with DPA. As expected, complexes Ru-1, Ru-2 and $[Ru(dmb)_3]^{2+}$ show poor upconversion capability, which is easily justified by the short lifetime of the $^3$MLCT state. Ru-3 and

Ru-4 show phosphorescence which is entirely quenched by DPA, which infers that an efficient TTET process is taking place. Upconversion quantum yields of 9.8% and 9.6% respectively were reported for the complexes. Although it would be expected that Ru-4 should have a higher efficiency, the driving force for the TTET process is smaller because of the smaller energy gap between the $^3$IL state of the complex and the $^3\pi$-$\pi^*$ of DPA ($\Delta E_{T\text{-}T}$ = 707 cm$^{-1}$ *vs* 2054 cm$^{-1}$). This work demonstrates that the $^3$IL state of Ru(II) polyimines is more efficient than the $^3$MLCT state for sensitizing TTA upconversion.

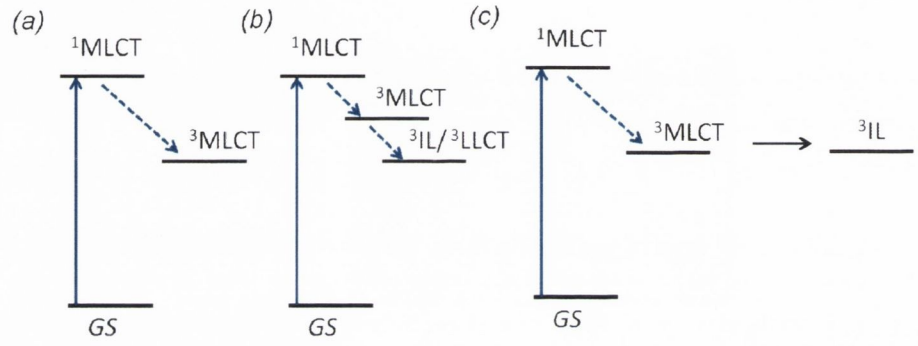


*Figure 3.4: Illustrative energy level diagram depicting the strategies to extend the triplet lifetimes for Ru polypyridyl complexes (a) Normal $^3$MLCT emission (Ru-1 and Ru-2); (b) $^3$IL/LLCT emission (Ru-3) and (c) $^3$MLCT emission with $^3$IL equilibrium (Ru-4).*

### 3.1.3 Developing cyclometalated Ir(III) complexes for TTA upconversion

Cyclometalated Ir(III) complexes routinely display weak absorption in the visible-light region, with few reports of complexes showing intense visible light absorption to date.[175] Combined with typical $T_1$ excited state lifetimes in the region of 5 μs,[176, 177] the application potential of these complexes in electroluminescent materials, and TTA upconversion based processes is limited. To combat this, the focus of research must now shift towards the design of Ir(III) complexes with enhanced photophysical properties. One method is to boost the lifetimes of their excited states. In 2006, Castellano *et al.* initiated this research drive with the reported successful use of $Ir(ppy)_3$ as a triplet sensitizer in TTA based upconversion, with pyrene and di-(*tert*-butyl)pyrene as acceptors/annihilators.[178] Although the UV-Vis absorption measured for the complex was centred in the blue region, and the complex possessed a short $T_1$ lifetime ($\tau$ = 1.55 μs), selective excitation of the triplet sensitizer was achieved at $\lambda$ = 450 nm, and upconverted fluorescence of pyrene was detected at $\lambda$ = 400 nm. This was a promising initial result,

however despite this, there has since been a paucity of further developments in the area of Ir(III) based sensitizers.[179]

### 3.1.3.1 Ir(III) 1,10-phenanthroline based triplet sensitizers for upconversion

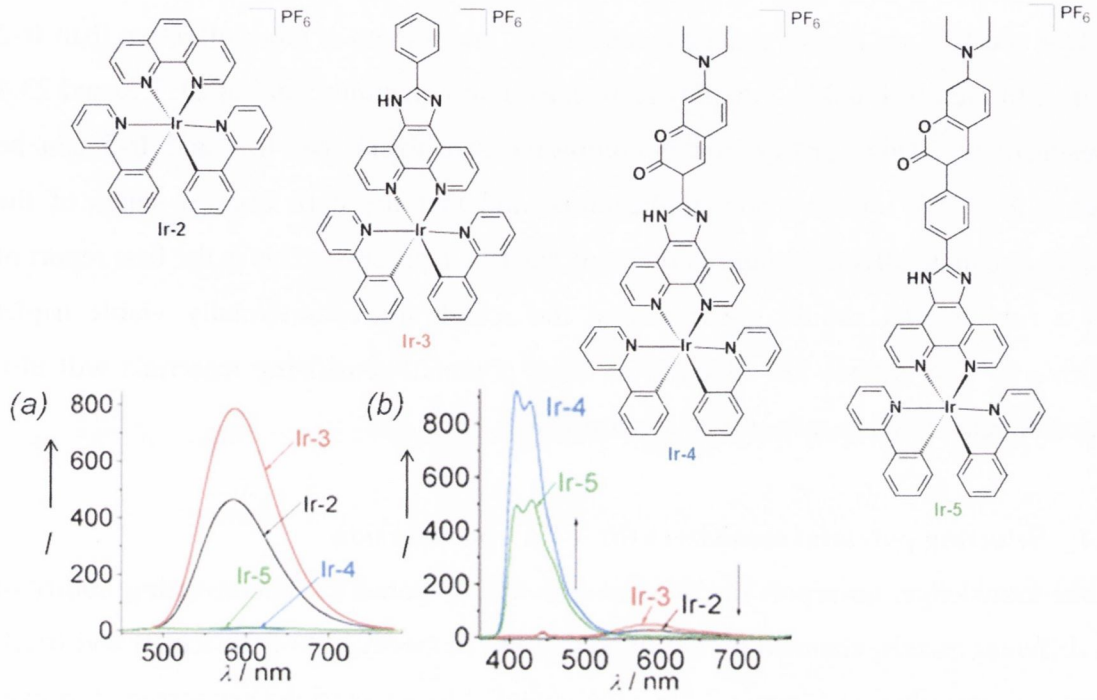


*Figure 3.5: Cyclometalated Ir(III) complexes used for TTA upconversion. Inset (a) phosphorescence of sensitizers alone ($\lambda_{ex}$ = 445 nm, 5 mW) and (b) Upconversion of the sensitizers with DPA as acceptor. Phosphorescence measured as a function of DPA concentration in 1.0 x $10^{-5}$ M in $CH_3CN$ at 20 °C.*[180]

Work by Thompson on square planar Pt(II) complexes with varying monoanionic pyridyl functionality[181] inspired Zhao and co-workers to design a series of Ir(III) 1,10-phenanthroline derivatives with coumarin functionality (Figure 3.5).[180] These complexes showed greater absorption in the visible region than Castellano's previously reported compounds, and possessed considerably longer-lived $^3$IL excited states [up to 75.5 μs (Ir-4)].[180] DFT calculations showed that the $T_1$ energy level of the coumarin derivatives is comparable to that of the metal coordination centre, and therefore likely that it would effectively perturb the triplet excited state of the complex. Included in Zhao's study was the 1,10-phenanthroline derivative Ir-1, which showed weak absorption in the visible region. Ir-1 did not produce any observable upconversion, and had a significantly smaller quenching constant than the Ir-3 and Ir-4 complexes (e.g. 1.71 x $10^4$ $M^{-1}$ for Ir-3 *vs* 5.51 x $10^5$ $M^{-1}$ for Ir-4). This indicated a relatively non-efficient TTET process and was also

observed for Ir-2.Figure 3.5(a) shows the emission spectra of the four sensitizers ($\lambda_{exc}$ = 445 nm). The phosphorescence peak areas of the complex Ir-4 and Ir-5 are considerably smaller than those of the corresponding emission peaks for Ir-2 and Ir-3. This suggests that the Ir-4 and Ir-5 complexes would be poor sensitizers for TTA. Figure 3.5(b) shows the upconverted emission of all four sensitizers after addition of DPA, which illustrates that Ir-4 and Ir-5 are in fact excellent sensitizers, and are much more effective than Ir-2 and Ir-3. In fact, Ir-4 and Ir-5 display an upconversion quantum yield of 21.3 % and 23.4 % respectively. This verifies that non-emissive sensitizers like Ir-4 and Ir-5 can be targeted for TTA upconversion applications, and that the dark excited states of the complexes can be effective energy donors of the TTET process. This is the first report of such a finding and should greatly assist the search for commercially viable triplet sensitizers. The criteria for selection of other potential sensitizing materials will also have to be reassessed to reflect this development.

### 3.1.4 Selecting potential sensitizers for TTA upconversion

To our knowledge, no report to date has directly compared the upconverting ability of two different metals, chelated by the same ligand. In theory, all of the Ru(II) and Ir(III) complexes described in Chapter 2 have the potential to act as triplet sensitizers, however further examination of their UV-Vis absorption spectra (Figure 3.6) and the room temperature triplet lifetime measurements revealed that a number of the complexes displayed weak MLCT absorption bands in the region of $\lambda$ = 450-500 nm, and shorter lifetimes than the reference complexes $[Ru(dmb)_3]^{2+}$ and $Ir(ppy)_3$. On the basis of the criteria previously discussed, the pyrenyl complexes **10** and **15** are the strongest candidates for further investigation. The limited number of studies on Ru(II) and Ir(III) complexes discussed in the literature to date, and the work by Zhao *et al.* on the dark excited states of Ir(III) coumarin derivatives as energy donors prompted the inclusion of the naphthyl complexes **9** and **14**, and HBC complexes **12** and **16** in the initial studies of our work. The HBC complexes display moderate absorption but unfortunately have demonstrated short triplet lifetimes. The naphthyl derivatives display MLCT absorption at higher energy, but have moderate triplet lifetimes.

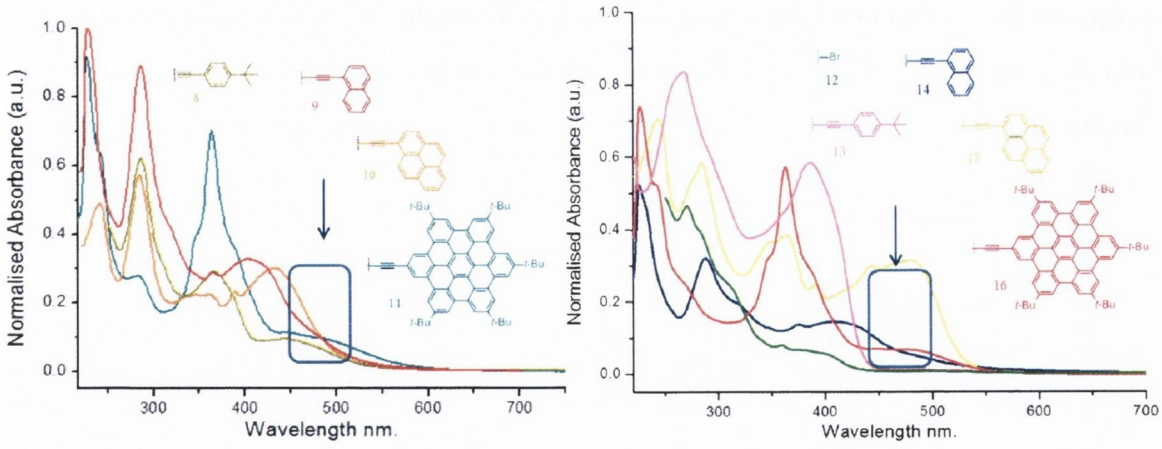


*Figure 3.6: A comparison of the UV-Vis absorption spectra of the Ru(II) complexes* ***8-11*** *and Ir(III) complexes* ***12-16*** *with highlighted area indicating the MLCT absorption from* $\lambda$ *= 450-500 nm.*

DPA was chosen as the triplet acceptor, as it possesses a triplet state energy (1.77 eV, $\lambda$ = 700 nm) that is lower than the complexes, thereby fulfilling the requirements of the TTA upconversion system. Using DPA as a triplet acceptor thereby requires that the excitation wavelength must be of lower energy so as emission is restricted to that generated by TTET process between the sensitizer and the upconverted fluorescence i.e. greater than $\lambda$ = 450 nm. On this basis, it is again imperative that the selected complexes display strong absorption above $\lambda$ = 450-500 nm. Initial measurements were carried out using a Horiba-Yvon Fluorolog FL-3-11 spectrofluorimeter. Figure 3.7 (a) shows the emission spectra of DPA obtained when the sample was excited at $\lambda$ = 478 nm. This control illustrates that no upconversion is observed from DPA alone. The complexes were prepared at 1 x $10^{-5}$ M concentration in dichloromethane, and thoroughly degassed by freeze-pump thaw before each respective emission spectrum was recorded. Increasing aliquots of DPA solution (1 x $10^{-5}$ M) were added between each measurement. Although multiple measurements were attempted, the intense lamp saturated the resulting emission spectra. Attempts to alleviate this problem included running the samples with an optical notch filter, and increasing the sample concentration.

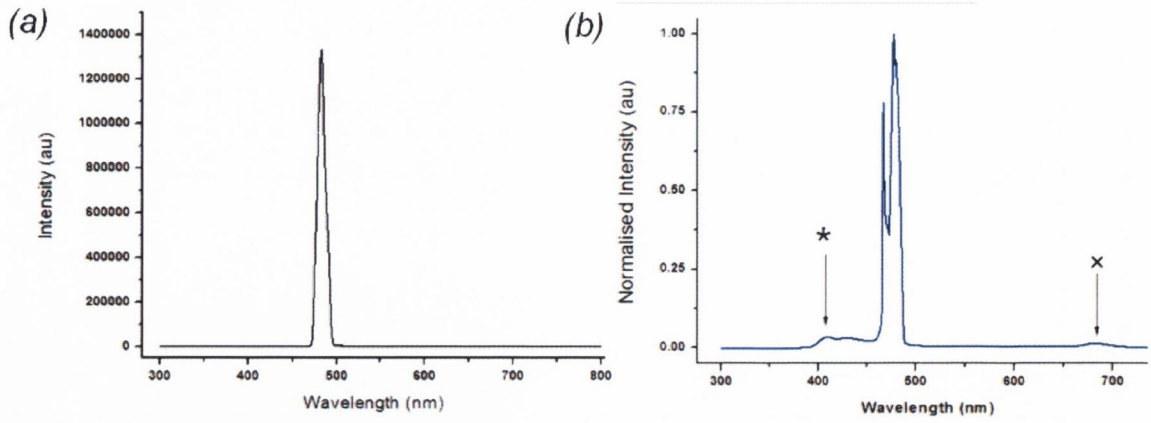


*Figure 3.7: (a) Control illustrating that no fluorescence is observed from DPA when excited at λ = 478 nm and (b) the emission spectra of* ***15*** *and DPA obtained when excited at λ = 478 nm with the incorporation of an optical notch filter. "*" indicates upconversion at λ = 420 nm and" x" the phosphorescence of* ***15*** *detected at λ = 680 nm.*

Figure 3.7(b) illustrates that upconverted emission is detected for **15** (*) at λ = 420 nm when the notch filter is incorporated into the instrumental setup. Although the intensity of the lamp signal at λ = 478 nm was notably reduced, this reduction was not adequate enough to permit accurate measurements of the concentration dependency of the upconverted emission with increasing additions of the triplet acceptor. If the samples are measured at the same concentration, and the spectrum is stopped before λ = 470 nm, crude measurements indicate that the iridium(III) complex is approximately eight times more efficient at upconverting the acceptor (Figure 3.8 (a) **10** < 20,000 cps, (b) **15** < 200,000 cps). This preliminary measurement suggests that the iridium metal is a stronger triplet sensitizer than the corresponding ruthenium(II) system.

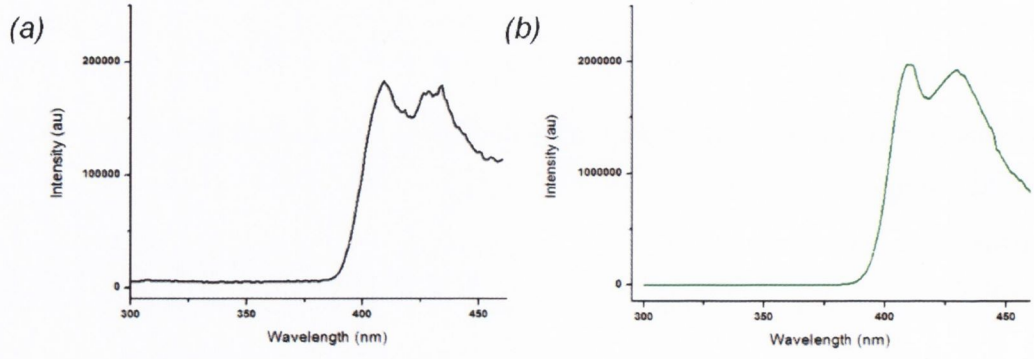


*Figure 3.8: Detected upconverted emission for (a)* ***10*** *and (b)* ***15*** *upon addition of 6 eq. of DPA ($\lambda_{exc}$ = 470 nm). The spectral window is limited to λ = 300-460 nm to illustrate that upconversion is detectable before λ = 470 nm, at which point the spectra becomes saturated by the scattered light from the lamp. Scale indicates that* ***15*** *is approximately 8 times more efficient at upconverting DPA than* ***10*** *when excited at λ = 478 nm.*

Measurements were then repeated using the naphthyl and HBC substituted complexes as triplet sensitizers. In the case of both naphthyl substituted complexes, no appreciable upconversion was observed from the Ru(II) complex **9** [see Figure 3.9 (a)], and weak upconverted fluorescence was generated by the Ir(III) complex **16**. This verifies that lower energy MLCT absorption generates stronger TTA sensitizers. The HBC derivatives **11** and **16** both displayed moderate upconversion when six equivalents of DPA were added. However by increasing the slit width and the further addition of 25 equivalents of DPA, the spectrum in Figure 3.9(b) was recorded.

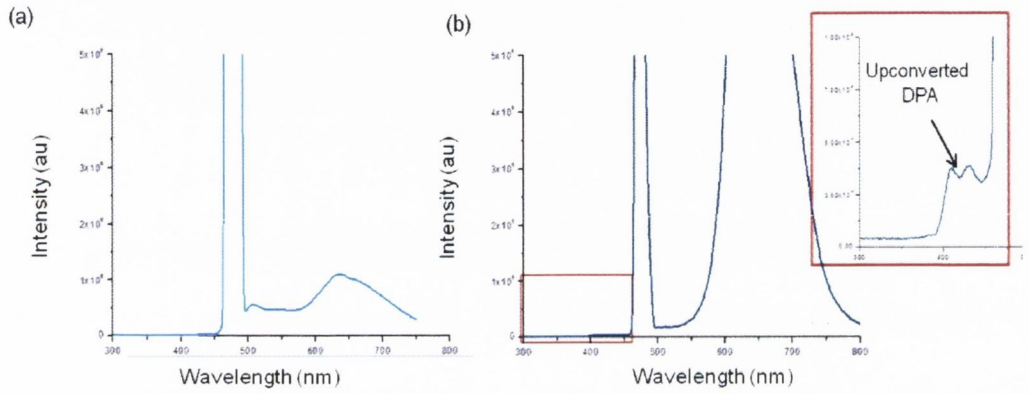


*Figure 3.9: (a) The emission spectra recorded for the Ru(II) naphthyl substituted complex **9** after the addition of 6 equivalents of DPA ($\lambda_{exc}$ = 478 nm), and (b) the emission spectra of Ir(III) HBC derivative **16** with 25 equivalents of DPA (inset shows upconverted DPA when the spectra is run between $\lambda$ = 300 and 450 nm.*

By directly comparing the two metals, this initial study suggests that when chelated to the same ligand, the iridium derivatives show superior ability as TTA sensitizers. Overall, the pyrenyl substituted 1,10-phenanthrolines appear to be stronger sensitizers than the other complexes. This is not surprising as both display superior extinction coefficients in the visible absorption spectra between $\lambda$ = 450-500 nm compared to all of the other aryl acetylene complexes as well as extended phosphorescence lifetimes.

#### 3.1.4.1.1 Further developments towards 10 and 15 as TTA sensitizers

To establish the concentration dependency of the samples and the overall value for the upconverting efficiency of **10** and **15**, further work was carried out in collaboration with Professor Jianzhang Zhao and his student Wanhua Wu at Dalian University of Technology in China. In order to directly compare our study with previous work, the compounds $Ir(ppy)_3$ and $[Ru(dmb)_3]^{2+}$ have been included as reference complexes (Figure 3.10) and were synthesised according to literature procedures in comparable yields.[119, 131] $Ir(ppy)_3$ undergoes rapid ISC, and the $^3$MLCT quantum yield is reported to

reach unity. It is photostable and exhibits high triplet energy (~20,000 $cm^{-1}$).[178] All measurements were performed using a continuous wave diode-pumped solid-state laser with output at $\lambda$ = 473 nm. All solutions were purged with argon for 30 minutes before the measurement was recorded. The typical laser power was 5mW (the diameter of the laser spot was 3mm; therefore the surface power density was calculated to be approximately 71 $mWcm^{-2}$).

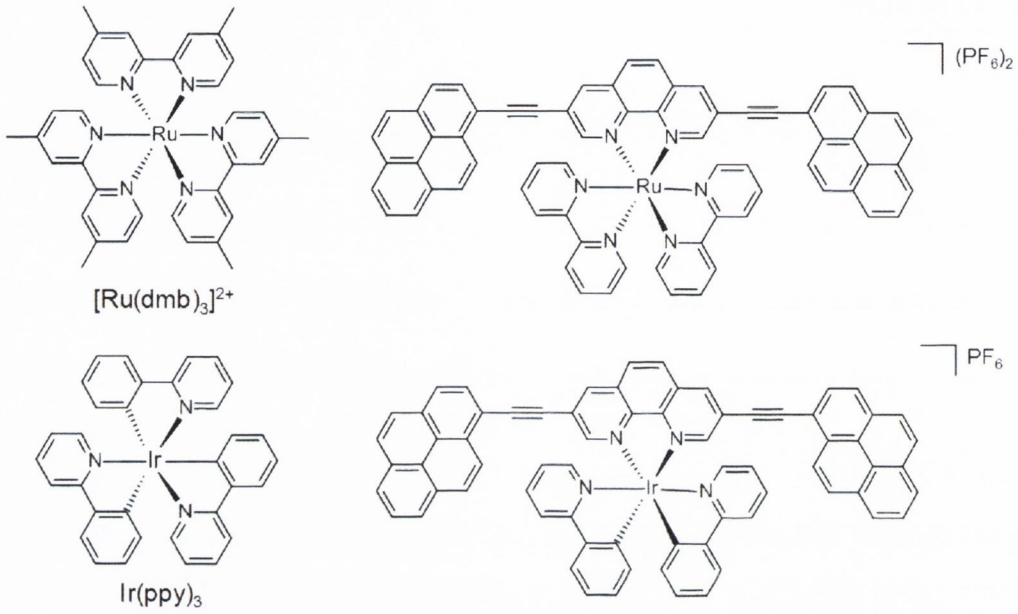


*Figure 3.10: Structures of reference compounds $Ir(ppy)_3$ and $[Ru(dmb)_3]^{2+}$ and synthesised complexes [(Ru (3,8-ethynylpyrene-1,10-phenanthroline)(bpy)$_2$)](PF$_6$)$_2$ (**10**) [Ir(ppy$_2$) (3,8-bis[2-(pyrene)ethynyl]-1,10-phenanthroline]PF$_6$ (**15**) which were selected for further TTA analysis.*

Figure 3.11(a) shows the overlaid emission spectra of **15**, the reference compound $Ir(ppy)_3$, and the triplet acceptor DPA. The emission intensity of $Ir(ppy)_3$ is five times greater than that of **15**. As previously discussed in Chapter 2, **15** displays intraligand (IL) emission as is characteristic of pyrene complexes.[129] As expected, DPA shows no observable emission. Figure 3.11(b) shows the emission of the acceptor upon addition of the DPA at a concentration of 4.0 x $10^{-5}$ M. A new emission is observed at $\lambda$ = 420 nm and $\lambda$ = 540 nm respectively. This indicates successful TTA upconversion of the DPA, and agrees with the steady-state fluorescence emission observed for the acceptor.[182] **15** generates considerably stronger upconverted fluorescence than $Ir(ppy)_3$ when used as the triplet sensitizer. This is consistent with the triplet excited state of **15** being more efficiently populated upon excitation, and indicative of a superior TTET process

occurring. Since phosphorescence is a competing process to TTET, **15** is another example of a weakly phosphorescent material being suitable for triplet sensitization in upconversion.[180]

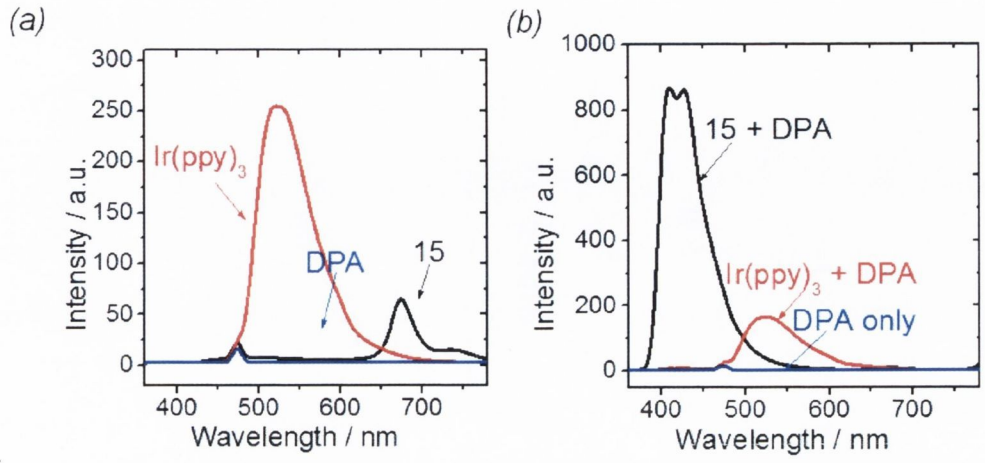


*Figure 3.11: (a) Overlaid fluorescence spectra obtained for $Ir(ppy)_3$, **15** and DPA before the acceptor is added to the sensitizers ($\lambda_{exc}$ = 473 nm) and (b) emission observed upon addition of DPA to the sensitizers. Concentration of the complexes = 1.0 x $10^{-5}$M, concentration of DPA = 4.0 x $10^{-5}$ M. ($CH_3CN$, 20 °C).*

The variation in the emission of the sensitizer **15** with increasing DPA concentration was explored [Figure 3.12 (a)]. Increasing blue fluorescence of the newly formed singlet excited state of DPA was observed upon excitation of the mixture of DPA and the complex with a $\lambda$ = 473 nm laser. The high upconversion efficiency of the complex is as a result of the long lifetimes of the $^3$IL excited state, and not a typical $^3$MLCT state.[125] Sensitizers with extended lifetimes enable an increased probability of an encounter between it and the acceptor, resulting in a more efficient TTET process and increase in the diffusion distance. Significant quenching of the phosphorescence at ca. $\lambda$ = 670 nm was observed with increased concentration of DPA. Higher quenching constants are also indicative of more efficient TTET. Figure 3.12(b) illustrates the calculation of the upconversion quantum yield with increasing concentration of DPA. Extrapolation of the curve indicates that the quantum yield is less than 10%.

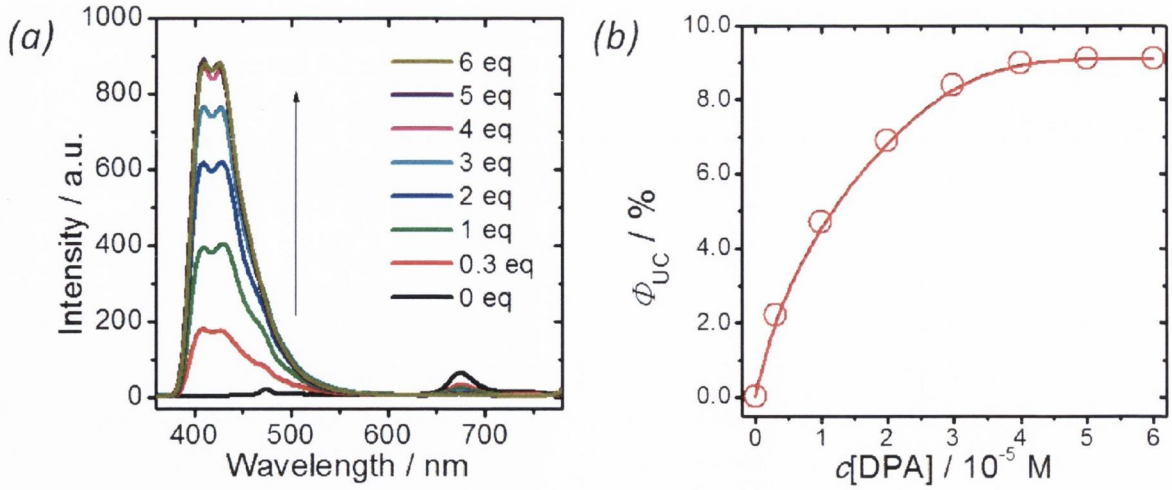


*Figure 3.12 (a) Emission spectra showing upconverted fluorescence observed with increasing DPA concentration and (b) upconversion quantum yield with **15** as triplet sensitizer with increasing DPA concentration; Excitation with λ = 473 nm laser (5 mW). [sensitizer] = 1.0 x $10^{-5}$M, $CH_3CN$, 20 °C.*

**3.1.4.1.2 Upconversion with 10 as the triplet sensitizer and DPA as the acceptor.**

The experimental conditions utilised for **15** and $Ir(ppy)_3$ were applied in the analysis of **10** and the reference compound, $[Ru(dmb)_3]^{2+}$. Figure 3.13(a) shows the overlaid emission spectra of **10** when excited with a λ = 473 nm laser, the emission spectra of DPA, and the upconverted fluorescence generated by the sensitizer when four equivalents of DPA are added. The emission intensity of **10** alone is considerably stronger than that obtained for the iridium(III) derivative **15**, however the upconverted fluorescence generated by the TTET from **10** to DPA is considerably weaker. Further measurements were attempted with increased laser intensity, and increasing concentrations of DPA. In all cases, poor upconversion was observed. The difference between the two complexes is approximately a factor of eight. This measurement is in agreement with the screening method previously utilised on the complexes in Figure 3.8, and suggests this method is a sufficient and reliable one for identifying potential candidates for TTA upconversion. The phosphorescence of **10** is effectively quenched on addition of DPA, which is indicative of an efficient TTET process.

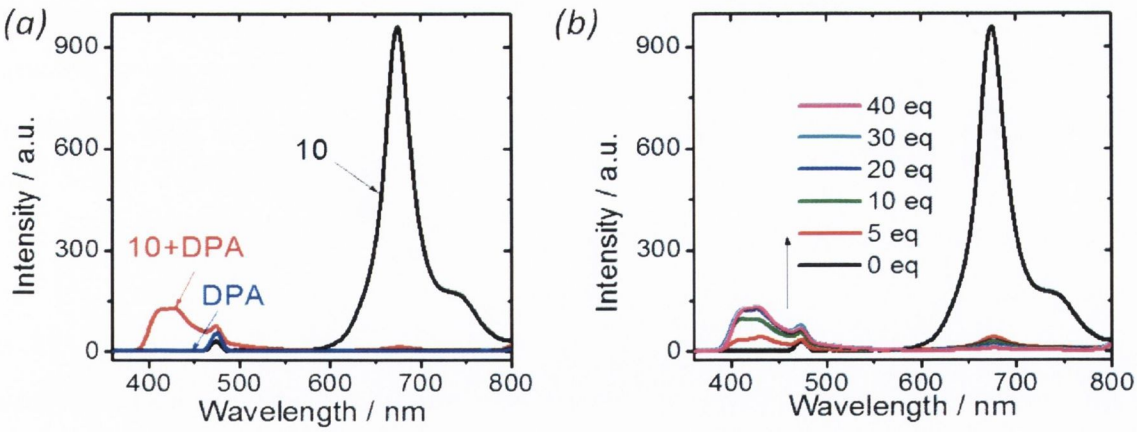


*Figure 3.13: Upconversion with (a)* ***10*** *as the sensitizer (concentration of the sensitizer = 1.0 x $10^{-5}$M, concentration of DPA = 4.0 x $10^{-5}$ M) and (b) upconverted emission observed with addition of increasing DPA concentration to* ***10*** *(MeCN ,20 °C).*

Figure 3.13(b) shows the DPA concentration dependency of upconverted emission generated by **10**. The response is remarkably different to the corresponding study of **15** from Figure 3.12, and shows that even with 40 equivalents of DPA, the maximum upconverted fluorescence is still approximately 8 times less than that observed for **15**. Given the intense phosphorescence of the complex, it is probable that there is an additional competing process occurring such as electron transfer within the complex itself.

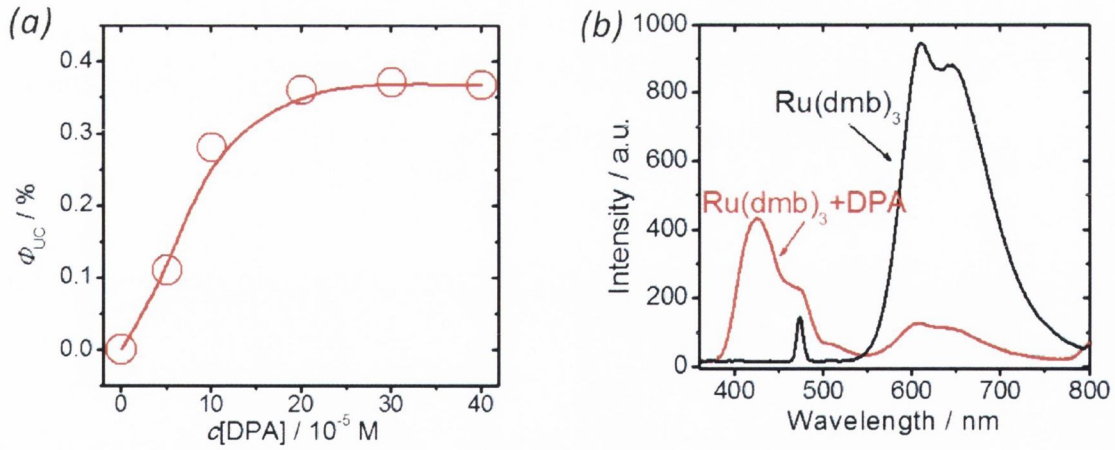


*Figure 3.14: (a) Calculation of the upconversion quantum yield with* ***10*** *as triplet sensitizer with increasing DPA concentration. (b) Overlaid emission spectra of $[Ru(dmb)_3]^{2+}$ and upconverted fluorescence generated by $[Ru(dmb)_3]^{2+}$ upon addition of DPA (concentration of the sensitizer = 1.0 x $10^{-5}$M, $CH_3CN$, 20 °C).*

Figure 3.14(b) shows the corresponding emission spectra obtained for the complex

$[Ru(dmb)_3]^{2+}$. Unlike **10**, the reference complex displays residual phosphorescence which suggests that it does not undergo efficient TTET in the upconversion process. $[Ru(dmb)_3]^{2+}$ has a reported upconversion quantum yield of 1% , while the calculated upconversion quantum yield of **10** under the same experimental conditions is less than 1% [Figure 3.14(a)].

As suggested by the preliminary screening experiments, the iridium complex **15** is approximately eight times more efficient at sensitizing DPA than the Ru(II) derivative **10**. This is almost certainly explained by the stronger MLCT absorption in the visible region of **15**, however it is also possible that a competing process, electron transfer, is occuring, or intramolecular electron transfer within **10** itself. This does not account for the difference between the measured $\Phi_{UC}$ for **10** (~1%), and the 3-pyrenyl-10-phenanthroline derivative (**Ru-4**, Figure 3.3) previously reported by Zhao and co-workers. **Ru-4** has a similar upconversion efficiency to the iridium complex **15** i.e. $\Phi_{UC}$ = 9.6%, which would suggest that the additional pyrenyl subunit has little affect on the efficiency of the complex. One proposed explanation for the unusual behaviour of **10** could be that the energy gap between the $^3$IL state of **10** and the $^3\pi$-$\pi^*$ state is considerably smaller than the corresponding energy gap of **15** and Ru-4. This would result in a reduction in the driving force for the TTET process, and has been previously observed in ruthenium(II) coumarin derivatives.[168] Although the inclusion of one pyrene chromophore appears to have a significant influence on the ruthenium(II) metal centre, two pyrene acetylene units may introduce a non-radiative decay pathway that is competing with the upconversion process.

### 3.1.4.2 Nanosecond time-resolved transient difference absorption spectroscopy for 10 and 15.

In order to further investigate the $T_1$ states of the complexes, the transient species were measured using nanosecond time-resolved transient difference absorption spectroscopy. Transient absorption spectroscopy is a useful technique which provides information on the electronic properties of the transient states, where a laser pulse is used to excite a molecule from the ground state to the excited state. The absorption is measured as a function of the elapsed time after excitation. The wavelength of the absorption band can be determined by the energy gap from the probed excited state to a state of higher energy.

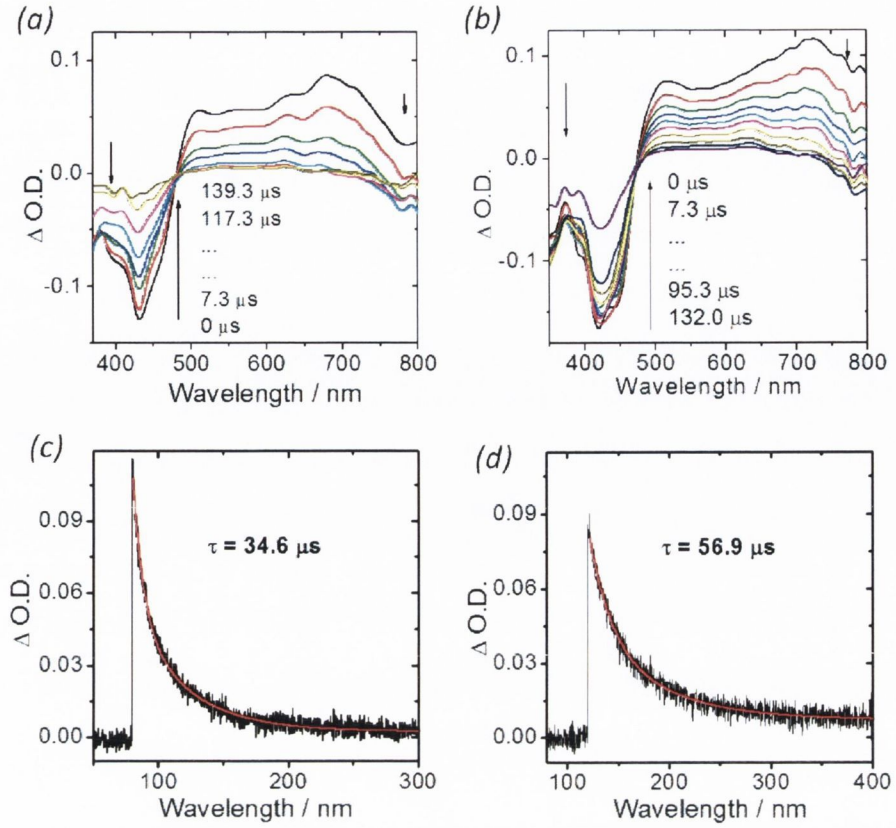


*Figure 3.15: Nanosecond time-resolved transient absorption spectra of (a)* ***15*** *and (b)* ***10*** *after pulsed excitation ($\lambda_{ex}$ = 355 nm). Arrows indicates the elapsed time after a 355 nm laser flash. Figure (c) and (d) show the corresponding decay traces obtained for the two complexes at λ = 600 nm ( c = 1.0 x10 $^{-5}$M, $CH_3CN$, 20 °C)*

Figure 3.15(a) shows the transient absorption spectra recorded for **15**. Significant ground bleaching was observed at λ = 435 nm, which is attributed to the $^3$IL absorption of the transient species. The presence of the ethynyl linker facilitates coupling between the 1,10-phenanthroline core and the pendant pyrene chromophores, and it is therefore highly likely that the $^3$IL state consists of contributions from both moieties. Similar transient difference absorption profiles have been observed for other pyrene complexes, and have been assigned as the mixed $^3$IL/$^3$LLCT emissive excited state, therefore we also assign the emissive state of **15** in this manner.[63, 130] Figure 3.15(b) shows the absorption spectra recorded for **10**, which shows a similar absorption band in the λ = 500-800 nm region. On this basis it can also been assigned to the $^3$IL/$^3$LLCT (pyrene localised) emissive excited state. The lifetimes of the complexes were also measured by monitoring the decay kinetics of the bleaching [**15** = 34.6 μs and **10** = 56.9 μs, Figure 3.15 (c) and (d)]. These extended lifetime values further support the assignment of $^3$IL/$^3$LLCT emissive excited state.

### 3.1.4.3 Calculating the singlet oxygen quantum yield of 10 and 15.

To investigate the nature of the transfer mechanisms of the triplet excited states of **10** and **15**, the singlet oxygen quantum yields ($\Phi_{\Delta}$) of the complexes were determined by Prof. Jianzhang Zhao and his research group in Dalian University in China. $^1O_2$ quantum yields ($\Phi_{\Delta}$) of the two complexes were calculated using 5, 10, 15, 20-tetraphenylporphyrin (TPP) as a reference standard and 1,3-diphenylisobenzofuran (DPBF) as a $^1O_2$ scavenger (Figure 3.16*)*. The absorbance of DPBF was adjusted to approximately 1.0 in air saturated $CH_2Cl_2$. The photosensitizer was added to the cuvette and the photosensitizers absorbance was adjusted to 0.2-0.3. The cuvette was irradiated with monochromatic light at the absorbance maxima for 10 seconds with repeat measurements for the absorbance maximum taken before each successive irradiation. The slope of the absorbance maxima of DPBF at $\lambda$ = 414 nm versus the accumulated photoirradiation time was calculated for both complexes.

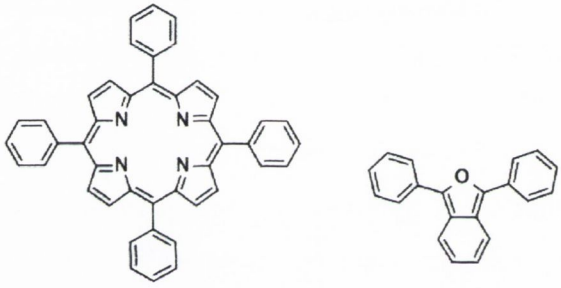


TPP DPBF

*Figure 3.16: The reference compound 5,10,15,20-tetraphenylporphyrin (TPP) and $^1O_2$ scavenger 1,3-diphenylisobenzofuran (DPBF) used in the calculation of the singlet oxygen quantum yields.*

The singlet oxygen quantum yield for each complex was then calculated using the following equation:

$$\Phi_{\Delta_{unk}} = \Phi_{std} \cdot \frac{m_{unk} F_{std}}{m_{std} F_{unk}}$$

where "*unk*" and "*std*" refer to the photosensitizer and the reference respectively, *m* is the slope of the difference in change in absorbance of DPBF ($\lambda$ = 414 nm) with irradiation time, and *F* refers to the absorption correction factor which is given by F=1-10-OD. Table 3.1 contains the values calculated for both complexes and the reference complex TPP.

*Table 3.1: The calculated singlet oxygen quantum yields of **10**, **15** and TPP.*

| | $\Phi_\Delta$ |
|---|---|
| TPP | 0.62 |
| **10** | 0.53 |
| **15** | 0.59 |

The calculated values for **10** and **15** are both within the expected range for ruthenium(II) and iridium(III) complexes, but surprisingly low considering the extended triplet lifetimes displayed by both complexes, which should enable efficient quenching of singlet oxygen. As both **10** and **15** display moderate singlet oxygen quantum yields (~0.5), it is therefore most likely that energy transfer is the dominate mechanism for singlet oxygen production. Electron transfer is typically dominant in complexes that display larger values of $\Phi_\Delta$. The comparable values for $\Phi_\Delta$ further supports the suggestion that the difference in the upconversion quantum yield between the two complexes is due to the weaker MLCT absorption displayed by **10** rather than different transfer mechanisms between the individual complexes and the triplet acceptor.

### 3.1.5 Theoretical calculations: to establish the lowest lying excited states of 10 and 15.

To further evaluate the photophysical properties of the two complexes, and to establish the lowest lying singlet excited states and triplet excited states, DFT/TDDFT calculations were carried out in collaboration with Professor Jianzhang Zhao in the University of Dalian in China. Figure 3.17 (a) and (b) shows the calculated isosurfaces of the spin density of both the ruthenium(II) (**10**) and iridium(III) complex (**15**). The isosurface of the spin density of both complexes is mainly localised on the pyrene chromophore, with a small contribution from the 1,10-phenanthroline moiety. The contribution of the metal centres and the auxilary ligands in **10**, and 2-phenylpyridine ligands of **15** appears to be minimal. This indicates that the major component of the triplet excited state of both complexes is the $^3$IL state, and is in agreement for other polyimine complexes with extended $\pi$-conjugation.[125, 168]

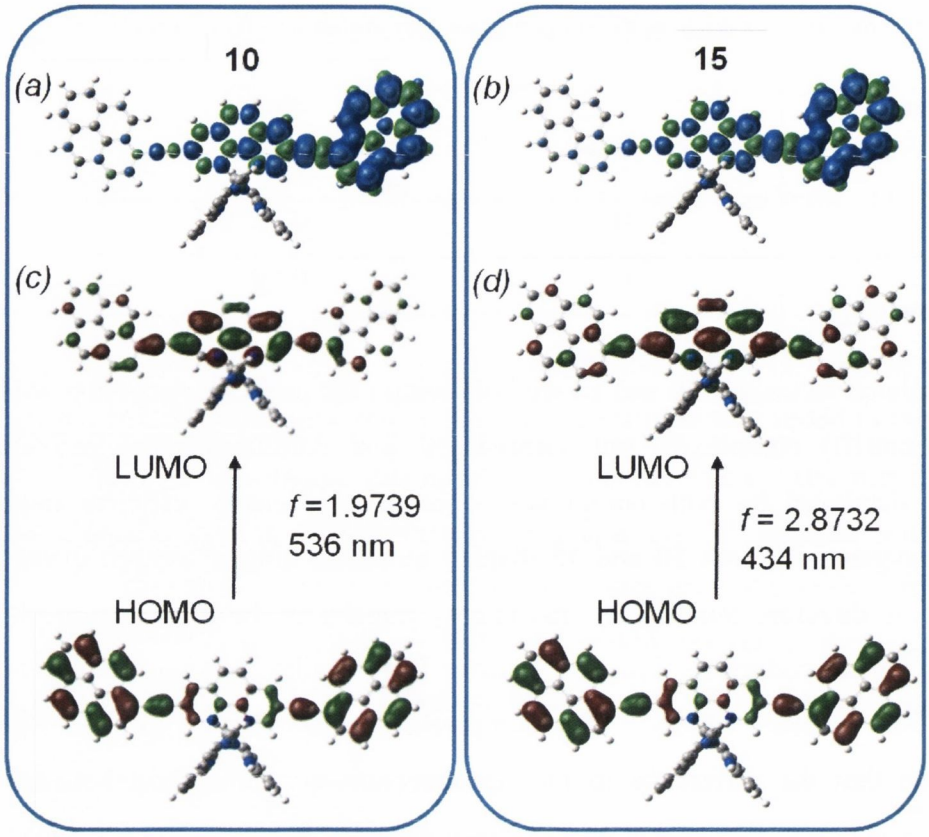


*Figure 3.17: (a) and (b) the calculated isosurfaces of spin density of **10** and **15** at the optimized triplet state geometries, (c) and (d) the corresponding frontier molecular orbitals depicting the HOMO-LUMO gaps for **10** and **15**. The calculations are at the B3LYP/6-31G(d)/LanL2DZ level using Gaussian 09W and toluene as solvent.*

Figure 3.17 (c) and (d) show the corresponding frontier molecular orbitals calculated for both complexes, and the calculated absorption wavelengths ($\lambda$ = 536 nm and 434 nm respectively). The iridium(II) complex **15** demonstrates a considerably higher oscillator strength which predicts a strong low energy absorption at $\lambda$ = 434 nm. The experimentally derived absorption appears as a broad band between $\lambda$ = 430 nm and 515 nm, and has previously been assigned in Chapter 2 as a predominately Ir-ppy→phen charge transfer transition. Based on the DFT/TDDFT calculations shown, this extended absorption also contains a significant contribution from the charge transfer between the pyrene chromophore to the central 1,10-phenanthroline. Although the calculated oscillator strength for the ruthenium derivative **10** is significant at $f$ = 1.9739, it is considerably less than the comparable value for **15**. This is surprising, as the extinction coefficients previously calculated for both complexes in Chapter 2, are almost identical [$\lambda$= 435 nm $\varepsilon$ = 29910 $M^{-1}$ $cm^{-1}$ (**10**) and $\lambda$ = 480 nm $\varepsilon$ = 31358 $M^{-1}$ $cm^{-1}$ (**15**)]. It is also worth considering that the 3-ethynyl pyrene derivative of **10**, has a broad $^{1}$MLCT

absorption at slightly higher energy ($\lambda_{abs}$ = 418 nm) and that the extinction coefficient of this band is elevated ($\varepsilon$ = 38800 $M^{-1}$ $cm^{-1}$) with respect to **10** and **15**, which may explain the superior upconverting ability of the complex.

*Table 3.2: Summary of selected parameters for the vertical excitation (UV-vis absorption and fluorescence emission) of complexes **10** and **15**. Electronic excitation energies (eV) and oscillator strengths (f), configurations of the low-lying excited states and fluorescent precursors. Based on the optimized ground state geometries.*

| | Electronic transition [a] | TDDFT/B3LYP/6-31G(d) | | | |
|---|---|---|---|---|---|
| | | Excitation energy | $f$ [b] | Composition [c] | CI [d] |
| **10** | | | | | |
| Absorption | $S_0 \rightarrow S_1$ | 2.31 eV (536 nm) | 1.9739 | $H \rightarrow L$<br>$H \rightarrow L+2$ | 0.3360<br>0.5648 |
| Triplet states | $T_0 \rightarrow T_1$ | 1.52 eV (816 nm) | 0.0000 | $H-1 \rightarrow L+4$<br>$H \rightarrow L$ | 0.4096<br>0.4271 |
| | $T_0 \rightarrow T_2$ | 1.60 eV (775 nm) | 0.0000 | $H-1 \rightarrow L$<br>$H-1 \rightarrow L+5$<br>$H \rightarrow L+4$ | 0.3481<br>0.3209<br>0.4532 |
| **15** | | | | | |
| Absorption | $S_0 \rightarrow S_1$ | 2.86 eV (434 nm) | 2.8732 | $H \rightarrow L$ | 0.6105 |
| Triplet states | $T_0 \rightarrow T_1$ | 1.56 eV (792 nm) | 0.0000 | $H-1 \rightarrow L+2$<br>$H \rightarrow L$ | 0.4173<br>0.4196 |
| | $T_0 \rightarrow T_2$ | 1.64 eV (757 nm) | 0.0000 | $H-1 \rightarrow L$<br>$H-1 \rightarrow L+3$<br>$H \rightarrow L+2$ | 0.3459<br>0.3291<br>0.4569 |

*Calculation was performed at B3LYP/6-31G(d) / LanL2DZ level with Gaussian 09W. [a] Only selected excited states were considered. Methanol was used as solvent. The numbers in brackets are the excitation energy in wavelength. [b] Oscillator strength. [c] H stands for HOMO and L stands for LUMO. Only the main configurations are presented. [d] Coefficient of the wavefunction for each excitations. The CI coefficients are in absolute values.*

To quantify the triplet excited states of both complex **10** and **15**, further DFT calculations were performed on the optimised geometries of the individual ground states. The lowest energy triplet $T_1$ of **10** is located at $\lambda$ = 816 nm, which is more red shifted than the experimental value of $\lambda$ = 626-753 nm. The difference between the measurements may be accounted for to some extent by solvent polarity. The computed value is based on calculations performed in methanol, however the poor solubility of the complexes

limited the experimental measurements to $CH_2Cl_2$. The lowest energy triplet $T_1$ of **15** is $\lambda$ = 792 nm which is closer agreement to the experimental value of $\lambda$ = 684-758 nm. The additional higher energy transitions $S_0 \rightarrow T_2$, calculated by DFT for both complexes at $\lambda$ = 775 nm (**10**) and $\lambda$ = 759 nm (**15**) are in agreement with the observed vibronic structure, and are a feature of pyrenyl complexes. As previously discussed in Chapter 2, the energy difference between the emission peaks matches the C≡C IR frequencies of **10** and **15**. On this basis, it can also be attributed to the emissive $^3$IL state. Table 3.2 contains a summary of the selected electronic excitation energies and oscillator strengths for both complexes

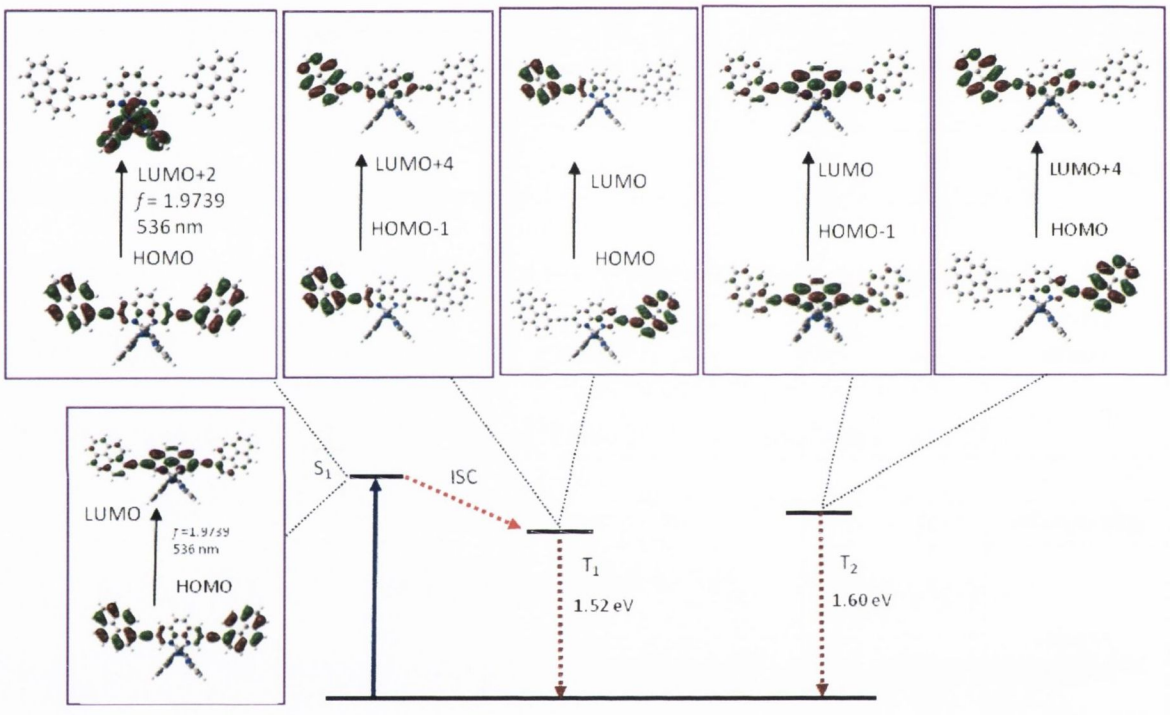


*Figure 3.18: Selected frontier molecular orbitals involved in the excitation and emission of **10**. Calculation was performed at B3LYP/6-31G(d) / LanL2DZ level with Gaussian 09W.*

Figure 3.18 and Figure 3.19 show the selected frontier molecular orbitals involved in the emission and excitation of both of the complexes, and confirm that the two degenerate lowest lying triplet excited states ($T_1$ and $T_2$) are localised on the pyrene moiety with a small contribution from the 1,10-phenanthroline ligand centre. This confirms that the emission of both complexes is due to the ligand centred triplet state ($^3$IL/LLCT), as previously indicated by transient absorption studies.

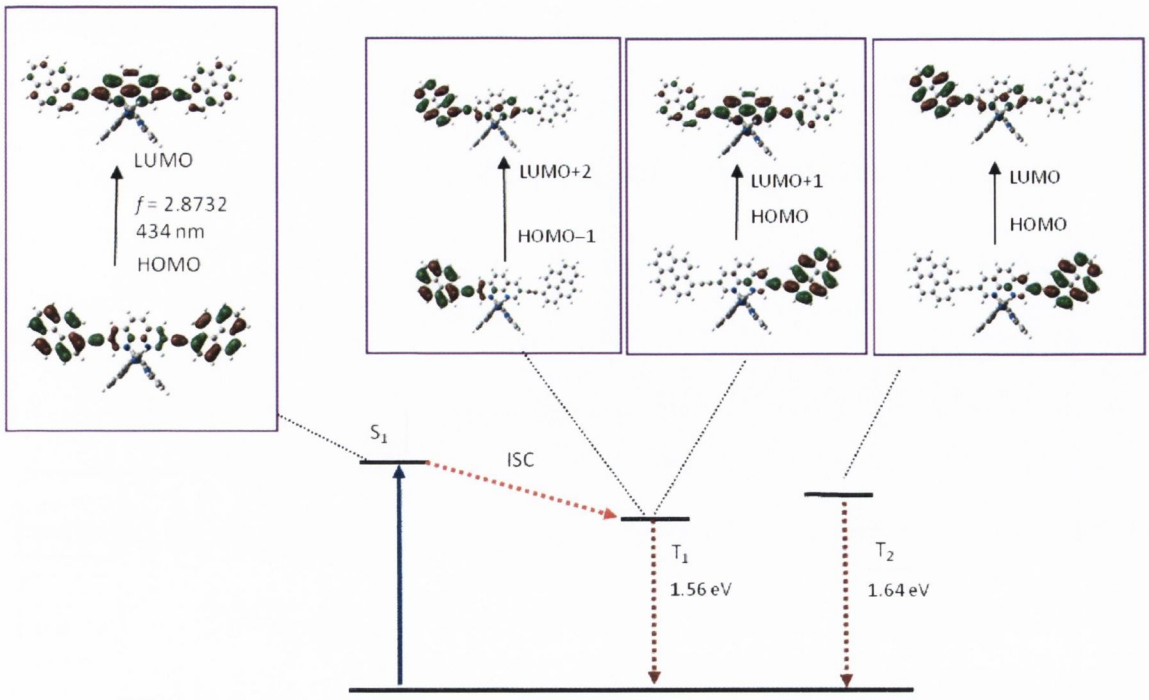


*Figure 3.19: Selected frontier molecular orbitals involved in the excitation and emission of **15**. Calculation was performed at B3LYP/6-31G(d) / LanL2DZ level with Gaussian 09W.*

## 3.2 Conclusions

This chapter successfully illustrates the development of a new screening system for TTA upconversion sensitizers using a typical fluorimeter setup, and the subsequent photophysical and computational investigation of complexes **10** and **15**. A comparison of the upconverting ability of two metals coordinated to the same ligand has shown that the cyclometallated iridium(III) complex displays a higher TTA upconversion efficiency than the corresponding ruthenium(II) derivative. Scheme 3.5 summarizes the overlaid upconversion process for each of the two sensitizers and DPA. Based on the results of the singlet oxygen quantum yield measurement, and DFT/TDDFT calculations, we are attributing the variation in the upconverting efficiency between the two complexes as being primarily due to the stronger absorption of **15** at the excitation wavelength ($\lambda$ = 473 nm), thereby enabling more efficient TTET to take place, and superior TTA upconversion to occur. However, the difference between the $\Phi_{UC}$ of **10** and the Ru(II) 3-ethynylpyrene- 1, 10-phenanthroline complex previously reported by Zhao and co-workers remains to be conclusively accounted for. It is possible that less efficient TTET may be occurring between our sensitizer and the DPA acceptor. Further quenching experiments will need to be undertaken to quantify this, primarily by investigating the

quenching of the triplet state lifetime, as well as further emission quenching experiments.

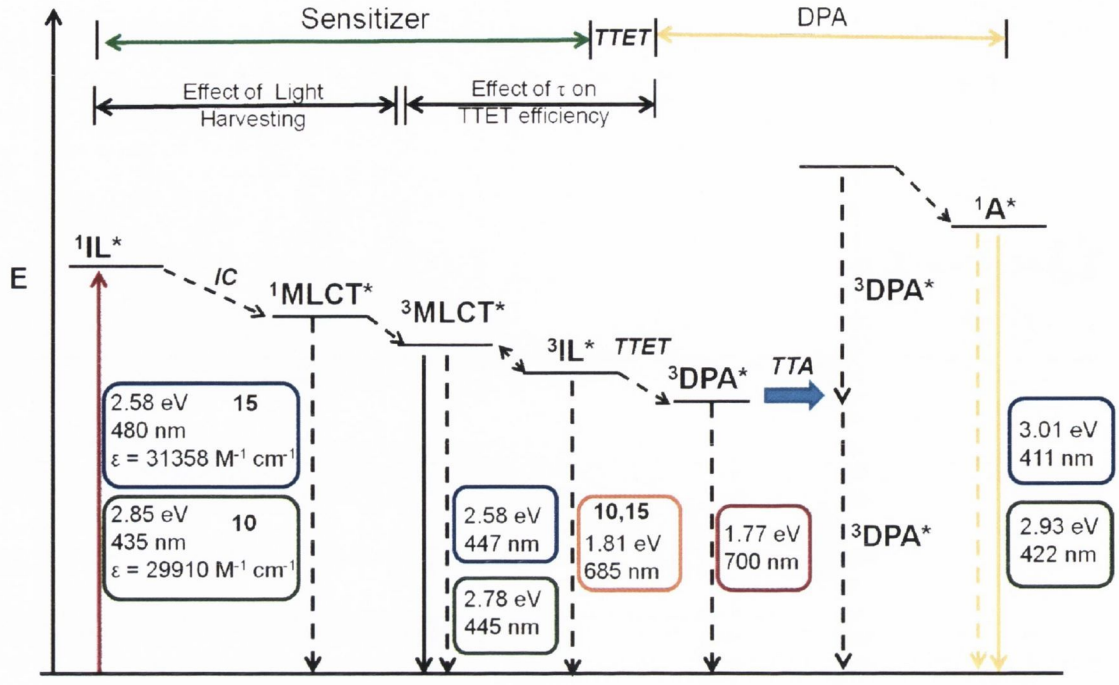


*Scheme 3.5: Qualitative Jablonski diagram summarising the overlaid upconversion process between DPA and individual complexes* ***10*** *(highlighted in green) and* ***15*** *(highlighted in blue). The emission wavelength for the $^3IL^*$ is the same for both complexes (orange inset), as is the energy of the $T_1$ excited state of DPA (1.77 eV).*

### 3.2.1 Future work

The exploitation of our newly developed screening system for potential triplet sensitizers is one of the primary focuses of this project's future work. The vast library of nitrogen doped compounds that have been previously synthesised within the Draper group may potentially yield many other triplet sensitizers which demonstrate high upconversion efficiency. Although recent reports of upconversion with terpyridine substituted complexes has been disappointing, significant progress has been made within the Draper group to develop these complexes for self-assembled monolayer on gold surfaces.[17, 64, 183] Literature studies have been restricted to upconversion with Ru(II), Zn(II) and Pt(II) terpyridine systems.[184, 185] We are interested in further exploiting our aryl terpyridines to compare the efficiency of other metals as TTA materials, such as iridium(III) and osmium(II) complexes. This screening process will also be used in turn to identify other transition metal complexes synthesised within the group which may also be successful candidates for singlet oxygen scavenging.

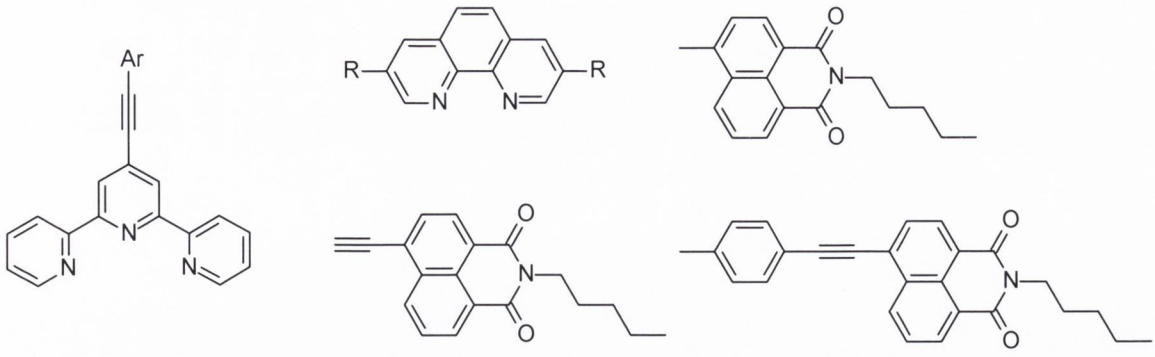


*Figure 3.20: Potential triplet sensitizers designed for future TTA studies as part of the on-going collaboration with Prof. Jianzhang Zhao.*

Work within the group is also on-going to design and extend the 3,8 substituted 1,10-phenanthroline family as efficient triplet sensitizers. The collaboration with Prof. Jianzhang Zhao is still in progress and current work aims to capitalise on the vast number of recent studies on upconversion with various chromophores[186, 187] and apply it to expand the 3,8 substituted 1,10-phenanthroline family. Work will focus on the design of new Ru(II) and Ir(III) complexes with strong absorption which extends further into the visible region of the spectra. One example of this work is a current study on the effect of the varying rigidity between a napthaleneimide (NI) chromophore and the 3,8-substituted 1,10-phenanthroline core. NI functionalised complexes show enhanced absorption in the blue range and extended lifetimes ($\tau_p$ ~ 650 μs), and should display improved upconversion efficiency over the pyrenyl systems examined in this project.[188] To our knowledge, no comparative studies between triplet sensitizer efficiency and linker rigidity have been reported for substituted 1,10-phenanthrolines (Figure 3.20). There is also significant scope to examine the variation in upconversion efficiency with varying 1,10-phenanthroline substitution, i.e. [2,9] vs [4,7] and [5,6] systems.

# 4 Large surface area ligands; extending 3,8-aryl 1,10-phenanthrolines

## 4.1 Extending 1,10-phenanthrolines towards the generation of large surface area nitrogen containing ligands and their potential applications.

Modification of 1,10-phenanthroline units to generate larger fused nitrogen systems would have the potential to develop a family of supergraphene-like materials whose properties would mimic those of larger heteroatom doped graphene systems. Such large surface ligands would have particular application in solar energy harvesting,as on complexation to transition metals they would be expected to generate "black-absorber" materials with enhanced luminescence properties.

The synthesis of large area aromatic ligands is frequently hampered by difficult multi-step syntheses. An exception to this is the synthesis of derivatives of 1,10-phenanthroline-5,6-dione, where condensation reactions between the dione and 1,2 diamines yields extended 1,10-phenanthroline based ligands such as dipyrido[3,2-a:2',3'-c]phenazine (dppz) and tetrapyrido[3,2-a: 2'3'-c:3'',2''-h:2''',3'''-j]phenazine (tpphz) (Figure 4.1).[189-191] This ligand family is generated *via* extension along the y-axis, and exhibits properties consistent with a "dual nature" i.e. individual contributions from two distinct moieties. This suggests that the increase in length with conjugation produces electronic decoupling across the aromatic platform. Turro *et al.* have reported individual contributions from the phenanthroline moiety and the phenazine moiety in Raman spectra for both the free tpphz ligand and the corresponding ruthenium(II) complex.[192] This has also been seen by Schafer and co-workers.[193]

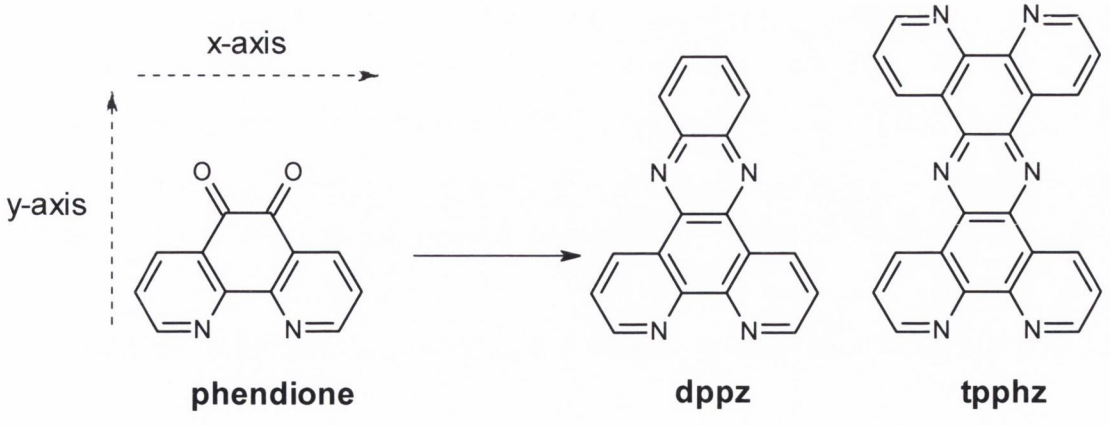


*Figure 4.1: Condensation reactions with phendione produces extended aromatic ligands such as dppz and tpphz. Dotted arrows indicate the two directions by which 1,10-phenanthroline derivatives can be extended.*

This multi-component nature extends to other members of the ligand family, such as the 2,3,5,6-tetrakis(2-pyridyl)pyrazine (tppz) ligand and its bimetallic complexes reported by Launey. The redox behaviour of the complexes show no interaction between the two metal centres, indicating the ligand was acting as two individual components.[194]

### 4.1.1 Extending the conjugation of 1,10-phenanthrolines with aryl substitutent coupling reactions.

An alternative synthetic methodology is to extend 1,10-phenanthrolines along the x-axis of the ligand through coupling reactions. To date, modification by this method has not produced fused phenanthroline systems, however cross-coupling reactions facilitate the use of many commercially available synthetic building blocks to generate highly aromatic systems. Despite the fact that very few examples of these materials currently exist in the literature, those reported offer a range of potential applications. The synthetic strategies adopted for some of this research will be discussed in this section.

#### 4.1.1.1 Carbazole substituted 1,10-phenanthroline ligands

Attaching 9,9-hexylfluorene substituents in the 3,8-position of the 1,10-phenanthroline core takes advantage of all the benefits previously discussed in Chapter 1, whilst also boosting the solubility and hydrophobicity of the ligand. Monkman *et al.* have described a series of mono-and di-substituted 1,10-phenanthrolines and their corresponding cationic bis-cyclometallated bis-ppy iridium(III) complexes for potential light emitting applications.[103] The ligands were prepared through a series of Suzuki-Miyaura cross-coupling reactions with fluorenylboronic esters. The carbazole ligands, such as **PHCB2** (Figure 4.2), were synthesised by a two-fold alkylation of the relevant fluorine precursor. The extended ligand $\pi$ system reduces the non-radiative intermolecular charge recombination which was reported by Bolink *et al.* for similar 4,7-diphenylphenanthroline derivatives.[108] Photoluminescence studies showed a considerable increase in the phosphorescence lifetimes for the symmetric 3,8 substituted compounds with increasing conjugation, over their mono-substituted analogues (**PHAl1** and **PHCB1**). The additional carbazole functionality incorporated into the extended structure improves not only the stability and processibility, but also the hole transport properties of the ligands and their corresponding iridium(III) complexes.[195] The complexes were used to prepare spin coated LECs consisting of ITO/PEDOT:PSS/iridium complex/Al, and were found to display a maximum brightness efficiency of 9 cd/A. It was observed that

the bulky side groups perturbed the diffusion of the counterions in the cell, resulting in longer "switch-on" times than similar literature examples. The bias required to drive the cells appears to be proportional to the number of side chains as well as the overall molecular weight of the complex. These findings suggest that 3,8-substituted 1,10-phenanthrolines with shorter alkyl chains could have potential in luminescent devices.

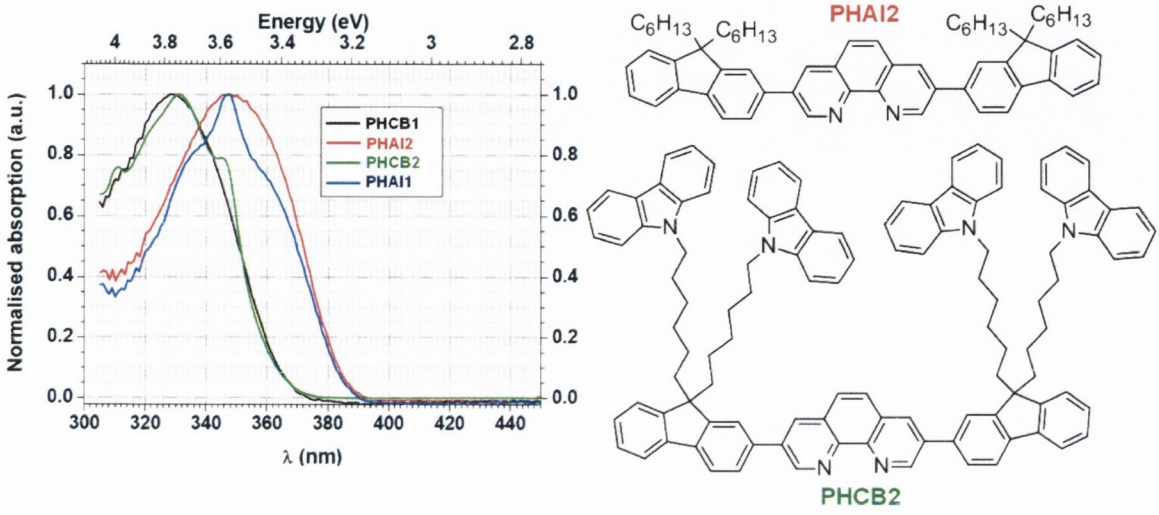


*Figure 4.2: Normalised electron absorption spectra of the ligands described by Monkman et al. and the 3,8-substituted derivatives of the series.* ***PHAI1*** *and* ***PHCB1*** *refer to the corresponding 3-substituted derivatives.*

**4.1.1.2 1,10-phenanthrolines suitable for electron-transporting materials in OLEDs.**

To consider the potential application of organic compounds as electron-transporting materials for light emitting devices, the compounds must fulfil several requirements. These include:

(i) good electron affinity and high electron mobility

(ii) good stability and the ability to form compact membranes

(iii) when excited should be able to avoid energy transfer of excited states as to ensure that exciton recombination occurs in the emissive layer of the device rather than the electron transporting layer (Figure 4.3).

To date, many of the tested organic compounds have displayed electron capture when integrated into devices. Those which have been deemed suitable are typically planar aromatic compounds with a high degree of conjugation. Examples include patents for oxadiazoles,[196] quinoxalines,[197] heterocyclic compounds with heteroatoms and cyano-polymers.[198] These materials are electron accepting, and have been shown to transport electrons efficiently with a forward bias.

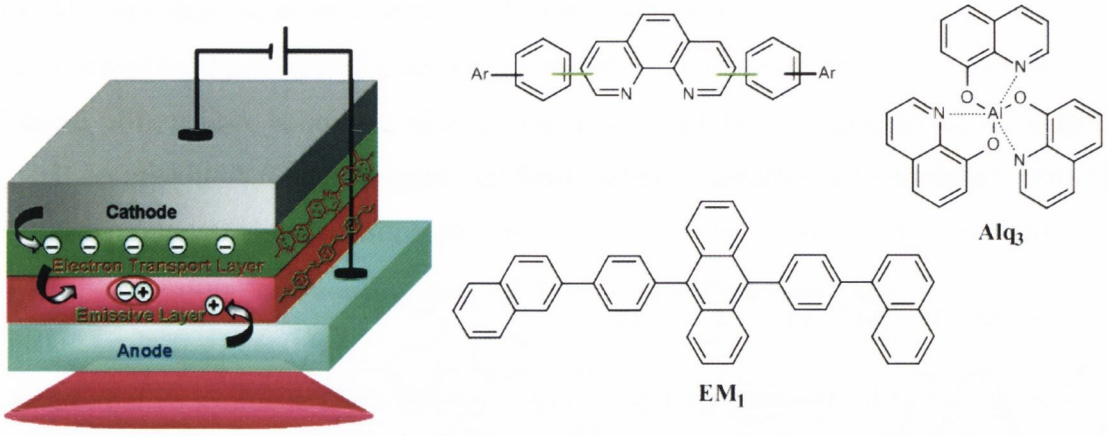


*Figure 4.3: Illustration depicting the design of an OLED (reproduced from review by Jenekhe et al.),[199] and the 1,10-phenanthroline compounds tested for their capability in the electron transport layer by Duan and co-workers. (Ar= pyridine, phenyl, biphenyl or naphthyl, — indictates substitution in the 2,9-, 3,8-, or 4,7- position. [200]Also shown are reference compounds $Alq_3$ and $EM_1$.*

The rigidity and planarity of the 1,10-phenanthroline core, combined with its low-lying HOMO, enhances the overall efficiency of the device. Modification of 1,10-phenanthrolines with electron deficient groups such as pyridyl or naphthyl rings perturbs the planarity of the periphery of the molecule thus improving the ability of the organic moiety to form homogeneous non-crystalline films under vacuum evaporation.[200] Duan and co-workers have examined the suitability of a novel family of aryl 1,10 phenanthrolines for these devices, with substitution in the 2,9-, 3,8- and 4,7- position of the diimine unit.[200] The 1,10-phenanthroline family was tested against tris(8-hydroxyquinolinato)aluminium ($Alq_3$), with the modified anthracene **$EM_1$** incorporated as the main component of the reference devices. For all of the tested compounds, the luminous intensity was notably higher (15.8 – 17.1 cd/A) than $Alq_3$ (13.2 cd/A), with other factors such as voltage and current density measuring comparably. This supports further research into the application of these systems in luminescent devices.

### 4.1.2 Extended polyaromatic frameworks with fused nitrogens.

Synthetic routes towards fused bidentate nitrogen systems with larger surface areas are frequently restricted by low yielding reactions such as the Skraup reaction. Two alternative strategies are to (a) couple extended *peri*-N-substituted polycyclic pyridines (such as isoquinoline) to generate perylene frameworks,[201] or (b) synthesis of a bipyridine ligand which then undergoes a dehydrogenation reaction.[202, 203] This approach

requires the pyridine moiety to be in the *cis* orientation so that the adjacent rings can undergo a second coupling reaction. Complexation to a metal centre aids the reaction of the uncyclised ligand by forcing it to orientate to the required geometry. Both synthetic routes yield a fused bidentate system which can be further modified to yield structures similar to the natural product eilatin.

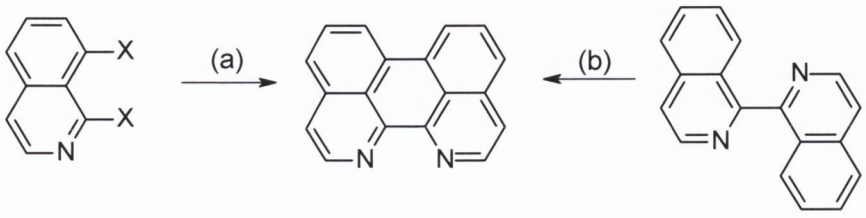


*Scheme 4.1: Two approaches taken to generate extended fused nitrogen system; (a) $Pd(OAc)_2$, $Bu_4NBr$, $K_2CO_3$, (ii) $Pd(PPh_3)_4$, reflux (b) Pd/C, 175 °C, 1 hr.*

Eilatin is a member of the pyridoacridine family, and is a natural product that is found in marine organisms. Eilatin possesses two bidentate coordination sites. The electron accepting nature of the nitrogen atoms, coupled with an extended aromatic core, facilitates charge transfer reactions. Dibenzoeilatin is a derivative of eilatin consisting of nine aromatic rings (Figure 4.4, **DBE**). Unlike eilatin and many other bridging systems, dibenzoeilatin is not planar due to steric interactions in the "bay" area of the structure (see $\mathbf{H_d}$, Figure 4.4). Bergman *et al.* have successfully synthesised a range of complexes of this ligand, with coordination to the Ru(II) metal centre causing a further deviation in the ligand from planarity.[204] This is due to additional steric interactions between the bipyridyl protons and the dibenzoeilatin platform. Palladium(II) complexes of these ligands have been found to be catalytically active in the copolymerisation of organic compounds such as styrene and carbon monoxide.[205]

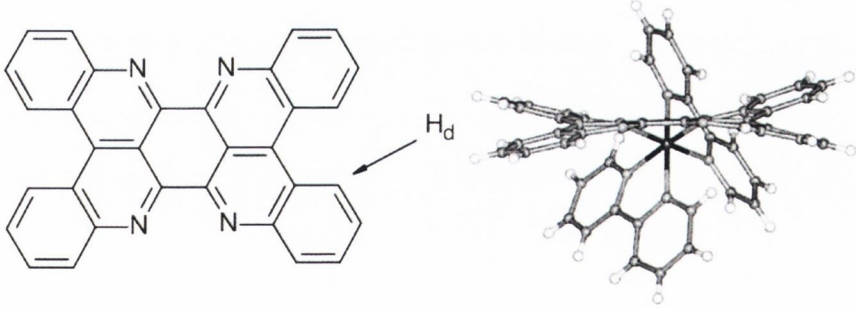


*Figure 4.4:(Left) The structure of the eilatin derivative **DBE**, with arrow indicating $\boldsymbol{H_d}$ which induces steric hindrance in the molecule causing a distortion from planarity. (Right) the crystal structure of the Ru(II) complex of **DBE** obtained by Bergman et al.*[204, 206]

### 4.1.3 Crescent-shaped 1,10-phenanthrolines and their application in DNA binding

Extended polycyclic aromatic systems which can adopt planar crescent shaped geometry have the potential to act as molecular wedges between two nucleosides through hydrogen bonding interactions. Such molecules can undergo base-pairing known as Watson-Crick pairing, and in targeted cases, have the ability to cause local geometrical distortions in areas of the DNA backbone. This is a valuable mode of action utilised by a wealth of anti-tumour drugs and antibiotics (e.g. quinoxaline antibiotics). The most important design feature of these compounds is that their hydrophobic moieties overlap with the heterocyclic nucleobases. This implies that molecules with extended surface area could be crucial to the development of next generation drugs (Scheme 4.2, inset).

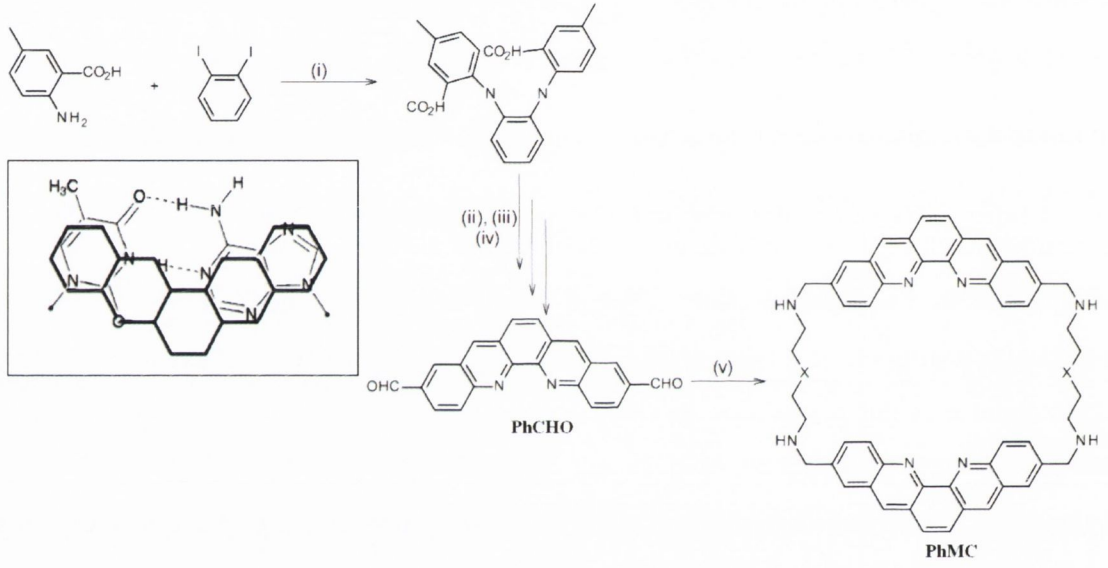


*Scheme 4.2: Pentacyclic compounds for nucleobase pairing: (i) Cu/CuI, n-pentanol, reflux,(ii) conc. $H_2SO_4$, 100 °C, (iii) Na, pentanol, reflux, $FeCl_3$, EtOH, $H_2O$, reflux, (iv) $SeO_2$, naphthalene, reflux, (v) n-propylamine, $CH_2Cl_2$/MeOH, rt; $NaBH_4$, $CH_2Cl_2$/MeOH, 0 °C. Inset depicts overlap of G-C base pair by a crescent shaped pentacyclic in the Watson and Crick base pairing mode (figure from Lehn et al.)*[207]

Work by Lehn *et al.* describes the synthetic methodology towards isomeric dibenzo[b,j]phenanthrolinedicarboxaldehydes which accomplishes the geometric overlap required for use as potential target drugs ([b,j] refers to the position of the nitrogen atoms relative to each other in the phenanthroline moiety of the final product).[207] The Freidländer condensation outlined in Chapter 1 to produce unsymmetrical 1,10-phenanthrolines was attempted by Lehn, but produced the required 6,7-dihydrodibenzophenanthroline precursor in poor yield. This led to an adaptation of

an Ullman-Goldberg condensation, which is commonly used in the synthesis of acridines (Scheme 4.2). Selectivity can be achieved through the use of *ortho*, *meta* or *para* diiodobenzene precursors, which enables the formation of either [1,10], [1,7] or [4,7] dibenzo[b,j]phenanthrolines. The bidentate dialdehyde (**PhCHO**) product is produced by a Na/pentanol reflux and mild oxidation with iron trichloride. Further condensation of the dialdehyde with the relevant diimine produces the macrocyclic product (**PhMC**). Diethylenetriamines are particularly suitable because they yield cyclic intercalators of a suitable size and geometry that can facilitate aromatic substrates. Protonation studies of the ligands show a high pH sensitivity which can be manipulated to generate different conformations, allowing for preferential binding of the substrates with DNA. Overall, the synthetic approach utilised in this work could be extended to generate other possible fused phenanthroline systems.

### 4.1.4 Ceramidonine chemistry in the development of nitrogen containing fused polycyclic polymers

Ceramidonine is a heart-shaped product produced from the high-temperature cyclodehydrogenation of 1-phenylamino-anthraquinone in sulfuric acid.[208] Bock and co-workers have employed this synthetic strategy to design extended nanoribbon-type polycyclics, and have successfully synthesised bifunctional diaminoarenes and dianthraquinones blocks with 1,10-phenanthroline-like substitutents deliberately posed on opposite sides of the central unit.[209] Tactical incorporation of nitrogens by appropriate choice of the azaarylamine precursor confers selective ligand functionality on the structure, and condensation yields products such as **ArA1** [Figure 4.5(b)]. The absorption spectra of (b) displays similar features to that of perylene dyes[210] with intense high energy absorptions below $\lambda$ = 350 nm, a gap zone from 350-450 nm, followed by a three peaks at lower energy ($\lambda$ = 450-560 nm) (Figure 4.5(c)). Figure 4.5(d) shows the unit cell containing two molecules of **ArA1** exhibiting $\pi$-$\pi$ interactions. The molecule is almost planar, with the two diazatetraphene fragments molecule (see grey and white) tilted at an angle of 24° with respect to each other. The C-C distance of 3.44 Å is close to that displayed in the interplanar distance of graphene sheets to form graphite (3.35 Å). Further development of this ceramidonine based synthetic strategy endeavours to produce heteroatom containing nanoribbons with larger surface areas such as **PolyArA2**, where the nitrogens can be strategically incorporated using the "bottom-up" approach.

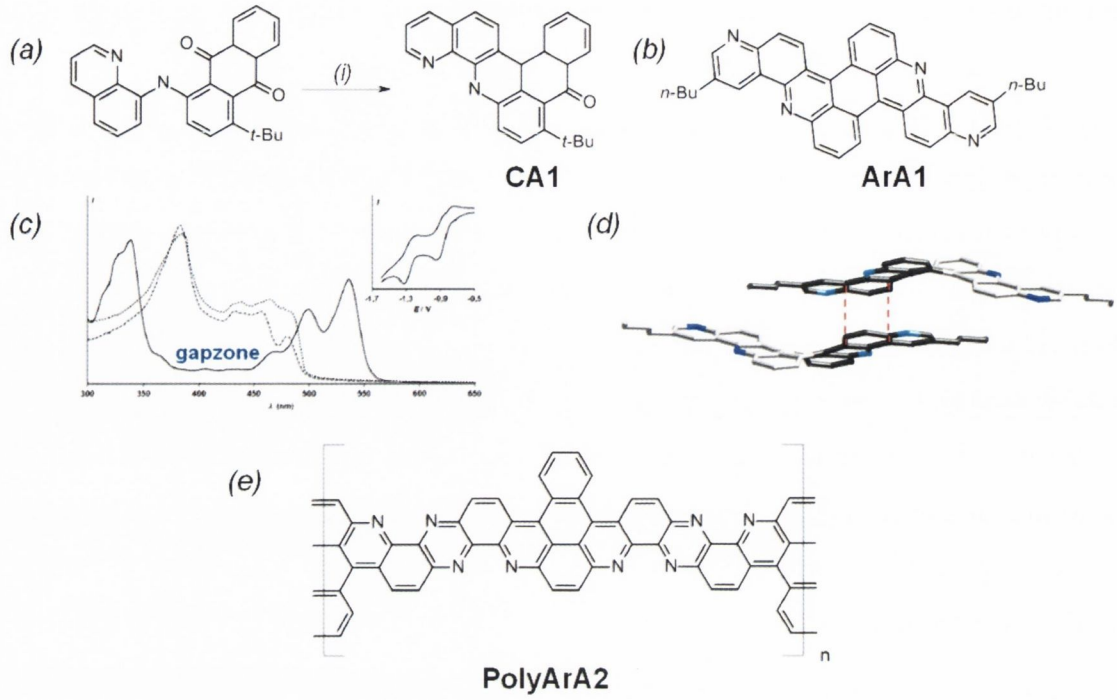


*Figure 4.5 (a) Acid-promoted decyclisation of aryl-amino-anthraquinones to produce pyridine-cermidonine (i) 70% $H_2SO_4$, 130 °C, 8 mins (b) product **ArA1** and (c) the absorption spectrum for **ArA1** (d) the unit cell of **ArA1**; (distance of 3.44 Å); and (e) further adaptation of the synthetic methodology could yield polymeric type tetraazaheterocycle materials such as the one shown.*[209]

### 4.1.5 Large fused heteroatom containing systems within the Draper group.

Investigations into the behaviour of heteroatom containing systems are on-going within the Draper group. This work is carried out an attempt to understand the mechanism of bond formation under Lewis acid-catalysed cyclodehydrogenation reactions. To date, the study has predominately centred around nitrogen heterosuperbenzenes, although recent publications have extended the scope of the investigation to include terpyridines[64] [Figure 4.6(a)] and pyridazines[49] [Figure 4.6(b)].[211] In all cases, the cyclodehydrogenation of the aromatic platform has proven to be more difficult and unpredictable than the all carbon analogues. Intramolecular arylation can be attempted using an extensive combination of reagents which includes $AlCl_3/CuCl_2$, DDQ in the presence of $MeSO_3H$, $Cu(OTf)_2/AlCl_3/CS_2$, $Pd(OAc)_2$/DMF, or $MoCl_5$ (either with or without $TiCl_4$ in chlorinated solvent). Ring closure has been most successful within our study using $FeCl_3/CH_3NO_2$ as reagents, although as previously discussed in the context of N-HSB chemistry in Chapter 1, this can generate a variety of partially fused products.

This problem extends to terpyridine systems, where ring closure adjacent to the nitrogen rings was found to be disfavoured [see Figure 4.6(a)]. Drs Gareth Cooke and Gearóid Ó Máille have applied the findings of King and co-workers to pyridazines, who proved the incorporation of methoxy substituents in the periphery of the aromatic system can further encourage ring closure through the arenium cation mechanism. [7, 212]

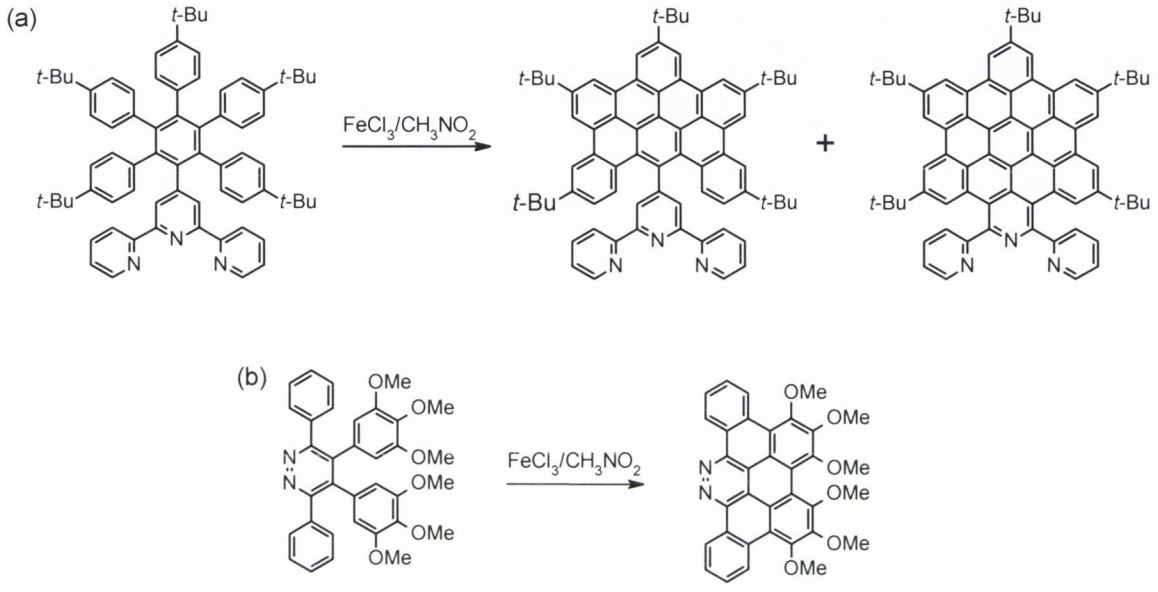


*Figure 4.6: Cyclodehydrogenation of nitrogen containing ligands (a) terpyridines, where ring closure adjacent to the nitrogen ring appears to be disfavoured and (b) pyridazines, where Drs. Gareth Cooke and Gearóid Ó Máille have shown the incorporation of methoxy substituents aids ring closure.*

The behaviour of sulfur containing compounds have also been examined, where preference for the formation of thiophene–thiophene intermolecular and intramolecular carbon–carbon bonds appears to take precedence over the formation of intramolecular thiophene-phenylene bonds [Figure 4.7(c)].[211] Chemical oxidation leads to the formation of the partially fused species, however electrochemical oxidation selectively enables bond formation in the more reactive 2- and 5- thiophene positions. This example illustrates the complexity of the cyclodehydrogenation mechanism, and the variation in the behaviour of different heteroatoms under similar conditions.

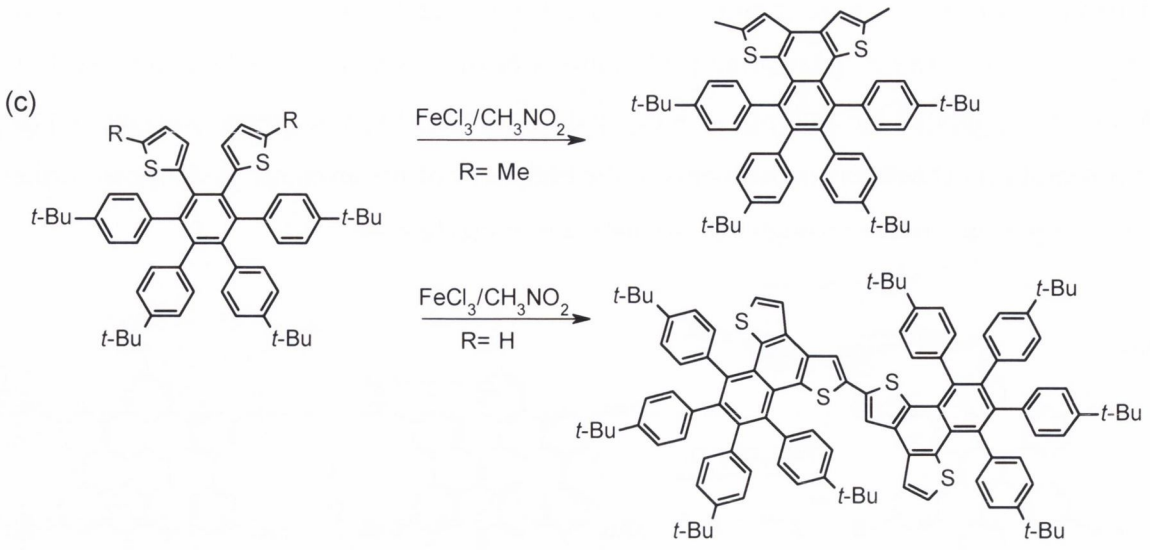


*Figure 4.7: Oxidative cyclodehydrogenation in thienyl polyphenylenes examined by Dr. Colin Martin.*[211]

## 4.2 Project Goal: The synthesis and carbon-carbon bond closure of large surface area 1,10-phenanthrolines.

This chapter details the functionalisation of 1,10-phenanthrolines *via* the incorporation of HBC type polyphenylenes. The systems are designed to enable comparisons to be made between the photophysical properties of the aryl acetylene derivatives outlined in Chapters 1 and 2. The peripheries of the compounds have *tert*- butyl functionality to enhance the overall solubility however the design rationale provides further scope for variation in the substitution pattern of the fragments. The proposed 1,10-phenanthroline family retain ligand functionality so that further complexation to iridium(III) and ruthenium(II) metal centres can be achieved. This work endeavours to further build on the extensive investigations carried out to date within the Draper group on heteroatom containing platforms such as pyridazines, and terpyridines.[9]

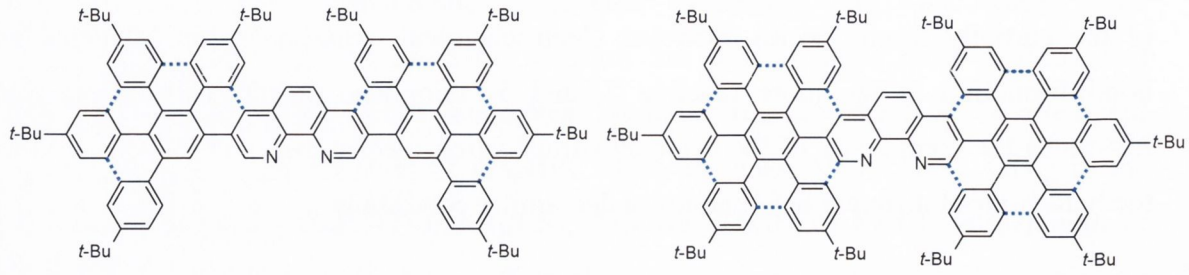


*Figure 4.8: The proposed design for the novel 1,10-phenanthroline ligands with (----) indicating the possible sites for carbon-carbon bond formation.*

### 4.2.1 Synthesis of ligands *via* Diels Alder [2+2] cycloaddition chemistry

A variety of synthetic routes are available in the design of large 1,10-phenanthrolines, some of which have been outlined in the previous sections, and in Chapter 1. Strategies such as Suzuki cross-coupling of the relevant boronic acid to brominated-1,10-phenanthrolines have been previously reported in favourable yields.[125] The primary synthetic strategy adopted in this work was based on a [2+4] Diels Alder cycloaddition of the required cyclopentadienone to an 3,8-aryl acetylene substituted 1,10-phenanthroline. This route was chosen as it enabled the use of several of the acetylene substituted 1,10-phenanthroline precursors utilised in the Sonogashira cross-coupling reactions in Chapter 1, as well further application of the [2+4] Diels Alder cycloaddition chemistry utilised for other systems in the Draper group.[18, 64, 213]

#### 4.2.1.1 Synthesis of 3, 8-bis[1,2,3,4-tetrakis(4-*tert*-butylphenyl)benzene]-1,10-phenanthroline (17) and 3, 8-bis[tribenzo[(*b, n, pqr*-5, 8, 11, 14-*tert*- butyl perylene]-1,10-phenanthroline (18)

The [2+4] Diels-Alder cycloaddition of the cyclopentadienone (**sm4**) and 3,8-diethynyl-1,10-phenanthroline (**sm7**) was attempted in a high temperature benzophenone melt with continuous monitoring by T.L.C. Unlike similar all-carbon Diels-Alder reactions, the starting materials were not consumed after 24 hours, and the reaction was left to proceed for an additional 48 hours.

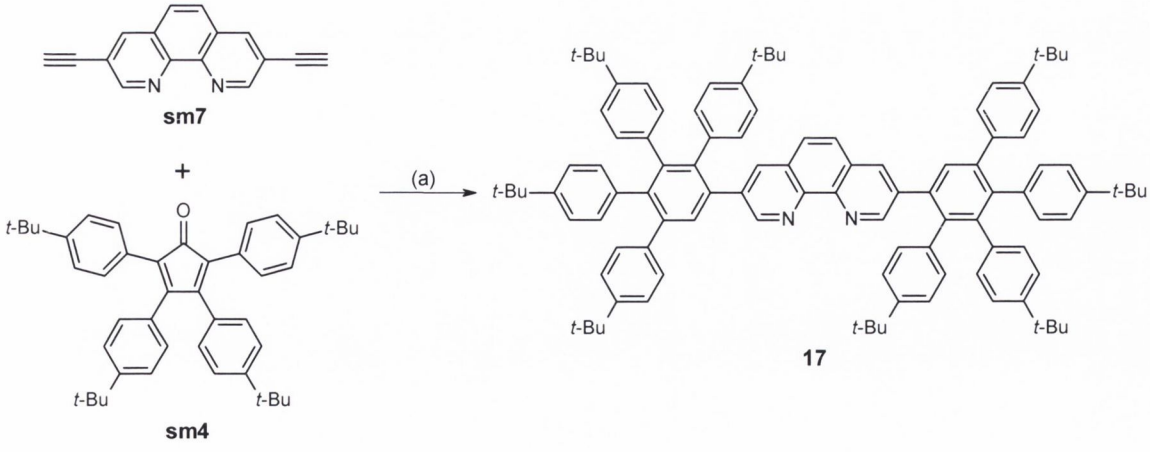


*Scheme 4.3:The [2+4] Diels-Alder cycloaddition with cyclopentadienone to form the 3 ,8- bis[1,2,3,4-tetrakis(4-tert-butylphenyl)benzene]-1,10-phenanthroline ligand **17**; (a) benzophenone, 320 °C, Ar, 2 days.*

Precipitation from methanol did not yield the pure product and additional purification by silica column chromatography was required. The final product (**17**) was finally isolated as a pale brown solid in a moderate yield (39 %), and analysed by MALDI-TOF spectrometry ($[M+H]^+$ m/z = 1390. 8982, calculated m/z = 1390.8906).

Oxidative cyclodehydrogenation of **17** was attempted using the iron(III) trichloride/nitromethane method. The reaction was carried out using 3 equivalents of the iron catalyst for every bond to be formed. The product was purified by silica column chromatography, eluting with $CH_2Cl_2$ to give a pale brown solid. Despite the inclusion of additional equivalents, analysis by a panoply of NMR experiments and mass spectrometry revealed that bond closure to the central 1,10-phenanthroline unit was not successful. The product was successfully isolated from the reaction as a pale brown solid (**18**), containing two tribenzoperylene-type units attached to the 1,10-phenanthroline unit. Despite the presence of the bidentate coordination site in the starting material, the MALDI-TOF spectroscopical analysis showed no coordination of the iron catalyst to the metal centre with the main peak at *m/z*= 1378.8041 corresponding to [M+H]+ (calculated m/z = 1378.8043). The reaction was repeated using additional equivalents of iron(III) trichloride, and allowing extended reaction time, but further ring closure was not detected.

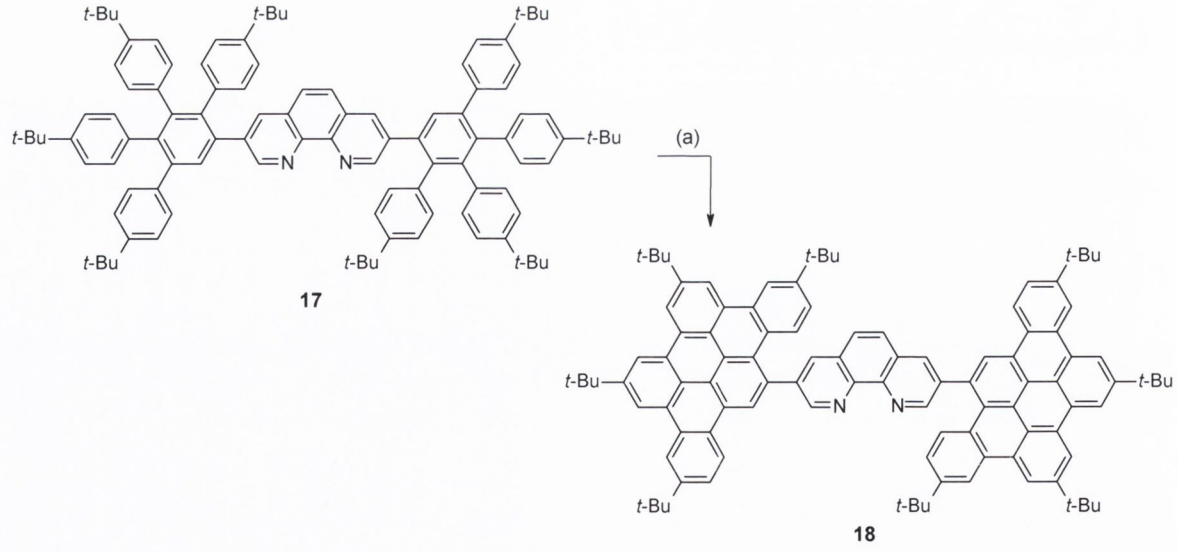


17 18

*Scheme 4.4: Oxidative cyclodehydrogenation of **17** to form **18**: (a) $FeCl_3$/ $CH_3NO_2$, $CH_2Cl_2$, Ar, overnight, R.T. Yield (63%).*

Examples of nitrogen-doped tribenzo[b,n,pqr] perylenes in the literature are very rare.[214] Drs Gareth Cooke and Gearóid Ó Máille have previously reported the synthesis of pyridazine ligands generated by the successful Diels Alder cycloaddition reaction between 3,6-dipyrimidyl-s-tetrazine (bptz) and an acetylene with varied functionality.[9] Compound **18** offers an unusual combination of a bidentate coordination site, whilst combining the properties of a 3,8-substituted 1,10-phenanthroline with multiple tribenzo[b,n,pqr]perylene functionality. The synthetic design of this ligand through the "bottom-up" approach provides further scope for the incorporation of long chains which should enhance the discotic nature of the ligand. This would offer potential liquid crystalline applications for this unusual family of hybrids. Yoshiyuki and co-workers have also successfully adapted tribenzo[b,n,pqr] perylenes for electroluminescent device application by substitution on the periphery of the disc with a variety of halogens, aryl, alkyl and amino groups, however the study was limited to either mono or di-substituted tribenzo[b,n,pqr] perylenes.[215]

Figure 4.9 shows the aromatic region of $^{1}$H NMR spectrum of compound **17**. The three signals corresponding to the 1,10-phenanthroline core were distinguished with the aid of a $^{1}$H-$^{1}$H COSY experiment, and appear at 9.05 ppm (●), 7.95 ppm (●) and 7.65 ppm (●) respectively each integrating for 2H. The three signals appear as doublets with smaller coupling constants (e.g. 7.95 ppm (●), $^{3}J$ = 2.52 Hz, see inset, Figure 4.9). The inset also shows the aliphatic ring with four distinct *tert*-butyl groups (the coloured squares indicate the corresponding phenyl ring), each integrating for eighteen protons. Selective NOE experiments through irradiation at the resonance frequency of each of the *tert*-butyl signals enabled the assignment of the corresponding phenyl ring. The $^{1}$H NMR spectrum displays eight distinct doublets between δ = 7.25 and 6.65 ppm, each doublet integrating for 4H as expected. Further examination of the $^{1}$H-$^{1}$H COSY experiment shown in Figure 4.9 confirms the assignment of the corresponding *ortho* and *meta* proton signals on each phenyl ring. The most deshielded pair of doublets at δ = 7.2 ppm (●) and δ = 7.1 ppm (●) were assigned using long-range HMBC experiments on the quaternary carbon which is adjacent to the singlet at δ = 7.5 ppm (●). The peripheral phenyl rings labelled as (● and ●) appear upfield of the other phenyl rings as four doublets, between 6.7 ppm and 6.95 ppm, each with larger $^{3}J$ coupling values of 12 Hz.

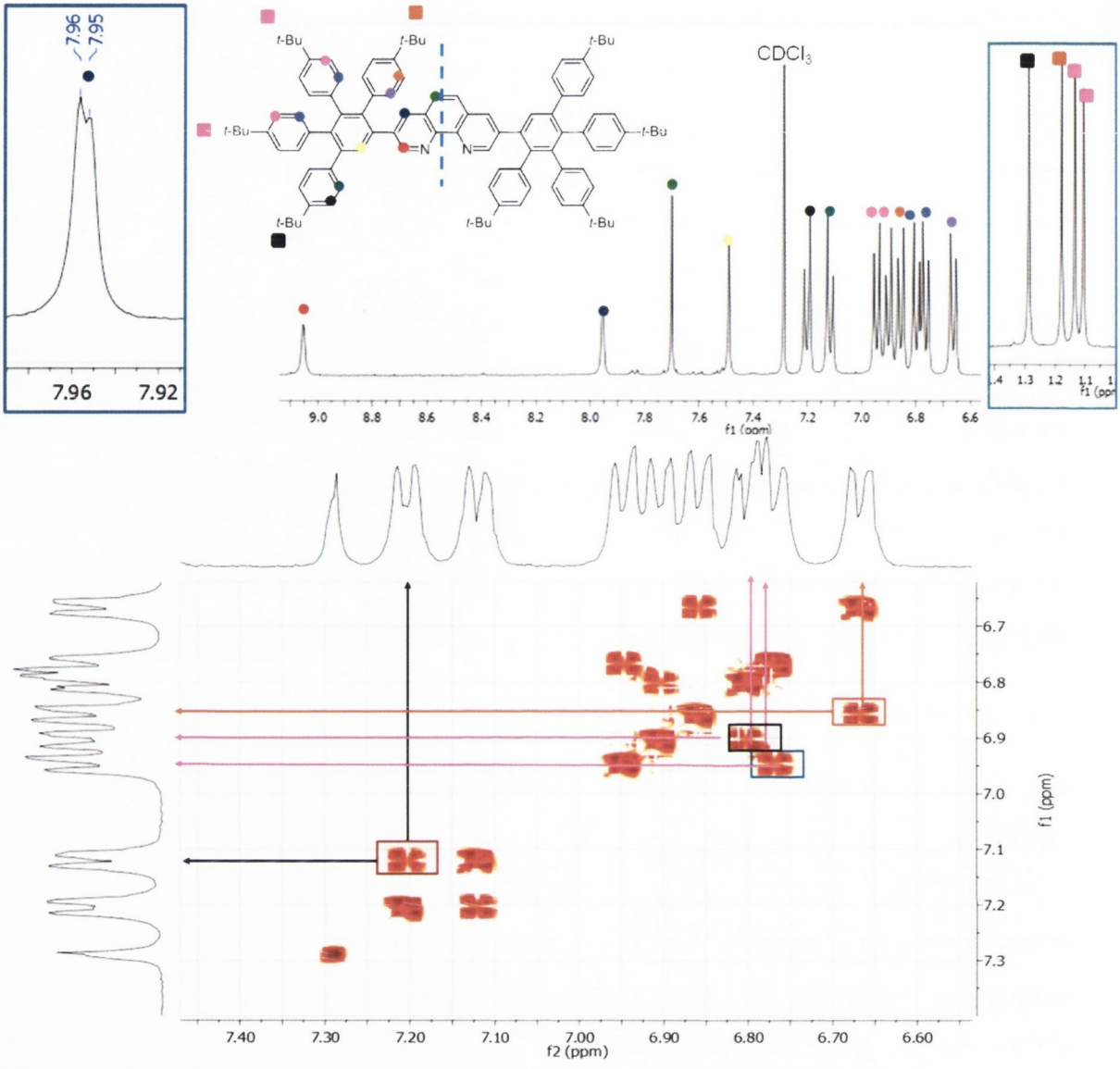


*Figure 4.9: Above; the aromatic region of the $^{1}H$ NMR spectrum obtained of* ***17*** *with inset showing (i) the doublet assigned as the proton adjacent to the nitrogen atom and (ii) aliphatic region (squares indicate adjacent phenyl ring). Below; the $^{1}H$-$^{1}H$ COSY experiment showing assignment of polyphenylene protons for* ***17*** *($CDCl_3$, RT, 600 MHz).*

The $^{13}C$ NMR spectrum for **17** is presented in Figure 4.10. The assignment was carried out with the aid of both HSQC experiments in an analogous method to that which will be discussed for compound **19** in Figure 4.12. As expected, the carbon adjacent to the nitrogen is the most deshielded signal at δ 151.5 ppm (●). The labelling scheme adopted for the *tert*-butyl region (see inset), refers to the adjacent proton signal of the phenyl ring in Figure 4.9. The four signals confirm the assignment of four distinct environments as previously assigned in the $^{1}H$ NMR spectrum. The unlabelled carbon signals refer to the

32 quaternary carbons and are in agreement with the number expected for the compound.

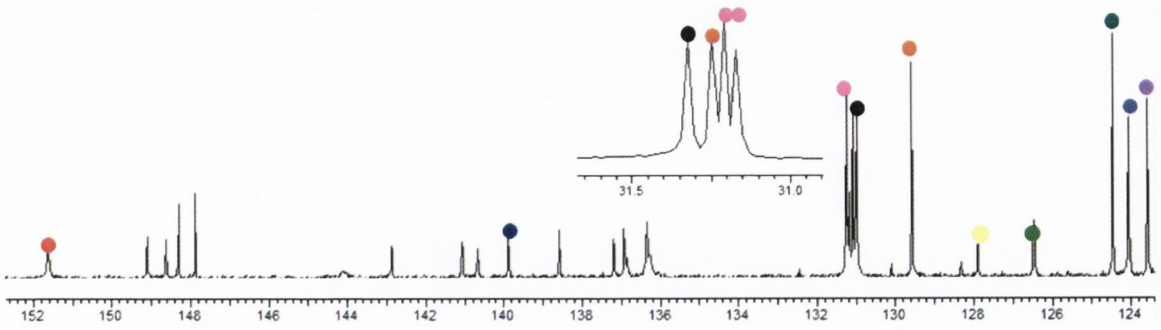


*Figure 4.10: $^{13}C$ NMR spectrum for **17**, with inset showing assigned tert-butyl groups. Colour scheme adopted refers to that in corresponding $^{1}H$ NMR spectrum (Figure 4.9). Unlabelled signals refer to the remaining 32 quaternary carbons ($CDCl_3$, 151 MHz, R.T.)*

Figure 4.11 shows the corresponding aromatic region of the $^{1}H$ NMR spectrum of compound **18**. All of the proton signals of the fused pendant have undergone a dramatic downfield shift as frequently seen upon cyclodehydrogenation in all carbon systems. The proton on the 1,10-phenanthroline (●) remains the most downfield signal at δ = 9.6 ppm, however a significant shift is still evident when compared to the corresponding signal in the $^{1}$ H NMR spectra of **17** (●, δ = 9.1 ppm**)**. The remaining protons on the 1,10-phenanthroline moiety were successfully identified with the aid of the $^{1}H$-$^{1}H$ COSY (Figure 12) at δ = 8.7 ppm (●) and δ = 9.1 ppm (●) respectively. Figure 4.11 shows the aromatic region of the $^{1}H$-$^{1}H$ COSY spectrum for **18**, and confirms the assignment of the protons on the 1,10-phenanthroline moiety (●●). The assignment of the aromatic protons of the benzo-perylene moiety was achieved through the use of a series of NOE experiments. The two singlets at δ = 9.25 ppm (●) and 9.15 ppm (●) each integrate for 2H, and have been assigned as the protons on the periphery of the benzo perylene pendent. Selective NOE experiments through irradiation of the *tert*-butyl resonance frequencies confirmed both signals lie adjacent to a *tert*-butyl group, which in combination with the integration values, confirms this assignment. The proton on the central phenyl ring of the fragment (labelled ●) was also identified through selective NOE experiments through irradiation at the resonance frequency δ = 8.8 ppm (●) (see inset, Figure 4.11). The protons appearing at δ = 8.96 ppm (●) and 8.87 ppm (●) respectively have been assigned in a similar manner. Two broad signals at δ 8.0 ppm and 7.2 ppm have replaced the distinct doublets previously evident in the starting material.

Each one integrates for 2H, and through selective long range coupling experiments have been identified as the protons on the periphery of the tri-benzoperylene disc (● and ●), adjacent to the back of the 1,10-phenanthroline core.

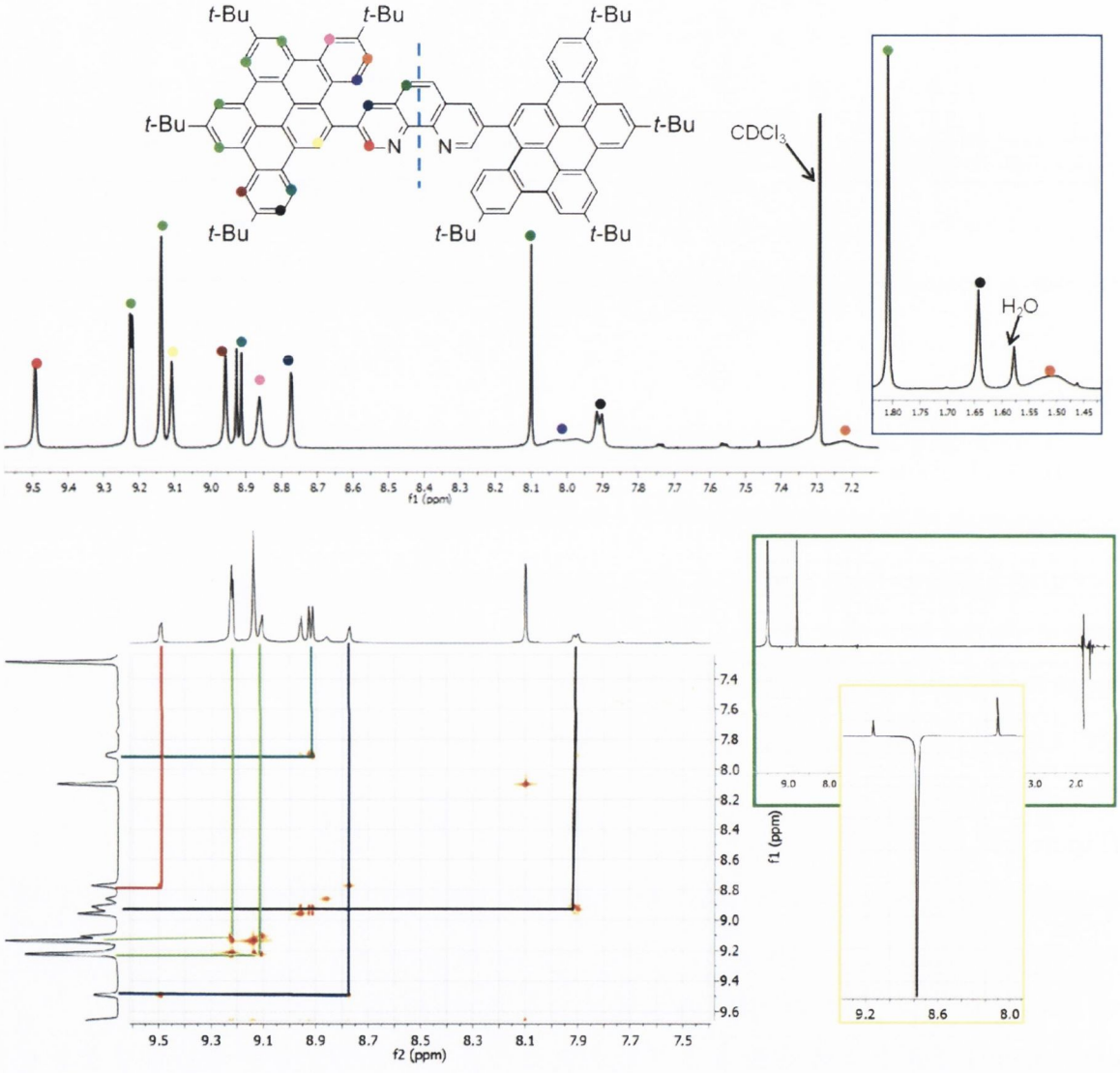


*Figure 4.11: Above: the aromatic region of the $^{1}H$ NMR spectrum of **18** with inset showing aliphatic region ($CDCl_3$, 400 MHz). Below: $^{1}H$-$^{1}H$ COSY spectrum of **18** with inset showing some examples of the selective NOE experiments carried out to assign the proton signals (i) adjacent to the tert butyl groups labelled (●) and (ii) proton labelled (●) ($CDCl_3$, 600 MHz, R.T.).*

Figure 4.12 shows the aromatic region of the DEPT 90° spectrum for **18**. The carbon signals were assigned using a 2D $^{1}H$-$^{13}C$ correlation experiment, a combination of which enabled full assignment of the aliphatic region of the spectrum as illustrated. The carbon signals from the 1,10-phenanthroline moiety have been highlighted to match the colour

scheme used for the $^{1}$H NMR experiment. No significant shift for the three signals is observed upon ring closure (i.e. **17** vs **18**) which further confirms that no bond closure to the 1,10-phenanthroline ring has taken place.

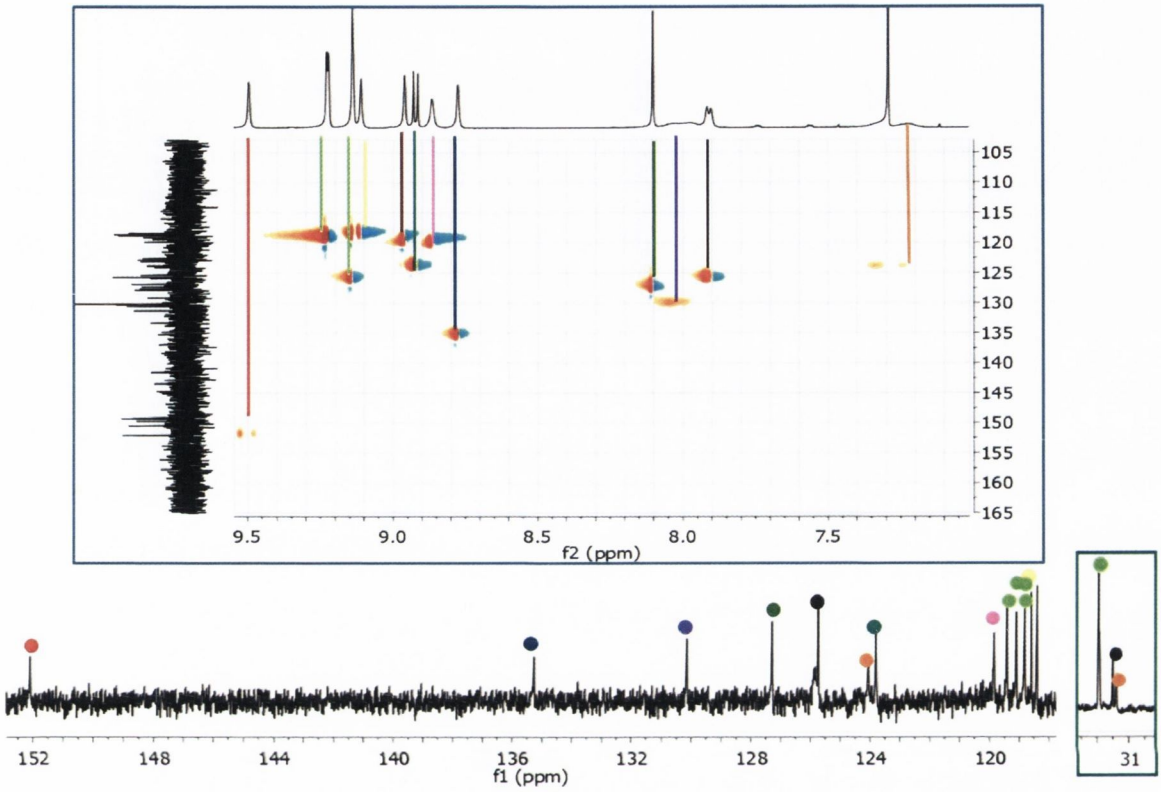


*Figure 4.12: DEPT 90° NMR experiment for* ***18*** *with inset showing tert-butyl carbons signals (adopted colour scheme matches that used in $^{1}$H NMR spectrum in Figure 4.11. ($CDCl_3$, RT, 151 MHz).*

### 4.2.1.2 X-ray crystallography of 18

Single crystals of **18** suitable for X-ray analysis were obtained by slow evaporation in $CH_2Cl_2$. The ligand crystallises in the $P2_1/c$ space group. Figure 4.13 shows the crystal structure obtained. It illustrates the large twist of the pendant tribenzoperylene fragments with respect to the central 1,10-phenanthroline unit. This distortion from planarity is 47.3° and 58.8° for each of the tribenzo[*b,n,pqr*]perylene substituents, and indicates why full ring closure to the 1,10-phenanthroline would require significant re-orientation of these rings.

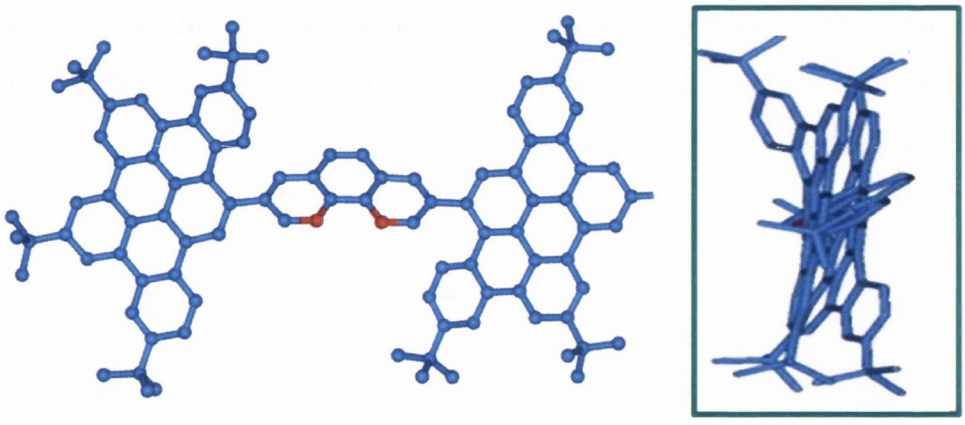

*Figure 4.13: Crystal Structure of* ***18*** *showing the high degree of twist between the 1,10-phenanthroline core and the fused pendant The nitrogen atoms are highlighted in red for clarity. Alternative view is presented in the inset.*

Figure 4.14 below illustrates the dimeric packing observed in the unit cell of **18**. The dimers pack in a head-to-tail manner, which appears to be driven by intermolecular interactions i.e. hydrogen bonding interaction between the nitrogen atoms of the 1,10-phenanthroline and the adjacent hydrogen atoms (see ----). The distance between the diimine cores is 3.8 Å, which is similar to the inter tribenzo[b,n,pqr]perylene distance at (3.76 Å). The dimers are arranged in a perpendicular brick-like fashion.

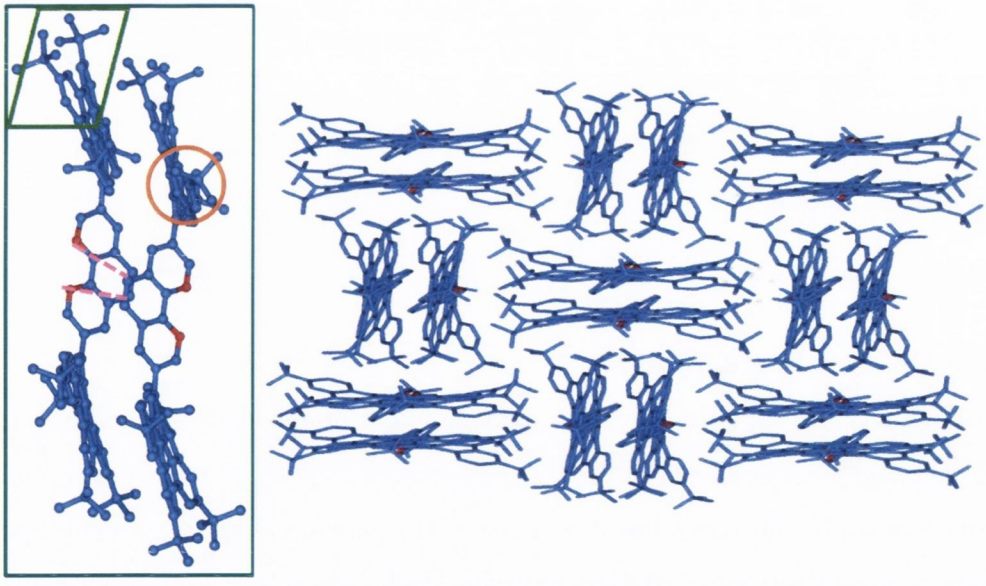

*Figure 4.14: The dimeric packing observed in the unit cell of* ***18****. Inset indicates the various twists observed within the single crystal (□ and O), and the intermolecular interactions between the dimer pair (-----).*

Finally, the inset highlighted in Figure 4.14 also demonstrates the considerable distortion within both of the attached aromatic fragments of the molecule which is indicated by O.

This distortion from planarity is even more evident in the twist of the peripheral *tert*-butyl phenyl fragments with respect to the tribenzo[b,n,pqr]perylene plane (12.9°).

### 4.2.2 Synthesis of 3,8-bis[2,3,4,5,6-pentakis(4-tert-butylphenyl)phenyl]-1,10-phenanthroline (19) and 3,8- bis[2,4,5-tris(4-tert-butylphenyl)-3,6-bis(4-methoxyphenyl)phenyl]-1,10-phenanthroline (20)

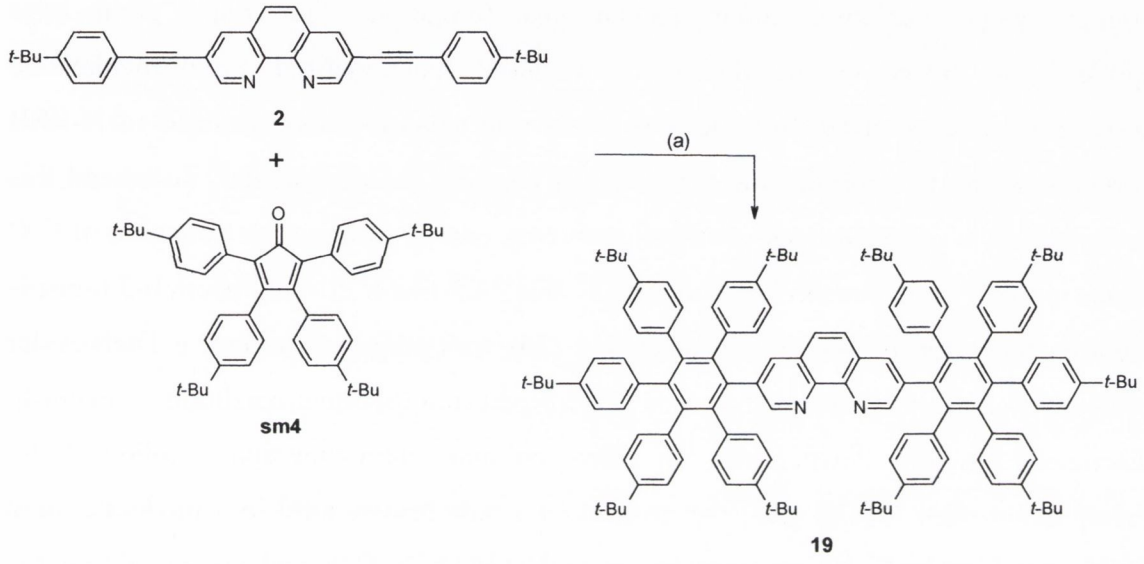


*Scheme 4.5: The [2+4] Diels-Alder cycloaddition with cyclopentadienone to form the 3,8- bis[1,2,3,4,5-pentakis(4-tert-butylphenyl)benzene]-1,10-phenanthroline ligand **19**;(a) benzophenone, 350 °C, Ar, 5 days.*

To further investigate the possibility of full ring closure to the 1,10-phenanthroline core, an additional *tert*-butyl phenyl ring was incorporated into the framework of the ligand. This was achieved by using the symmetrical aryl acetylene substituted 1,10-phenanthroline **2** whose synthesis was discussed in Chapter 1. The Diels-Alder [2+4] cycloaddition of the ligand with the cyclopentadienone **sm4** was attempted in a high temperature benzophenone melt at 320 °C under argon. The reaction was monitored by thin layer chromatography for several days. The product began to form after four days, however, traces of both starting materials were still evident. To encourage the reaction toward completion, the temperature was increased to 340 °C and left for an additional 24 hours. The crude product was precipitated from cold methanol, however traces of both starting materials in the solution required additional purification with column chromatography to give the product as a pale brown solid in a poor yield (27%). MALDI-TOF spectroscopic analysis agreed with the proposed product *m/z* = 1654.0825

corresponding to $[C_{124}H_{137}N_2]$ (calculated value = *m/z* 1654.0704). Further attempts at elevated temperatures to force the reaction to completion did not improve the overall yield of the reaction.

As previously discussed, King and co-workers have established that the incorporation of *o,p* activating groups (such as methoxy substituents) into the periphery of oligophenylenes can direct intramolecular bond formation.[7] The Draper group have applied this theory in the design of methoxy functionalised cyclopentadienone derivatives such as **sm10** (Scheme 4.6) to aid ring closure in the synthesis of N-HSB derivatives, and to minimise the formation of partially fused products.[8] To extend this investigation to other nitrogen containing systems, and to promote the formation of C-C bonds to the 1,10-phenanthroline centre, 3,8- bis[2,4,5-tris(4-tert-butylphenyl)-3,6-bis(4-methoxyphenyl)phenyl]-1,10-phenanthroline (**20**) was prepared through a Diels-Alder cycloaddition with **2**. The reaction was performed using the same conditions previously discussed for **19**. Purification by silica column chromatography, followed by precipitation from MeOH gave the product as a pale brown solid in a moderate yield (34%). Analysis by NMR spectroscopy, as well as MALDI-TOF analysis agreed with the formation of product **20**. [(Found $[M+H]^+$ m/z = 1669.9111, calculated m/z = 1669.9123, $C_{116}H_{121}N_2O_8$].

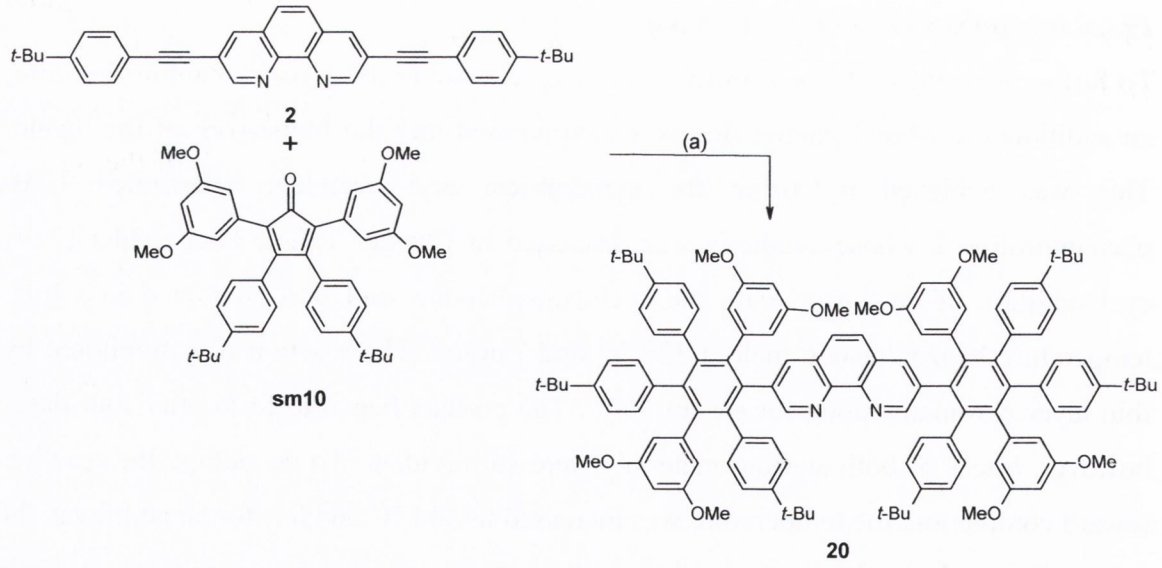


*Scheme 4.6: The [2+4] Diels-Alder cycloaddition reactionwith cyclopentadienone* ***sm10*** *to form 3,8- bis[2,4,5-tris(4-tert-butylphenyl)-3,6-bis(4-methoxyphenyl)phenyl]-1,10-phenanthroline (**20**); (a) benzophenone melt, 340 °C, Ar, 5 days.*

### 4.2.2.1 $^{1}H$ and $^{13}C$ NMR spectroscopic characterisation of 19 and 20

The $^{1}H$ NMR spectrum of **19** in $CDCl_3$ is shown in Figure 4.15 below. The plane of symmetry through the centre of the molecule greatly simplifies the spectrum. The assignment of the three protons of the 1,10-phenanthroline core were confirmed using $^{1}H$-$^{1}H$ COSY, and appear at δ = 8.75 ppm (•), δ = 7.57 ppm (•) and δ = 7.15 ppm (•) respectively. These signals are slightly more shielded than the corresponding signals of ligand **17**, [δ = 9.0 ppm (•), δ = 7.95 ppm (•) and δ = 7.65 ppm (•)], which suggests that the incorporation of the additional *tert*-butyl substituted phenyl ring has a significant effect on the 1,10-phenanthroline moiety. Polyphenylene substituents typically exhibit a high degree of rotation about the central phenyl which renders the opposite phenyl groups equivalent. This results in the phenyl protons appearing as two broad multiplets between δ 6.65 and 6.85 ppm, which integrate for 40 H, but whose individual components cannot be assigned. The inset shows three *tert*-butyl environments, which integrate for 90 H (ten *tert*-butyl groups), in the ratio of 1: 2: 2. Irradiation at the resonance frequency of each of the *tert*-butyl signals did not aid the further assignment of the phenyl rings. Also shown is the MALDI-TOF analysis which agrees with the formation of the product $[M+H]^{+}$ [calculated m/z = 1655.0724, $C_{124}H_{137}N_2$].

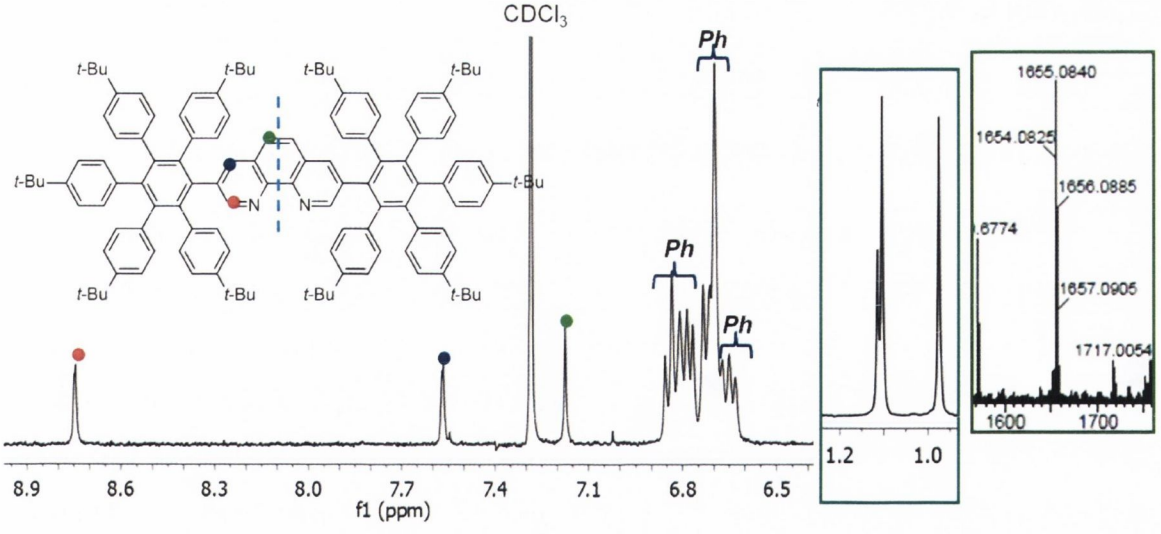


*Figure 4.15: $^{1}H$ NMR spectrum of **19** with inset showing aliphatic region ($CDCl_3$, 400 MHz, R.T.), and the MALDI-TOF spectrometry analysis for **19**.*

The $^{13}C$ NMR spectrum of **19** was assigned using DEPT analysis as shown in Figure 4.16. The three 1,10-phenanthroline protons are easily distinguishable, with the phenyl signals appearing astwo overlapping groups at ~δ 131.0 ppm and δ 123 ppm.

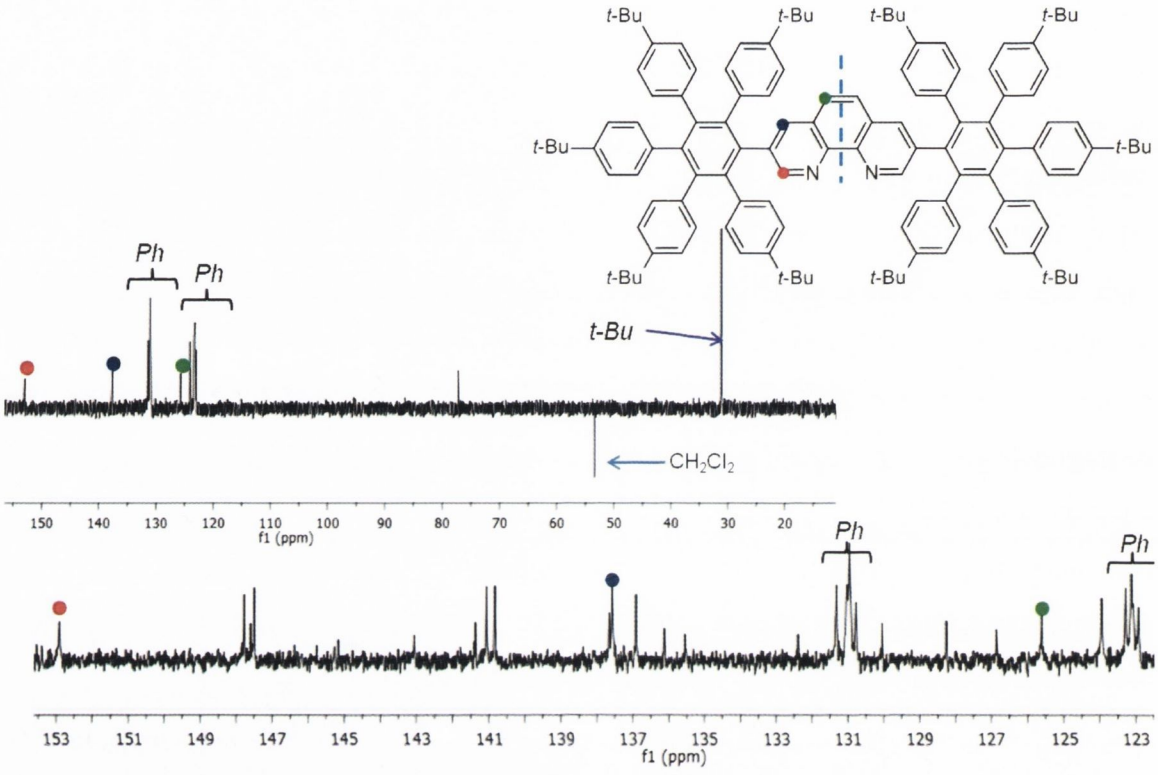


*Figure 4.16: $^{13}C$ NMR spectrum, showing the aromatic region of **19** and the DEPT experiment confirming assignment of the C-H signals of each phenyl groups. The remaining unlabelled signals are quaternary carbons (151 MHz, $CDCl_3$, R.T.).*

The corresponding $^{1}H$ NMR spectrum for compound **20** is shown below. The incorporation of the two methoxy functionalised rings has drastically changed the upfield region of the spectrum, with the addition of a broad multiplet at δ = 5.8 - 6.1 ppm. This integrates for 12 H and has been assigned to the overlapping signals of 3 protons situated on the methoxy phenyl rings. The two *tert*-butyl multiplets now appear as two better resolved multiplets, integrating for 24 H in total. The inset also shows the aliphatic region of the spectrum, which confirms that both methoxy substituted rings are inequivalent, as expected.

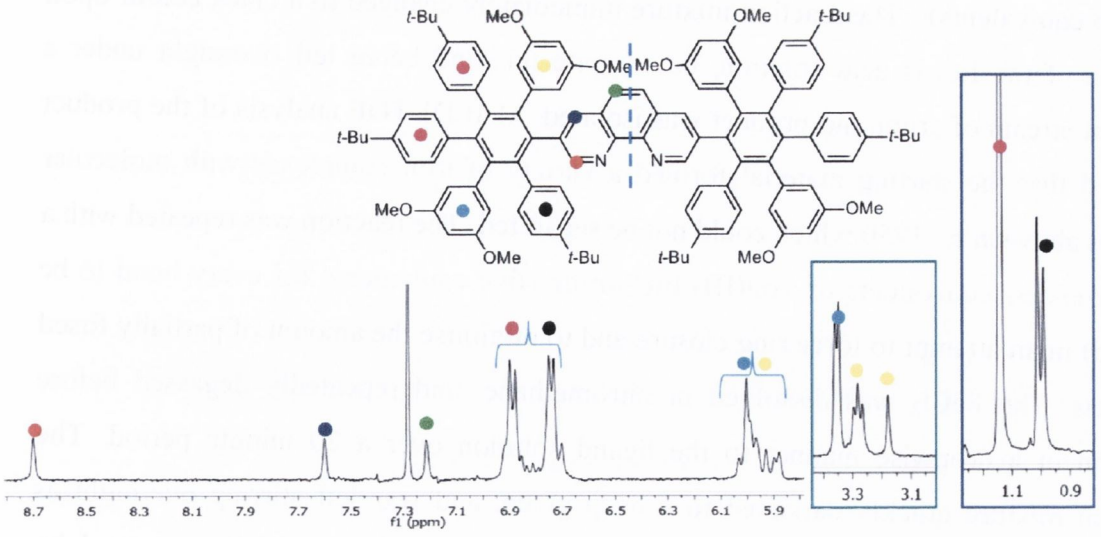


*Figure 4.17: $^1H$ NMR spectra of **20** with inset showing methoxy and tert-butyl signals in the aliphatic region ($CDCl_3$, 400 MHz, R.T.).*

Figure 4.17: $^1H$ NMR spectra of **20** with inset showing methoxy and tert-butyl signals in the aliphatic region ($CDCl_3$, 400 MHz, R.T.).contains the $^1H$ and $^{13}C$ chemical shifts for the three polyphenylenes compounds **17**, **19** and **20**. The proton adjacent to the nitrogen (●) becomes slightly more shielded on-going from **17** to **20**. The remaining protons (●,●) undergo a considerable upfield shift upon the inclusion of an additional *tert*-butyl phenyl ring. The addition of the methoxy groups in the framework of the polyphenylenes unit renders all of the phenyl groups inequivalent, yet appears to have a marginal affect on the proton and carbon environments of the 1,10-phenanthroline centre.

*Table 4.1: Selective proton signals of the1,10-phenanthroline portion of compounds 17, 19 and 20*

| *H* | **17** δ $^1H$ and $^{13}C$ (ppm) | **19** δ $^1H$ and $^{13}C$ (ppm) | **20** δ $^1H$ and $^{13}C$(ppm) |
|---|---|---|---|
| ● | 9.0, 151.5 | 8.8, 152.9 | 8.7, 153.3 |
| ● | 7.95, 139 | 7.57, 138.7 | 7.6, 137.6 |
| ● | 7.65 126.5 | 7.15, 125.9 | 7.2, 125.9 |

### 4.2.3 Cyclodehydrogenation of 19 and attempted cyclodehydrogenation of 20.

The oxidative cyclodehydrogenation of **19** was attempted in a manner analogous to that of **18**, using three equivalents of iron(III) trichloride for every C-C bond to be formed

(e.g. 36 equivalents). The reaction mixture immediately changed to a black colour upon addition of the Lewis acid solution, but despite this and being left overnight under a constant stream of argon, no product was isolated. MALDI-TOF analysis of the product revealed that the starting material formed a variety of iron complexes with molecular weights above *m/z* =1750 which could not be separated. The reaction was repeated with a greater excess equivalents of iron(III) trichloride (five equivalents for every bond to be formed) in an attempt to force ring closure and to minimise the amount of partially fused products. The $FeCl_3$ was dissolved in nitromethane, and repeatedly degassed before addition in a dropwise manner to the ligand solution over a 20 minute period. The reaction mixture quickly darkened to a deep green, and was left stirring overnight as before. The mixture was purified, and the iron waste was successfully removed by repeated washings with a basic aqueous solution of EDTA. Although a small amount of starting materials were recovered, a dark brown solid (**21**) which was highly green fluorescent in solution was isolated by precipitation from $CH_2Cl_2$/hexane.

The characterisation of larger fused polycyclic hydrocarbon compounds is frequently hampered by poor solubility and the tendency of the planarised sheets to aggregate at higher concentrations. Müllen *et al.* have reported many larger all-carbon systems by relying on the isotopic distribution pattern of MALDI-TOF and APCI Laser-Desorption/Ionization Time of Flight (LD-TOF) mass spectrometry to distinguish between partially fused and fully fused products when the attempted separation of the products has proven to be futile.[216, 217] As the closure of each carbon bond results in a reduction of the molecular weight by two mass units, identification of what can be a plethora of products can only be achieved by a highly resolved isotopic distribution. Analysis of **21** by mass spectrometry was attempted using both LD-TOF and solid state analysis; however detection above m/z =1200 proved to be impossible using the instrumentation set-up available. Optimisation of the MALDI-TOF analysis was achieved on utilising higher sample concentrations dissolved in the minimum amount of HPLC grade $CH_2Cl_2$ using [Glu1]-Fibrinopeptide B (1570.6 g $mol^{-1}$ as a matrix (m/z = 1570). This gave at peak at m/z = 1629.8821 which corresponds to $[M+H]^+$ where "M" refers to the fully fused product **21**. The peak shown at m/z = 1664.8484 (see inset, Scheme 4.6) corresponds to **21** plus the addition of one chloride ion $[M+Cl]^-$.

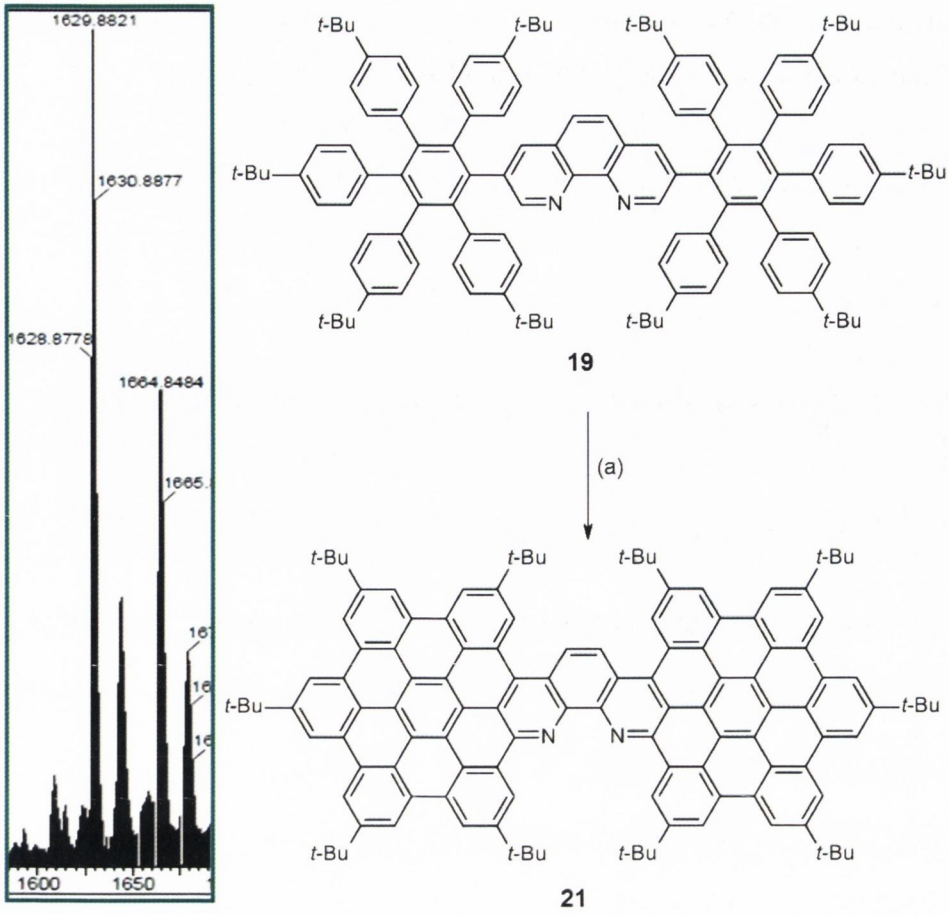


*Scheme 4.7: Cyclodehydrogenation of* ***19*** *to produce the fully aromatised product* ***21*** *(a) $FeCl_3$, $CH_3NO_2$ and $CH_2Cl_2$, R.T., Ar, overnight with inset shows magnified MALDI-TOF analysis confirmed the formation of* ***21****.*

Figure 4.18 shows the $^1$H NMR spectrum obtained for **21** in $CDCl_3$. The tendency of the ligand to undergo stacking at higher concentrations, combined with the poor solubility of the ligand in all deuterated solvents available prevented more resolved spectra from being obtained at both room and higher temperatures. The two defined multiplets which appear at δ = 6.9-6.6 ppm in the $^1$H NMR spectrum of the starting material have been replaced with a broad singlet appearing at δ = 9.4 ppm (●) which integrates for 18 H. The remaining protons appear as an adjacent downfield broad singlet at δ = 9.95 ppm (●) and δ = 10.9 ppm (●) both of which integrate for 2 H respectively. These have been assigned as the proton nearest to the nitrogen in the periphery of the HBC disc. Despite numerous attempts in a variety of solvents, $^{13}$C data for the product could not be obtained.

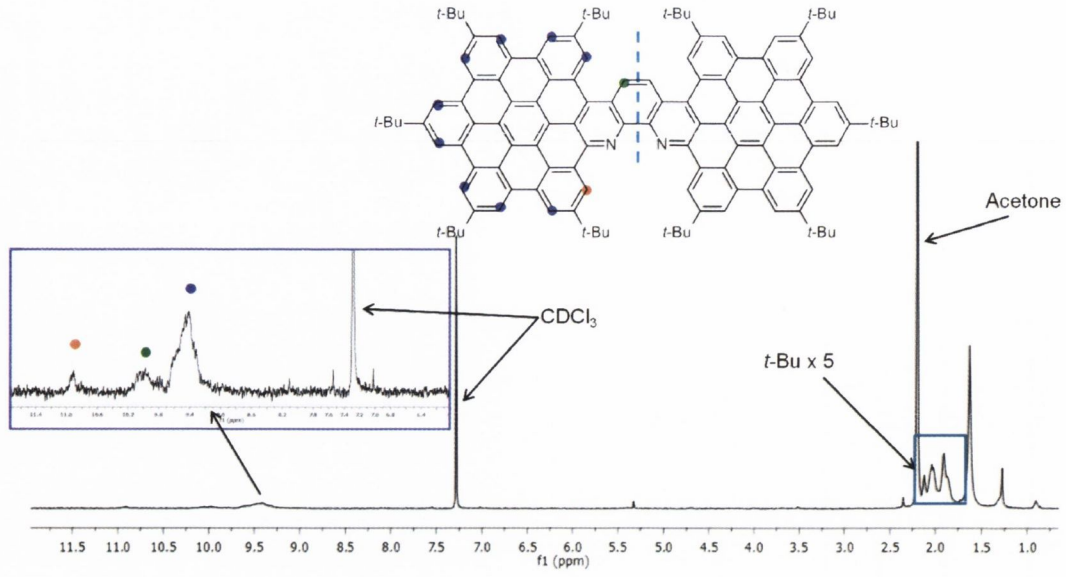


*Figure 4.18: $^1H$ NMR spectrum obtained for **21** with inset showing magnified aromatic region displaying three broad singlets which have been assigned according to the labelling shown ($CDCl_3$, 600 MHz, RT).*

### 4.2.3.1 The attempted cyclodehydrogenation of 20

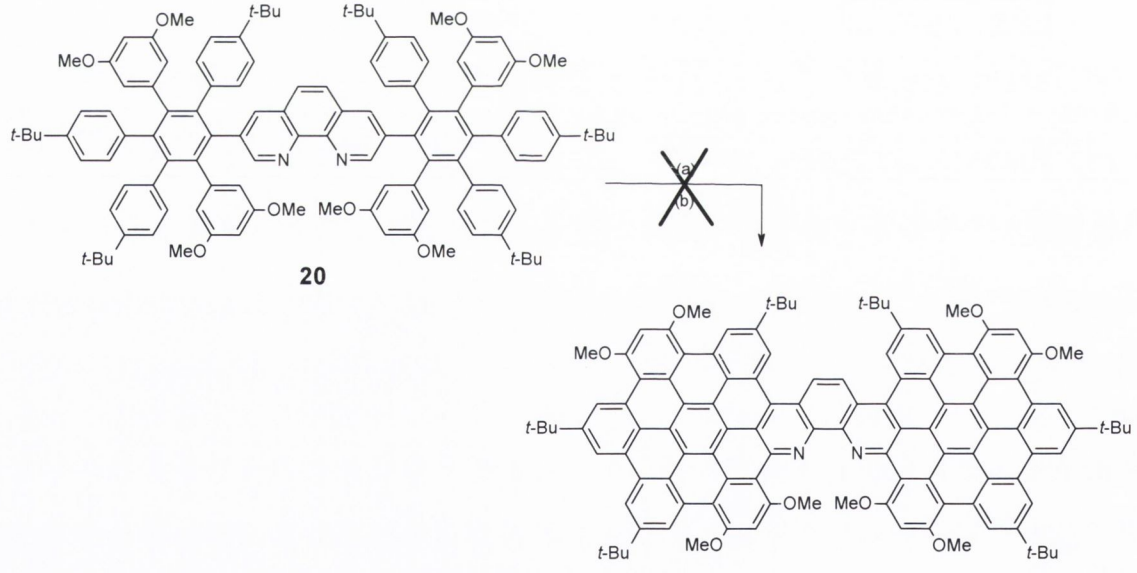


*Scheme 4.8: Attempted cyclodehydrogenation of **20** using (a) $FeCl_3/CH_3NO_2$ and (b) boron trifluoride diethyl etherate and PIFA both of which proved to be unsuccessful reagents.*

The reaction was repeated using the methoxy derivative **20**. Despite the inclusion of additional equivalents of iron(III)trichloride, no bond closure was detected. The reaction was then repeated using alternative reagents, namely boron trifluoride diethyl etherate and bis (trifluoroacetoxy)iodobenzene (PIFA), however the starting material was again

recovered. This was surprising, as the modification of the polyphenylene moiety to include methoxy substituents has previously enhanced the reaction efficiency in other nitrogen containing systems within the group. Other reagent systems such as $AlCl_3/CuCl_2$ and DDQ in $MeSO_3H$ are currently being investigated, as well as modification of the ligand design to incorporate methoxy groups on adjacent phenyl rings.

### 4.3 Photophysical study of ligands 17-21

The UV-Vis absorption spectra of the ligand family **17** -**21** (1 $x10^{-5}$ M, $CH_2Cl_2$) is presented in Figure 4.19. Ligand centred $\pi$-$\pi^*$ transitions due to the 1,10-phenanthroline moiety typically appear at $\lambda$ = 286 nm. These transitions are dramatically weaker than the ligand series discussed in Chapter 1, with the exception of the methoxy derivative **20**. This is an indication of the poorer communication between the 1,10-phenanthroline core and the substituents when an acetylene linker is omitted from the ligand design. Overall, the UV-Vis absorption spectra of **17**, **19** and **20** display broad featureless bands which are typical of many polyphenylenes derivatives previously reported by the Draper group as well as the aryl polyphenylene derivative 6 discussed in Chapter 1. This is explained by the large twist between the outer rings of polyphenylene derivatives with respect to the central phenyl ring. The addition of methoxy groups (**19** vs. **20**) results in an increase in the molar absorptivity ($\varepsilon$) across the range $\lambda$ = 250-350 nm, and is indicative of the increase in electron donation from the substituents (MeO vs. *tert*-butyl). As discussed in Chapter one, the increase in electron donating ability of the substituents results in increased charge transfer character. Similar to the parent compound 1,10-phenanthroline, 3,8- substituted derivatives of 1,10-phenanthroline with electron-donating substituents exhibit stabilization of electron charge transfer in their excited states. This has been observed for the methoxy and dimethylamino substituted 1,10-phenanthrolines reported by Joshi *et al.* and results in both the absorption and emission maxima of the spectra being red shifted.[45]

The addition of a fifth substituted phenyl ring (i.e **18**→**19**) also results in a significant red shift of the lowest energy band by approximately 50 nm. This bathochromic shift is further enhanced by the addition of the methoxy substituted phenyl rings (**19** vs. **20**). A similar trend has been previously reported by Armaroli *et al.* for 2,9- methoxy phenyl substituted 1,10-phenanthrolines. The change in absorption and emission features were

ascribed by Armaroli to the oxygen/nitrogen electron repulsion effect between molecules in solution, as well as N-H hydrogen bonding to the methoxy group. This results in a further distortion in the planarity of the molecule which causes a further broadening of the absorption bands.[24]

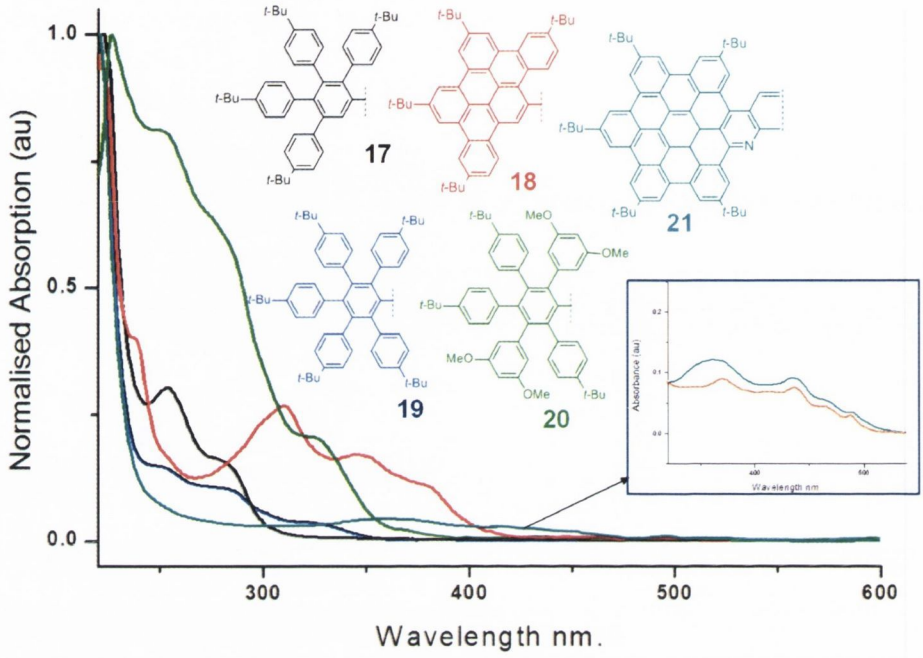


*Figure 4.19: Normalised UV-Vis absorption spectra of the ligand series (1 x $10^{-5}$M, $CH_2Cl_2$) with inset showing magnified region of the lower energy bands of* ***21*** *in $CH_2Cl_2$ (—) and toluene (—).*

Finally, the cyclised ligands **18** and **21** exhibit considerable bathochromic shifts of their lower energy bands when compared to the unfused derivatives, with **21** displaying a weak low energy band extending to $\lambda$ = 490 nm. (see inset, Figure 4.19). This trend has been reported by the Draper group for other fused nitrogen containing ligands.[17] Planar rigid molecules with high degrees of symmetry typically display well-resolved vibrational bands with broad structured absorptions. Some evidence of this trend is evident in the UV-Vis absorption spectrum of **18** when compared to its precursor **17**, as the former demonstrates significantly higher molar absorptivity values in the region $\lambda$ = 300-400 nm. In particular, the intense absorption band between $\lambda$ 350-400 nm in the spectrum of **18** is indicative of 1,10-phenanthrolines functionalised with a larger chromophore. [125] The omission of the absorption band at $\lambda$ = 350-400 nm in the spectrum of **21** is a further indication that the ligand is no longer behaving as an aryl substituted 1,10-phenanthroline, and may be further evidence of ring closure to the bidentate core. Interestingly, Müllen and co-workers reported a spectroscopic analysis of all carbon

HBC dimeric and trimeric compounds where the introduction of a rigid superfluorene bridge between two HBC units resulted in significant bathochromic shift and a broadening of the UV-Vis absorption bands being observed.[218] Müllen justified this observation by remarking that the 0→0 transition that was previously forbidden in C-C linked HBC dimer, becomes a partially allowed transition in the superfluorene analogue due to an increase in conjugation and planarity, and a decrease in symmetry. If this explanation is extended to the ligands systems in this study, it is possible than the bidentate ligand centre of **21** is no longer behaving as a 1,10-phenanthroline moiety, but instead as a bidentate centre integrated into a larger graphene-type sheet. This system is poorly soluble in most organic solvents, however the corresponding UV-Vis absorption spectrum was recorded in toluene to investigate the dependence of **21** on solvent polarity (see inset, Figure 4.19). The slight blue shift observed in $CH_2Cl_2$ confirms that the lower energy bands are predominately n→π* in character. All of the ligands exhibit marginal dependence on solvent polarity, which is characteristic of spin-allowed transitions that are π→π* in origin, and is indicative of a redistribution of electron density within the same π framework.

*Table 4.2: Summary of the UV-Vis absorption energies and relative extinction coefficients for ligands **17-21**.*

| Compound | $\lambda_{max}$[nm](ε x $10^4$ [$M^{-1}$ $cm^{-1}$]) |
|---|---|
| **17** | 286 (6.15), 330 (1.04), 442 (1.01) |
| **18** | 288 (6.16), 320 ( 2.53) 345 (2.87), 380 (0.9), 417 *sh* (0.6) |
| **19** | 256 (3.62), 270 (3.87), 300 (3.17), 318 *sh* (2.63), (386), 400 (2.29), 433 *sh* |
| **20** | 228 (8.48), 253 (3.74), 366 (3.77), 389 (2.79), 438 *sh* (3.77), |
| **21** | 368 (3.43), 435 (3.08), 470 (1.80), 490 (1.25) |

### 4.3.1 Protonation studies of 18 and 21

To further investigate the photophysical effect of C-C bond closure to the 1,10-phenanthroline moiety, and for comparison with the aryl acetylenes 1,10-phenanthrolines in Chapter one, a protonation study of **18** and **21** was then undertaken. Figure 4.20 shows the UV-Vis absorption spectrum obtained for **18** upon addition of 5 μL aliquots of trifluoroacetic acid to the ligand solution ($CH_2Cl_2$, 1 x $10^{-5}$ M). Although the overall changes to all the absorption bands upon protonation are not as drastic as those observed

in the aryl acetylene functionalised derivatives in chapter one, the trend remains the same across the family of ligands. The most prominent feature is a decrease in the absorption band at $\lambda$ = 350 nm, coupled with the small bathochromic shift, confirming the n–$\pi^*$ nature of the band. The appearance of a new lower energy band in the tail of the spectrum at $\lambda$ = 420-480 nm (see inset, Figure 4.20) is in line with the trend observed in the aryl acetylene ligands in Chapter 1, and is indicative of some intramolecular charge transfer character from the tribenzoperylene fragment to the 1,10-phenanthroline core (tribenzoperylene → phen$H^+$). It is expected that mono-protonation is occuring, given the observations previously discussed in Chapter 1. Two isosbestic points are observed at $\lambda$ = 322 and 390 nm respectively between the 1$^{st}$ and 17$^{th}$ equivalent of acid. This is indicative of an equilbrium between the neutral and protonated species. Both isobestic points are compromised on further additons of acid.

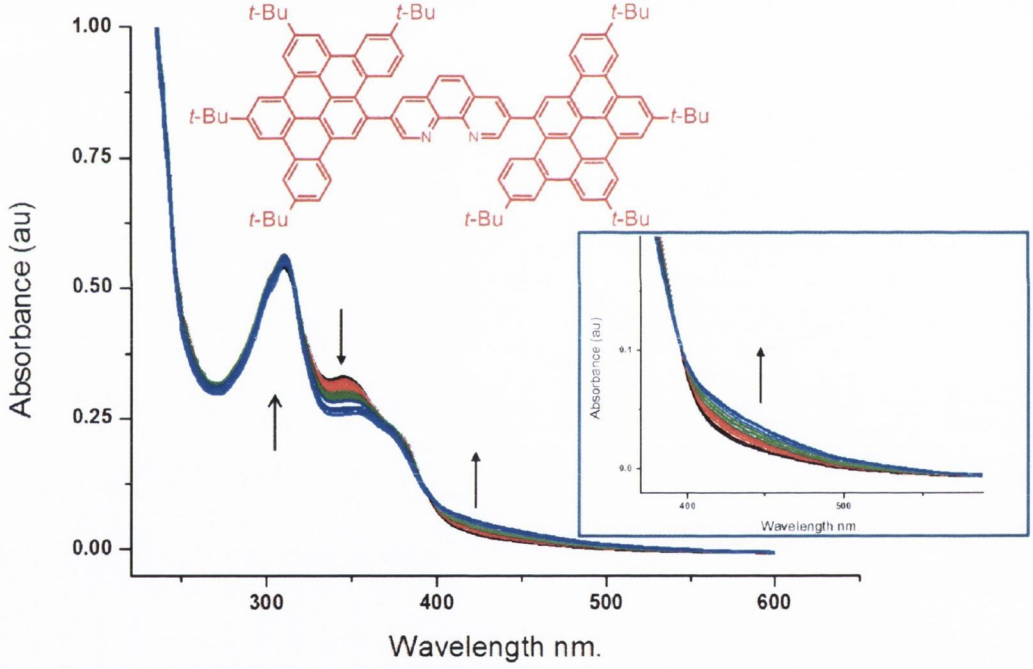


*Figure 4.20: The UV-Vis absorption spectrum of* ***18*** *(1 x $10^{-5}$M) upon sequential addition of 5 µL aliquots of trifluroacetic acid (1 x $10^{-5}$M).*

Figure 4.21 shows the corresponding titration undertaken for the fully fused ligand **21** under the same conditions. Upon addition of $H^+$, a new higher energy band is formed at $\lambda$ = 355 nm with a gradual reduction in the absorption intensity of the lower energy bands between $\lambda$ = 365 nm – 500 nm confirming their n-$\pi^*$ nature. No appreciable change in the tail of the spectrum suggests marginal charge transfer character within the ligand, which may be an indication of the considerable effect of bond closure to the 1,10-phenanthroline core on the overall communication between the diimine centre and the

appending aromatic moieties. A single isosbestic point is detectable at λ = 355 nm, which confirms an equilibrium between the neutral and newly protonated form. Although a significant number of aliquots of acid were added, no further appreciable change was observed.

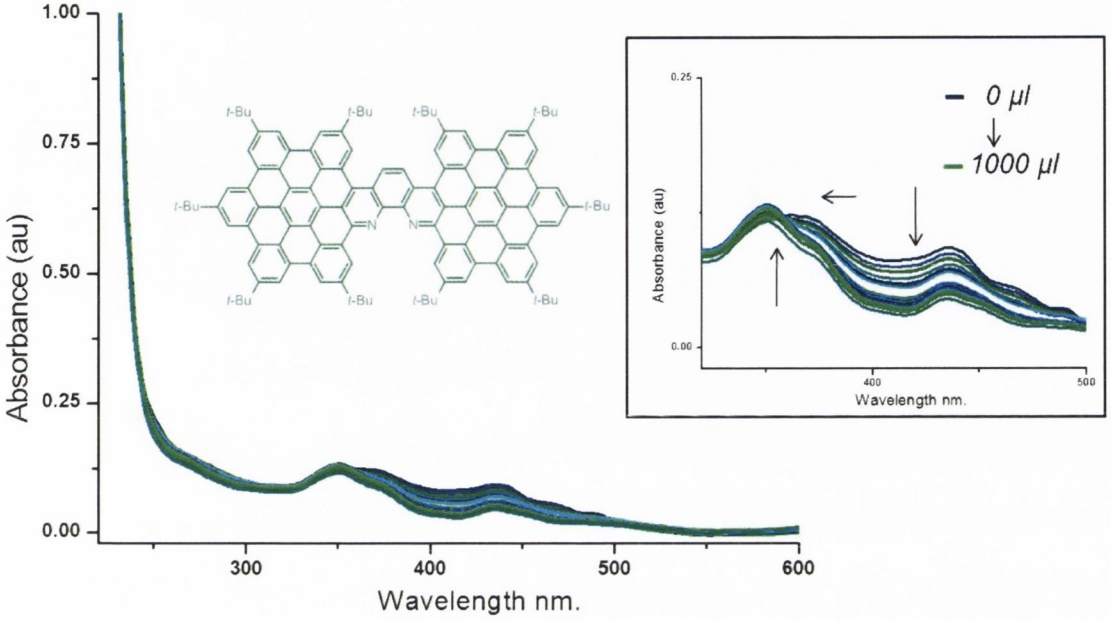


*Figure 4.21: Sequential addition of $CF_3COOH$ (5 µl aliquots of 1 x $10^{-5}$M in $CH_2Cl_2$) to a solution of* ***21****(1 x$10^{-6}$ M in $CH_2Cl_2$) with inset showing magnified region of the spectra (λ =320 nm-500 nm).*

To further investigate the effect of the addition of acid to the ligand, an emission titration was carried out on **21** ($CH_2Cl_2$, 1 x $10^{-5}$ M). The unprotonated species displays a highly structured emission profile with two structured emission maxima at at λ = 510 and 545 nm. This structure is broader than the emission profile commonly observed within the Draper group for other fused nitrogen ligands such as N-HSB, which can be attributed to π-stacking, and is in agreement with the $^1$H NMR spectrum obtained for the ligand. Figure 4.22 shows the spectrum obtained after addition of $CF_3COOH$ (2.5 µL aliquots of 1 x $10^{-6}$ M in $CH_2Cl_2$) to a solution of the ligand (1 x$10^{-6}$ M in $CH_2Cl_2$). There is an overall quenching of both of the emission bands at λ = 510 and 545 nm after the addition of 240 equivalents of the acid. Upon excitation at the maximum absorption wavelength ($\lambda_{max}^{abs}$ = 368 nm), the emission maximum at $\lambda_{em}$ = 505 nm gradually undergoes complete fluorescence quenching with increasing additions of the acid. This is indicative of n-π* contribution to the bands. The most surprising feature of the spectrum is the lack of the formation of a lower energy band that was previously observed for all of the aryl acetylene ligands investigated in Chapter 1, and for other 3,8-substituted 1,10-

phenanthroline ligands. However this supports the evidence that there is no significant intermolecular charge transfer between the 1,10-phenanthroline moiety and the graphene segments i.e. the ligand is behaving as one whole unit.

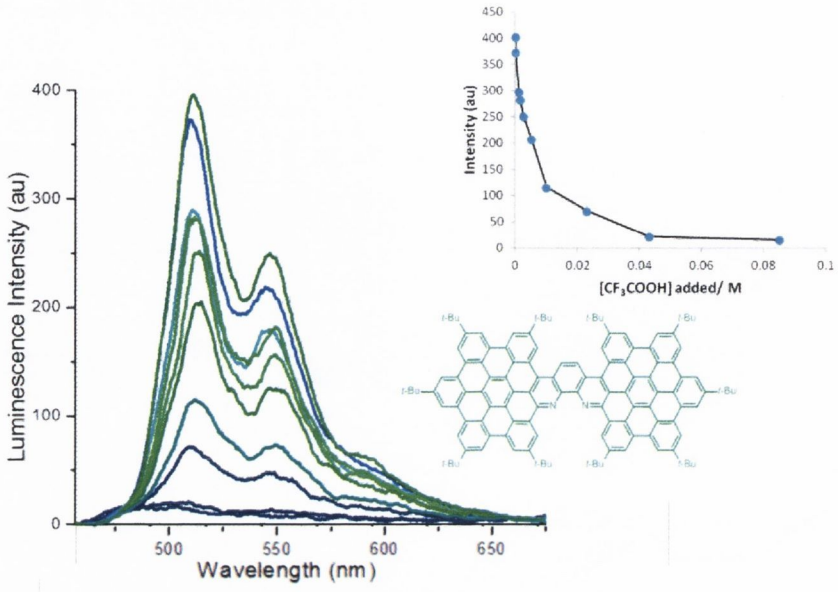


*Figure 4.22: Emission quenching observed in **21** due to the addition of 5 μL aliquots of 0.1 M $CF_3COOH$ with inset showing a plot of change of emission intensity vs. concentration of acid added at $\lambda_{max}$ 505 nm.*

### 4.3.2 Emission properties of ligands 17-21

The room temperature photoluminescence data was recorded for each respective ligand ($1 \times 10^{-5}$ M, $CH_2Cl_2$ solutions), as well as the corresponding data at 77 K using butyronitrile as solvent. For comparative purposes, the polyphenylenes **17**, **19** and **20** will be discussed separately to the fused ligands **18** and **21**.

The overlaid room temperature and low temperature emission spectra of **17**, **19** and **20** are presented in Figure 4.23. All three ligands display a broad high energy emission bands centred at $\lambda_{max} \sim =$ 380 nm at room temperature. An increase in substitution to the centre phenyl ring results in a marginal blue shift in the high energy band e.g. **17** ($\lambda_{max} \sim =$ 385 nm) *vs* **19** ($\lambda_{max} \sim =$ 376 nm). The addition of the electron donating group results in a small red shift in the $\lambda_{max}$ of the polyphenylene emission **20** ($\lambda_{max} \sim =$ 380 nm). The excitation spectrum of **20** is also presented, illustrating that a small Stokes shift is observed between it and the corresponding emission spectrum of the ligand. This suggests that a small geometric change is occurring between the ground state ($S_0$) and the singlet excited state ($S_1$). This observation, in combination with the nanosecond lifetimes

recorded for each ligand ($\tau$ =7-13 ns), confirms the assignment of emission from the polyphene as $^1(\pi\text{-}\pi^*)$.[219]

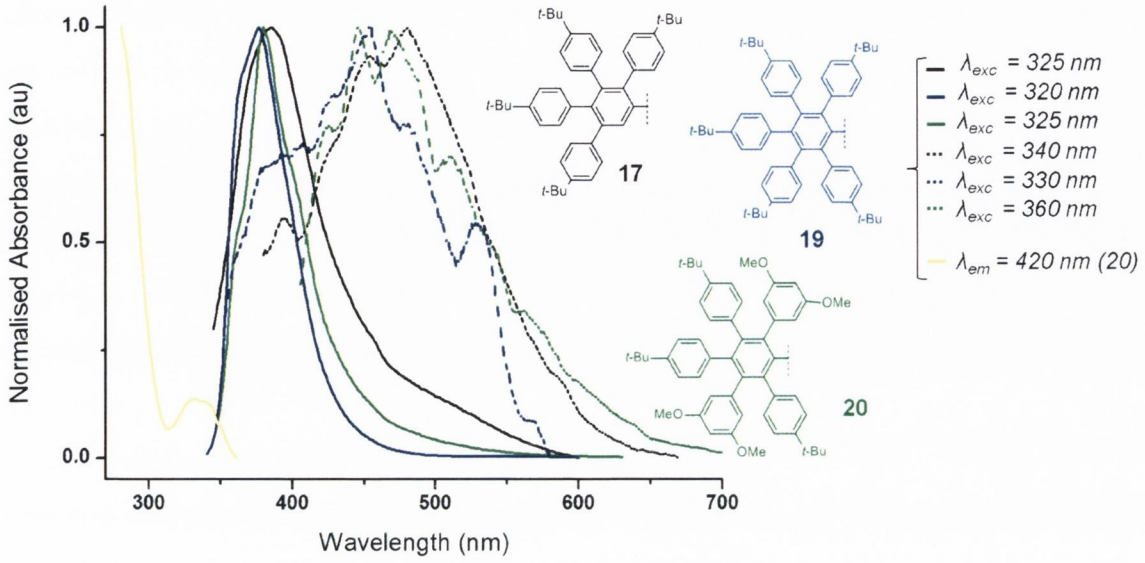


*Figure 4.23: Normalised room temperature (-) and low temperature emission spectra recorded for compounds **17**, **19** and **20** in $CH_2Cl_2$, with excitation wavelengths. Also included is the excitation spectrum of **20** (yellow).*

Several changes are observed on examination of emission spectra at 77 K. The emission bands of all three ligands have under gone a bathochromic shift, and the emission maxima are now all centred at approximately $\lambda$ ~450 nm. The emission bands have become more structured at lower temperatures which suggests partial $^3(\pi\text{-}\pi^*)$ character within the emission bands. The lifetimes of the ligands are enhanced relative to their room temperature measurements, and now range from $\tau$ = 15-18 ns, with the methoxy derivative displaying the longest of the three. The low temperature lifetimes are however, not sufficiently extended to warrant the assignment of phosphorescence. It is therefore likely the broad emission band contains two contributions, i.e. both $^1(\pi\text{-}\pi^*)$ and $^3(\pi\text{-}\pi^*)$ character. The values obtained for the lifetimes are thereby assigned as the higher energy $^1(\pi\text{-}\pi^*)$ moiety within the emission band that is likely to have undergone a blue-shift at lower temperatures. The vibronic character is attributed to the $^3(\pi\text{-}\pi^*)$ contribution at lower energys i.e. $\lambda$ = 450-600 nm. Attempts to determine a value for the lower energy emission were not successful as it was outside the range of the experimental set-up. This is in-line with a study of 1,0-phenanthrolines with anisyl derivatives by Armaroli *et al.* Armaroli also reported both $^1(\pi\text{-}\pi^*)$ and $^3(\pi\text{-}\pi^*)$ contributions within the low temperature emission bands for the ligands. The lifetime of

he long lived phosphorescence was attributed to phosphorescence deactivation from the lowest $^3(\pi\text{-}\pi)^*$ level and was reported to be in the range of $\tau$ = 0.9- 1.6 s.[24, 69]

Figure 4.24 shows the room temperature excitation and emission spectral data recorded for the fused ligands **18** and **21** in $CH_2Cl_2$. As previously discussed, the absorption and emission spectra of nitrogen-doped aromatic systems are dominated by (n,π*) and (π-π*) transitions. The excitation spectra of both ligands are presented and are in full agreement with the $\lambda_{max}$ observed in the UV-Vis absorption measurements, both of which are also presented in Figure 4.24, i.e. **18** $\lambda_{max}$ = 314 nm, 349 nm and 380nm and **21** $\lambda_{max}$ = 368 nm, 435 nm, 470nm and 490 nm. The lowest excited transition state of **18** is assigned as a π-π* transition, which is supported by spectral changes observed in the protonation studies earlier in the chapter. The lower energy bands of **21** have retained the structure observed in the UV-Vis spectrum, which suggests that it retains single monomeric character in solution. An additional low energy band at $\lambda$ = 485 nm is featured in the excitation spectrum of **21**, and is not present in the absorption spectra. This is assigned as the forbidden 0⟶0 transition, and is as a result of the additional degree of symmetry present in **21**.

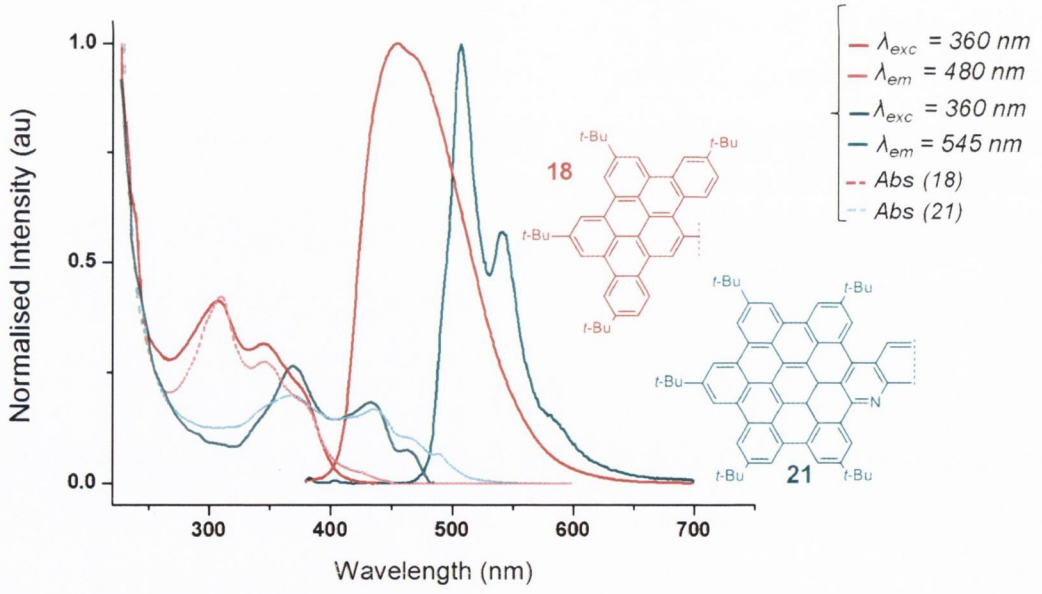


*Figure 4.24: Normalised room temperature excitation (---) and emission spectra (-), overlaid with the UV-Vis absorption spectra recorded for compounds **18** and **21** in $CH_2Cl_2$, with relevant wavelengths shown. (1 x $10^{-5}$M).*

The emission spectrum of **18** at room temperature is centred at $\lambda_{max}$ = 450 nm, and is red-shifted with respect to the precursor **21** ($\lambda_{max}^{em}$ = 380 nm). The broad emission is indicative of the twisted configuration adopted by the tri-benzo perylene pendents, and

the molecules overall distortion from planarity. The extended emission tail observed in the unfused derivatives is also evident, which further confirms the distorted conformation. A high degree of symmetry is evident between the excitation and emission spectrum of the ligand, however the large Stokes shift observed between the two spectra (~4250 $cm^{-1}$) is suggestive of a geometrical change between the ground state and the excited state species.

The addition of aromatic rings to the nitrogen fused platform results in a reduction of the lowest $\pi$-$\pi^*$ transition, thereby increasing the number of bonding and anti-bonding levels available. This results in a bathochromic shift in the emission maximum on going from **21** to **21**, and is very similar to the trend observed in the Draper group between N-HSB and it's partially fused derivatives. Excitation of the ligand (**21**) at $\lambda$ = 360 nm results in three emission maxima at $\lambda_{em}$ = 505, 545 and 595 nm, and an emission tail which extends to 700 nm. The intensity of these bands did not vary with different excitation wavelengths. This vibronic structure and emission maxima correlate well to the data reported by Drs. Dan Gregg and Buddhie Lankage within the Draper group for other nitrogen doped graphene systems.[8, 59] Contrary to that observed in the spectra of **18**, a small Stokes shift is observed (~ 690 $cm^{-1}$), which suggests very little conformational change between the molecules ground and excited state species. This is to be expected, given the high degree of planarity in the structure and is in agreement with the formation of additional C-C bonds to the 1,10-phenanthroline moiety. The room temperature lifetime measurements for the ligands are almost identical (~ 8 ns, see Table 4) with mono-exponential decays observed for both compounds. These lifetimes are in further agreement with emission arising from the $^1(\pi$-$\pi^*)$ transition.

The corresponding low temperature data for both ligands is presented in Figure 4.25. The vibronic structure of the emission band of **21** at 77K is very similar to that observed at room temperature. Both emission spectra undergo a marginal red shift in the rigid matrix (**18** ~ 194 $cm^{-1}$, **21** ~ 384 $cm^{-1}$). The structure of the emission band of **18** remains broad and featureless, with similar intensity to the corresponding room temperature measurement. The effect of bond closure to the 1,10-phenanthroline core is evident in the difference in band structure when the two emission bands are compared. The increased intensity of the emission maxima of **21**, particularly at $\lambda$ = 555 nm is explained by the highly conjugation structure experiencing an increase in rigidity and $\pi$- stacking at lower

temperatures. The extended lifetimes observed for both compounds at 77 K are due to the rigidity of the matrix (**18** $\tau$ = 14.3 ns, **21** $\tau$ = 13 ns).

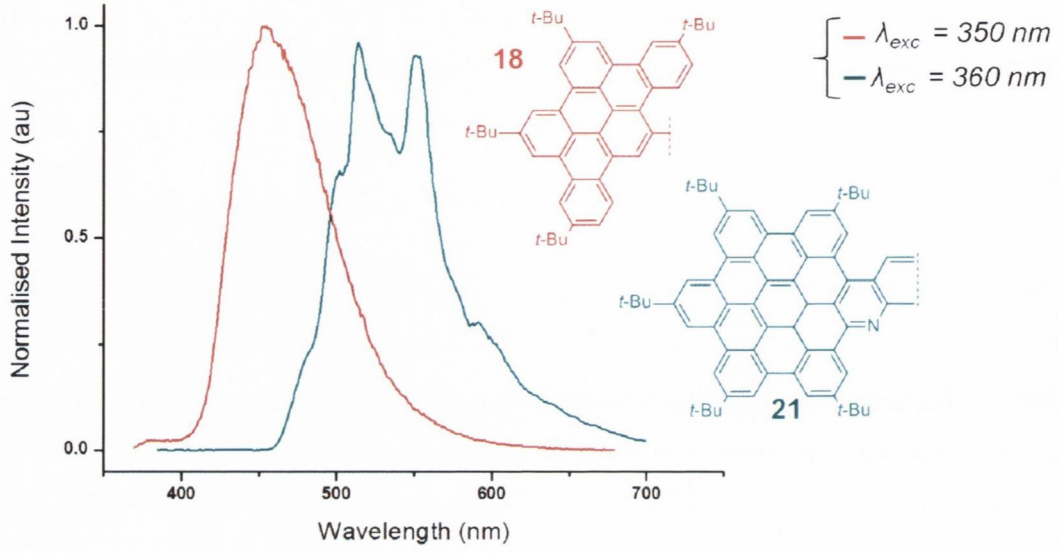


*Figure 4.25: Emission spectra (77 K for **18** and **21** (butyronitrile (glass), 1 x $10^{-5}$ M).*

Table 4.3 contains a summary of the photophysical measurements of the five 1,10-phenanthroline ligands. Both the emission wavelengths and the lifetime measurements are comparable to each other, and to the aryl acetylene ligands discussed in Chapter 1. The overall trend is as predicted, a red shift in emission maxima is observed upon both ring closure and the addition of electron donating groups e.g *tert*-butyl vs. methoxy substitution on the phenyl ring.

*Table 4.3: Photophysical measurements of ligands **17-21** at room and low temperature.*

| | **Medium (T[K])** | **$\lambda_{em}$[nm] ($\lambda_{exc}$[nm])** | **$\tau$ [ns] ( $\lambda_{exc}$ / $\lambda_{em}$ nm)** |
|---|---|---|---|
| **17** | $CH_2Cl_2$ (298) | $380_{max}$ (325) | 7.2 ns (295/370) |
| | Butyronitrile (77) | 396, $455_{max}$,485 (340) | 15 ns (340/455) |
| **18** | $CH_2Cl_2$ (298) | $453_{max}$ (360) | 8 ns (295/370) |
| | Butyronitrile (77) | $457_{max}$, (350) | 14.3 ns (370/500) |
| **19** | $CH_2Cl_2$ (298) | $376_{max}$ (320) | 6.6 ns (295/370) |
| | Butyronitrile (77) | 380, 445 $_{max}$, 525 (330) | 17 ns (340/445) |
| **20** | $CH_2Cl_2$ (298) | $385_{max}$ (325) | 13 ns (295/380) |
| | Butyronitrile (77) | 385, $450_{max}$, 525 (360) | 18 ns (340/450) |
| **21** | $CH_2Cl_2$ (298) | 505 $_{max}$, 545, 595 (360) | 7.6 ns (370/505) |
| | Butyronitrile (77) | 515 $_{max}$, 555, 595 (350) | 13 ns (460/515) |

**Complexes of large surface area ligands**

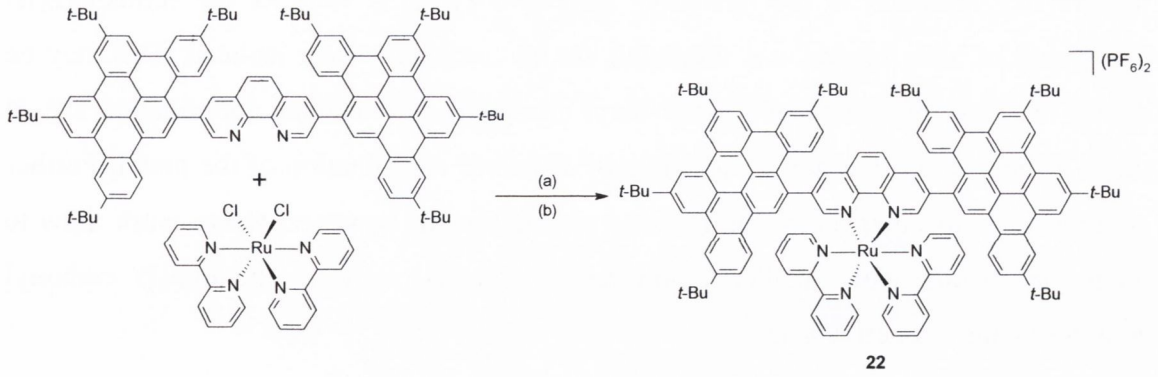


*Scheme 4.9: Synthesis of [Ru(bpy)$_2$(**18**)](PF$_6$)$_2$ to give **22** (a) Ethylene glycol monoethylether, ethanol, 150 °C, Ar, overnight (b) sat. KPF$_6$ solution.*

Although the overall yields of the ligand series **17-21** were quite low, two complexes were synthesised according to the procedures outlined in Chapter 2. Similar to the larger aryl acetylene ligands previously discussed, the poor solubility of **18** required changing from a solvent with a higher boiling point i.e. ethylene glycol monoethyl ether. The resulting complex (**22**) also required further purification by silica column chromatography, before it was redissolved in the minimum amount of ethylene glycol (~2 mL) precipitated with a solution of saturated $KPF_6$ as a dark red powder in a yield of 69 % (Scheme 4.9).

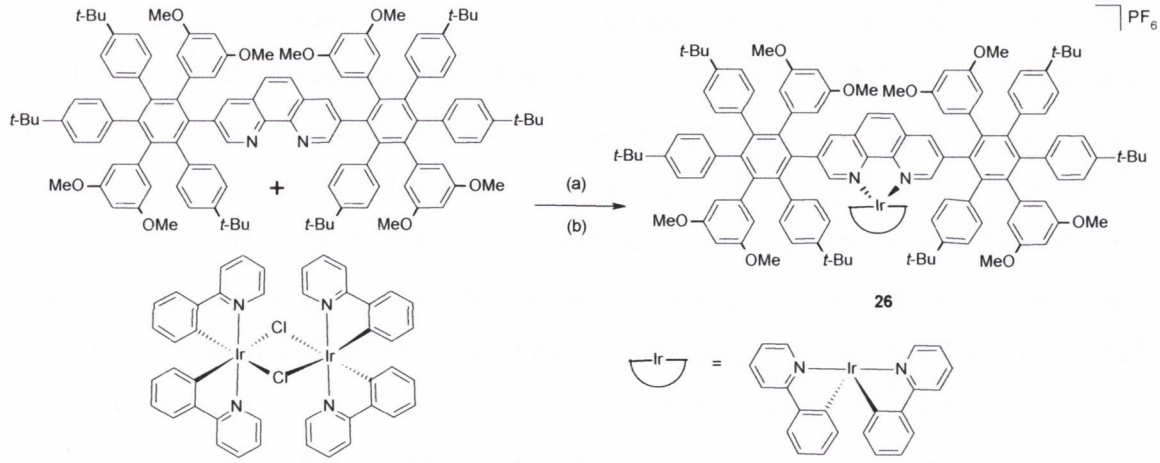


*Scheme 4.10: Synthesis of [Ir(ppy)$_2$(**20**)](PF$_6$) to give **23** (a)$CH_2Cl_2$: MeOH (1:1, v/v), reflux, Ar, 2 hrs, (b) sat. $NH_4PF_6$ solution.*

The cyclometalated iridium(III) complex of the methoxy polyphenylene derivative **20** was synthesised from $Ir(ppy)_2Cl_2$ according to the procedure outlined in Chapter 2, in a

poor yield of 37% (**23**, Scheme 10). The synthesis of the corresponding cyclometalated iridium(III) complex of the *tert*-butyl derivative (**19**), as well as the ruthenium(II) complexes of both ligands was attempted but no complexes were isolated. This may be due to the close proximity of the *tert*-butyl groups to the bidentate coordination site of the 1,10-phenanthroline moiety which may disfavour coordination of the metal. Further complexation to other metal centres was not attempted, however, future work aims to focus on metals with smaller co-ordinating ligands such as rhenium(I) carbonyl complexes and copper(I) salts.

Table 4.4 shows the MALDI-TOF analysis for **22** and **23**, which confirmed the formation of both the complexes. The isotopic distribution pattern of both products correlated well with the calculated m/z value as shown.

*Table 4.4: MALDI-TOF analysis of complexes **22** and **23** ($CH_3CN$).*

| Complex | Molecular Ion | Formula | Found *m/z* (%) | Calculated *m/z* |
|---|---|---|---|---|
| **22** | $[M-(PF_6)]^+$ | $[C_{124}H_{115}N_6F_6PRu]^+$ | 1935.7831 | 1935.7947 |
| **23** | $[M-(PF_6)]^+$ | $[C_{135}H_{136}N_4O_8Ir]^+$ | 2169.9939 | 2169.9988 |

The aromatic region of the $^1H$ NMR spectra of **22** is presented in Figure 4.26. As indicated by the quality of the spectra, the complex is poorily soluble at higher concentrations in most solvents. Despite repeated measurements in deuterated $CH_3CN$ and DMF, the quality of the resulting spectra did not improve. The protons on the periphery of the tri-benzoperylene pendant are assigned with the aid of long range coupling experiments, using the same technique outlined in the assignment of the ligand. The majority of the proton signals appear as a cluster in an overlapping multiplet between $\delta$ = 8.7 ppm and 9.0 ppm, with no significant downfield shift upon coordination to the metal centre. The proton labelled (●) appears as it did in the $^1H$ NMR of the free ligand, as a broad signal which is now overlapping with the solvent peak at 7.27 ppm. Three signals in the aliphatic region of the spectrum integrate for 90 H as expected, and confirm the presence of three different *tert*-butyl environments. Two of the protons on the 1,10-phenathroline core have undergone a considerable downfield shift, integrate for 2 H and appearing at $\delta$ = 9.8 (●) and 9.4 (●) respectively. The third proton remains upfield at 8.1 ppm (●). The auxiliary ligands have been assigned using a $^1H$-$^1H$ COSY experiment as before, and are shown in Figure 4.26 with he MALDI-TOF analysis of the

complex. The poor solubility of the complex prevented the $^{13}C$ spectrum of **22** from being obtained.

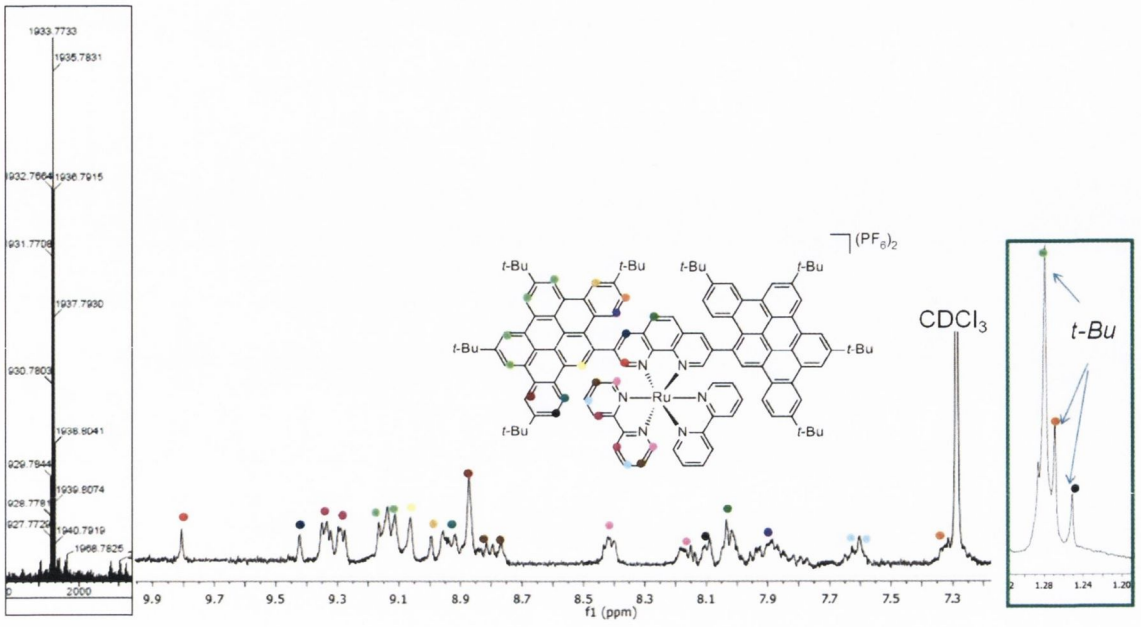


*Figure 4.26: The aromatic region of the poorly resolved $^{1}H$ NMR spectra of **22**. Inset shows three t-Bu signals in the aliphatic region and MALDI-TOF analysis confirming the presence of $[M+PF_6]^+$ m/z 1935.7831,(calculated m/z = 1935.7947)*

The $^{1}H$ NMR of the iridium(III) complex **23** is presented in Figure 27. Although the symmetrical plane through the centre of the 1,10-phenanthroline ring greatly simplifies the assignment of the complex, each of the polyphenylene rings appear as five distinct environments, which results in 29 proton signals in the aromatic region. The assignment of the auxiliary ligand was aided by the presence of two distinct triplets at δ 8.0 ppm and δ 7.1 ppm. With the aid of a $^{13}C$-$^{1}H$ COSY experiment , the shielded doublet at δ 6.3 ppm (•) was confirmed as the proton adjacent to the nitrogen of the phenylpyridyl ligand. The remaining signals on the ligand were identified using the $^{1}H$-$^{1}H$ COSY experiment shown. Selective long range NOESY and TOCSY experiments, similar to the procedure used in the assignment of the ligand family, enabled identification of all three proton signals on each of the two methoxy-phenyl rings and their corresponding methoxy protons in the aliphatic region [Figure 4.28(a) and (b)]. This process was also used to confirm the assignment of the *tert*-butyl phenyl ring (•) on the periphery polyphenylene moiety, with the aid of $^{4}J$ interactions between the protons adjacent to the methoxy signals on the neighbouring spin system [Figure 4.28(c)].

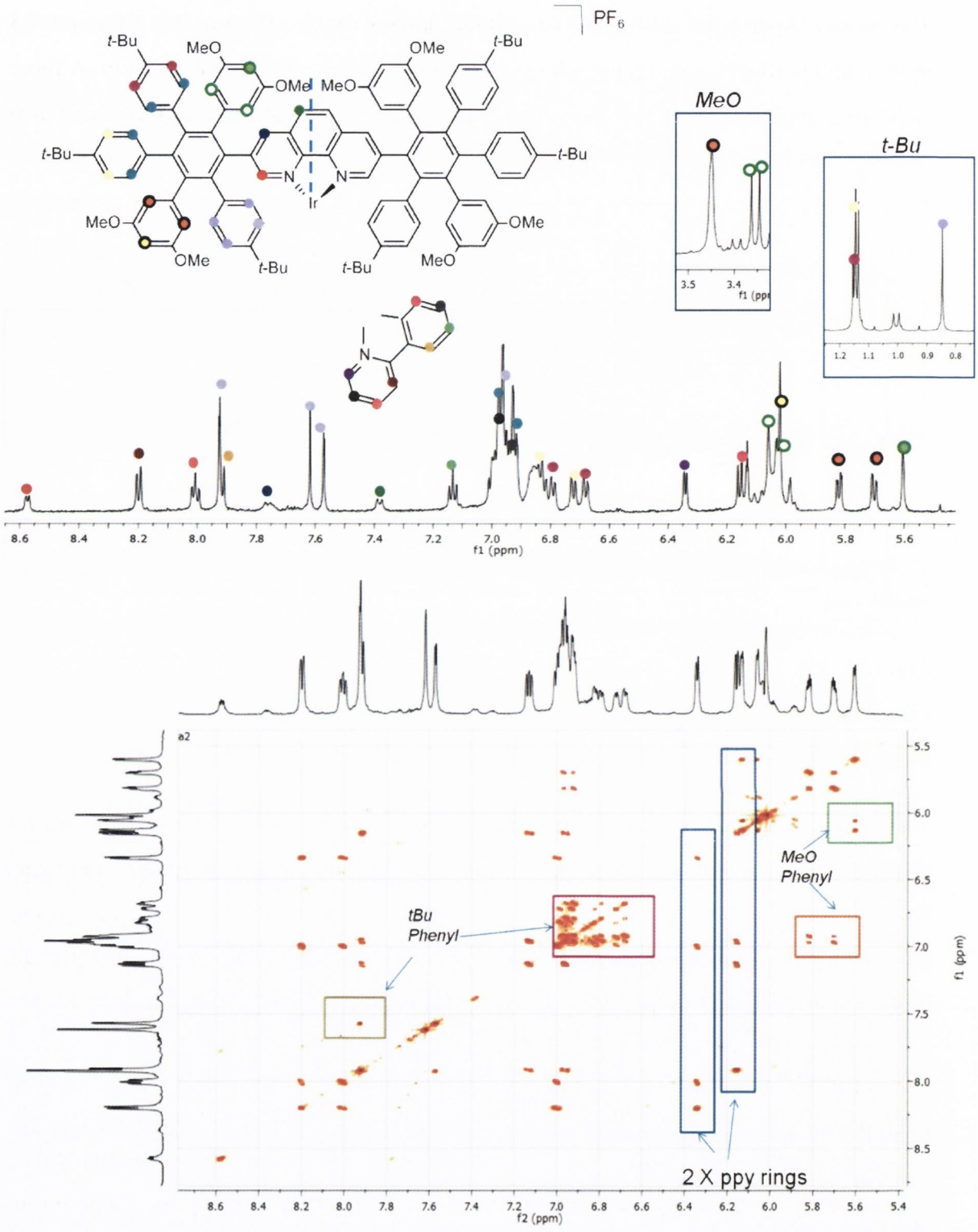


*Figure 4.27: Above: aromatic region of the $^{1}H$ NMR spectrum of **23** with inset showing the methoxy and tert-butyl signals of the aliphatic region of the spectra, and below: $^{1}H$-$^{1}H$COSY showing identification of various spin systems ($CD_3CN$, 600 MHz, R.T).*

This assignment was further confirmed by the small coupling constants possessed by each of protons on the ring (•). The protons on the ring are dramatically deshielded after complexation to the metal centre, due to the neighbouring auxiliary phenylpyridine rings.

The protons have been allocated as the three doublets at δ 7.9 ppm, 7.7 ppm and 7.5 ppm, with the fourth signal lying within the large multiplet centred at δ 6.9 ppm. A more conclusive assignment of the individual signals was not possible. The remaining two *tert*-butyl functionalised rings appear as four doublets (δ 6.7-6.9 ppm), each integrating for 2H, and a broad multiplet (δ 6.9-7.0 ppm, 14 H), four of which correspond to protons labelled (●). The remaining signals are due to the 1,10-phenanthroline moiety, with the most deshielded doublet at 8.5 ppm designated as the proton adjacent to the nitrogen (●).

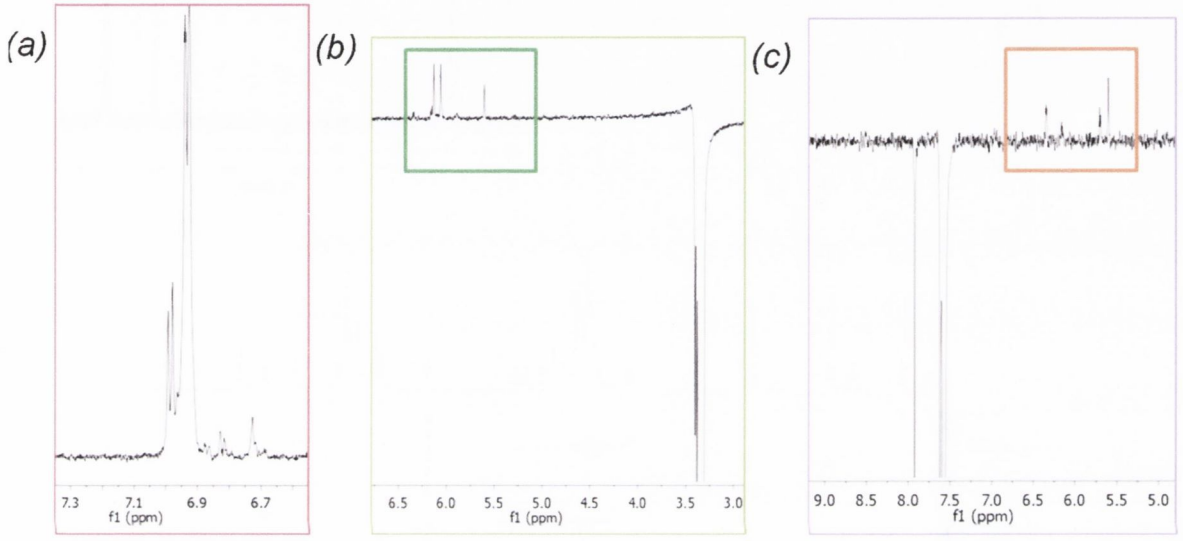


*Figure 4.28: Some examples of long range NOESY and TOCSY experiments which enabled the identification of (a) the protons in each of the tert-butyl phenyl ring spin systems, (b) the corresponding methoxy signals in the aliphatic region and (c)the methoxy substituted ring adjacent to the tert-butyl phenyl ring labelled (●) for* ***23****. Colour scheme of individual boxes corresponds to that adopted in the* $^{1}H$ *NMR.*

The corresponding $^{13}C$ NMR spectrum for **23** is presented in Figure 29. As before, additional assignment of the quaternary carbons was achieved through 2D HMBC experiments. This experiment was utilised to specifically locate the two quaternary carbons of the phenylpyridine ligands, as well as the quaternary carbons located on the methoxy and *tert*-butyl functionalised rings. These have been highlighted using the labelling scheme adopted in the $^{1}H$ NMR spectrum. The dramatic downfield shift experienced by the protons on the ring adjacent to the 2-phenylpyridine ligands (●), is also reflected in the $^{13}C$ spectrum below [δ 150 ppm and 140 ppm (**26**) *vs* ~132 ppm (**23**)].

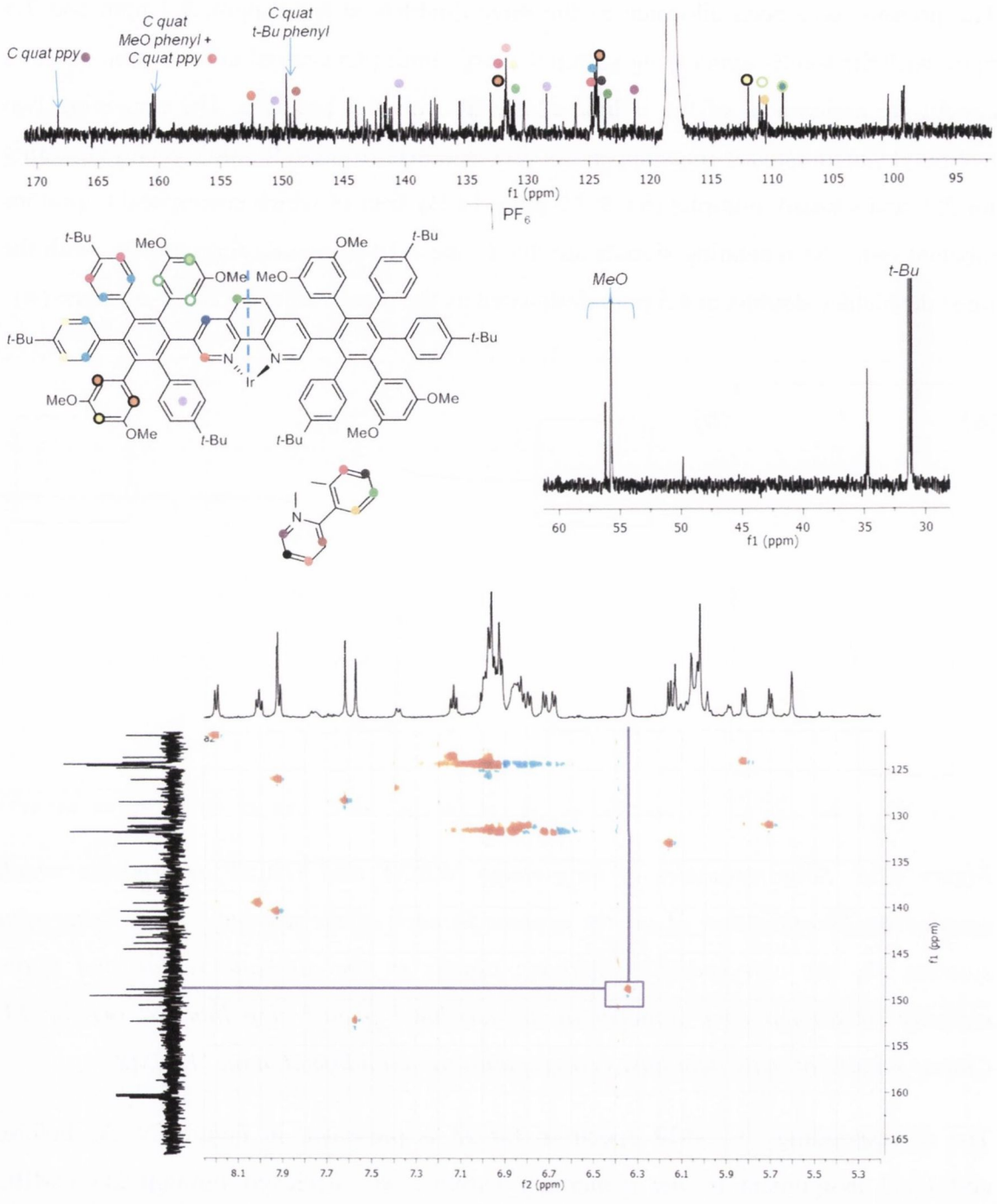


*Figure 4.29: Above: the $^{13}C$ NMR spectrum of iridium complex* ***23*** *with magnified area showing methoxy and tert-butyl carbon signals. The unlabelled signals in aromatic region correspond to the remaining quaternary carbons. Below: the $^{13}C$ -$^{1}H$ COSY experiment used to identify the proton adjacent to the nitrogen on the auxiliary ligand (•) ($CD_3CN$, 151 MHz, R.T.)*

## 4.4 The photophysical properties of 22 and 2

The UV-Vis absorption spectra of the two complexes are presented in Figure 4.30 below. The high energy bands of both spectra are comprised of π-π* transitions due to the 1,10-phenanthroline moiety and its peripheral ligand, and typically appear at λ = 286 nm.[204] The ruthenium(II) complex 22 displays absorption bands that are considerably more structured than the iridium(III) polyphenylene complex 23. This is explained by planarised conformation of the tri-benzoperylene fragments, and enables the identification of π-π* and n-π* transitions in the UV-Vis absorption spectrum. The prominent absorption band between λ 350-400 nm is a indicative of a 1,10-phenanthroline functionalised with C-C linked large chromophores[125] The equivalent feature is also present in the absorption spectra of 23, but has a considerably lower extinction coefficient (Table 4.5). Two intense lower energy bands at λ = 424 nm and λ= 450 nm are assigned as spin-allowed MLCT transition [d(Ru)→(N^N)], both of which display high extinction coefficients of ε ~1 x $10^{-4}$ $M^{-1}$ $cm^{-1}$.[121] Finally, a strongly absorbing lower energy band that stretches to λ = 500 nm is assigned as an $^{1}$MLCT transition from the ruthenium(II) metal centre to the 1,10-phenanthroline chromophore.

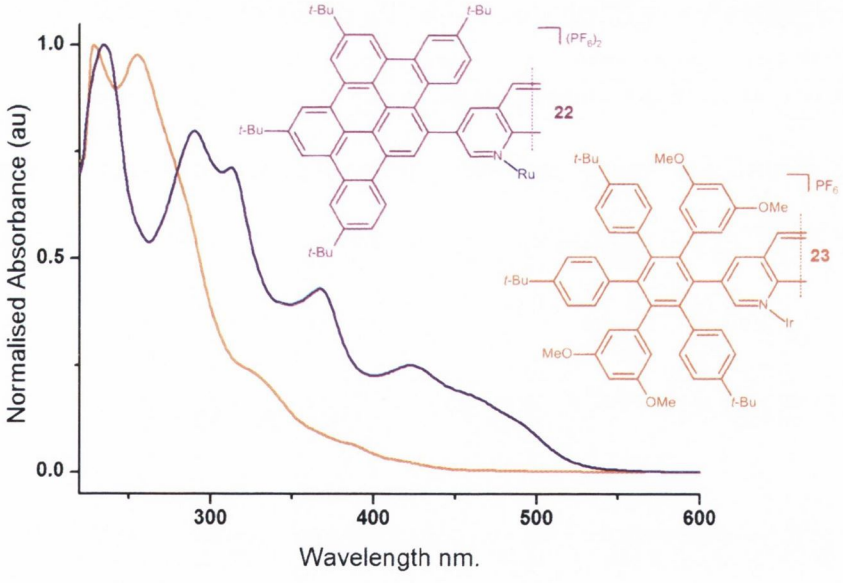


*Figure 4.30: Normalised UV-Vis absorption spectrum for complexes **22** and **23** (1 x 10-**5** M, $CH_2Cl_2$). Auxiliary ligands on metal complexes are omitted for clarity.*

The strong molar absorptivity coefficient (ε) of the high energy bands of **23** (λ = 250-300 nm) is attributed to the presence of the electron-donating methoxy groups in the ligand framework.[24] The electron/repulsion induced by the presence of the OMe groups

previously observed in the absorption spectrum of the ligand, is still evident in the UV-Vis absorption spectrum of the complex. There is a slight shoulder detectable at $\lambda_{abs}$=295 nm for the iridium(III) complex, and is assigned as a $\pi$-$\pi^*$ transition within the ppy ligand. Weaker absorption bands at lower energy have been reported for similar systems as spin allowed CT transitions, where the CT is from the HOMO residing on the metal to a phenanthroline-ligand based $\pi^*$ orbital. The extent of delocalisation of the HOMO over the metal [$d\pi(Ir) \rightarrow \pi^*(phen)$] and ppy ligand [$\pi(ppy) \rightarrow \pi^*(phen)$] determines the overall nature of the transition i.e. MLCT or LLCT.[115]

*Table 4.5: UV-Vis absorption spectra maxima and their corresponding extinction coefficients (ε) for complexes **22** and **23** ($CH_2Cl_2$, 1 x $10^{-5}$M).*

| Complex | $\lambda_{max}$[nm](ε x $10^4$ [$M^{-1}$ $cm^{-1}$]) |
|---|---|
| **22** | 233 (9.9), 291 (8.02), 314 (7.12), 368 (4.2), 423 (2.4), 468 (1.62), 486 *sh,* |
| **23** | 254 (6.16), 286 *sh* (3.87), 328 (1.34), 383 (0.4), 418 *sh* (0.3) |

To assess the solvent dependency of both metal complexes, the corresponding UV-Vis absorption spectra were recorded in toluene and acetonitrile. As expected, both complexes exhibit analogous behaviour to the complexes in Chapter 2 i.e. solvent polarity exhibits marginal influence over the position of lower energy absorption bands.

*Table 4.6: UV-Visible absorption maxima (λ, nm) of the lowest energy absorption bands of **22** and **23** in different solvents.*

| Complex | $CH_3CN$ | $CH_2Cl_2$ | Toluene |
|---|---|---|---|
| **22** | 366, 417, 466 | 368, 423, 468 | 369, 417, 464 |
| **23** | 330, 379 | 328, 383 | 328, 385 |

### 4.4.1 The excitation and emission spectra of 22 and 23 (298 K and 77 K).

The excitation and emission spectra for the ruthenium(II) complex are presented in Figure 4.31. Three distinguishable excitation maxima correlate with the UV-Vis absorption maxima of the lower energy bands shown in Figure 4.30 i.e. $\lambda_{exc}$ = 362 nm, 418 nm and 465 nm. The degassed solution of the complex displays strong red phosphorescence at room temperature, emitting at $\lambda_{em}^{max}$ = 625 nm. The emission wavelength is invariant to excitation wavelength. The complex displays moderate

vibronic structure at 298 K. The energy difference between the two emission maxima ($\lambda_{em}^{max}$ = 625 and 674 nm) is calculated to be 1138 $cm^{-1}$. This is in line with the aryl C-H wagging vibration values calculated for the larger aryl acetylene complexes in Chapter 2 (e.g. **10** = 1102 $cm^{-1}$). The room temperature lifetime of the triplet state of **22** is $\tau$ = 2.5 μs. Similar Ru(II) diimine complexes with larger C-C linked aryl substituents have been reported by Castellano and Zhao.[128, 220, 221] It is hypothesised that the introduction of the C-C linked fluorophore introduces a ligand localised $^3(\pi\text{-}\pi^*)$ which is considered to be almost isoenergetic with the $^3$MLCT state. This can establish an equilibrium between the $^3(\pi\text{-}\pi)^*$ and the $^3$MLCT states, with the long-lived $^3(\pi\text{-}\pi^*)$ now acting as an energy reservoir transferring energy to the $^3$MLCT emissive state. This results in a slightly extended phosphorescence lifetime i.e. 0.5 μs → ~2.5 μs. On this basis, the emissive state of **22** is also assigned as $^3$MLCT emissive state, but the incorporation of the tri-benzoperylene moiety is likely to result in similar equilibrium between the ligand localised $^3(\pi\text{-}\pi^*)$ of the organic fluorophore and the MLCT state.

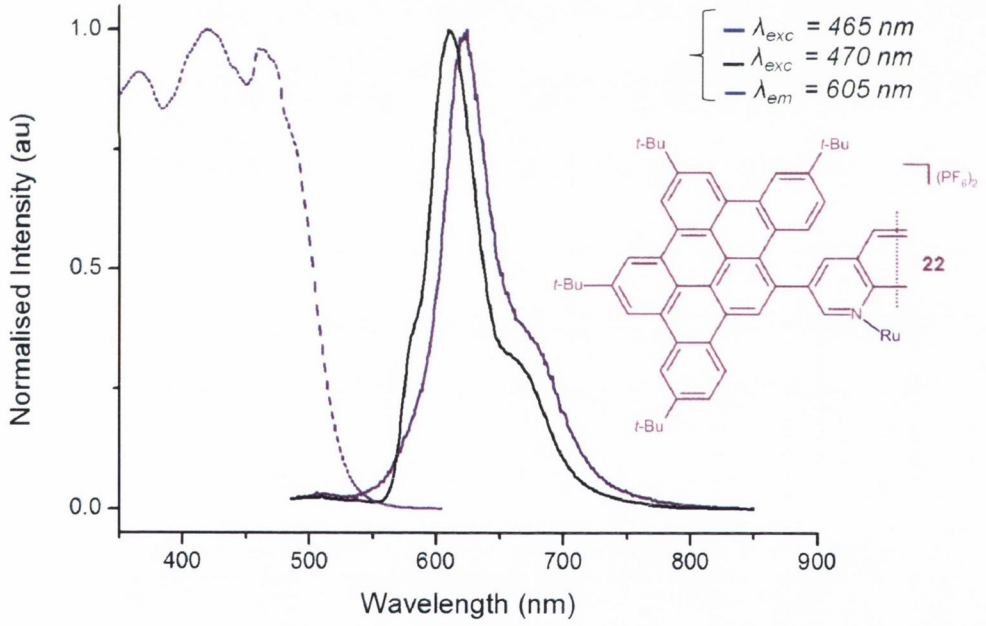


*Figure 4.31: Normalised excitation (---) and emission spectra (—) for **22**. Relative wavelengths are shown. The emission spectra at 77 K is labelled in black (1 x $10^{-5}$ M, RT = $CH_2Cl_2$, 77 K.= butyronitrile). Auxiliary bipy ligands omitted for clarity.*

The low temperature emission of **22** was measured in butyronitrile glass at 1 x $10^{-5}$ M concentration. The emission band retains a similar degree of vibronic structure at 77K (—, Figure 4.31), and undergoes a small blue-shift, with a rigidochromic shift of 527 $cm^{-1}$. This is in-line with other Ru(II) MLCT emitters and confirms the emissive state of

the complex as the $^3$MLCT state. The low temperature measurement of the lifetime of the triplet state of **22** shows a considerably extended triplet lifetime of 13.6 μs. This increase is consistent with a decreasing thermal population of the non-radiative d-d state. The corresponding room temperature and low temperature excitation and emission spectra for **23** are presented in Figure 4.32. Unlike **22**, the room temperature spectrum is broad and featureless, and is centred at $\lambda_{em}$ = 560nm. There is a significant blue shift between the room temperature and low temperature emission spectra for the complex. The separation between the two emission bands was calculated to be 1575 cm$^{-1}$, which is smaller than similar iridium(III) 1,10-phenanthroline systems, but is within the range of other iridium(III) and ruthenium(II) complexes whose emissive state have been assigned as MLCT.[115] The lifetime of the excited state of **23** is 1.6 μs at room temperature, which is marginally longer than the triplet lifetime of [Ir(ppy)(1,10-phenanthroline)][$PF_6$].[182] This value, in combination with a larger Stokes shift, is indicative of a $^3$CT state. The lifetime of the complex at 77 K was also measured, and is 5.8 μs. This extension further supports the assignment of the $^3$MLCT state and is within the range of comparable systems.[222]

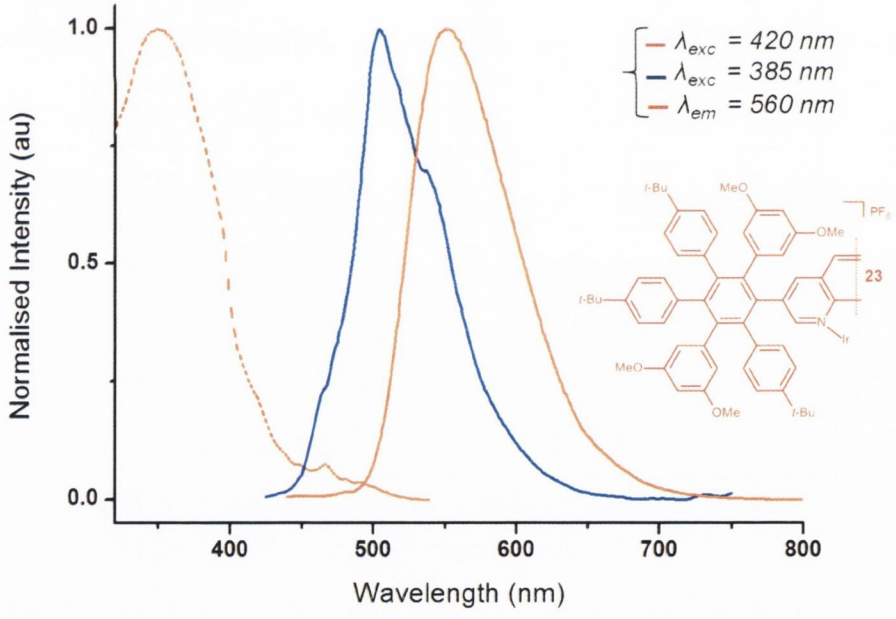


*Figure 4.32: Normalised excitation (---) and emission spectra (—) for **23**. Relative wavelengths as shown. The emission spectra at 77 K is labelled in blue (1 x 10$^{-5}$ M, R.T. = $CH_2Cl_2$, 77 K.= butyronitrile glass). Auxiliary ppy ligands omitted for clarity.*

Table 4.7 contains a summary of the luminescence data obtained for complexes **22** and **23**. As expected, the ruthenium(II) polypyridyl complex shows longer lifetimes at room and low temperature, and increased emission vibronic structure. This is attributed to the

presence of the increased π-conjugation in the ligand framework and the energy transfer occurring from the $^3(\pi\text{-}\pi^*)$ to the $^3$MLCT state.

*Table 4.7: Photophysical measurements for complexes **22** and **23**.*

| | Medium (T[K]) | $\lambda_{em}$[nm] ($\lambda_{exc}$[nm]) | τ [ns] ( $\lambda_{exc}$ / $\lambda_{em}$ nm) |
|---|---|---|---|
| **22** | $CH_2Cl_2$ (298) | $623_{max}$, 675 (465) | 2.5 μs (370/625) |
| | Butyronitrile (77) | $610_{max}$, 665 (470) | 13.6 μs (460/610) |
| **23** | $CH_2Cl_2$ (298) | $555_{max}$ (420) | 1.6 μs (370/555) |
| | Butyronitrile (77) | $503_{max}$, 536 (385) | 5.8 μs (370/505) |

### 4.4.2 The potential application of 22 as a triplet sensitizer for TTA based upconversion.

After consideration of the poor UV-Vis absorption of **23** at lower energies, in combination with the shorter lifetime measurements of the excited states, the complex was deemed unsuitable for potential application in TTA. However work is on-going to design derivatives of **23** with better absorption in the required range λ = 450-500 nm. Based on the strong absorption band at λ = 450 - 500 nm displayed by the ruthenium(II) complex **22** (Figure 4.30) and the reasonably long triplet lifetime measurements (τ = 2.5 μs), the decision was taken to screen the compound as an additional potential triplet sensitizer. The measurements were performed using identical parameters to those used in the screening of the complexes in Chapter 3. The sample was prepared at 1 $x10^{-5}$ M concentration, and degassed thoroughly by the freeze-pump thaw method. The emission spectra of the complex was recorded when the sample was excited at $\lambda_{exc}$ = 478 nm to ensure no trace of fluorescence from the complex was detected between λ = 400-450 nm. Six equivalents of DPA were added, and the emission spectrum was again recorded up to λ = 450 nm. Upconversion of the acceptor was successfully detected. Based on the relevant intensity of the upconverted fluorescence recorded by the sample under the same conditions (6 equivalents), the complex is predicted to have upconversion efficiency similar to the ruthenium(II) pyrenyl complex. This is surprising given that the lifetime of the complex is considerably shorter than **10** (1.2 μs *vs* 56 μs), and suggests that further modification of the design of the complex may produce a very efficient triplet sensitizer. Despite the addition of further equivalents of DPA, the phosphorescence of **22** could not be quenched up to 25 equivalents (see ----, Figure

4.33), and the corresponding unconverted fluorescence recorded is of a similar intensity to that recorded for the iridium pyrenyl complex **15** at the same concentration of DPA. This is again surprising since the triplet lifetime and the absorption of **22** is much less than **10**.

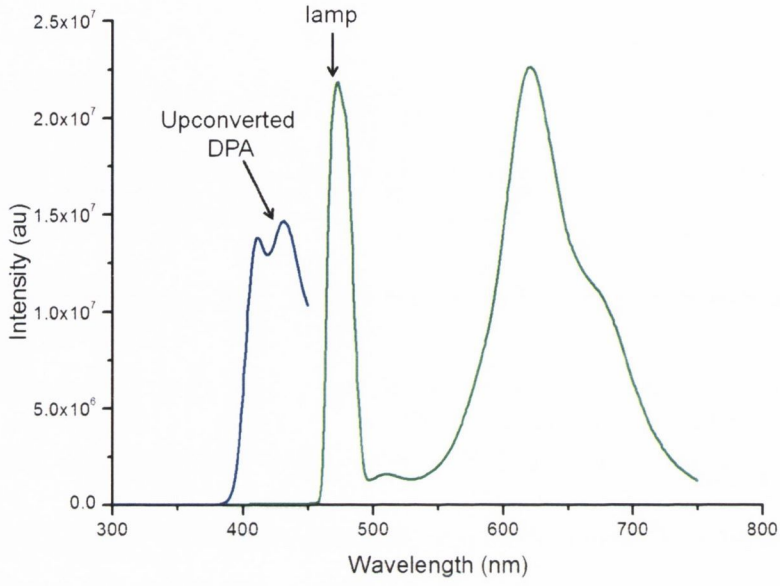


*Figure 4.33: The upconverted fluorescence detected for* ***22*** *at* $1x10^{-5}$*M upon addition of 25 equivalents of DPA (blue line, when the spectra is run between 300-450 nm), and the entire spectrum (between* $\lambda$ *=300 and 750 nm).*

### 4.5 Conclusions and future work

This chapter outlines the synthesis of a new family of five large surface area 1,10-phenanthroline ligands and a photophysical study of their emissive behaviour. The photophysical behaviour of the polyphenylene based ligands (**17**, **18** and **20**) is similar to that previously observed for the precursors of N-HSB. The ligands display broad fluorescence emission at room temperature, with moderate lifetimes in the nanosecond range. At lower temperatures, both fluorescence and phosphorescence contributions are detected, which agrees with assignments made by Armaroli for anisyl 1,10-phenanthroline ligands. This project has demonstrated the C-C bond closure to the 1,10-phenanthroline moiety is possible, unlike other nitrogen containing systems previously studied within the Draper group (e.g. terpyridines).[64] The protonation studies of **19** and **21** have demonstrated that closure to the central diimine moiety produces photophysical behaviour which is more in line with fully fused systems, rather than 3,8-substituted 1,10-phenanthrolines. Electrochemical studies are underway to further clarify the extent of this behaviour. Modification of the design of **21** is also currently underway in order to

generate similar systems with wider applications, and improved solubility. Optimisation of the synthetic route is required so that surface behaviour of the ligand can be studied. It is believed that the incorporation of alkyl chains around the periphery of aromatic platform may also confer liquid crystalline behaviour on the ligand

The synthesis of complexes of the large surface area ligands using metals with smaller auxiliary ligands should overcome the restrictions of the size of the coordination site available in the ligands, thereby enhancing the overall potential yields of the complexes and enabling broader photophysical and electrochemical studies to be undertaken. The initial focus of the study will be on rhenium(I) tricarbonyl systems and copper(I) complexes.

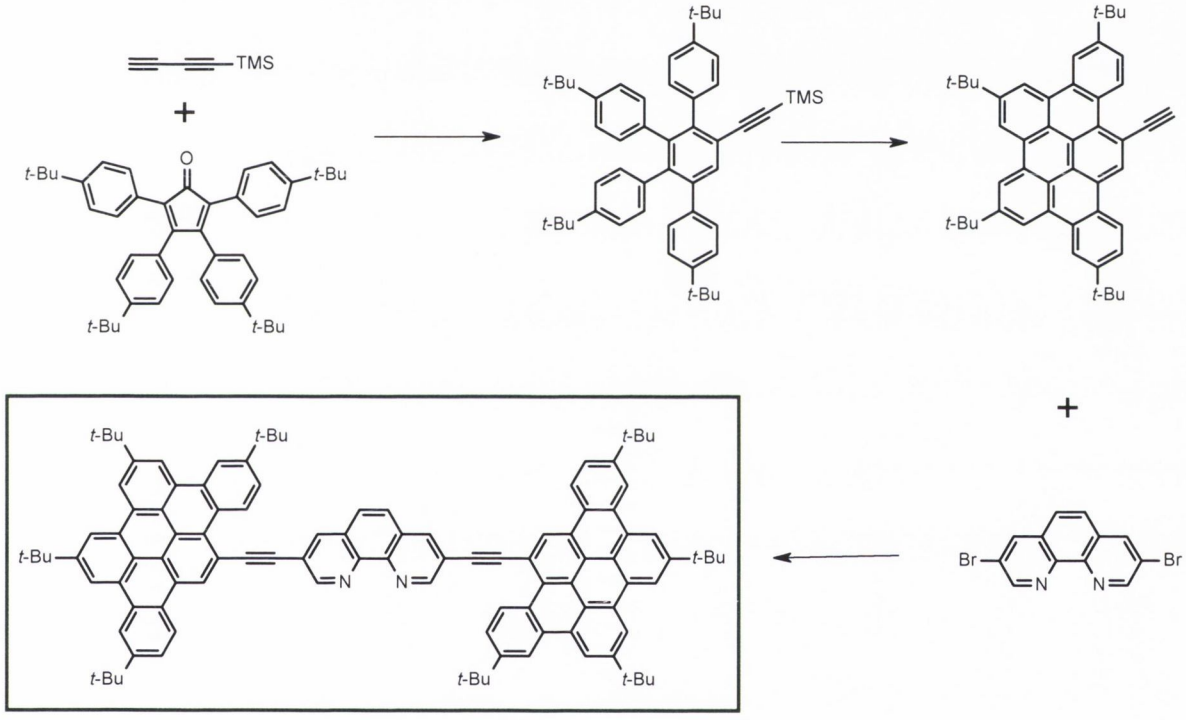


*Figure 4.34: The proposed synthetic route to the tribenzo[b,n,pqr]perylene acetylene substituted 1,10-phenanthroline ligand towards the generate of iridium(III) and ruthenium(II) complexes as TTA triplet sensitizers.*

Based on the preliminary investigation undertaken in this study, it is believed that incorporation of an acetylene linker between the tribenzo[b,n,pqr]perylene pendent and the 1,10-phenanthroline core may produce a triplet sensitizer with stronger absorption at $\lambda$ = 450-500 nm, while simultaneously increasing the triplet lifetime of the complex. This would not only generate higher values of $\varepsilon$, but in turn produce a more efficient TTET

process between the complex and the acceptor, thereby enhancing the value of $\eta$, the upconversion capability. The proposed synthetic route towards this new ligand is outlined below, and is based on the design of the ligands previously discussed in this Chapter 1. This route offers the potential of further modification of the aromatic platform by alternating the substituents on the cyclopentadienone precursor. The corresponding ruthenium(II) and iridium(III) complexes could also be synthesised by using the on-the-complex coupling approach discussed in Chapter 3, which would enable higher yields of the complexes to be achieved.

# 5 Experimental

## 5.1 Experimental Details

Unless otherwise stated, all reactions were carried out under an inert atmosphere of either nitrogen or argon using standard Schlenk and vacuum line techniques. Solvents were dried using appropriate drying agents and distilled under a nitrogen atmosphere, dichloromethane and diisopropylamine distilled over $CaH_2$ and THF and toluene over sodium/benzophenone. Starting materials 1-ethynyl pyrene (Alfa Aesar), ethynyltrimethylsilane, CuI, $Pd(PPh_3)_4$, 2,2'-bipyridine, $PPh_3$ and (Sigma Aldrich) and standard solvents were used without further purification. Flash chromatography was performed using silica gel (Sigma Aldrich) as the stationary phase. $RuCl_3.xH_2O$ and $IrCl_3.H_2O$ were purchased from Alfa Aesar.

The known compounds 1,4-dimethylpiperazine-2,3-dione (DMPD) [61], bis(4-*tert*-butylphenyl)acetylene [223], *cis*-$PdCl_2(PPh_3)_2$ [224], *cis*-$Ru(bpy)_2Cl_2.H_2O$ [119] and $[Ir(ppy)_2(\mu\text{-}Cl)]_2$ [131] were synthesised according to literature procedures. The synthesis of 1,3-bis(4-*tert*-butylphenyl)propan-2-one (**sm2**) [225] 1,2-bis-(4-*tert*-butylphenyl)ethane-1,2-dione (**sm3**) [61] and 2,3,4,5-tetra-(4-*tert*-butylphenyl)cyclopenta-2,4-dienone (**sm4**)[226] have previously been reported. 4-iodo-4'-*tert*-butylphenylacetylene (**sm5**),[17] 1-(4-iodophenyl)-2,3,4,5,6-penta-*tert*-butylphenyl-benzene (**sm6**), [17] 1-(4-trimethylsilylethynylphenyl-2,3,4,5,6-penta-(4-*tert*- butylphenyl)benzene (**sm7**), [18] 1-(4-ethynylphenyl)-2,3,4,5,6-penta-(4-*tert*-butylphenyl)benzene (**sm8**) [18] and 2-ethynyl-5,8,1,14,17-penta-tert-butylhexa-*peri*-hexabenzocoronene (**sm9**)[17] have been previously reported by the Draper group and were synthesised accordingly in comparable yields. For this reason, the experimental procedure has not been included.

Microwave reactions were carried out in a CEM Discover S-Class Single Mode Microwave reactor. All reactions were performed in specialised sealed 'snap-cap' vials under pressure.

Electrospray mass spectra were recorded on a Micromass-LCT spectrometer. Electron impact mass spectra were measured on a Waters corp. GCT Premier electron impact mass spectrometer. MALDI-TOF mass spectra were recorded on a Waters MALDI-QTOF Premier spectrometer using an α-cyano-4-hydroxy cinnamic acid matrix. Accurate mass spectra were referenced against Leucine enkeplin (555.6 g $mol^{-1}$) or

[Glu$^1$]-Fibrinopeptide B (1570.6 g mol$^{-1}$) and reported to within 5 ppm. All samples were dissolved in THF or MeCN unless otherwise stated.

IR spectra (reported in cm$^{-1}$) were made as neat samples and were recorded on a Perkin-Elmer Spectrum 100 FT-IR spectrometer equipped with a Universal-ATR sampling accessory. Elemental analyses were performed in the Microanalytical Laboratory, University College Dublin. Melting points are given uncorrected and were measured in capillary tubes using a Griffin melting point apparatus.

NMR spectra were recorded in $CDCl_3$, $CD_3CN$ or $CD_2Cl_2$ on (i) Bruker Avance DPX-400 MHz spectrometer (operating at 400.13 for $^1$H, 100.6 MHz for $^{13}$C); (ii) Bruker AV-400 MHz spectrometer operating at 400.13 MHz for $^1$H, 100.6 MHz for $^{13}$C or (iii) Bruker AV-600 MHz spectrometer (600.13 MHz for $^1$H, 150.6 MHz for $^{13}$C). $^1$H and $^{13}$C NMR spectra were referenced relative to TMS ($\delta$ 0.00 ppm). $^{13}$C NMR spectra were proton decoupled. Chemical shifts ($\delta$) are reported in ppm and coupling constants ($J$) in Hertz.

Photophysical Measurements: All photophysical measurements were carried out with solutions containing in 1 x 1 cm$^2$ quartz cuvettes in HPLC grade solvents. UV-Visible absorption spectra were recorded on a Shimadzu UV-2450 spectrophotometer. Emission and excitation spectra were obtained on a Perkin-Elmer LS55 fluorimeter or on a Horiba-Jobin-Yvon Fluorolog FL-3-11 spectrophotometer with double grating emission amd excitation monochromators. Emission lifetime measurements were performed with an IBH Datastation HUB 5000F using NanoLED pulsed diode laser excitation sources of appropriate wavelength. Appropriate excitation repetition rates were chosen in order to ensure that no re-excitation of the sample occurred until the decay has reached the baseline. TAC (time to amplitude convertor) ranges were set at approximately twenty times the expected average decay time, and were less than the reciprocal of the source repetition rate. To prevent pile-up, the start-stop ratio ($\alpha$) was maintained at less than 2%. If the repetition rates required were > 100 kHz, the experiments were carried out in reverse mode. Data was fit using monoexponential decays where possible, while attempting to maintain a $\chi^2$ statistic of ~ 1, a Durbin-Watson statistic of ~ 2, a random spread of residuals with approximately 60 % of residuals within one standard deviation

of the fitted parameter, and over 99 % of the residuals within 3 standard deviations. When these parameters could not be satisfied (particularly where non-random behaviour was observed in the residuals plot), biexponential fits were obtained instead. The same criteria as above were applied to these residuals/fits. For shorter lifetimes (in the nanosecond range), the instrument response factor (IRF) was estimated through running a scattering solution with the detector set to the excitation wavelength. When reconvolution failed, this IRF estimate was used to aid analysis through tail fitting. The solvents and compounds used in this study were of spectroscopic grade. The optical density of the solutions at the excitation wavelength was less 0.15 when recorded in a 1 cm pathlength cuvette. Low temperature measurements were carried out in a thin tube in a quartz Dewar filled with liquid nitrogen.

Upconversion: TTA upconversion and upconversion was carried out in the University of Dalian, by the group of Prof Jianzhang Zhao. The upconversion was carried out with two continuous wave diode-pumped solid-state lasers (DPSSLs) with outputs at 473 and 532 nm, respectively (the power was tunable in the range of 0–200 mW). A reflecting lens was used to direct the laser beam into the sample cell so that the laser beam was not directed toward the detector window of the fluorospectrometer. A small black box was used to trap the laser beam behind the sample cell to suppress the scattered laser; thus, no notch filter was necessary. All the solutions were purged with Ar for 30 min before the measurements were taken. The typical laser power was 5 mW (the diameter of the laser spot was 3 mm; thus, the power density of the laser was about 71 $mWcm^{-2}$). Nanosecond time-resolved transient difference absorption spectra were recorded on a LP 920 laser flash photolysis spectrometer (Edinburgh Instruments, Livingston, UK). The samples were purged with nitrogen or argon for 30 minutes before any measurements were taken. The samples were excited with a 355 nm laser and the transient signals were recorded on a Tektronix TDS 3012B oscilloscope

TDDFT computational methods: Geometry optimizations were calculated by using the B3LYP functional with the 6–31G(d)/LanL2DZ basis set. The vertical excitation energy was calculated with the TDDFT method based on the singlet ground-state geometry. The spin-density of the triplet excited state was calculated with their energy-minimized triplet geometries. The solvents were used in the calculations (CPCM model). All calculations

were performed with the Gaussian 09W software (Gaussian Inc.). All computational measurements were carried out by Prof Jianzhang Zhao research group.

Crystal and structural experimental data are summarised in Table 1 in the Annex. Selected bond lengths and angles are given in the discussion. The single crystal analyses was performed by Dr. Longsheng Wang in Trinity College with a Bruker SMART APEX CCD diffractometer (compound **18**) using graphite monochromated $M_o$-$K_\alpha$ ($\lambda$ = 0.71073 Å) at the temperature given in the table. Intensities were corrected for Lorentz and polarisation effects and for absorption by SADABS. Space group were determined from systematic absences and checked for higher symmetry. The structure was solved by direct methods using SHELXS and refined on $F^2$ using all data by full-matrix least-squares procedures with SHELX-97. All non-hydrogen atoms were refined with anisotropic displacement parameters. Hydrogen atoms were included in calculated positions with isotropic displacement parameters 1.3 times the isotropic equivalent of their carrier carbons. Absolute structure determination was based on the Flack parameter. The functions minimised were $\Sigma w(F_o^2\text{-}F_c^2)$, with $w=[\sigma^2(F_o^2) + (aP)^2 + bP]^{-1}$, where P = $=[\max(F_o^2) + 2(F_c^2]/3$. In all cases, final Fourier synthesis showed no significant residual electron density in chemically sensible positions.

## 5.2 Experimental Procedure

### 1-ethynylnaphthalene (1)

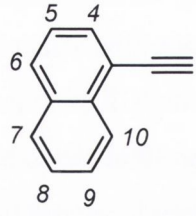


1-bromonaphthalene (1.5 g, 7.25 mmol) was added to pre-dried DMF: $NHEt_2$ (2:5, 15 mL) in a microwave vessel. $Pd(PPh_3)_2Cl_2$ (304 mg, 0.435 mmol) and CuI (82.7 mg, 0.435 mmol) were added, and the solution was bubbled with argon for 15 minutes. 1-ethynyltrimethylsilane (748 mg, 7.61 mmol) was added *via* syringe, and the vessel was rapidly sealed. The reaction mixture was irradiated at 125 °C for 20 mins, allowed to cool and acidified with a 2 M solution of HCl (~30 mL). The crude product was extracted into $CH_2Cl_2$, dried over $MgSO_4$ and the solvents removed under reduced pressure. The protected product was purified by silica column chromatography elueting

with hexane to give a yellow oil. The oil was deprotected overnight in THF: MEOH (1:1, v/v, 20 mL), stirring at room temperature. The solvents were removed *in vacuo*. The residue was dissolved in $CH_2Cl_2$, and washed with a 2 M solution of HCl (15 mL) and water. The organic layers were combined, dried over $MgSO_4$, and the solvent reduced to give the product as a light yellow oil. **Yield**: (650 mg, 4.27 mmol, 59%).

**$^1$H HMR** (400.1 MHz, $CDCl_3$) δ (ppm):8.37 (d, $^3J_{HH}$ = 8.3 Hz, 2H, H), 7.84 (d, $^3J_{HH}$ = 8.0 Hz, 2H, H) ,7.74 (d, $^3J_{HH}$ = 7.1 Hz, 2H, H), 7.51 (t, $^3J_{HH}$ = 7.3 Hz, 2H, H), 7.40 (t, $^3J_{HH}$ = 8.1 Hz, 2H, H).

**ESI-MS** ($CH_2Cl_2$, m/z): [M] calculated for [$C_{12}H_8$]: 152.0626. Found 152.0629

**3,8-bis[2-(4-*tert*-butylphenyl)ethynyl]-1,10-phenanthroline (2)**

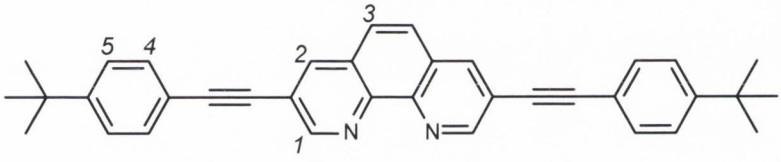


3,8-dibromo-1,10-phenanthroline (300 mg, 0.893 mmol) was dissolved in predried THF: $^i$Pr$_2$NH (3:1, 30 mL), $Pd(PPh_3)_4$ (124 mg, 12 mol%) was added to the Schlenk, and the solution was degassed by the freeze-pump thaw method three times. The mixture was heated to 70 °C, and allowed to stir for 15 mins. 4-*tert*-butylphenyl acetylene (0.327 mL, 1.81 mmol) was added slowly dropwise, and the reaction mixture was left to stir overnight at 70 °C, under argon. The volume of the solvent was reduced *in vacuo*, the residue was redissolved in $CH_2Cl_2$ (~100 mL), washed with a solution of HCl (2 M, ~50 mL), and washed with water. The organic layers were combined and dried over $MgSO_4$. The solvent was removed, and the product purified by column chromatography on silica eluting with diethyl ether. The product was obtained as a pale yellow solid. **Yield**: (247 mg, 0.498 mmol; 55.8%).

**$^1$H NMR** (400.1 MHz, $CDCl_3$) δ (ppm):9.24 (d, $J$ = 1.84 Hz, 2H, $H^1$), 8.38 (d, $J$ = 1.88 Hz, 2H, $H^2$), 7.83 (s, 2H, $H^3$), 7.6 (d, $J$ = 8.36 Hz, 4H, $H^4$), 7.46 (d, $J$ = 8.28 Hz, 2H, $H^5$), 1.35 (s, 18H, ($CH_3$)$_3$).

**$^{13}$C NMR** (100 MHz, $CDCl_3$) δ (ppm): 153.1 (2C, $C_1$), 138.0, (2C, $C_{quat}$), 134.6 (2C, $C_{quat}$) 131.8 (2C, $C_4$), 131.5 (2C, $C_2$),129.3 (2C, $C_{quat}$), 127.0 (2C, $C_3$),126.4 (2C, $C_{quat}$)

125.58 (2C, $C_5$), 119.3 (2C, $C_{quat}$), 94.7 (2C, $C_{quat}$, C≡C), 91.2 (2C, $C_{quat}$, C≡C), 34.8 (2C, $C(CH_3)_3$), 30.8 (18 C,$(CH_3)_3$).

**IR** (vbar/ $cm^{-1}$) 3137 (m, C≡*C-H*) 2959 (C-H alkane), 2212 (C≡C), 1505, 1422, 1462, 1362, 1203, 1104, 1017, 905 (C-H aromatic), 834, 799, 730 and 703.

**HRMS** (THF): calculated for $C_{36}H_{33}N_2$. $[MH]^+$ m/z : 493.2644, found : 493.2653

**CHN**: Calculated for $C_{36}H_{33}N_2$ $0.5CH_2Cl_2$: C: 81.8, H: 6.5, N: 5.16. Found C: 82.05, H: 6.9, N: 5.69

**m.p.** 241-244 °C.

**3,8-bis[2-(1-naphthyl)ethynyl]-1,10-phenanthroline (3)**

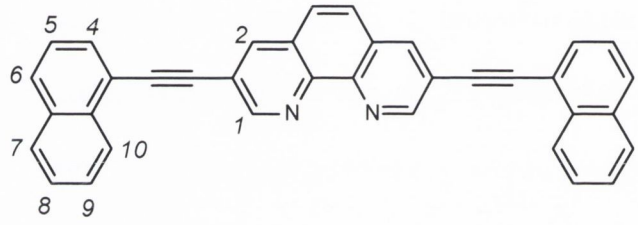


3,8-dibromo-1,10-phenanthroline (250 mg, 0.746 mmol) and $Pd(PPh_3)_4$ (103.4 mg, 0.09 mmol) were dissolved in distilled THF: $^iPrNH_2$ (3:1, v/v, ~45 mL) and heated to 70 °C under argon. 1-ethynylnaphthalene (232.5 mg, 1.53 mmol) was added dropwise *via* syringe, and the reaction was left overnight stirring at 70 °C. The reaction was allowed to cool to room temperature, and excess solvents were removed under pressure. The crude mixture was acidified with HCl (2 M, ~40 mL), and extracted into diethyl ether. The organic layers were combined, washed with water and dried with $MgSO_4$. The solvents were removed *in vacuo*, and the residue was purified by silica column chromatography, eluting with $CH_2Cl_2$: hexane, 1:1. The product was isolated as a yellow/orange solid

**Yield**: (172 mg, 0.498 mmol; 48 %).

**$^1$H NMR** (400.1 MHz, $CDCl_3$) δ (ppm): 9.28 (d, $J$ = 1.84 Hz, 2H, $H^1$), 8.32 (d, $J$ = 1.88 Hz, 2H, $H^2$), 8.2 (d, $J$ = 8.1 Hz, 2H, $H^{10}$), 7.98 (d, $J$ = 8.1 Hz, 2H, $H^7$), 7.94 (d, $J$ = 8.1 Hz, 2H, $H^6$) 7.89 (d, $J$ = 7.1 Hz, 2H, H) 7.46 (t, $J$ = 2.3 Hz, 2H, $H^5$), 7.51 (t, $J$ = 7.3 Hz, 2H, H), 7.40 (t, $J$ = 8.1 Hz, 2H, H).

**$^{13}$C NMR** (100 MHz, $CDCl_3$) δ (ppm): 207.3 (2C, $C_{quat}$,), 153.4 (2C, $C_1$), 144.3 (2C, $C_{quat}$) 138.1 (2C, $C_{quat}$) 133.2 (2C, $C_{quat}$) 131.1 (2C, $C_4$), 131.5 (2C, $C_2$), 128.7 (2C, $C_{quat}$), 128.3 (2C, $C_{10}$), 128.0 (2C, $C_6$), 127.9 (2C, $C_7$) 127.2 (2C, $C_3$), 126.3 (2C, $C_9$) 126.1 (2C, $C_8$), 125.9 (2C, $C_5$), 125.58 (2C, $C_{quat}$), 94.7 ($C_{quat}$, C≡C), 91.3 ($C_{quat}$, C≡C).

**IR** (vbar/ $cm^{-1}$) 3149 (m, C≡*C-H*), 2952 (C-H alkane), 2210 (C≡C), 1495, 1462, 1420, 1362, 1221, 1017, 1109, 905 (C-H aromatic), 834, 792, 731 and 707.

**HRMS** (THF): calculated for $C_{36}H_{23}N_2$: $[MH]^+$ m/z: 482.1699, found: 482.1697.

**CHN**: Calculated for $C_{36}H_{22}N_2$; C:89.98, H 4.19 N: 5.83 Found: C: 89.91, H: 4.42; N: 5.67.

**m.p.** 261-265 °C

**Cu(I) 3,8-bis[2-(4-*tert*-butylphenyl)ethynyl]-1,10-phenanthroline (4)**

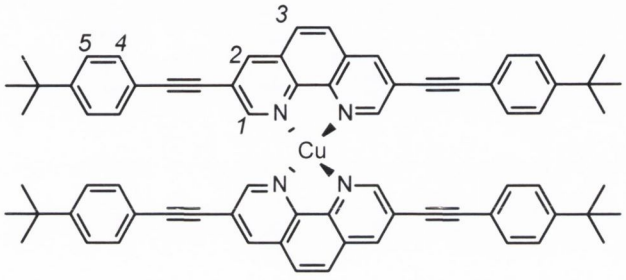


3,8-di-bromo-1,10-phenanthroline (82 mg, 0.167 mmol) was dissolved in $CH_2Cl_2$ (~8 mL) and $[Cu(MeCN)_4]PF_6$ (31 mg, 0.083 mmol) was added. The reaction was stirred under argon for two hours. The solvent was reduced *in vacuo*, and cold hexane (~2 mL) was added dropwise. The precipitate was filtered, washed with diethyl ether and dried to give a yellow/orange solid. **Yield**: (48.3 mg, 0.046 mmol, 55.8%).

**$^1$H NMR** (600.1 MHz, $CDCl_3$,) δ (ppm): 8.95 (d, $J$ = 1.2 Hz, 4H, $H^2$), 8.67 (d, $J$ = 1.2 Hz, 4H,$H^1$), 8.05 (s,4H, $H^3$), 7.7 (d, $J$ = 8.36 Hz, 4H, $H^4$), 7.53 (d, $J$ = 8.28 Hz, 4H, $H^5$), 1.38 (s, 36H, ($CH_3$)$_3$).

**$^{13}$C NMR** (151 MHz,$CDCl_3$) δ (ppm): 153.8 (4C,$C_1$), 131.2 (8C,$C_4$), 130.9 (4C,$C_2$), 126.2 (4C,$C_3$), 125.1 (8C,$C_5$), 119.3 (4C,$C_{quat}$), 94.1 (4C,$C_{quat}$, C≡C), 91.8 (4C,$C_{quat}$, C≡C), 35.1 (4C,$C_{quat}$, $C(CH_3)_3$), 32.8 (12 C,($CH_3$)$_3$)

**IR** (vbar/ $cm^{-1}$) 2963 (C-H alkane), 2209 (C≡C), 1595, 1434, 1365, 1296, 1147, 1104, 906, 834 (C-H aromatic), 799, 714, 703, 678.5.

**HRMS** ($CH_2Cl_2$) (m/z): $[M-PF_6]^+$ ($C_{72}H_{64}CuN_4$): Calc. 1047.4425, Found 1047.4419.

**CHN**: Calculated for $C_{72}H_{64}CuN_4$: C: 82.13 H: 6.51 N: 5.32 Found C: 81.69 H: 6.8 N: 5.45

**3,8-bis(2-pyren-1-ylethynyl)-1,10-phenanthroline (5)**

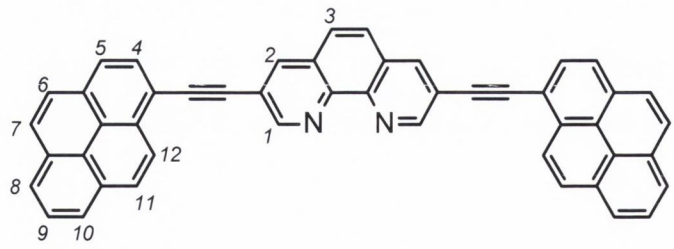


3,8-dibromo-1,10-phenanthroline (150 mg, 0.448 mmol) was dissolved in a mixture of dry DMF: $NHEt_2$ (5:2, ~15 mL) in a microwave vessel and $Pd(PPh_3)_4$ (62 mg, 0.053 mmol)was added. The solution was bubbled with argon for 5 minutes, before being sealed and irradiated with microwave heating for 3 minutes at 75 °C. The solution was cooled to 60 °C, 1-ethynylpyrene (207.6 mg, 0.92 mmol) was quickly added and the vessel resealed. The mixture was irradiated for a further 20 minutes at 125 °C, allowed to cool and acidified with a solution of HCl (2 M, ~30 mL). The crude product was extract into $CH_2Cl_2$, washed with water and dried over $MgSO_4$. The solvents were removed under pressure and the residue was purified by silica column chromatography, eluting with $CH_2Cl_2$: hexane (1:1). The product was isolated as an orange solid. **Yield**: (90.2 mg, 0.143 mmol, 32%)

**$^1$H NMR** (600.1 MHz, $CDCl_3$) δ (ppm): 9.4 (d, $J$ = 1.2 Hz, 2H, $H^1$), 8.62 (d, $J$ = 12 Hz, 2H, $H^{12}$), 8.45 (d, $J$ = 1.2 Hz, 2H, $H^2$), 8.25-8.15 (m, 6H, $H^{6,7,11}$), 8.07 (d, $J$ = 8.28 Hz, 2H, $H^5$), 8.07 (d, $J$ = 8.28 Hz, 2H, $H^4$), 8.02-7.9 (m, 6H, $H^{8,9,10}$).

**$^{13}$C NMR** (151.1 MHz, $CDCl_3$) δ (ppm): 151.7 (2C, $C_1$), 138.4 (2C, $C_2$), 132.5 (2C, $C_{quat}$), 131.6 (2C, $C_{quat\ pyr}$), 131.14 (2C, $C_{quat\ pyr}$), 130.4 (2C, $C_{pyr}$) , 129.5 (2C, $C_{pyr}$), 128.8 (2C, $C_{pyr}$),127.3 (2C, $C_{pyr}$), 126.3 (2C, $C_{pyr}$), 126.2 ($C_3$), 125.8 (2C, $C_{pyr}$), 125.7 (2C, $C_{pyr}$), 125.6 (2C, $C_{pyr}$), 124.5 (2C, $C_{pyr}$), 124.2 (2C, $C_{quat\ pyr}$), 116.6 (2C, $C_{quat\ pyr}$), 93.7 ($C_{quat}$, C≡C), 87.5 ($C_{quat}$, C≡C),

**IR** (νbar/ $cm^{-1}$) 2963 (C-H alkane), 2198 (C≡C), 1598, 1581, 1462, 1433, 1391, 1217, 1186,, 1142, 1095,970, 908, 841 (C-H aromatic), 819, 757, 714, 727, 678.

**HRMS** ($CH_2Cl_2$) (m/z): $[C_{48}H_{24}N_2+H]^+$ Calc. 629.2012; Found 629.2015.

**CHN**: Calculated for $C_{48}H_{24}N_2$ C: 91.7, H: 3.85 N: 4.46; Found C: 90.9 H: 4.68. N: 4.42

**m.p.**: 271-274 ° C

**3,8-bis[2-[4-[2,3,4,5,6-pentakis(4-*tert*-butylphenyl)phenyl]phenyl]ethynyl]-1,10-phenanthroline (6)**

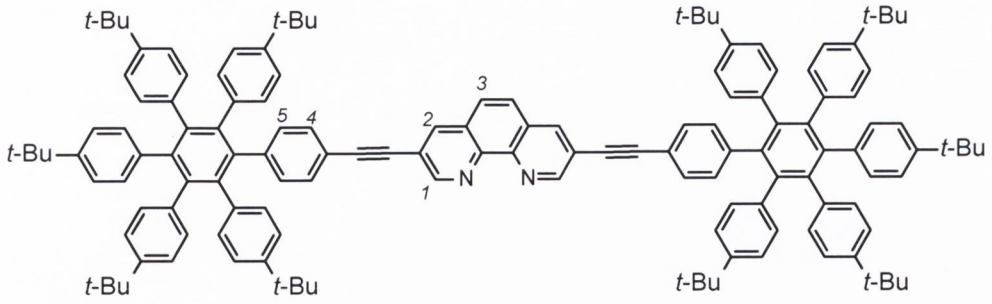


3,8-dibromo-1,10-phenanthroline (25 mg, 0.075 mmol) was added to THF:$NHEt_2$ (3:1, ~15 mL) and bubbled with argon for 15 minutes. $Pd(PPh_3)_4$ (10.3 mg, 0.01 mmol) was added and the solution was heated to 90 °C. 1,2,3,4,5-pentakis(4-tert-butylphenyl)-6-(4-ethynylphenyl)benzene (129 mg, 0.153 mmol) was dissolved in THF (~8 mL) ,bubbled with argon for 10 mins, and transferred *via* cannula dropwise to the 3,8-dibromo-1,10-phenanthroline solution. The reaction was stirred at 90 °C for three days under argon. The solution was cooled, the solvents removed *in vacuo*, and the residue was washed with a solution of HCl (2 M, ~15 mL). The crude product was extracted into $CH_2Cl_2$, washed with water, and dried over $MgSO_4$. The product was purified by silica column chromatography, eluting with $CH_2Cl_2$: hexane (2:1) and isolated as a pale brown solid. **Yield** :(65 mg, 0.035 mmol, 46 %).

**$^1$H NMR** (400.1 MHz, $CDCl_3$) δ (ppm): 9.0 (d, $J$ = 1.2 Hz, 2H, $H^1$), 8.19(d, $J$ = 1.2 Hz, 2H, $H^2$), 7.7 (d, $J$ = 1.2 Hz, 2H, $H^3$), 6.85 (m, 20H, $H^{Ph}$), 6.75 (d, $J$ = 8.5 Hz, 4H, $H^5$), 6.7-6.6 (m, 20H, $H^{Ph}$), 6.58 (d, $J$ = 8.5 Hz, 4H, $H^4$).

**$^{13}$C NMR** (151 MHz, $CDCl_3$) δ (ppm): 153.7 (2C, $C_1$), 147.1 (2C, $C_{quat}$), 146.2 (2C, $C_{quat}$), 145.9 (2C, $C_{quat}$), 142.2(2C, $C_{quat}$), 140.87 (2C, $C_{quat}$), 140.8 (2C, $C_{quat}$), 138.9 (2C, $C_{quat}$), 138.7 (2C, $C_2$), 137.4 (2C, $C_{quat}$), 132.5 (2C, $C_{quat}$), 131.3 (2C, $C_4$), 127.9 (2C, $C_3$), 123.3 (2C, $C_5$) 93.7 ($C_{quat}$, C≡C), 84.7 ($C_{quat}$, C≡C), 34.4-34.31 (m, $C_{quat}$, $C(CH_3)_3$), 31.2-31.1 (m, 30 C, $C(CH_3)_3$).

**IR** (νbar/ $cm^{-1}$) 3288 (m, C≡*C-H*), 3037, 2961, 2900, 3865, 2125 (C≡C), 1652, 1611, 1562, 1464, 1389, 1563, 1270, 1193, 1152, 1105, 1020, 860, 826, 780, 675.

**HRMS** ($CH_2Cl_2$, m/z): [M] calculated for $[C_{140}H_{144}N_2]$: 1854.1402 Found 1854.1396

**m.p.** > 275 °C (decomp)

**2-[4-(2-ethynyl-5,8,11,14,17-penta-*tert*-butylhexa-*peri*-hexabenzocoronene)buta-1,3-diynyl] -5,8,11,14,17-penta-*tert*-butylhexa-*peri*-hexabenzocoronene (7)**

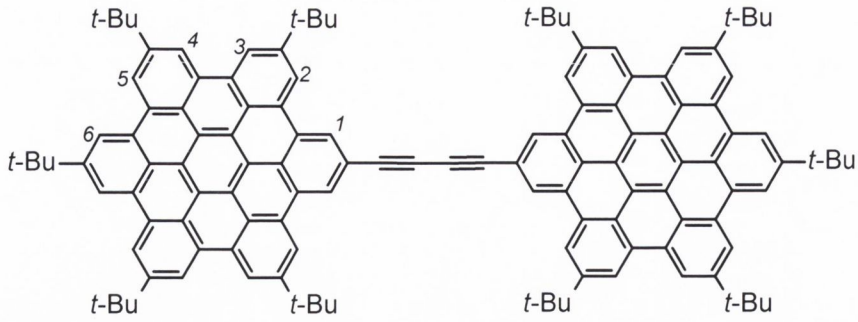


3,8-dibromo-1,10-phenanthroline (20 mg, 0.06 mmol) was added to DMF:$NHEt_2$ (4:1, ~15 mL) and bubbled with argon for 15 minutes. $Pd(PPh_3)_4$ (8.27 mg, 0.01 mmol) was added and the solution was heated to 70 °C. 2-ethynyl-5,8,11,14,17-penta-*tert*-butylhexa-*peri*-hexabenzocoronene (103 mg, 0.123 mmol) was dissolved in DMF (~8 mL) and bubbled with argon for 10 mins, and transferred dropwise to the 3,8-dibromo-1,10-phenanthroline solution. The reaction was left overnight stirring at 70 °C under argon. The solution was cooled, the solvents removed *in vacuo*, and the residue was washed with a solution of HCl (2 M, ~15 mL). The crude product was extracted into $CH_2Cl_2$, washed with water, and dried over $MgSO_4$. The product was isolated by silica column chromatography, eluting with $CH_2Cl_2$: hexane (2:1) as a pale brown solid. **Yield**: (87 mg, 0.0451 mmol, 42%).

**$^1$H NMR** (600 MHz, $CD_2Cl_2$) δ (ppm): 9.19 (s, 4H, $H^6$), 9.10 (s, 4H, $H^5$), 9.07 (s, 4H, $H^4$), 8.95 (s, 4H, $H^3$), 8.73 (s, 4H, $H^2$), 8.68 (s, 4H, $H^1$), 1.94 (s, 18H, $C(CH_3)_3$), 1.89 (s, 36H, $C(CH_3)_3$), 1.81 (s, 36H, $C(CH_3)_3$).

**$^{13}$C NMR** (151 MHz, $CD_2Cl_2$) δ (ppm): 150.7 (2C, $C_{quat}$), 133.9 (2C, $C_{quat}$), 131.9 (2C, $C_{quat}$), 131.6 (2C, $C_{quat}$), 131.7 (2C, $C_{quat}$), 129.9 (2C, $C_{quat}$), 121.15 (2C, $C_1$), 121 (2C, $C_3$), 120.9 (2C, $C_6$), 120.87 (2C, $C_4$), 120.7 (2C, $C_5$), 95.26 ($C_{quat}$, *C*≡*C*), 37.48-37.35 (m, $C_{quat}$, $C(CH_3)_3$), 33.6-33.4 (m, 30 C, $C(CH_3)_3$),

**IR**(νbar/ $cm^{-1}$) 3289 (m, C≡*C*-*H*), 3036, 2961, 2904, 2865, 2107 (C≡C), 1741, 1611, 1576, 1511, 1476, 1459, 1393, 1361, 1267, 1270, 1201, 1147, 1118, 1105, 1020 (s, br), 944, 865, 831, 780, 745, 672.

**HRMS** (m/z, $CH_2Cl_2$): [M] calculated for [$C_{140}H_{144}N_2$]: 1684.9546 Found 1684.9529

**m.p.** > 280 °C

**[Ru(bipy)$_2$ (3,8-bis[2-(4-*tert*-butylphenyl)ethynyl]-1,10-phenanthroline)](PF$_6$)$_2$ (8)**

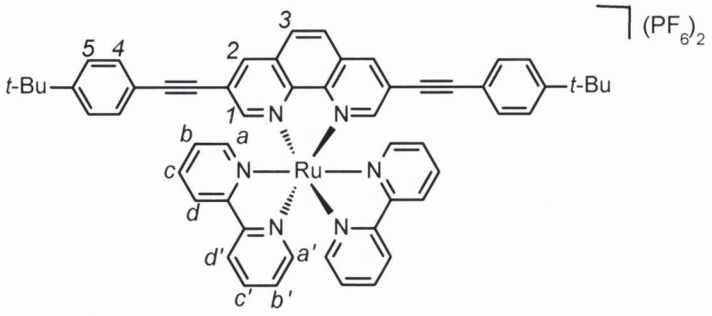


Ru(bipy)$_2$(3,8-dibromo-1,10-phenanthroline) $PF_6$ (75 mg, 0.089 mmol), CuI (2.1 mg, 12 mol%) and $Pd(PPh_3)_2Cl_2$ (7.4 mg, 12 mol%) were dissolved in dry degassed THF (8 mL). $^{i}Pr_2NH$ (4 mL) was added *via* cannula and the solution was allowed to stir for 5 minutes. *tert*- Butyl phenyl acetylene (27.8 mg, 0.176 mmol) was added dropwise and the resulting solution was left to stir overnight at room temperature. The solution was acidified with a solution of 2M HCl.(~15 mL), extracted into $CH_2Cl_2$, and washed with water. The organic layers were combined and dried over $MgSO_4$. The solvent was removed in *vacuo* and the complex was purified by silica column chromatography using $CH_3CN$:$KNO_3$:$H_2O$ (10:1:1.5, v/v) as solvent. The organic fractions were combined, washed with water and dried over $MgSO_4$.The solvent was removed, the residue was dissolved in acetone, and ethylene glycol was added (~3 mL). A saturated solution of $KPF_6$ was added dropwise until a precipitate was observed. The pure complex was isolated by filtration, and washed with diethyl ether (~20 mL) to give red crystalline solid. **Yield** (83 mg, 0.069 mmol, 78 %).

**$^1$H NMR** (600 MHz, $CD_3CN$) ), δ(ppm): 8.74 (d, *J*= 1.2 Hz, 2H, $H^2$), 8.57 (d, *J*= 12 Hz, 2H, $H^{d'}$) 8.54 (d, *J*= 12 Hz, 2H, $H^d$), 8.28 (s, 2H, $H^3$) 8.19 (d, *J*= 1.2 Hz, 2H, $H^1$) 8.05 (t, *J*= 6 Hz, 2H, $H^{c'}$), 8.12 (t, *J*= 6 Hz, 2H, $H^c$) 7.85 (d, *J*= 8 Hz, 2H, $H^{a'}$), 7.66 (d, *J*= 8 Hz, 2H, $H^a$). 7.5 (m, 10H, $H^{4/5b''}$) 7.29 (t, *J*= 6 Hz, 2H, $H^b$)

**$^{13}$C NMR** (151 MHz,$CD_3CN$), δ (ppm): 157.2 (2C, $C_{quat\ bpy}$) 156.9 (2C, $C_{quat\ bpy}$), 154.5 (2C, $C_1$), 153.5 (2C, $C_{phen\ quat}$), 152.4 (2C, $C_{a/a'}$), 152.3 (2C, $C_{a/a'}$), 146.0 (2C, $C_{quat\ phen}$), 138.6 (2C, $C_2$), 138.6 (2C, $C_{c/c'}$), 138.5 (2C, $C_{c/c'}$), 132.3 (4C, $C_4$), 130.9 (2C,$C_{quat}$), 128.5 (2C, $C_3$), 127.4 (2C, $C_{b/b'}$),127.3 (2C, $C_{b/b'}$), 125.8 (4C,$C_5$), 124.3(2C, $C_{d/d'}$),124.2 (2C, $C_{d/d'}$) 93.9 (2C, C≡C), 85.9 (2C, C≡C), 34.2 (2C, $C(CH_3)_3$).30.4 (2C, $C(CH_3)_3$).

**IR**(vbar/ $cm^{-1}$): 2961 (C-H stretching), 2210 (C≡C), 1737, 1582 1511, 1466 (C-C aromatic ring), 1445, 1436, 1421, 1368, 1268 (C-H rocking phen), 1105, 1016, 1016, 832 (C-H aromatic), 766, 732, and 720 .

**HRMS** (m/z, $CH_2CN$), calculated for $C_{56}H_{48}F_6N_6PRu$ $[M+PF_6]^+$: 1051.2623 Found: 1051.2626

**CHN**: Calculated for $C_{56}H_{48}F_{12}RuN_6P_2$: calculated: C: 56.24 H: 4.05; N: 7.03; found; C 55.38 H 3.52 N 6.89

**[Ru(bipy)$_2$ (3,8-bis[2-(1-naphthyl)ethynyl]-1,10-phenanthroline)](PF$_6$)$_2$ (9)**

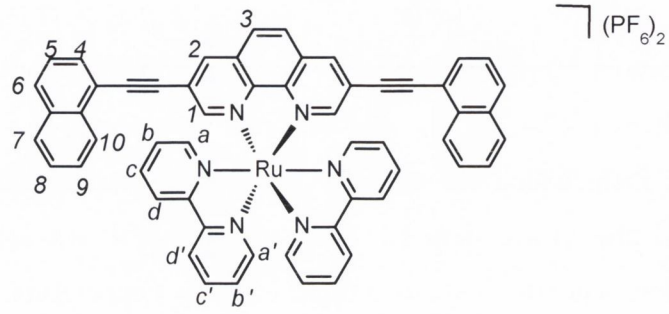


Ru(bipy)$_2$(3,8-dibromo-1,10-phenanthroline) $PF_6$ (78 mg, 0.087 mmol), CuI (3 mg, 12 mol%) and $Pd(PPh_3)_2Cl_2$ (5 mg, 12 mol%) were dissolved in dry degassed DMF (8 mL). $^iPr_2NH$ (4 mL) was added *via* cannula and the solution was allowed to stir for 5 minutes. 1-ethynyl-naphthalene (27 mg, 0.178 mmol) was added dropwise and the resulting solution was left to stir overnight at room temperature. The solution was acidified with a solution of 2M HCl.(~15 mL), extracted into $CH_2Cl_2$, and washed with water. The organic layers were combined and dried over $MgSO_4$. The solvent was removed in *vacuo* and the complex was purified by silica column chromatography using $CH_3CN$:$KNO_3$:$H_2O$ (10:1:1.5, v/v) as solvent. The organic fractions were combined, washed with water and dried over $MgSO_4$.The solvent was removed, the residue was dissolved in acetone, and ethylene glycol was added (~3 mL). A saturated solution of $KPF_6$ was added dropwise until a precipitate was observed. The pure complex was isolated by filtration, and washed with diethyl ether (~20 mL) to give red crystalline solid. **Yield**: (71 mg, 0.060 mmol, 69 %)

**$^1$H NMR** (600 MHz, $CD_3CN$) δ(ppm): 8.98 (d, *J*= 1.2 Hz, 2H, $H^2$), 8.58 (d, *J*= 12 Hz, 2H, $H^{d'}$) 8.55 (d, *J*= 12 Hz, 2H, $H^d$), 8.35 (d, *J*= 12 Hz, 2H, $H^{10}$), 8.29 (d, *J*= 1.2 Hz, 2H, $H^1$) , 8.27 (t, *J*= 6 Hz, 2H, $H^{c'}$), 8.1-8.09 (m, 4H, $H^{3/7/c}$), 7.9 (d, *J*= 8 Hz, 2H $H^a$), 7.83 (d, *J*= 12Hz, 2H, $H^4$), 7.71 (d, *J*= 8.5 Hz, 2H, $H^{a''}$),7.7-7.6 (m, 6H, $H^{6/8/9}$), 7.58 (t, *J*= 8 Hz, 2H, $H^5$), 7.32 (t, *J*= 6 Hz, 2H, $H^6$.

**$^{13}$C NMR** (151 MHz,$CD_3CN$) δ (ppm): 157.2 (2C, $C_{quat\ bpy}$) 156.9 (2C, $C_{quat\ bpy}$), 154.3 (2C, $C_1$), 153.2 (2C, $C_{a/a'}$), 153.1 (2C, $C_{a/a'}$), 146.0 (2C, $C_{quat\ phen}$), 138.7 (2C, $C_2$), 138.6

(2C, $C_{c/c'}$), 138.5 (2C, $C_{c/c'}$),132.7 (2C,$C_{quat\ naph}$), 132.5 (2C,$C_{quat\ naph}$), 131.4 (2C,$C_{quat}$), 131.2 (2C,$C_{quat}$), 130.8 (2C,$C_{4/6/7}$), 130.6 (2C, $C_{4/6/7}$), 130.3 $C_{4/6/7}$) 129.8 (2C, $C_3$), 129.7 (2C, $C_{10}$), 127.4 (2C, $C_{b/b'}$),127.3 (2C, $C_{b/b'}$), 127.0 (2C,$C_5$), 125.2 (2C, $C_{8/9}$), 125.1 (2C, $C_{8/9}$), 124.2 (2C, $C_{d/d'}$),124.1 (2C, $C_{d/d'}$) 93.7 (2C, C≡C), 89.2 (2C, C≡C).

**IR**(νbar/ $cm^{-1}$): 2961 (C-H stretching), 2202 (C≡C), 1736, 1587 1509, 1468 (C-C aromatic ring), 1445, 1435, 1421, 1368, 1275 (C-H rocking phen), 1105, 1016, 1016, 831 (C-H 'oop' aromatic), 766, 732, and 718 .

**HRMS** (m/z, $CH_2CN$), calculated for $C_{56}H_{36}F_6N_6PRu$ $[M+PF_6]^+$: 1039.1493 Found: 1039.1512.

**CHN**: Calculated for $C_{56}H_{36}F_{12}RuN_6P_2$: calculated: C: 56.81.78; H: 3.06; N: 7.10; found; C 54.93 H 3.63 N 7.02.

**[Ru(bipy)$_2$ (3,8-bis[2-(1-pyrenyl)ethynyl]-1,10-phenanthroline)](PF$_6$)$_2$ (10)**

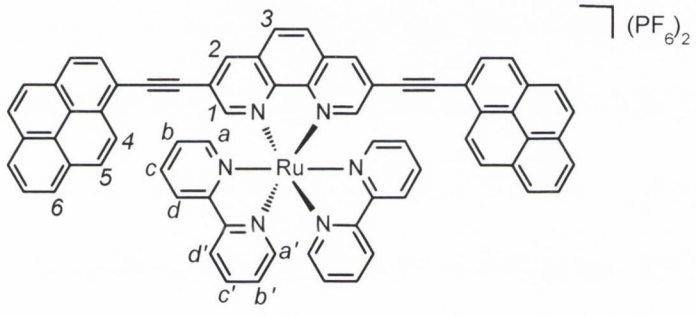


Ru(bipy)$_2$(3,8-dibromo-1,10-phenanthroline) $PF_6$ (51 mg, 0.067 mmol), CuI (3 mg, 12 mol%) and $Pd(PPh_3)_2Cl_2$ (6 mg, 12 mol%) were dissolved in dry degassed DMF (8 mL). $^iPr_2NH$ (4 mL) was added *via* cannula and the solution was allowed to stir for 5 minutes. 1-ethynyl-pyrene (43.6 mg, 0.164 mmol) was dissolved in still-dried degassed DMF and added *via* syringe, and the resulting solution was left to stir overnight at 70 $^{o}$ C under argon. The solution was acidified with a solution of 2 M HCl.(~15 mL), and filtered to isolate the crude solid. The crude solid was dissolved in $CH_2Cl_2$, washed with water and the organic layers combined and dried over $MgSO_4$. The solvent was removed in *vacuo* and the complex was purified by silica column chromatography using $CH_3CN$:$KNO_3$:$H_2O$ (10:1:1.5, v/v) as solvent. The organic layer was combined, dried over $MgSO_4$, and solvents removed *in vacuo*. The residue was dissolved in acetone, and ethylene glycol was added (~3 mL). A saturated solution of $KPF_6$ was added dropwise until a precipitate was observed. The pure complex was isolated by filtration, and washed with diethyl ether (~15 mL) to give a dark red crystalline solid. **Yield**: (51 mg, 0.038 mmol, 57%)

**$^1$H NMR** (600 MHz, $CD_3CN$) ) δ(ppm): 8.96 (d, *J*= 1.2 Hz, 2H, $H^2$), 8.65 (d, *J*= 12 Hz, 2H, $H^{d'}$) 8.57 (d, *J*= 12 Hz, 2H, $H^d$), 8.45 (d, *J*= 12 Hz, 2H, $H^4$) 8.39 (m, 8H, $H^{1/3/5/pyr}$), 8.31 (m, 6H, $H^{pyr}$) 8.26-8.18 (m, 8H, $H^{c'/6/pyr}$), 8.1 (t, *J* = 8 Hz, $H^{c'}$), 7.97 (d, *J*= 8 Hz, 2H $H^{a'}$), 7.8 (d, *J*= 8Hz, 2H, $H^a$). 7.59 (t, *J*= 4 Hz, 2H, $H^{b'}$) 7.36 (t, *J*= 4 Hz, 2H, $H^b$).

**$^{13}$C NMR** (151 MHz,$CD_3CN$) δ (ppm): 162.2 (2C, $C_{quat\ bpy}$), 162.0 (2C, $C_{quat\ bpy}$), 155.2 (2C, $C_1$), 153.2 (2C, $C_{a/a'}$), 153.1 (2C, $C_{a/a'}$), 148.8 (2C, $C_{quat\ phen}$), 139.3 (2C, $C_2$), 138.6 (2C, $C_{c/c'}$), 138.5 (2C, $C_{c/c'}$), 132.7 (2C,$C_{quat}$), 132.5 (2C,$C_{quat}$), 131.8 (2C,$C_{quat}$), 131.6 (2C,$C_{quat}$), 131.1 (2C,$C_{quat}$), 130.3 (2C, $C_{pyr}$), 129.7 (2C, $C_3$), 126.9 (2C, $C_{b/b'}$), 126.9 (2C, $C_{b/b'}$), 126.6 (2C, $C_{py}$), 126.4 (2C, $C_{pyr}$), 125.9 (2C, 2C, $C_6$), 125.4 (2C,$C_5$), 125.2 (2C, $C_{d/d'}$), 125.1 (2C, $C_{d/d'}$), 123.2 (2C, $C_{quat}$) 96.1 (2C, C≡C), 91.3 (2C, C≡C).

**IR**(νbar/ $cm^{-1}$): 3049 (m, C≡*C-H*), 2961, 2866 (C-H stretching), 2210 (C≡C), 1736, 1587 1506, 1465 (C-C aromatic ring), 1448, 1421, 1365, 1268 (C-H rocking phen), 1105, 1016, 1016, 831 (C-H aromatic), 766, 732, and 718 .

**HRMS** (m/z, $CH_2CN$), calculated for $C_{71}H_{52}F_6N_6PRu$ $[M+PF_6]^+$: 1190.1436 Found: 1190.1434

**CHN**: Calculated for $C_{71}H_{52}F_{12}RuN_6P_2$: calculated: C: 61.78; H: 3.8; N: 6.09; found; C 60.93 H 3.64 N 5.97

**[Ru(bipy)$_2$(3,8-bis[2-ethynyl-5,6,11,14,17-penta-*tert*-butylhexa-*peri*-hexabenzocoronene]-1,10-phenanthroline)](PF$_6$)$_2$ (11)**

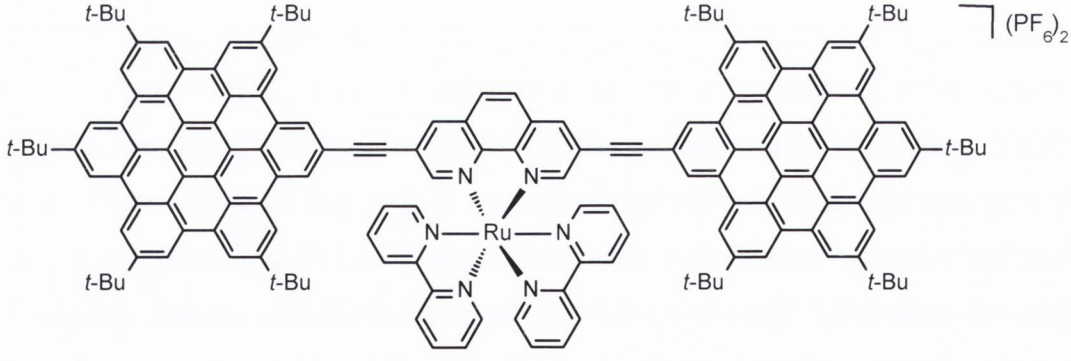


$Ru(bipy)_2$ (3,8-dibromo-1,10-phenanthroline) $PF_6$ (40 mg, 0.045 mmol), $Pd(PPh_3)_2Cl_2$ (5 mg, 12 mol%) and CuI (3mg, 12 mol%) were dissolved in still-dried degassed DMF (8 mL). $^iPr_2NH$ (3 mL, still dried and degassed) was added *via* cannula and the solution was allowed to stir for 30 minutes. 1-ethynyl-HBC (73 mg, 0.090 mmol) was dissolved in still-dried degassed DMF and added dropwise *via* syringe. The resulting solution was left to stir overnight at room temperature under argon. The solution was acidified with 5% HCl (~25 mL), and taken up in $CH_2Cl_2$. The organic layer was washed with water (x

3) and dried over $MgSO_4$. The solvent was removed *in vacuo*, and the crude residue was washed with $CHCl_3$ to remove any unreacted ligand or catalyst. The residue was dissolved in acetone (~2 mL),and ethylene glycol (~3 mL) was added. The acetone was evaporated and a saturated solution of $KPF_6$ was added dropwise to give a red precipitate. The precipitate was filtered, and washed with diethyl ether. The product was isolated as a dark red/black crystalline solid. **Yield**: (69 mg, 0.028 mmol, 65%)

**$^1$H NMR** (600 MHz, $CD_2Cl_2$) δ(ppm): 9.4-9.1 (m, 34H), 7.7 (m, 2H, $H^{bipy}$), 7.6 (m, 2H, $H^{bipy}$), 7.5 (m, 2H, $H^{bipy}$), 1.95 (s, 25H, $C(CH_3)_3$), 1.67 (s, 47H, $C(CH_3)_3$) 1.3 (s, 27H, $C(CH_3)_3$).

**IR** (νbar/ $cm^{-1}$): 3062 (m, C≡*C-H*), 2961, 2866 (C-H stretching), 2204 (C≡C), 1738, 1606, 1583, 1509, 1477 (C-C aromatic ring), 1423, 1391, 1269 (C-H rocking phen), 1217, 1, 1114, 1063, 1016, 907, 867, 838 (C-H aromatic), 772, 755, 730 and 703.

**HRMS** (m/z, $CD_2Cl_2$), calculated for $C_{160}H_{136}F_6N_6PRu$ $[M+PF_6]^+$ 2387.3112 Found: 2387.3127

**[Ir(ppy)$_2$ (3,8-dibromo-1,10-phenanthroline)](PF$_6$) (12)**

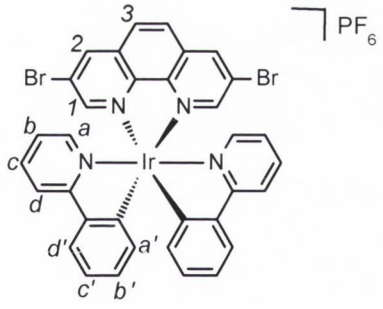


$[Ir(ppy)_2Cl]_2$ (54.3 mg, 0.05 mmol) was dissolved in $CH_2Cl_2$ and heated to 40 °C. 3,8-dibromo-1,10-phenanthroline (50.25 mg, 0.15 mmol) was dissolved in $CH_2Cl_2$: MeOH (1:1, v/v, ~6 mL,) and added slowly. The reaction was left to reflux for 2 hours. The solution was cooled, the solvent was reduced to ~2 mL *in vacuo* and a concentrated solution of $NH_4PF_6$ in MeOH was added dropwise until a precipitate formed. The precipitate was isolated by filtration, washed with cold methanol and diethyl ether and allowed to dry as a pale orange solid. **Yield**: (91 mg, 0.109 mmol, 73 %)

**$^1$H NMR** (600.1 MHz, $CD_3CN$) δ(ppm): 8.92 (d, $J$ = 2.4 Hz, 2H, $H^2$), 8.23 (d, $J$ = 2.4 Hz, 2H, $H^1$) , 8.09 (d, $J$ = 12 Hz, 2H, $H^{d'}$), 7.85 (m, 4H, $H^{c+d'}$), 7.51 (d, $J$ = 12 Hz, 2H,

$H^{a}$), 7.13 (t, $^{3}J_{HH}$ = 12 Hz, 2H, $H^{c'}$),7.01 (t, $J$ = 12 Hz, 2H, $H^{b'}$), 6.92 (t,$J$ = 12 Hz, 2H, $H^{c}$), 6.37 (d, $J$ = 12 Hz, 2H, $H^{a'}$)

**$^{13}$C NMR** (151 MHz, $CD_3CN$) δ(ppm):151.8 (2C, $C_1$), 149.3 (2C, $C_a$), 143.2 ($C_{quat}$), 139.9 (2C, $C_2$), 138.3 (2C, $C_{quat}$), 138.1 (2C, $C_{d'}$), 131.2 (2C, $C_{b'}$), 129.9 (2C,$C_{a'}$), 128.0 (2C, $C_3$),127.2 (2C,$C_{quat}$) 124.5 (2C, $C_b$), 123.0 (2C, $C_c$), 122.5 (2C, $C_{c'}$) 119.1 (2C, $C_d$),117.2 (2C, $C_{quat}$).

**IR** (vbar/ $cm^{-1}$): 3062 (m, C≡*C-H*), 1607, 1583, 1567, 1583 (C-C aromatic ring), 1478, 1438, 1418, 1337, 1216, 1164, 1142 (C-H rocking phen), 1063, 969, 934, 835.3 (C-H aromatic), 784, 734, 669, 602 (C-Br)

**HRMS** (m/z, $CH_3CN$): calculated for $C_{34}H_{22}Br_2IrN_4$ $[M\text{-}PF_6]^+$ 836.9841, found : 836.9845.

**CHN**: Calculated for $C_{34}H_{22}Br_2F_6IrN_4P$ C:41.52, H: 2.25, N: 5.70, Found C: 40.95 H: 1.95. N: 5.70

**[Ir(ppy)$_2$ (3,8-bis[2-(4-*tert*-butylphenyl) ethynyl]-1,10-phenanthroline)](PF$_6$) (13)**

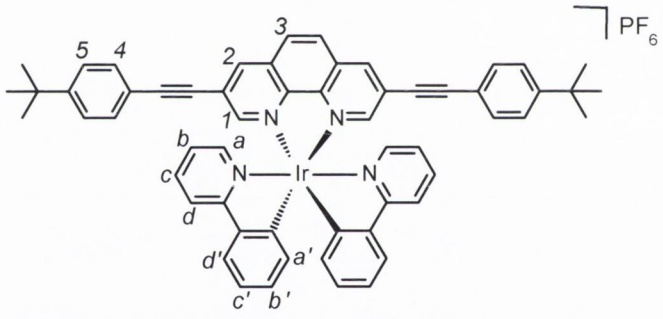


[Ir(ppy)$_2$ (3,8-dibromo-1,10-phenanthroline)](PF$_6$) (61 mg, 0.064 mmol), and Pd(PPh$_3$)$_4$ (4.5 mg, 0.004 mmol) were placed in a 50 mL Schlenk and the flask was purged (x3). Pre-dried THF (10 mL) and $NEt_3$ (2 mL) were degassed by freeze-pump thaw, and transferred *via* cannula to the Schlenk. The solution was left to stir at room temperature for 20 minutes under argon. *tert*-Butyl phenyl acetylene (21 mg, 0.133 mmol) was added dropwise *via* syringe. The reaction mixture was heated to 60 °C and stirred overnight under argon. The solvent level was reduced *in vacuo*. The crude mixture was extracted into $CH_2Cl_2$, washed with water and dried over $MgSO_4$. The impure solid was purified by a silica plug, eluting with $CH_2Cl_2$. The fractions were concentrated and a concentrated solution of ammonium hexafluorophosphate was added (~2 mL). The precipitate was filtered to give an orange solid. **Yield**: (48.8 mg, 0.03 mmol, 67 %).

**$^1$H NMR** (600.1 MHz, $CD_2Cl_2$) δ(ppm): 8.91 (d, $J$ = 2.4 Hz, 2H, $H^2$), 8.29 (d, $J$ = 2.4 Hz, 2H, $H^1$) 8.29 (s, 2H, $H^3$) 8.09 (d, $J$ = 12 Hz, 2H, $H^{d'}$), 7.9 -7.8(m, 4H, $H^{c+d'}$) 7.6-7.5 (m, 10H, $H^{a, 4+5}$), 7.13 (t, $J$ = 12 Hz, 2H, $H^{c'}$),7.01 (t, $J$ = 12 Hz, 2H, $H^{b'}$), 6.92 (t,$J$ = 12 Hz, 2H, $H^c$), 6.37 (d, $J$ = 12 Hz, 2H, $H^{a'}$)

**$^{13}$C NMR** (151 MHz, $CD_2Cl_2$) δ(ppm): 153.4 (2C, $C_1$), 152.5 (2C, $C_{quat}$), 148.8 (2C, $C_{quat}$), 148.6 (2C, $C_{quat}$), 144.8 (2C, $C_{quat}$), 143.6 (2C, $C_{quat}$), 140.4 (2C, $C_2$), 138.2 (2C,$C_{d'}$), 131.9 (2C, $C_{b'}$), 131.8 (4C, $C_4$), 131.8 (2C,$C_{quat}$), 138.2 (2C, $C_{d'}$), 129.9 (2C,$C_{a'}$), 128.0 (2C, $C_3$),127.2 (2C,$C_{quat}$), 125.1 (4C, $C_5$), 124.9 (2C, $C_b$), 123.5 (2C, $C_c$), 122.9 (2C, $C_d$), 122.5 (2C, $C_{c'}$) 119.7 (2C, $C_{quat}$), 118.2 (2C,$C_{quat}$) , 97.6 (2C, C≡C), 83.9 (2C, C≡C), 34.2 (2C, $C(CH_3)_3$),30.4 (2C, $C(CH_3)_3$).

**IR** (νbar/ $cm^{-1}$) 3047, 2961, 2207 (C≡C), 1608, 1584, 1506, 1479 (C-C aromatic ring), 1423, 1268, 1226 (C-H rocking phen), 1105, 1064, 1063, 831 (C-H aromatic), 756, and 730.

**HRMS** (m/z, $CH_3CN$) : calculated for $C_{58}H_{48}IrN_4$ $[M\text{-}PF_6]^+$ : 993.3548 found : 993.3540

**CHN**: Calculated for $C_{58}H_{48}F_6IrN_4P$ C: 61.2 , H: 4.25 N: 4.92 Found C: 61.70 H: 4.30. N: 4.92

**[Ir(ppy)$_2$ (3,8-bis[2-(1-naphthyl) ethynyl]-1,10-phenanthroline)](PF$_6$) (14)**

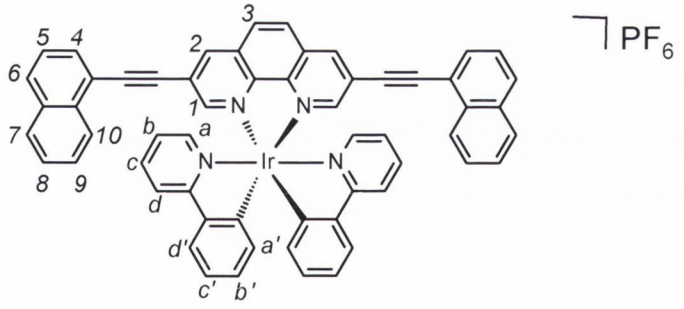


[Ir(ppy)$_2$(3,8-dibromo-1,10-phenanthroline)](PF$_6$) (80 mg, 0.093 mmol), CuI (5 mg, 0.001mmol) and Pd(PPh$_3$)$_2$Cl$_2$ (6.5 mg, 0.001 mmol) were placed in a 50 mL Schlenk and the flask was purged with argon (x3). Pre-dried DMF (8 mL) and $NEt_3$ (2 mL) were degassed by freeze-pump thaw, and transferred *via* cannula to the Schlenk. The solution was left to stir at room temperature for 20 minutes under argon. 1-ethynyl naphthyl (29 mg, 0.094 mmol) was added dropwise *via* syringe. The reaction was stirred overnight under argon. The solvent level was reduced *in vacuo*. The crude mixture was acidified with an aqueous solution of 2 M HCl (~25 mL) and extracted into $CH_2Cl_2$. The organic layer was washed with water and dried over $MgSO_4$. The impure solid was purified by a silica plug, eluting with $CH_2Cl_2$:hexane (1:1, v/v). The fractions were combined, the

solvents were reduced *in vacuo* and a concentrated solution of $NH_4PF_6$ was added (~2 mL). The precipitate was filtered to give an orange solid. **Yield**: (57.4 mg, 0.058 mmol, 63 %)

**$^1$H NMR** (600.1 MHz, $CD_2Cl_2$) δ(ppm): 8.5 (d, $J$ = 2.4 Hz, 2H, $H^2$), 8.43 (d, $J$ = 2.4 Hz, 2H, $H^1$), 8.3 (s, 2H, $H^3$), 8.25(d, $J$ = 12 Hz, 2H, $H^{10}$), 8.13 (d, $J$ = 12 Hz, 2H, $H^d$), 8.09 (d, $J$ = 12 Hz, 2H, $H^{d'}$), 8.07 (d, $J$ = 12 Hz, 2H, $H^6$), 8.09 (d, $J$ = 12 Hz, 2H, $H^7$), 7.95 (d, $J$ = 12 Hz, 2H, $H^{d'}$), 7.87 (t, $J$ = 8.5 Hz, 2H, $H^c$), 7.84 (d, $J$ = 12 Hz, 2H, $H^4$), 7.73 (t, $J$ = 8.5 Hz, 2H, $H^{8/9}$),7.66 (m, 6H, $H^{8/9/a}$), 7.58 (t, $J$ = 8.5 Hz,2H, $H^5$), 7.2 (t, $J$ = 8.5 Hz, 2H, $H^{c'}$), 7.18 (t, $J$ = 8.5 Hz, 2H, $H^{b'}$), 6.96 (t, $J$ = 8.5 Hz, 2H, $H^{b'}$) and 6.5 (d, $J$ = 12 Hz, 2H, $H^{a'}$).

**$^{13}$C NMR** (151 MHz, $CD_2Cl_2$) δ(ppm): 155.7 (2C, $C_1$),152.5 (2C, $C_{quat}$), 149.8 (2C, $C_a$), 148.6 (2C, $C_{quat}$), 144.6 (2C, $C_{quat}$), 143.9 (2C, $C_{quat}$), 139.8 (2C, $C_2$), 138.2 (2C,$C_c$), 131.8 (2C,$C_{quat}$), 130.1 (2C,$C_5$), 129.9 (2C,$C_{a'}$), 128.5 (2C, $C_3$),127.5 (2C,$C_7$), 126.7 (2C,$C_{8/9}$), 126.3 (2C,$C_{10}$), 125.9 (2C,$C_5$), 125.1 (2C, $C_{quat}$), 124.9 (2C, $C_b$), 123.1 (2C, $C_c$), 122.7 (2C, $C_d$), 122.2 (2C, $C_{c'}$) 119.7 (2C, $C_{quat}$), 118.2 (2C,$C_{quat}$), 114.2(2C,$C_{quat}$), 114.0 (2C,$C_{quat}$), 113.9 (2C,$C_{quat}$), 95.9 (2C, C≡C), 85.3 (2C, C≡C).

**IR** (vbar/ $cm^{-1}$): 3049, 2202 (C≡C), 1720, 1607, 1583, 1507, 1489 (C-C aromatic ring), 1423, 1372, 1225 (C-H rocking phen), 1064, 932, 909, 833 (C-H aromatic), 800, 756, and 729.

**HRMS** (m/z, $CD_3CN$), calculated for $C_{28}H_{36}IrN_4$ $[M\text{-}PF_6]^+$ : 981.2574 Found: 981.2658

**CHN**:($C_{70}H_{22}F_6IrN_4P$): Calculated for $C_{58}H_{36}F_6IrN_4P$ C:61.86, H: 3.22 N: 4.98 Found C: 59.70 H: 3.01. N: 4.71

**[Ir(ppy)$_2$ (3,8-bis[2-(1-pyrenyl) ethynyl]-1,10-phenanthroline)](PF$_6$) (15)**

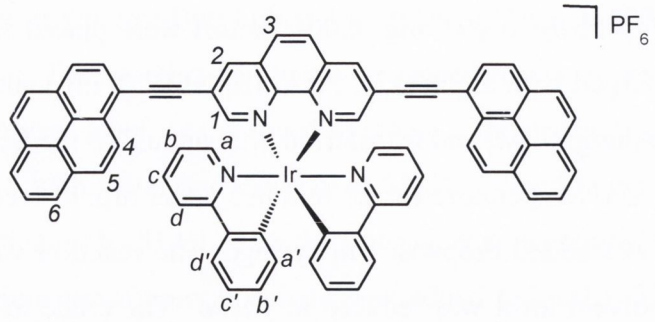


Ir(ppy)$_2$(3,8-dibromo-1,10-phenanthroline) $PF_6$ (64 mg, 0.065 mmol) and $Pd(PPh_3)_4$ (9 mg, 12 mol%) were dissolved in still-dried degassed THF (30 mL). $^iPr_2NH$ (10 mL, still dried and degassed) was added *via* annula and the solution was allowed to stir for 5

minutes. 1-ethynyl-pyrene (30 mg, 2.3 mmol) was dissolved in still-dried degassed THF and added *via* syringe, and the resulting solution was left to stir overnight at 70 °C under Ar. Solvents were removed *in vacuo*, 5% HCl was added (~25 mL) the crude solid was dissolved $CH_2Cl_2$. The mixture was washed with water and the organic layers combined and dried over $MgSO_4$. The solvent was reduced to ~2 mL, and a saturated solution of $NH_4PF_6$ in MeOH was added dropwise to give a red precipitate. **Yield**: (59 mg, 0.046, 71%)

**$^1$H NMR** (600 MHz, $CD_2Cl_2$),δ(ppm): 9.2 (d, *J* = 2.5 Hz, 2H, $H^2$), 8.7 (d, *J* =12 Hz, 2H, $H^4$), 8.5 (d, *J* = 2.5 Hz, 2H, $H^1$), 8.4-8.1 (m,12H, $H^{3/6/\ d/pyr}$), 7.95 (d, *J* = 12 Hz, 2H, $H^{d'}$), 7.86 (t, *J* = 8.5 Hz, 2H, $H^c$), 7.58 (d. *J*= 12 Hz, 2H, $H^a$), 7.38 (t, *J*= 4.5 Hz, 2H, $H^{b'}$), 7.2 (t, *J*= 4 Hz, 2H, $H^{c'}$), 7.12 (t, *J*= 4 Hz, 2H, $H^b$), 6.57 (d, *J*= 12 Hz, 2H, $H^{a'}$).

**$^{13}$C NMR** (151 MHz, $CD_2Cl_2$) δ (ppm): 168 (2C, $C_{quat\ ppy}$), 154.5(2C, $C_1$), 149.2 (2C, $C_{quat}$ ), 148.8 (2C, $C_a$), 146.2 (2C, $C_{quat}$), 144.3 (2C, $C_{quat\ phen}$), 140.1 (2C, $C_{quat}$), 139.1 (2C, $C_2$), 138.6 (2C, $C_c$) 132.7 (2C, $C_{quat}$), 132.6 (2C, $C_{quat}$), 131.8 (2C, $C_a$), 130.3 (2C, $C_b$), 129.6(2C, $C_3$), 129.3 (2C, $C_{pyr}$), 129.2 (2C, $C_{pyr}$), 126.9 (2C, $C_{pyr}$), 126.9 (2C, $C_{pyr}$), 126.3 (2C, $C_{pyr}$), 126.2 (2C, $C_{pyr}$), 125.0 (2C, $C_4$), 124.4 (2C, $C_{d'}$), 123.2 (2C, $C_{c'}$), 122.9 (2C, $C_b$), 132.6 (2C, $C_{quat}$),120.2(2C, $C_{quat}$) 115.1 (2C, $C_{quatpyr}$), 96.7 (2C, C≡C), 89.3 (2C, C≡C).

**IR** (νbar/ $cm^{-1}$): 2962, 2200 (C≡C), 1585, 1507, 1479 (C-C aromatic ring), 1423, 1364, 1267 (C-H rocking phen), 1105, 932, 908, 832 (C-H aromatic), and 729.

**HRMS** (m/z,$CD_3CN$), calculated for $C_{70}H_{48}IrN_4$ $[M\text{-}PF_6]^+$ 1133. 3187, Found: 1133.3195

**CHN**:($C_{70}H_{22}F_6IrN_4P$): Calculated for $C_{70}H_{48}F_6IrN_4P$ C:65.77, H: 3.47, N: 5.70 Found C: 63.80 H: 2.93. N: 4.72.

**[Ir(ppy)$_2$(3,8-bis[2-ethynyl-5,8,11,14,17-penta-*tert*-butylhexa-*peri*-hexabenzocoronene)1,10-phenanthroline)](PF$_6$) (15)**

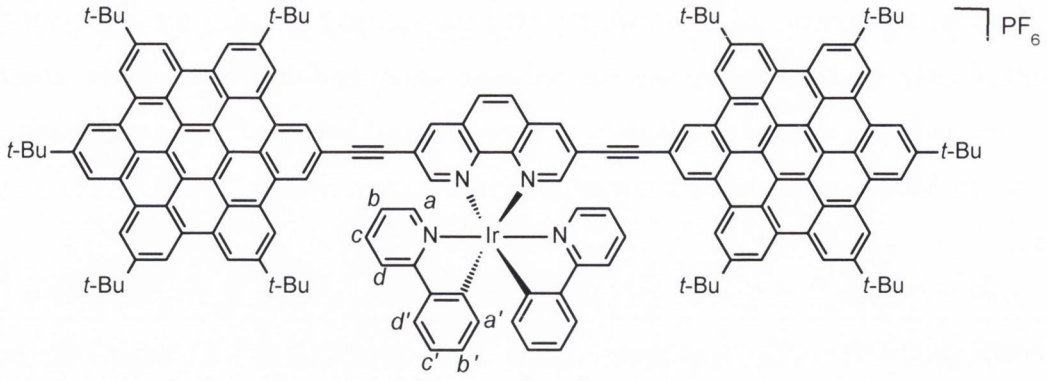


Ir(ppy)$_2$(3,8-dibromo-1,10-phenanthroline) PF$_6$ (26 mg, 0.03 mmol), Pd(PPh$_3$)$_2$Cl$_2$ (5 mg, 12 mol%) and CuI (3 mg, 12 mol%) were dissolved in still-dried degassed DMF (8 mL). $^{i}$Pr$_2$NH (3 mL, still dried and degassed) was added *via* cannula and the solution was allowed to stir for 30 minutes. 1-ethynyl-HBC (30 mg, 0.061 mmol) was dissolved in still-dried degassed DMF and added dropwise *via* syringe. The resulting solution was left to stir overnight at room temperature under argon. The solution was acidified with an aqueous solution of 2 M HCl (~25 mL), and taken up in $CH_2Cl_2$. The organic layer was washed with water and dried over $MgSO_4$. The solvent was reduced to ~2 mL, and a saturated solution of $NH_4PF_6$ in MeOH was added dropwise to give a red precipitate. The precipitate was filtered, and washed with diethyl ether. The product was isolated as a dark red/black crystalline solid. **Yield** (38 mg, 0.016 mmol, 55%)

**$^1$H NMR** (600 MHz, $CD_2Cl_2$), δ(ppm): 9.4-8.8 (m, 32H, $H^{HBC}$), 8.6 (d, $J$ = 2.52Hz, 2H, $H^{phen}$), 8.25 (d, $J$ = 8 Hz, 2H, $H^{ppy}$), 8.1 (d, $J$ = 8 Hz, 2H, $H^{ppy}$), 8.04 (d, $J$ = 8 Hz, 2H, $H^{ppy}$), 7.8 (d, $J$ = 8 Hz, 2H, $H^{ppy}$), 7.43 (t, $J$ = 4.5 Hz, 2H, $H^{c'}$), 7.39 (t, $J$ = 4.5 Hz, 2H, $H^{b'}$), 6.73 (d, $J$ = 8 Hz Hz, 2H, $H^{a'}$), 1.95-1.73 (br, 105H,C($CH_3$)$_3$).

**IR** (vbar/ cm$^{-1}$): 3062 (m, C≡*C-H*), 2953, 2865 (C-H stretching), 2196 (C≡C), 1738, 1606, 1581, 1507, 1478 (C-C aromatic ring), 1423, 1369, 1307, 1260 (C-H rocking phen), 1223, 1200, 1114, 1063, 1031, 941, 867, 838 (C-H aromatic), 755, 746 and 730.

**HRMS** (m/z, $CD_2Cl_2$), calculated for $[C_{162}H_{136}IrN_4]^+$ [M-PF$_6$]$^+$ 2331.0439 Found: 2331.0622.

**3, 8-bis[1, 2 ,3 ,4-tetrakis(4-*tert*-butylphenyl) benzene]-1,10-phenanthroline (17)**

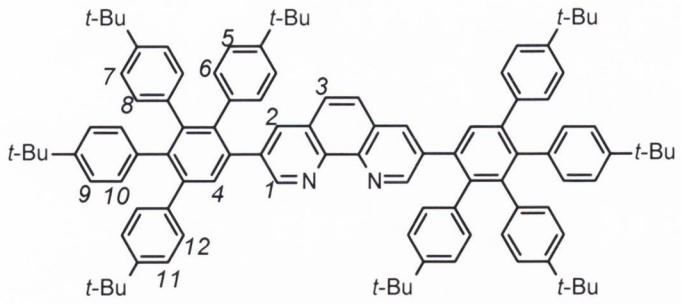


3,8-diethynyl-1,10-phenanthroline (115 mg, 0.505 mmol) and 2,3,4,5-tetrakis(4-tert-butylphenyl)- cyclopenta-2,4-dien-1-one (615 mg, 1.01 mmol) and benzophenone (1.5 g, 0.75 mmol) were placed in a 25 mL RBF. The RBF was attached to a condenser which had been flushed with argon. The reaction was heated to 200 °C, and allowed to stir for one hour. The temperature was slowly increased to 320 °C and the reaction was left stirring under argon for 3 days. The reaction was cooled, and dissolved in the minimum of $CH_2Cl_2$. Excess cold MeOH was added, and the crude solution was left in the fridge for two hours. The resulting precipitate was filtered, washing with cold methanol (~ 15 mL) and then further purified by column chromatography, eluting with $CH_2Cl_2$: hexane (2:1, v/v). The fractions were combined and the solvent removed *in vacuo* to give a cream solid. **Yield**: (273.8 mg, 0.197 mmol, 39 %).

**$^1$H NMR** (600 MHz, $CDCl_3$), δ(ppm): 9.05 (d, $J$ = 2.52 Hz, 2H, $H^1$), 7.95 (d, $J$ = 2.52Hz, 2H, $H^2$),7.65 (d, $J$ = 2.52 Hz, 4H, $H^3$), 7.5 (s, 2H, $H^4$), 7.2 (d, $J$ = 12 Hz, 4H, $H^{11}$), 7.1 (d, $J$ = 12 Hz, 4H, $H^{12}$) 6.95 (d, $J$ = 12 Hz, 4H, $H^{7/9}$), 6.9 (d, $J$ = 12 Hz, 4H, $H^{7/9}$), 6.84 (d, $J$ = 12 Hz, 4H, $H^5$) 6.77 (d, $J$ = 12 Hz, 4H, $H^{8/10}$) 6.75 (d, $J$ = 12 Hz, 4H, $H^{8/10}$) 6.66 (d, $J$ = 12 Hz, 4H, $H^6$), 1.3 (s, 18H, $C(CH_3)_3$), 1.17 (s, 18H, $C(CH_3)_3$), 1.15 (s, 18H, $C(CH_3)_3$), 1.1 (s,18H,$C(CH_3)_3$).

**$^{13}$C NMR** (151 MHz, $CDCl_3$) δ(ppm): 151.43 (2C, $C_1$), 149.20 (2C, $C_{quat}$), 148.3 (2C, $C_{quat}$), 143.2 (2C, $C_{quat}$), 141.2 (2C, $C_{quat}$), 147.9 (2C, $C_{quat}$), 142.8 (2C, $C_{quat}$), 140.9(2C, $C_{quat}$), 140.6 (2C, $C_{quat}$), 139.5 (2C, $C_2$), 138.7 (2C, $C_{quat}$), 137.2 (2C, $C_{quat}$), 136.9 (2C, $C_{quat}$),136.3 (2C, $C_{quat}$), 131.9-131.3 (12C, $C_{7,9,11}$), 129.5 (4C, $C_5$), 127.8 (2C, $C_4$), 126.4 (2C, $C_3$), 124.5(4C, $C_{8,10}$), 124.1 (4C, $C_{8/10}$), 123.5 (2C, $C_6$), 123.2 (2C, $C_6$), 34.4-34.31 (m, 8C, $C(CH_3)_3$), 31.2-31.1 (m, 24 C, $C(CH_3)_3$).

**IR** (vbar/ $cm^{-1}$) 2958 (C-H alkane), 2911, 2863, 1742, 1607, 1505 (C-C aromatic ring), 1475, 1461, 1392, 1271, 1202, 1116, 1105 (C-H rocking phen), 1042, 922, 857, 838 (C-H aromatic), 817, 772, 755, 742, 679, 658.

**HRMS** (THF): calculated for $C_{104}H_{113}N_2$ $[M+H]^+$ m/z : 1390.8906, found : 1390. 8982.

**m.p.** > 270 °C

**3, 8-bis[tribenzo[(*b, n, pqr*-5, 8, 11, 14-*tert*- butyl perylene]-1,10-phenanthroline (18)**

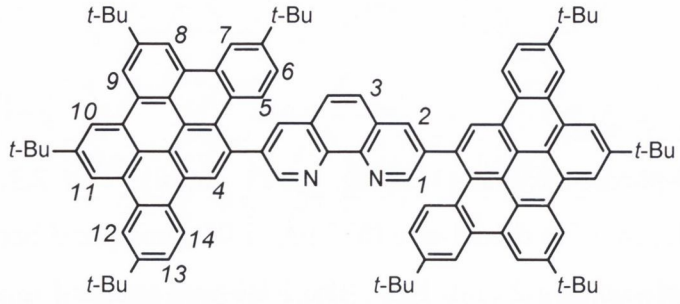


3, 8-bis[1,2,3,4-tetrakis(4-*tert*-butylphenyl)benzene]-1,10-phenanthroline (**17**) (130 mg, 0.094 mmol) was dissolved in dry degassed $CH_2Cl_2$ (~70 mL)in a three neck RBF. The solution was bubbled with argon for 15 minutes. Iron(III) chloride (606.9 mg, 3.74 mmol) was quickly added to a 10 mL Schlenk. Nitromethane (~ 4 mL) was added, and the iron trichloride solution was degassed by the freeze-pump thaw method (x3). The solution was added dropwise *via* cannula to the ligand solution. The reaction was stirred overnight under a constant stream of argon. The reaction was quenched with MeOH (~50 mL), and a brown/yellow colour was observed. $CH_2Cl_2$ (~100 mL) was added, the product was extracted, washed with water (x3) and dried over $MgSO_4$. The organic layer was concentrated and purified by silica column chromatography, eluting with $CH_2Cl_2$. The product was isolated as a brown solid. **Yield** (86 mg, 0.063 mmol, 67%)

**$^1$H NMR** (600 MHz, $CDCl_3$), δ(ppm): 9.5 (d, $J$ = 3 Hz, 2H, $H^1$), 9.21 (s, 4H, $H^{8/9/10/11}$), 9.13 (s, 4H, $H^{8/9/10/11}$),9.1 (s, 2H, $H^4$), 8.95 (s, 2H, $H^{12}$), 8.93 (d, $J$ = 12 Hz, 2H, $H^{14}$) 8.85 (s, 2H, $H^7$), 8.78 (s, 2H, $H^2$), 8.1 (s, 2H, $H^3$), 8.05 (br, 2H, $H^5$), 7.9 (d, $J$ = 12 Hz, 2H, $H^{13}$), 7.2 (br, 2H, $H^6$), 1.8 (s, 36H,C(C$H_3$)$_3$), 1.65 (s, 18H,C(C$H_3$)$_3$), ), 1.50 (br, 18H,C(C$H_3$)$_3$).

**$^{13}$C NMR** (151 MHz, $CDCl_3$), δ(ppm): 152.2 (2C, $C_1$), 150.5 (2C, $C_{quat}$), 149.6 (2C, $C_{quat}$),149.2 (2C, $C_{quat}$),149.1 (2C, $C_{quat}$),141.5 (2C, $C_{quat}$), 135.2 (2C, $C_2$), 131.9(2C, $C_{quat}$), 130.6 (2C, $C_{quat}$), 130.3 (2C, $C_5$), 130.3 (2C, $C_{quat}$), 130.2 (2C, $C_{quat}$), 129.1(2C, $C_{quat}$),127.7 (2C, $C_3$), 127.6 (2C, $C_{quat}$), 127.3 (2C, $C_{quat}$), 126.8(2C, $C_{13}$), 125.9-125.2 (8C, $C_{8,9,10,11}$), 122.9 (2C, $C_6$),122.7 (2C, $C_{14}$), 119.9 (2C, $C_7$), 119.35 (2C, $C_{8/9/10/11}$), 119.2 (2C, $C_4$), 118.7 (2C, $C_{quat}$), 118.5 (2C, $C_{quat}$), 118.4 (2C, $C_{quat}$), 35.7-35.02 (m, 8C $C$(CH$_3$)$_3$), 31.9-31.3 (m, 24 C, C($C$H$_3$)$_3$).

**IR** (vbar/ $cm^{-1}$) 3107 (C-H aromatic), 2958 (C-H alkane), 2920, 2872, 1745, 1613, 1585, 1515 (C-C aromatic ring), 1475, 1461, 1392, 1271, 1202, 1116, 1105 (C-H rocking phen), 1042, 922, 857, 838 (C-H aromatic), 817, 772, 755, 742, 679, 658

**HRMS** (THF): calculated for $C_{104}H_{101}N_2$ $[M+H]^+$ m/z : 1378.8043, found : 1378.8041

**m.p.** > 270 °C

**3,8-bis[2,3,4,5,6-pentakis(4-*tert*-butylphenyl)phenyl]-1,10-phenanthroline (19)**

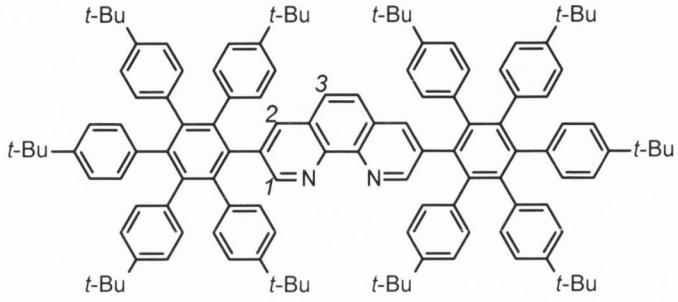


3,8-Bis[2-(4-tert-butylphenyl)ethynyl]-1,10-phenanthroline (58 mg, 0.118 mmol) and 2,3,4,5-tetrakis(4-tert-butylphenyl)- cyclopenta-2,4-dien-1-one (144 mg, 0.2356 mmol) and benzophenone (1 g, 0.5 mmol) were placed in a 25 mL RBF. The RBF was attached to a condenser which had been flushed with argon. The reaction was heated to 200 °C, and allowed to stir for one hour. The temperature was slowly increased to 340 °C and the reaction was left stirring under argon for five days. The reaction was cooled, and dissolved in the minimum of $CH_2Cl_2$. Excess cold MeOH was added, and the crude solution was left in the fridge for two hours. The resulting precipitate was isolated by filtration and then further purified by column chromatography, eluting with $CH_2Cl_2$: hexane (2:1, v/v). The fractions were combined and the solvent removed *in vacuo* to give a cream solid. **Yield**: (52 mg, 0.032 mmol, 27 %).

**$^1$H NMR** (600 MHz, $CDCl_3$), δ(ppm): 8.75 (d, $J$ = 1.2 Hz, 2H, $H^1$), 7.55 (d, $J$ = 1.2 Hz, 2H, $H^2$),7.18 (d, $J$ = 1.2 Hz, 2H, $H^3$), 6.9-6.6 (m, 40H, $H^{Ph}$) 1.13 (s, 18H,C($CH_3$)$_3$), 1.1(s, 36H,C($CH_3$)$_3$), 0.9 (s,36H,C($CH_3$)$_3$).

**$^{13}$C NMR** (151 MHz, $CDCl_3$) δ(ppm):153.0 (2C, $C_1$), 148.1 (2C, $C_{quat}$), 147.9 (2C, $C_{quat}$), 143.1 (2C, $C_{quat}$), 141.2 (2C, $C_{quat}$), 140.9 (2C, $C_{quat}$), 138.7 (2C, $C_2$),137.1 (2C, $C_{quat}$), 136.1 (2C, $C_{quat}$), 135.4 (2C, $C_{quat}$), 131.5-130.5 (m,$C_{Ph}$), 128.3 (2C, $C_{quat}$), 126.9 (2C, $C_{quat}$), 125.9 (2C, $C_3$), 124 (2C, $C_{quat}$), 123.0 (m, $C_{Ph}$), 34.6-34.4 (m, $C_{quat}$, $C(CH_3)_3$), 31.83 (30C, C($CH_3$)$_3$).

**IR** (vbar/ $cm^{-1}$) 2960 (C-H alkane), 2903, 2867, 1739, 1602, 1510 (C-C aromatic ring), 1475, 1461, 1390, 1361, 1271, 1202, 1116, 1105 (C-H rocking phen), 1021, 922, 855.3, 834 (C-H aromatic), 815, 780, 755, 742, 679, 660

**HRMS** (THF): calculated for $C_{124}H_{137}N_2$ $[M+H]^+$ m/z : 1655.0724, found : 1655.0840.

**m.p.** > 270 °C

**3,8-bis[2,4,5-tris(4-*tert*-butylphenyl)-3,6-bis(4-methoxyphenyl)phenyl]-1,10-phenanthroline (20)**

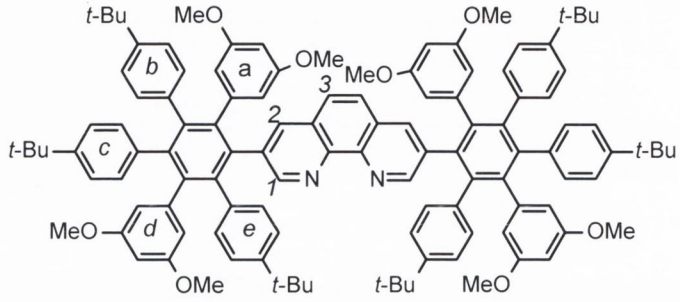


3,8-Bis[2-(4-tert-butylphenyl)ethynyl]-1,10-phenanthroline (50 mg, 0.101 mmol) and 3,4-bis(4-tert-butylphenyl)-2,5-bis(3,5-dimethoxyphenyl)cyclopenta-2,4-dien-1-one (126 mg, 0.204 mmol) and benzophenone (1 g, 0.5 mmol) were placed in a 10 mL RBF. The RBF was attached to a condenser which had been flushed with argon. The reaction was heated to 200 °C, and allowed to stir for one hour. The temperature was slowly increased to 340 °C and the reaction was left stirring under argon for five days. The reaction was cooled, and dissolved in the minimum of $CH_2Cl_2$. The crude mixture was purified by silica column chromatography, eluting with $CH_2Cl_2$: hexane (2:1, v/v). The fractions were combined and the solvent removed. Excess cold MeOH was added, and the crude solution was left in the fridge for two hours. The resulting precipitate was isolated by filtration to give a pale brown solid. **Yield**: (57.3 mg, 0.034 mmol, 34 %).

**$^1$H NMR** (600 MHz, $CDCl_3$), δ(ppm): 8.7 (d, $J$ = 1.2 Hz, 2H, $H^1$), 7.6 (d, $J$ = 1.2 Hz, 2H, $H^2$),7.21 (d, $J$ = 1.2 Hz, 2H, $H^3$), 6.9 (m, 12H, $H^{b/c/e}$), 6.72 (m, 12H, $H^{b/c/e}$), 6.05- 5.85 (m, 12H, $H^{a/d}$), 3.38 (d, $J$ = 8.5 Hz, $OCH_3^d$), 3.28 (t, $J$ = 6.0 Hz 4H, $OCH_3^a$), 3.17 (s, 2H, $OCH_3^a$), 1.15 (s, 36H,C($CH_3$)$_3$), 1.01 (d, $J$ = 8.5 Hz,18H,C($CH_3$)$_3$).

**$^{13}$C NMR** (151 MHz, $CDCl_3$) δ(ppm): 153.3 (2C, $C_1$), 147.3 (2C, $C_{quat}$), 147.1 (2C, $C_{quat}$), 143.0 (2C, $C_{quat}$), 142.5 (2C, $C_{quat}$), 140.9 (2C, $C_{quat}$), 137.6 (2C, $C_2$),137.2 (2C, $C_{quat}$), 135.9 (2C, $C_{quat}$), 135.5 (2C, $C_{quat}$), 131.7-130.9 (m, $C_{b/c/e}$), 128.1 (2C, $C_{quat}$), 126.9 (2C, $C_{quat}$),125.9 (2C, $C_3$), 124.3 (2C, $C_{quat}$), 123.0 (2C, $C_{b/c/e}$),112.5 (2C, $C_{a/d}$), 112.1 (2C, $C_{a/d}$),, 55.4 (C, $OCH_3$) 55.2 (C,$OCH_3$), 31.83 (6C, C($CH_3$)$_3$).

**IR** (vbar/ $cm^{-1}$) 2960 (C-H alkane), 2903, 2867, 1738, 1602, 1510 (C-C aromatic ring), 1461, 1391, 1362, 1269, 1202, 1116, 1104 (C-H rocking phen), 1018, 934, 855.3 (C-H aromatic), 769, 755, 678

**HRMS** (THF): calculated for $C_{116}H_{121}N_2O_8$ $[M+H]^+$ m/z : 1669.9123, found : 1669.9111.

**m.p.** > 270 °C

**Cyclodehydrogentation of 3,8-bis[2,3,4,5,6-pentakis(4-*tert*-butylphenyl)phenyl]-1,10-phenanthroline (19), product 21.**

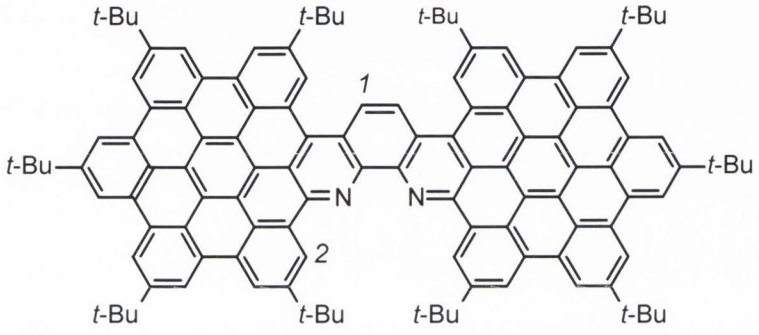


3,8-bis[2,3,4,5,6-pentakis(4-tert-butylphenyl)phenyl]-1,10-phenanthroline (**19**) (55 mg, 0.033 mmol) was dissolved in dry degassed $CH_2Cl_2$ (~70 mL) in a three neck RBF. The solution was bubbled with argon for 15 minutes. Iron(III) chloride (321.4 mg, 1.98 mmol) was quickly added to a 10 mL Schlenk. Nitromethane (~ 4 mL) was added, and the iron trichloride solution was degassed by the freeze-pump thaw method (x3). The solution was added dropwise *via* cannula to the ligand solution over five minutes. The reaction was stirred overnight under a constant stream of argon. The reaction was quenched with MeOH (~50 mL), and a brown/yellow colour was observed. The MeOH was removed *in vacuo* and the crude mixture was dissolved in $CH_2Cl_2$ (~25 mL), the product was extracted, washed with a basic aqueous solution of EDTA (x3), and then with water (x3). The organic layers were combined and dried over $MgSO_4$. The organic layer was concentrated and purified by silica column chromatography, eluting with diethyl ether. The product was isolated as a yellow/brown solid. **Yield**: (9 mg, 0.005 mmol, 15 %)

**$^1$H NMR** (600 MHz, $CDCl_3$) δ(ppm): 10.9 (s, 2H, $H^2$), 9.95 (s, 2H, $H^1$) 9.4 (br, 18H), 2.1-1.75 (m, 90H,C($CH_3$)$_3$).

**HRMS** ($CH_2Cl_2$): calculated for $C_{124}H_{113}N$ $[M+H]^+$ m/z : 1669.8858, found : = 1629.8821.

**3, 8-bis[tribenzo[(*b, n, pqr*-5, 8, 11, 14-*tert*- butyl perylene]-1,10-phenanthroline [Ru(bipy$_2$)(3,8-bis[tribenzo[(*b, n, pqr*-5, 8, 11, 14-*tert*-butyl perylene]-1,10-phenanthroline)](PF$_6$)$_2$ (22)**

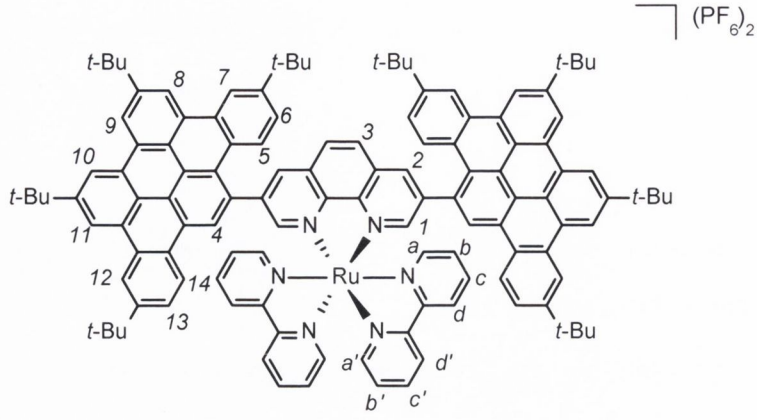


Ethylene glycol monoethylether (10 mL) was bubbled with argon in a two necked RBF for 15 minutes. 3,8-bis[tribenzo[(*b, n, pqr*-5, 8, 11, 14-*tert*-butyl perylene]-1,10-phenanthroline (30 mg, 0.022 mmol) was added and the solution was left to stir for a further 15 mins under nitrogen. EtOH was added dropwise until the ligand had completely dissolved. *cis*-[Ru(bipy)$_2$Cl$_2$].H$_2$O (10.7 mg, 0.021) was added and the solution was heated to 150 °C. The solution was refluxed overnight under argon. The reaction was cooled to room temperature, and filtered through celite to remove any unreacted ligand. The crude complex was purified on a short silica plug, eluting with a solution of CH$_3$CN:KNO$_3$:H$_2$O (10:1:1.5, v/v). The fractions were combined, the solvent level reduced, and extracted into CH$_2$Cl$_2$, The organic layer was combined, dried over MgSO$_4$, and solvents removed *in vacuo*. The residue was dissolved in acetone, and ethylene glycol was added (~3 mL). A saturated solution of KPF$_6$ was added dropwise until a precipitate was observed. The pure complex was isolated by filtration, and washed with diethyl ether (~15 mL) to give a dark red crystalline solid. **Yield** (28 mg, 0.014 mmol, 69%)

**$^1$H NMR** (600 MHz, CDCl$_3$) δ(ppm): 9.79 (s, 2H, H$^1$), 9.46 (d, $J$ = 1.2 Hz, H$^2$), 9.35 (d, $J$ = 8.0 Hz, 2H, H$^{d/d'}$), 9.28 (d, $J$ = 8.0 Hz, 2H, H$^{d/d'}$), 9.1 (m, 8H, H$^{8/9/10/11}$), 9.02 (s, 2H, H$^4$), 9.02 (s, 2H, H$^7$), 8.94 (br, 2H, H$^{14}$), ), 8.88 (s, 2H, H$^{12}$), 8.82 (m, 4H, H$^{b/b'}$), 8.4 (m, 2H, H$^{a/a'}$), 8.19 (m, 2H, H$^{a/a'}$), 8.1 (d, $J$ = 8 Hz, 2H, H$^{13}$), 8.08 (s, 2H, H$^3$), 7.9 (br, 2H, H$^5$), 7.6 (m, 4H, H$^{c/c'}$), 7.3 (br, 2H, H$^7$) , 1.28 (s, 36H,C(C$H_3$)$_3$), 1.26 (s, 18H,C(C$H_3$)$_3$), ), 1.2 (s,18H,C(C$H_3$)$_3$).

**IR** (νbar/ $cm^{-1}$) 3036, 2960, 2919, 2850, (C-H alkane),1738, 1584, 1510 (C-C aromatic ring), 1463,1435, 1420, 1391, 1364, 1260, 1206, 1189, 1091 (C-H rocking phen), 1018, 905, 835.3 (C-H aromatic), 798, 753, 727, 712, 677.

**HRMS** ($CH_3CN$): calculated for $C_{124}H_{115}N_6F_6PRu$ $[M+PF_6]^+$ m/z = 1935.7831, found m/z = 1935.7831

**[Ir(ppy$_2$)(3,8-bis[2,4,5-tris(4-*tert*-butylphenyl)-3,6-bis(4-methoxyphenyl)phenyl]-1,10-phenanthroline)](PF$_6$) (23)**

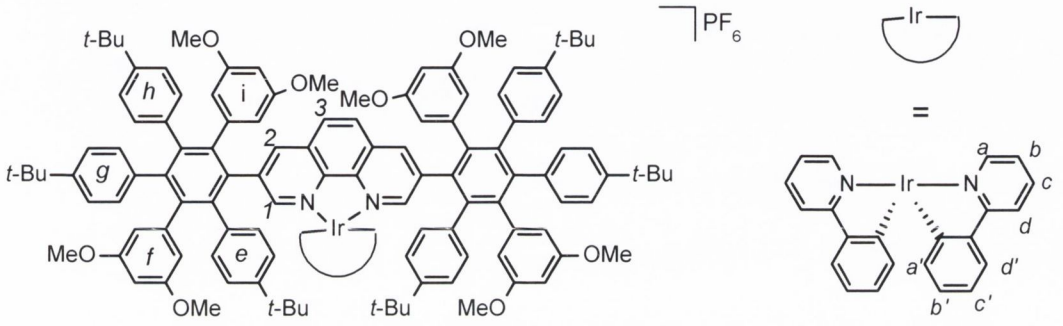


$[Ir(ppy)_2Cl]_2$ (4.8 mg, 0.005 mmol) was dissolved in $CH_2Cl_2$ (~2 mls) and stirred under argon for five minutes. 3,8-bis[2,4,5-tris(4-tert-butylphenyl)-3,6-bis(4-methoxyphenyl)phenyl]-1,10-phenanthroline (15 mg, 0.009 mmol) was dissolved in $CH_2Cl_2$: MeOH (3 mL, 1;1 v/v), and added slowly. The solution was heated to 40 °C and stirred under argon for 2 hours. The solution was allowed to cool. A saturated solution of $NH_4PF_6$ in MeOH was added dropwise until a precipitate had formed. The precipitate was filter, washed with diethyl ether (~8 mL), to give an orange solid. **Yield:** (7.7 mg, 0.003 mmol, 37%).

**$^1$H NMR** (600 MHz, $CD_3CN$) δ(ppm): 8.6 (d, *J* = 6 Hz, 2H, $H^1$), 8.2 (d, *J* = 8.4 Hz, 2H, $H^{d'}$), 8.0 (t, *J* = 7.8 Hz, 2H, $H^b$), 7.92 (m, 4H, $H^{e/d'}$), 7.76 (d, *J* = 7.6 Hz, 2H, $H^2$), 7.6 (s, 2H, $H^e$), 7.57 (d, *J* = 1.2 Hz, 2H, $H^e$), 7.38 (d, *J* = 6 Hz, 2H, $H^3$), 7.13 (t, *J* = 6 Hz, 2H, $H^{c'}$), 7.02-6.9 (m, 8H, 6.72 (d, *J* = 12 Hz, 2H, $H^g$), 6.68 (d, *J* = 8.4 Hz, 12H, $H^h$), 6.34 (d, *J* = 12 Hz, 12H, $H^a$), 6.16 (d, *J* = 8.4 Hz, 12H, $H^{a'}$), 6.07-5.97 (m, 6H, $H^{f/i'}$), 5.82 (dd, *J* = 12, 1.8 Hz, 2H, $H^f$), 5.7(dd, *J* = 12, 1.8 Hz, 2H, $H^f$), 5.6 (s, 2H, $H^i$), 3.45 (s, 12H, $OCH_3^f$), 3.36 (s, 6H, $OCH_3^i$), 3.35 (s, 6H, $OCH_3^i$), 1.18 (m,36H, $C(CH_3)_3^{g/h}$), 0.85 (s,36H, $C(CH_3)_3^e$).

**$^{13}$C NMR** (151 MHz, $CD_3CN$) δ(ppm):168.37 (2C, $C_{quat\ ppy}$), 160.7-160.4 (6C, $C_{quat}$), 152.5 (2C, $C_1$),149.8 (2C, $C_{quat}$), 149.5 (2C, $C_{quat}$),148.9 (2C, $C_a$), 144.5 (2C, $C_{quat}$), 143.9 (2C, $C_{quat}$), 143.2 (2C, $C_{quat}$), 141.9 (2C, $C_{quat}$), 141.7 (2C, $C_e$), 141.7 (2C, $C_e$),

141.5 (2C, $C_{quat}$), 141.2 (2C, $C_{quat}$), 141.1 (2C, $C_{quat}$), 140.4 (2C, $C_{quat}$),, 139.5 (2C, $C_{quat}$), 137.5 (2C, $C_{quat}$), 133.5 (2C, $C_c$),132.9 (2C, $C_{quat}$),, 131.8 (2C, $C_f$), 131.6 (2C, $C_h$), 131.2 (2C, $C_g$), 131.1 (2C, $C_{quat}$),, 131.0 (2C, $C_{quat}$), 130.3 (2C, $C_{a'}$), 128.5 (2C, $C_e$), 126.0 (2C, $C_{b'}$), 124.8 (2C, $C_d$), 124.5 (2C, $C_{g/h}$), 124.4 (2C, $C_f$), 124.3 (2C, $C_{c'}$), 124.1 (2C, $C_3$),121.2 (2C, $C_d$), 112.1 (2C, $C_g$), 111.8 (2C, $C_i$), 111.7 (2C, $C_i$), 56.2-55.1(8C, $OCH_3$) 31.c (6C, $C(CH_3)_3$).

**IR** (νbar/ $cm^{-1}$) 2960, 2903, 2867, (C-H alkane), 1738, 1593, 1510 (C-C aromatic ring), 1460, 1421, 1391, 1362, 1269, 1202, 1104, 1018 (C-H rocking phen), 907, 832 (C-H aromatic), 798, 778, 738, 700, 679.

**HRMS** ($CH_3CN$): calculated for $C_{135}H_{136}N_4PO_8IrF_6$ $[M+PF_6]^+$ m/z = 2169.9988, found m/z = 2169.9939

1. J. Meisenheimer and K. Witte, *Reports of the German Chemical Society*, 1903, **36**, 4153-4164.
2. R. WeitzenbÃ¶ck and A. Klingler, *Monatshefte fÃ¼r Chemie und verwandte Teile anderer Wissenschaften*, 1918, **39**, 315-323.
3. W. W. H. Wong, J. Subbiah, S. R. Puniredd, B. Purushothaman, W. Pisula, N. Kirby, K. Mullen, D. J. Jones and A. B. Holmes, *Journal of Materials Chemistry*, 2012, **22**, 21131-21137.
4. M. Yin, J. Shen, W. Pisula, M. Liang, L. Zhi and K. Mullen, *Journal of the American Chemical Society*, 2009, **131**, 14618-14619.
5. P. Rempala, J. Kroulik and B. T. King, *Journal of the American Chemical Society*, 2004, **126**, 15002-15003.
6. D. J. Jones, B. Purushothaman, S. Ji, A. B. Holmes and W. W. H. Wong, *Chemical Communications*, 2012, **48**, 8066-8068.
7. B. T. King, C. R. Robertson, P. Rempala, C. L. Hilton, J. D. Korinek and L. M. Gortari, *The Journal of Organic Chemistry*, 2007, **72**, 2279-2288.
8. B. Lankage, L. Wijesinghe and S. M. Draper, *Unpublished Results, Trinity College Dublin*.
9. G. Cooke, G. M. O Maille, R. Quesada, L. Wang, S. Varughese and S. M. Draper, *Dalton Transactions*, 2011, **40**, 8206-8212.
10. A. M. van de Craats and J. M. Warman, *Advanced Materials*, 2001, **13**, 130-133.
11. S. Flores-Torres, G. R. Hutchison, L. J. Soltzberg and H. D. Abruna, *Journal of the American Chemical Society*, 2006, **128**, 1513-1522.
12. R. Ziessel and C. Stroh, *Tetrahedron Letters*, 2004, **45**, 4051-4055.
13. R. Ziessel, V. Grosshenny, M. Hissler and C. Stroh, *Inorganic Chemistry*, 2004, **43**, 4262-4271.
14. K.-Y. Kim, S. Liu, M. E. Kasse and K. S. Schanze, *Inorganic Chemistry*, 2006, **45**, 2509-2519.
15. B. El Hamaoui, F. Laquai, S. Baluschev, J. Wu and K. Mullen, *Synthetic Metals*, 2006, **156**, 1182-1186.
16. C. D. Simpson, G. Mattersteig, K. Martin, L. Gherghel, R. E. Bauer, H. J. Rader and K. Mullen, *Journal of the American Chemical Society*, 2004, **126**, 3139-3147.
17. F. A. Murphy and S. M. Draper, *The Journal of Organic Chemistry*, 2010, **75**, 1862-1870.
18. D. Nolan, B. Gil, F. A. Murphy and S. M. Draper, *European Journal of Inorganic Chemistry*, 2011, **2011**, 3248-3256.
19. R. H. Manske, *Chemical Reviews*, 1942, **30**, 113-144.
20. G. Accorsi, A. Listorti, K. Yoosaf and N. Armaroli, *Chemical Society Reviews*, 2009, **38**, 1690-1700.
21. J. P. Sauvage, Dietrich-Buchecker, C.O. , *Wiley-VCH, Weinheim, Germany*, 1999.
22. B. N. Bandyopadhyay and A. Harriman, *Journal of the Chemical Society, Faraday Transactions 1: Physical Chemistry in Condensed Phases*, 1977, **73**, 663-674.
23. G. M. Badger and I. S. Walker, *Journal of the Chemical Society*, 1956, 122-126.
24. A. Listorti, A. Degli Esposti, R. S. K. Kishore, V. Kalsani, M. Schmittel and N. Armaroli, *Journal of Physical Chemistry A*, 2007, **111**, 7707-7718.
25. B. Bosnich, *Accounts of Chemical Research*, 1969, **2**, 266-273.
26. F. H. Case, *Journal of Organic Chemistry*, 1951, **16**, 1541-1545.
27. D. Tzalis, Y. Tor, F. Salvatorre and S. Jay Siegel, *Tetrahedron Letters*, 1995, **36**, 3489-3490.
28. T. J. Kress and S. M. Costantino, *Journal of Heterocyclic Chemistry*, 1973, **10**, 409-410.
29. A. Bencini and V. Lippolis, *Coordination Chemistry Reviews*, **254**, 2096-2180.
30. Y. Jahng, R. P. Thummel and S. G. Bott, *Inorganic Chemistry*, 1997, **36**, 3133-3138.
31. E. C. Glazer, D. Magde and Y. Tor, *Journal of the American Chemical Society*, 2007, **129**, 8544-8551.
32. T. Forster, *Discussions of the Faraday Society*, 1959, **27**, 7-17.
33. D. L. Dexter, *The Journal of Chemical Physics*, 1953, **21**, 836-850.

34. H. S. Joshi, R. Jamshidi and Y. Tor, *Angewandte Chemie-International Edition*, 1999, **38**, 2722-2725.
35. C. S. Creaser, Sodeau, J.R, , *Perspectives in Modern Chemical Spectroscopy (Ed.: D.L. Andrews), Springer, Berlin*, 1990, 103-136.
36. K. Biradha, M. Aoyagi and M. Fujita, *Journal of the American Chemical Society*, 2000, **122**, 2397-2398.
37. C. J. Kuehl, S. D. Huang and P. J. Stang, *Journal of the American Chemical Society*, 2001, **123**, 9634-9641.
38. M. J. E. Resendiz, J. C. Noveron, H. Disteldorf, S. Fischer and P. J. Stang, *Organic Letters*, 2004, **6**, 651-653.
39. D. W. Bruce and K. E. Rowe, *Liquid Crystals*, 1995, **18**, 161-163.
40. L. Douce, A. El-ghayoury, R. Ziessel and A. Skoulios, *Chemical Communications*, 1999, 2033-2034.
41. R. Ziessel, G. Pickaert, F. Camerel, B. Donnio, D. Guillon, M. l. Cesario and T. Prange, *Journal of the American Chemical Society*, 2004, **126**, 12403-12413.
42. S. J. P. Bousquet and D. W. Bruce, *Journal of Materials Chemistry*, 2001, **11**, 1769-1771.
43. R. Ziessel, L. Douce, A. El-ghayoury, A. Harriman and A. Skoulios, *Angewandte Chemie International Edition*, 2000, **39**, 1489-1493.
44. A. El-ghayoury, L. Douce, A. Skoulios and R. Ziessel, *Angewandte Chemie International Edition*, 1998, **37**, 2205-2208.
45. H. S. Joshi, R. Jamshidi and Y. Tor, *Angewandte Chemie International Edition*, 1999, **38**, 2721-2725.
46. Y. Saitoh, T.-a. Koizumi, K. Osakada and T. Yamamoto, *Canadian Journal of Chemistry*, 1997, **75**, 1336-1339.
47. W. Wu, W. Wu, S. Ji, H. Guo, P. Song, K. Han, L. Chi, J. Shao and J. Zhao, *Journal of Materials Chemistry*, 2010, **20**, 9775-9786.
48. S. Nagarajan, C. Barthes and A. Gourdon, *Tetrahedron*, 2009, **65**, 3767-3772.
49. G. O'Maille and S. M. Draper, *Thesis (unpublished results)*, 2013.
50. D. Villemin and F. Caillot, *Tetrahedron Letters*, 2001, **42**, 639-642.
51. M. Larhed and A. Hallberg, *Journal of Organic Chemistry*, 1996, **61**, 9582-9584.
52. J.-X. Wang, B. Wei, Y. Hu, Z. Liu and Y. Yang, *Synthetic Communications*, 2001, **31**, 3885-3890.
53. L. Ã–hberg and J. Westman, *Synlett*, 2001, **2001**, 1893-1896.
54. M. Nüchter, U. Müller, B. Ondruschka, A. Tied and W. Lautenschläger, *Chemical Engineering & Technology*, 2003, **26**, 1207-1216.
55. D. M. P. Mingos and D. R. Baghurst, *Chemical Society Reviews*, 1991, **20**, 1-47.
56. J. V. Lockard, S. Kabehie, J. I. Zink, G. Smolentsev, A. Soldatov and L. X. Chen, *The Journal of Physical Chemistry B*, 2010, **114**, 14521-14527.
57. S. Kabehie, M. Xue, A. Z. Stieg, M. Liong, K. L. Wang and J. I. Zink, *Journal of the American Chemical Society*, 2010, **132**, 15987-15996.
58. Andrew C. Benniston, A. Harriman, Donald J. Lawrie and Sarah A. Rostron, *European Journal of Organic Chemistry*, 2004, **2004**, 2272-2276.
59. S. M. Draper, D. J. Gregg and R. Madathil, *Journal of the Americal Chemical Society*, 2002, **124**, 3486-3487.
60. H. Desabbayes, J. C. Clement, P. Laurent, G. Tanguy and N. Thilmont, *Organometallics*, 1988, **7**, 2293-2299.
61. U. T. Muellerwesterhoff and M. Zhou, *Journal of Organic Chemistry*, 1994, **59**, 4988-4992.
62. D. B. Biradar and H.-M. Gau, *Chemical Communications*, 2011, **47**, 10467-10469.
63. S. Ji, W. Wu, W. Wu, H. Guo and J. Zhao, *Angewandte Chemie International Edition*, **50**, 1626-1629.
64. A. Graczyk, F. A. Murphy, D. Nolan, V. Fernandez-Moreira, N. J. Lundin, C. M. Fitchett and S. M. Draper, *Dalton Transactions*, 2012, **41**, 7746-7754.
65. E. Clar, C. T. Ironside and M. Zander, *Journal of the Chemical Society*, 1959, 142-147.

66. B. N. Bandyopadhyay and A. Harriman, *Journal of the Chemical Society-Faraday Transactions I*, 1977, **73**, 663-674.
67. I. B. Berlman, *Handbook of Fluorescence Spectra of Aromatic Molecules , Academic Press, New York*, 1971.
68. E. C. Constable, M. Neuburger, P. Reesel, G. E. Schneider, J. A. Zampese, C. E. Housecroft, F. Monti, N. Armaroli, R. D. Costa and E. Orta, *Inorganic Chemistry*.
69. N. Armaroli, L. Decola, V. Balzani, J. P. Sauvage, C. O. Dietrichbuchecker and J. M. Kern, *Journal of the Chemical Society-Faraday Transactions*, 1992, **88**, 553-556.
70. N. Armaroli, P. Ceroni, V. Balzani, J.-M. Kern, J.-P. Sauvage and J.-L. Weidmann, *Journal of the Chemical Society, Faraday Transactions*, 1997, **93**, 4145-4150.
71. J. Zhao and L. Xu, *Inorganica Chimica Acta*, 2008, **361**, 2385-2395.
72. N. Armaroli, J.-F. Eckert and J.-F. Nierengarten, *Chemical Communications*, 2000, 2105-2106.
73. A. Moissette, Y. Batonneau and C. Braumard, *Journal of the American Chemical Society*, 2001, **123**, 12325-12334.
74. V. Balzani and S. Campagna, *Photochemistry and Photophysics of Coordination Compounds I*, Springer, 2007.
75. L. Giribabu, V. K. Singh, C. Vijay Kumar, Y. Soujanya, V. Gopal Reddy and P. Yella Reddy, *Advances in OptoElectronics*, **2011**, 8.
76. K. K.-W. Lo, T. K.-M. Lee, J. S.-Y. Lau, W.-L. Poon and S.-H. Cheng, *Inorganic Chemistry*, 2007, **47**, 200-208.
77. M. I. J. Polson, F. Loiseau, S. Campagna and G. S. Hanan, *Chemical Communications*, 2006, **0**, 1301-1303.
78. K. Kalayandundarm, *Photochemistry of Polypyridine and Porphyrin Complexes*, 1ed.
79. B. O'Regan and M. Gratzel, *Nature*, 1991, **353**, 737-740.
80. M. K. Nazeeruddin, A. Kay, I. Rodicio, R. Humphrey-Baker, E. Müller, P. Liska, N. Vlachopoulos and M. Grätzel, *Journal of the American Chemical Society*, 1993, **115**, 6382-6390.
81. A. El-ghayoury, A. Harriman and R. Ziessel, *The Journal of Physical Chemistry A*, 2000, **104**, 7906-7915.
82. D. B. MacQueen, J. R. Eyler and K. S. Schanze, *Journal of the American Chemical Society*, 1992, **114**, 1897-1898.
83. M. Hissler, A. El-ghayoury, A. Harriman and R. Ziessel, *Angewandte Chemie International Edition*, 1998, **37**, 1717-1720.
84. E.-G. Abdelkhrim, H. Anthony, K. Abderrahim and Z. Raymond, *Angewandte Chemie International Edition*, 2000, **39**, 185-189.
85. A. Harriman, M. Hissler, A. Khatyr and R. Ziessel, *Chemical Communications*, 1999, **0**, 735-736.
86. E. Badaeva, Albert, V. V., Kilina, S., Koposov, A., Sykova, M., Tretiak, S., *Physical Chemistry Chemical Physics*, 2009, **12**, 8902-8913.
87. D. V. Kozlov, D. S. Tyson, C. Goze, R. Ziessel and F. N. Castellano, *Inorganic Chemistry*, 2004, **43**, 6083-6092.
88. C. Goze, D. V. Kozlov, F. N. Castellano, J. Suffert and R. Ziessel, *Tetrahedron Letters*, 2003, **44**, 8713-8716.
89. I. E. Pomestchenko and F. N. Castellano, *The Journal of Physical Chemistry A*, 2004, **108**, 3485-3492.
90. A. De Nicola, Y. Liu, K. S. Schanze and R. Ziessel, *Chemical Communications*, 2003, **0**, 288-289.
91. R. J. Watts, G. A. Crosby and J. L. Sansregret, *Inorganic Chemistry*, 1972, **11**, 1474-1483.
92. M. Hissler, A. El-ghayoury, A. Harriman and R. Ziessel, *Angewandte Chemie*, 1998, **110**, 1804-1807.
93. A. Harriman, A. Mayeux, C. Stroh and R. Ziessel, *Dalton Transactions*, 2005, **0**, 2925-2932.
94. D. J. Hurley and Y. Tor, *Journal of the American Chemical Society*, 2002, **124**, 3749-3762.

95. D. J. Hurley and Y. Tor, *Journal of the American Chemical Society*, 1998, **120**, 2194-2195.
96. D. J. Hurley and Y. Tor, *Journal of the American Chemical Society*, 2002, **124**, 13231-13241.
97. B. Chiswell and S. E. Livingstone, *Journal of Inorganic and Nuclear Chemistry*, 1964, **26**, 47-51.
98. S. C. Rasmussen, M. M. Richter, E. Yi, H. Place and K. J. Brewer, *Inorganic Chemistry*, 1990, **29**, 3926-3932.
99. A. P. Wilde, K. A. King and R. J. Watts, *The Journal of Physical Chemistry*, 1991, **95**, 629-634.
100. I. M. Dixon, J.-P. Collin, J.-P. Sauvage, L. Flamigni, S. Encinas and F. Barigelletti, *Chemical Society Reviews*, 2000, **29**, 385-391.
101. W. A. Wickramasinghe, P. H. Bird and N. Serpone, *Journal of the Chemical Society, Chemical Communications*, 1981, **0**, 1284-1286.
102. P. Didier, I. Ortmans, A. Kirsch-De Mesmaeker and R. J. Watts, *Inorganic Chemistry*, 1993, **32**, 5239-5245.
103. X. Zeng, M. Tavasli, I. F. Perepichka, A. S. Batsanov, M. R. Bryce, C.-J. Chiang, C. Rothe and A. P. Monkman, *Chemistry – A European Journal*, 2008, **14**, 933-943.
104. H. Lin, M. E. Cinar and M. Schmittel, *Dalton Transactions*, **39**, 5130-5138.
105. A. Valore, E. Cariati, C. Dragonetti, S. Righetto, D. Roberto, R. Ugo, F. De Angelis, S. Fantacci, A. Sgamellotti, A. Macchioni and D. Zuccaccia, *Chemistry – A European Journal*, **16**, 4814-4825.
106. E. M. Simmons and J. F. Hartwig, *Journal of the American Chemical Society*, **132**, 17092-17095.
107. R. M. Harshorn and D. A. House, *J. Chem. Soc., Dalton Trans.*, 1998, 2577.
108. H. J. Bolink, L. Cappelli, E. Coronado, M. Gratzel, E. Orta, R. D. Costa, P. M. Viruela and M. K. Nazeeruddin, *Journal of the American Chemical Society*, 2006, **128**, 14786-14787.
109. K. Binnemans, J. C. B. K.A. Gschneidner and V. K. Pecharsky, in *Handbook on the Physics and Chemistry of Rare Earths*, Elsevier, Editon edn., 2005, vol. Volume 35, pp. 107-272.
110. K. Binnemans and C. Garller-Walrand, *Chemical Reviews*, 2002, **102**, 2303-2346.
111. C. Y. Yang, V. Srdanov, M. R. Robinson, G. C. Bazan and A. J. Heeger, *Advanced Materials*, 2002, **14**, 980-983.
112. L. Matthews and E. T. Knobbe, *Chemistry of Materials*, 1993, **5**, 1697-1700.
113. Y.-F. Yuan, T. Cardinaels, K. Lunstroot, K. Van Hecke, L. Van Meervelt, C. GÃ¶rller-Walrand, K. Binnemans and P. Nockemann, *Inorganic Chemistry*, 2007, **46**, 5302-5309.
114. Q. Shu, L. Birlenbach and M. Schmittel, *Inorganic Chemistry*, 2012, **51**, 13123-13127.
115. R. V. Kiran, C. F. Hogan, B. D. James and D. J. D. Wilson, *European Journal of Inorganic Chemistry*, **2011**, 4816-4825.
116. H. Yang, L. Li, L. Wan, Z. Zhou and S. Yang, *Inorganic Chemistry Communications*, **13**, 1387-1390.
117. P. J. Connors, D. Tzalis, A. L. Dunnick and Y. Tor, *Inorganic Chemistry*, 1998, **37**, 1121-1123.
118. J.-P. Collin, D. Jouvenot, M. Koizumi and J.-P. Sauvage, *Inorganic Chemistry*, 2005, **44**, 4693-4698.
119. B. P. Sullivan, D. J. Salmon and T. J. Meyer, *Inorganic Chemistry*, 1978, **17**, 3334-3341.
120. Q.-X. Zhen, B.-H. Ye, Q.-L. Zhang, J.-G. Liu, L. Hong, L.-N. Ji and L. Wang, *Journal of Inorganic Biochemistry*, 1999, **76**, 47-53.
121. A. Juris, V. Balzani, F. Barigalletti, C. S., P. Belser and A. Von Zelewsky, *Coordination Chemistry Reviews*, 1988, **84**, 85-277.
122. W. Wu, S. Ji, W. Wu, H. Guo, X. Wang, J. Zhao and Z. Wang, *Sensors and Actuators B: Chemical*, **149**, 395-406.
123. A. Harriman, M. Hissler and R. Ziessel, *Physical Chemistry Chemical Physics*, 1999, **1**, 4203-4211.

124. L. Chouai, F. Wu, Y. Jang and Randolph P. Thummel, *European Journal of Inorganic Chemistry*, 2003, **2003**, 2774-2782.
125. S. Ji, W. Wu, W. Wu, P. Song, K. Han, Z. Wang, S. Liu, H. Guo and J. Zhao, *Journal of Materials Chemistry*, **20**, 1953-1963.
126. M. Hissler, A. Harriman, A. Khatyr and R. Ziessel, *Chemistry – A European Journal*, 1999, **5**, 3366-3381.
127. C. Goze, D. V. Kozlov, D. S. Tyson, R. Ziessel and F. N. Castellano, *New Journal of Chemistry*, 2003, **27**, 1679-1683.
128. D. S. Tyson, K. B. Henbest, J. Bialecki and F. N. Castellano, *The Journal of Physical Chemistry A*, 2001, **105**, 8154-8161.
129. J. Hu, J. H. K. Yip, D.-L. Ma, K.-Y. Wong and W.-H. Chung, *Organometallics*, 2008, **28**, 51-59.
130. D. S. Tyson and F. N. Castellano, *The Journal of Physical Chemistry A*, 1999, **103**, 10955-10960.
131. S. Sprouse, K. A. King, P. J. Spellane and R. J. Watts, *Journal of the American Chemical Society*, 1984, **106**, 6647-6653.
132. R. H. Friend, R. W. Gymer, A. B. Holmes, J. H. Burroughes, R. N. Marks, C. Taliani, D. D. C. Bradley, D. A. D. Santos, J. L. Bredas, M. Logdlund and W. R. Salenek, *Nature*, 1999, **397**, 121.
133. S. Bettington, M. Tavasli, M. R. Bryce, A. S. Batsanov, A. L. Thompson, H. A. Al Attar, F. B. Dias and A. P. Monkman, *Journal of Materials Chemistry*, 2006, **16**, 1046-1052.
134. M. Lepeltier, T. Kwok-Ming Lee, K. Kam-Wing Lo, L. Toupet, H. Le Bozec and V. Guerchais, *European Journal of Inorganic Chemistry*, 2005, **2005**, 110-117.
135. M. K. Nazeeruddin, R. Humphry-Baker, D. Berner, S. Rivier, L. Zuppiroli and M. Graetzel, *Journal of the American Chemical Society*, 2003, **125**, 8790-8797.
136. F. Neve, A. Crispini, S. Campagna and S. Serroni, *Inorganic Chemistry.*, 1999, **38**, 2250-2258.
137. C. A. Parker and C. G. Hatchard, *Proc. Chem. Soc. London*, 1962, 386.
138. C. A. Parker, in *Advances in Photochemistry*, John Wiley & Sons, Inc., Editon edn., 2007, pp. 305-383.
139. M. P. T. G.F. Stelmakh, *Opt. Spectrosc*, 1980, **49**.
140. R. R. Islangulov, D. V. Kozlov and F. N. Castellano, *Chemical Communications*, 2005, 3776-3778.
141. D. Papkovsky and T. O' Riordan, *Journal of Fluorescence*, 2005, **15**, 569-584.
142. S. K. Sugunan, U. Tripathy, S. M. K. Brunet, M. F. Paige and R. P. Steer, *The Journal of Physical Chemistry A*, 2009, **113**, 8548-8556.
143. S. Baluschev, V. Yakutkin, T. Miteva, G. Wegner, T. Roberts, G. Nelles, A. Yasuda, S. Chernov, S. Aleshchenkov and A. Cheprakov, *New Journal of Physics*, 2008, **10**, 013007.
144. H. Zhang, Y. Li, I. A. Ivanov, Y. Qu, Y. Huang and X. Duan, *Angewandte Chemie International Edition*, **49**, 2865-2868.
145. C. Reinhard, R. Valiente and H. U. Gudel, *The Journal of Physical Chemistry B*, 2002, **106**, 10051-10057.
146. A. Monguzzi, J. Mezyk, F. Scotognella, R. Tubino and F. Meinardi, *Phys. Rev. B*, 2008, **78**, 195112.
147. T. F. Schulze, J. Czolk, Y.-Y. Cheng, B. Fuckel, R. W. MacQueen, T. Khoury, M. J. Crossley, B. Stannowski, K. Lips, U. Lemmer, A. Colsmann and T. W. Schmidt, *The Journal of Physical Chemistry C*, **116**, 22794-22801.
148. E. L. Cates, S. L. Chinnapongse, J.-H. Kim and J.-H. Kim, *Environmental Science & Technology*, **46**, 12316-12328.
149. J.-H. Kim and J.-H. Kim, *Journal of the American Chemical Society*, **134**, 17478-17481.
150. A. Monguzzi, R. Tubino and F. Meinardi, *Physical Review B*, 2008, **77**, 155122.
151. J. Zhao, S. Ji and H. Guo, *RSC Advances*, **1**, 937-950.
152. Y. Y. Cheng, B. Fuckel, T. Khoury, R. Clady, M. J. Y. Tayebjee, N. J. Ekins-Daukes, M. J. Crossley and T. W. Schmidt, *J. Phys. Chem. Lett.*, **1**, 1795.

153. Y. Y. Cheng, T. Khoury, R. Clady, M. J. Y. Tayebjee, N. J. Ekins-Daukes, M. J. Crossley and T. W. Schmidt, *Phys. Chem. Chem. Phys.*, **12**, 66.
154. T. N. Singh-Rachford, A. Haefele, R. Ziessel and F. N. Castellano, *Journal of the American Chemical Society*, 2008, **130**, 16164-16165.
155. J. Saltiel, G. R. March, W. K. Smothers, S. A. Stout and J. L. Charlton, *Journal of the American Chemical Society*, 1981, **103**, 7159-7164.
156. S. Kobayashi, K. Kikuchi and H. Kokubun, *Chemical Physics Letters*, 1976, **42**, 494-497.
157. J. D. Spikes, *J. Photochem. Photobiol B: Biol*, 1990, **6**, 259.
158. W. Spiller, Wohrle, D., Schulz-Ekloff, W., Ford, T., Schneider, G., and Stark, J., *J. Photochem. Photobiol B: Biol. A: Chem*, 1996, **95**, 161.
159. M. C. a. G. Palumbo, N.A. , *Toxicol. Environ. Chem* 1988, **17**, 103.
160. M. C. DeRosa and R. J. Crutchley, *Coordination Chemistry Reviews*, 2002, **233**, 351-371.
161. W. Spiller, Kliesch, H., Wohrle, D., Hackbarth, S., Roder, B., and Schurpfeil, G., *Journal of Porphyrins and Phthalocyanines* 1998, **2**, 145-158.
162. C. Tanielian and G. Heinrich, *Photochemistry and Photobiology*, 1995, **61**, 131-135.
163. Q. G. Mulazzani, H. Sun, M. Z. Hoffman, W. E. Ford and M. A. J. Rodgers, *The Journal of Physical Chemistry*, 1994, **98**, 1145-1150.
164. D. Garcìa-Fresnadillo, Y. Georgiadou, G. Orellana, A. M. Braun and E. Oliveros, *Helvetica Chimica Acta*, 1996, **79**, 1222-1238.
165. R. M. Hochstrasser and M. Ritchie, *Transactions of the Faraday Society*, 1956, **52**, 1363-1373.
166. S. Baluschev, V. Yakutkin, G. Wegner, T. Miteva, G. Nelles, A. Yasuda, S. Chernov, S. Aleshchenkov and A. Cheprakov, *Applied Physics Letters*, 2007, **90**, 181103-181103.
167. P. B. Merkel and J. P. Dinnocenzo, *Journal of Luminescence*, 2009, **129**, 303-306.
168. W. Wu, S. Ji, W. Wu, J. Shao, H. Guo, T. D. James and J. Zhao, *Chemistry – A European Journal*, **18**, 4953-4964.
169. M. Abrahamsson, M. Jager, R. J. Kumar, T. Osterman, P. Persson, H.-C. Becker, O. Johansson and L. Hammarstrom, *Journal of the American Chemical Society*, 2008, **130**, 15533-15542.
170. S. Leroy-Lhez, C. Belin, A. D'Aleo, R. M. Williams, L. De Cola and F. Fages, *Supramolecular Chemistry*, 2003, **15**, 627.
171. N. Armaroli, *ChemPhysChem*, 2008, **9**, 371-373.
172. N. D. McClenaghan, Y. Leydet, B. a. Maubert, M. T. Indelli and S. Campagna, *Coordination Chemistry Reviews*, 2005, **249**, 1336-1350.
173. T. N. Singh-Rachford and F. N. Castellano, *Coord. Chem. Rev.*, **254**, 2560.
174. R. R. Islangulov and F. N. Castellano, *Angewandte Chemie International Edition*, 2006, **45**, 5957-5959.
175. K. Hanson, A. Tamayo, V. V. Diev, M. T. Whited, P. I. Djurovich and M. E. Thompson, *Inorganic Chemistry*, 2010, **49**, 6077-6084.
176. K. K.-W. Lo, C.-K. Chung, T. K.-M. Lee, L.-H. Lui, K. H.-K. Tsang and N. Zhu, *Inorganic Chemistry*, 2003, **42**, 6886-6897.
177. M. C. DeRosa, D. J. Hodgson, G. D. Enright, B. Dawson, C. E. B. Evans and R. J. Crutchley, *Journal of the American Chemical Society*, 2004, **126**, 7619-7626.
178. W. Zhao and F. N. Castellano, *Journal of Physical Chemistry A*, 2006, **110**, 11440-11445.
179. S. M. Borisov and I. Klimant, *Analytical Chemistry*, 2007, **79**, 7501-7509.
180. J. Sun, W. Wu, H. Guo and J. Zhao, *European Journal of Inorganic Chemistry*, **2011**, 3165-3173.
181. J. Brooks, Y. Babayan, S. Lamansky, P. I. Djurovich, I. Tsyba, R. Bau and M. E. Thompson, *Inorganic Chemistry*, 2002, **41**, 3055-3066.
182. L. Ma, H. Guo, Q. Li, S. Guo and J. Zhao, *Dalton Transactions*, 2012, **41**, 10680-10689.
183. F. A. Murphy, S. Suárez, E. Figgemeier, E. R. Schofield and S. M. Draper, *Chemistry – A European Journal*, 2009, **15**, 5740-5748.
184. P. Du and R. Eisenberg, *Chemical Science*, 2010, **1**, 502-506.

185. T. N. Singh-Rachford, A. Nayak, M. L. Muro-Small, S. b. Goeb, M. J. Therien and F. N. Castellano, *Journal of the American Chemical Society*, 2010, **132**, 14203-14211.
186. J. Sun, F. Zhong, X. Yi and J. Zhao, *Inorganic Chemistry*, 2013, **52**, 6299-6310.
187. A. A. Rachford, S. b. Goeb and F. N. Castellano, *Journal of the American Chemical Society*, 2008, **130**, 2766-2767.
188. J. E. Yarnell, J. C. Deaton, C. E. McCusker and F. N. Castellano, *Inorganic Chemistry*, 2011, **50**, 7820-7830.
189. M. Li, P. Lincoln and J. Andersson, *The Journal of Physical Chemistry B*, **115**, 7923-7931.
190. K. Butsch, R. Gust, A. Klein, I. Ott and M. Romanski, *Dalton Transactions*, **39**, 4331-4340.
191. B. Schafer, H. Gorls, M. Presselt, M. Schmitt, J. Popp, W. Henry, J. G. Vos and S. Rau, *Dalton Transactions*, 2006, 2225-2231.
192. W. Chen, Turro, C., Friedman, L. A., Barton, J. K., Turro., N. J., *Journal of Physical Chemistry B*, 1997, **101**, 6995-7000.
193. J. R. Schoonover, W. D. Bates and T. J. Meyer, *Inorganic Chemistry*, 1995, **34**, 6421-6422.
194. J. Bolger, Gourdon, A., Ishow, E., Launey, J. P., *Inorganic Chemistry*, 1996, **35**, 2937-2944.
195. H. Zhen, C. Jiang, W. Yang, J. Jiang, F. Huang and Y. Cao, *Chemistry – A European Journal*, 2005, **11**, 5007-5016.
196. F. Emmerling, I. Orgzall, B. Dietzel, B. Schulz and J. Larrucea, *Journal of Molecular Structure*, **1030**, 209-215.
197. C. T.-C. HUANG HEH-LUNG , LEE HAO-CHUN in *European Patent Office Publication Number US2012305901 (A1) Application Number US201213567028*, Editon edn., 2012.
198. , 2012.
199. A. Babel and S. A. Jenekhe, *J. Am. Chem. Soc.*, 2003, **125**, 13656.
200. YONG QIU; XUXIA SUN; YINKUI LI; XUEYAN REN; JUAN QIAO; LIAN DUAN, *European Patent Office Publication Number CN20101258747 20100820* 2010.
201. T. L. Andrew, B. VanVeller and T. M. Swager, *Synlett*, **2010**, 3045-3048.
202. E. C. Glazer and Y. Tor, *Angewandte Chemie, International Edition in English*, 2002, **41**, 4022-4025.
203. O. Schmelz, A. Mews, T. Basche, A. Herrmann and K. Mullen, *Langmuir*, 2001, **17**, 2861-2865.
204. S. D. Bergman, D. Gut, M. Kol, C. Sabatini, A. Barbieri and F. Barigelletti, *Inorganic Chemistry*, 2005, **44**, 7943-7950.
205. S. D. Bergman, I. Goldberg, C. Carfagna, L. Mosca, M. Kol and B. Milani, *Organometallics*, 2006, **25**, 6014-6018.
206. S. D. Bergman, I. Goldberg, A. Barbieri, F. Barigelletti and M. Kol, *Inorganic Chemistry*, 2004, **43**, 2355-2367.
207. O. Baudoin, M.-P. Teulade-Fichou, J.-P. Vigneron and J.-M. Lehn, *The Journal of Organic Chemistry*, 1997, **62**, 5458-5470.
208. A. H. Cook and W. Waddington, *Journal of the Chemical Society (Resumed)*, 1945, **0**, 402-405.
209. P. Sarkar, I.-R. Jeon, F. Durola and H. Bock, *New Journal of Chemistry*, **36**, 570-574.
210. A. Sanguineti, M. Sassi, R. Turrisi, R. Ruffo, G. Vaccaro, F. Meinardi and L. Beverina, *Chemical Communications*, **49**, 1618-1620.
211. C. J. Martin, B. Gil, S. D. Perera and S. M. Draper, *European Journal of Organic Chemistry*, **2011**, 3491-3499.
212. G. C. Gearoid O'Maille, and Sylvia M. Draper, *Unpublished Results*, 2013.
213. D. J. Gregg, E. Bothe, P. Hofer, P. Passaniti and S. M. Draper, *Inorganic Chemistry*, 2005, **44**, 5654-5660.
214. S. Tokita, Hiruta. K, Ishikawa, S.,Kitahara, K., Nishi, H., *Synthesis*, 1982, **10**, 854-855.
215. N. Masakatsu, S. Takehiko, I. Tsutomu and T. Yoshiyuki, Editon edn., 2002, vol. Application number JP20020088228 20020327

216. M. D. Watson, A. Fechtenkotter and K. Mullen, *Chemical Reviews*, 2001, **101**, 1267-1300.
217. K. Yoshimura, L. Przybilla, S. Ito, J. D. Brand, M. Wehmeir, H. J. Räder and K. Müllen, *Macromolecular Chemistry and Physics*, 2001, **202**, 215-222.
218. J. Wu, M. D. Watson, N. Tchebotareva, Z. Wang and K. Müllen, *Journal of Organic Chemistry*, 2004, **69**, 8194-8204.
219. R. P. Wayne, *Principles and Applications of Photochemistry, Oxford Press*, 1980.
220. D. S. Tyson, C. R. Luman, X. Zhou and F. N. Castellano, *Inorganic Chemistry*, 2001, **40**, 4063-4071.
221. W. Wu, J. Sun, S. Ji, W. Wu, J. Zhao and H. Guo, *Dalton Transactions*, **40**, 11550-11561.
222. P. I. Djurovich, D. Murphy, M. E. Thompson, B. Hernandez, R. Gao, P. L. Hunt and M. Selke, *Dalton Transactions*, 2007, **0**, 3763-3770.
223. P. T. Herwig, V. Enkelmann, O. Schmelz and K. Mullen, *Chemistry-a European Journal*, 2000, **6**, 1834-1839.
224. J. H. Price, A. N. Williamson, R. F. Schramm and B. B. Wayland, *Inorganic Chemistry*, 1972, **11**, 1280-1284.
225. H. D. Abbayes, J. C. Clement, P. Laurent, J. J. Yaouanc, G. Tanguy and B. Weinberger, *Journal of Organometallic Chemistry*, 1989, **359**, 205-214.
226. V. S. Iyer, M. Wehmeier, J. D. Brand, M. A. Keegstra and K. Mullen, *Angewandte Chemie-International Edition in English*, 1997, **36**, 1604-1607.

# Annex

**Table 1**. Crystal data and structure refinement for 1,10-phenanthroline ligand (18)

| | | |
|---|---|---|
| Identification code | w | |
| Empirical formula | C106 H112 N2 O4 | |
| Formula weight | 1477.98 | |
| Temperature | 150(2) K | |
| Wavelength | 0.71073 Å | |
| Crystal system | Monoclinic | |
| Space group | P2(1)/c | |
| Unit cell dimensions | a = 27.404(6) Å | α= 90°. |
| | b = 18.182(4) Å | β= 91.36(3)°. |
| | c = 18.596(4) Å | γ = 90°. |
| Volume | 9263(3) $Å^3$ | |
| Z | 4 | |
| Density (calculated) | 1.060 $Mg/m^3$ | |
| Absorption coefficient | 0.063 $mm^{-1}$ | |
| F(000) | 3176 | |
| Crystal size | 0.40 x 0.30 x 0.28 $mm^3$ | |
| Theta range for data collection | 1.34 to 25.00°. | |
| Index ranges | -32<=h<=25, -21<=k<=16, -22<=l<=19 | |
| Reflections collected | 53197 | |
| Independent reflections | 16301 [R(int) = 0.0790] | |
| Completeness to theta = 25.00° | 99.8 % | |
| Absorption correction | Semi-empirical from equivalents | |
| Max. and min. transmission | 0.9826 and 0.9753 | |
| Refinement method | Full-matrix least-squares on $F^2$ | |
| Data / restraints / parameters | 16301 / 88 / 1033 | |
| Goodness-of-fit on $F^2$ | 1.104 | |
| Final R indices [I>2sigma(I)] | R1 = 0.1008, wR2 = 0.2985 | |
| R indices (all data) | R1 = 0.1786, wR2 = 0.3541 | |
| Largest diff. peak and hole | 0.912 and -0.352 $e.Å^{-3}$ | |